Study of Gamow-Teller Transitions of $T_z = -2$ ^{64}Se and $T_z = -1$ ^{66}Se

Tesis
entregada a la
Universidad de Chile
en cumplimiento parcial de los requisitos
para optar al grado de
Doctor en Ciencias con mención en Física
Facultad de Ciencias

por

Pablo Antonio Aguilera Jorquera

Marzo, 2020

Director de Tesis: **Dr. Hugo Arellano Sepúlveda**

Co-Directores de Tesis: **Dr. Francisco Gabriel Molina Palacios**

Dra. Berta Rubio Barroso

GLOSSARY

A10E700 / A11E700 Reconstruction algorithm where the Y-side energy of the MinTxMaxEy pixel can sum the energy of one of the neighbouring Y-side strip (see Section 4.2) within the same DSSSD / neighbouring DSSSD, with an energy threshold of 700 keV.

D000, D110, D111, NMD Distance condition between the decay event and ion event position (see Section 4.2) where the implant is in the same pixel (D000), within one of the nine neighbouring pixels (D110), and within one of the 27 neighbouring pixels including other DSSSDs (D111), or without a distance condition (NMD).

DSSSD Double Sided Silicon Strip Detector (see Section 3.1).

EURICA Euroball at RIKEN Cluster Array. Array of HPGe detectors used to measure the γ radiation emitted during a decay (see Section 3.2).

IAS Isobaric Analogue State.

IMME Isobaric mass multiplet equation (see Section 8.1).

MinTxMaxEy Reconstruction of a β event in WAS3ABi where the pixel with the minimum time on the X-side and maximum energy on the Y-side of the DSSSD is identified as the one where the decay event took place (see Section 4.2).

PID Particle identification plot (see Section 2.3), this is the mass over charge ratio as a function of the atomic number.

RIBF RI Beam Factory. Accelerator complex located in RIKEN Nishina Center (Tokyo), where the experiment took place during 2015 (see Section 2).

TNN Trends of neighbouring Nucleus. In AME2016 [WAK+17] and in Nubase2016 [AKW+17] the #is used to indicate when a nuclear value was extrapolated from its neighbouring nuclides when no experimental information is available.

WAS3ABi Wide-range Active Silicon-Strip Stopper Array for Beta and Ion detection. Array of silicon detectors used to measure position, energy and time for ions, βs, and protons (see Sec. 3.1).

Contents

List of Figures

List of Tables

RESUMEN EN CASTELLANO

En este trabajo se estudia por primera vez la desintegración beta de dos isótopos de selenio, ^{64}Se y ^{66}Se, mediante una reacción de fragmentación de un haz primario de ^{78}Kr sobre un blanco de berilio. Este experimento se realizó durante el año 2015 en la instalación RIBF de RIKEN Nishina Center en Tokio. Dado que estos núcleos exóticos se encuentran a cuatro nucleones de la estabilidad, hasta la fecha de realización de este experimento no había sido posible producir un haz lo suficientemente intenso para conseguir la estadística suficiente para llevar a cabo este tipo de estudios, siendo actualmente RIBF la instalación que produce los haz primarios más intensos en el mundo. Tras la reacción de fragmentación, los llamados fragmentos, núcleos producto de todos los canales de reacción, son separados e identificados en vuelo por el separador de partículas BigRIPs, para luego ser implantados en un detector de Silicio segmentado de doble capa (DSSSD) denominado WAS3ABi. Este detector permite determinar la posición geométrica de la implantación, así como medir la energía depositada por las partículas emitidas en una desintegración beta, positrones y protones, en este caso los más estudiados. De esta forma se es posible correlacionar los eventos de implantación con los de desintegración permitiendo medir los períodos de semi-desintegración de los núcleos de interés ^{64}Se y el ^{66}Se: $T_{1/2}$ =22.6(14) ms y $T_{1/2}$ =57.6(15) ms, respectivamente. Los núcleos hijos ^{64}As, ^{63}Ge y ^{66}As, también se desintegran β^+ con períodos de semi-desintegración comprables del orden de cientos de milisegundos. Afortunadamente estos núcleos hijos también fueron producidos por otros canales de reacción, identificados e implantados en WAS3ABi durante el experimento lo cual permitió determinar su período de semi-desintegración de forma independiente resultando $T_{1/2}$ =152.60(33) ms, $T_{1/2}$ =62.69(71) ms y $T_{1/2}$ =95.77(23) ms, para el ^{63}Ge, ^{64}As

y ^{66}As, respectivamente.

Para los núcleos emisores de protones ^{64}Se y ^{64}As, además del período de semi-desintegración se obtuvo el valor de branching de protones, $B_p = 48.02(89)\%$ y $B_p = 4.4(1)\%$, respectivamente. Además se identificaron, por primera vez, ocho energías de protones en la desintegración del ^{64}Se y once en la del ^{64}As.

Con el fin de estudiar el esquema de niveles de desintegración beta de cada núcleo, rodeando a WAS3ABi se ubicó un arreglo de detectores de Germanio Hiper Puro denominado EURICA, con la finalidad de realizar espectroscopia gamma a las desintegraciones. De esta forma fue posible imponer condiciones de coincidencia beta-gamma, de donde se obtuvieron los espectros gamma de cada núcleo. De esta forma se identificaron las transiciones gamma correspondientes a cada desintegración: siete en la del ^{64}Se, diecinueve en ^{64}As, quince en el ^{63}Ge y diez en el ^{66}Se, de los cuales en este trabajo se observaron por primera vez siete picos gama en la desintegración del ^{64}Se, quince en la del ^{64}As, once en al del ^{63}Ge y ocho en la del ^{66}Se. En el caso de la desintegración del ^{66}As no se observó ningún pico gamma, lo que siguiere que esta desintegración sólo puebla el estado fundamental en el ^{66}Ge.

Luego de identificar las transiciones gamma correspondientes a cada desintegración se impusieron condiciones de coincidencia gamma-gamma de tal forma de determinar cuales de ellos son emitidos en cascada y de esta forma construir el esquema de niveles. Para la desintegración del ^{64}Se se observó por primera vez nueve estados excitados, seis de los cuales emiten protones y un estado excitado en el núcleo hijo ^{63}Ge. En el caso de la desintegración del ^{64}As, cuatro estados excitados habían sido observados previamente en la literatura y otros dieciséis fueron identificados por primera vez, de los cuales seis son emisores de protones. En la desintegración del ^{63}Ge cuatro estados excitados ya habían sido reportados en la literatura y siete fueron

observados por primera vez. El caso del ^{66}Se se observaron siete estados excitados de los cuales cinco se observaron por primera vez en este trabajo.

En relación al valor experimental del exceso de masas, a la fecha no se han medido las masas para el ^{64}Se ni el ^{64}As, contando solo con estimaciones obtenidas a partir de extrapolaciones de núcleos más ligeros. En este trabajo se usó la Isobaric Mass Multiplet Equation (IMME) junto con las energías obtenidas de protones y gammas en el ^{64}As junto con el valor del exceso de masas del ^{64}Ga y del ^{64}Zn para obtener el exceso de masas del ^{64}As a partir de nuestros datos, obteniéndose un valor de $\mathbf{-39597(44)\ keV}$ para su estado fundamental. Análogamente se evaluó la curva en para el ^{64}Se donde se obtuvo un exceso de masas de $\mathbf{-27429(88)\ keV}$ para su estado fundamental.

ABSTRACT

This work corresponds to the first study of the beta decay of two exotic nuclei in an experiment performed during 2015 at RIBF in the RIKEN Nishina Center (Tokyo, Japan), the $T_z = -2$ ^{64}Se and the $T_z = -1$ ^{66}Se. These nuclei were produced by a fragmentation reaction using a primary beam of ^{78}Kr over a beryllium target. Since these exotic nuclei needs four beta decays to reach the stability, up to this experiment such a strong beam was not available in order to obtain enough statistic to carry out this type of experiment, being RIBF that produce the most intense beams around the world. After the reaction inside the target, fragments are separated, identified by the BigRIPs mass separator, to further being implanted in Double Sided Silicon Strip Detector (DSSSD) named WAS3ABi (active stopper). This detector allows to determine the geometric position where the implantation took place, as well as measure the energy deposited by a charged particle. Correlating implantation and decay events it was possible to measure the half-lives of nuclei of interest ^{64}Se and ^{66}Se: $T_{1/2} = 22.6(14)$ ms and $T_{1/2} = 57.6(15)$ ms. Daughter nuclei ^{64}As, ^{63}Ge and ^{66}As, also decay by β^+, having comparable half-lives of the order of hundred of milliseconds. Fortunately these nuclei also were produced, identified and implanted in the WAS3ABi active stopper, allowing one to measure their half-lives independently, obtaining $T_{1/2} = 152.60(33)$ ms, $T_{1/2} = 62.69(71)$ ms and $T_{1/2} = 95.77(23)$ ms, for ^{63}Ge, ^{64}As and ^{66}As. Beta-delayed proton emitter nuclei not only the half-life was determined, but also its proton branching, being $B_p = 48.02(89)\%$ and $B_p = 4.4(1)\%$. Indeed, eight proton energies were identified in ^{64}Se and ^{64}As decays.

To obtain the beta decay of each nuclei an array of HPGe detectors, named EURICA, were placed surrounding WAS3ABi, which was used to perform γ-ray

spectroscopy to the decays. Imposing conditions between the implanted nuclei and the beta-gamma coincidences the γ-ray spectra were obtained for each nuclei. Thus, γ-rays belongings to each decay were identified, seven for ^{64}Se, nineteen for ^{64}As, fifteen for ^{63}Ge and ten for ^{66}Se. From these, seven were observed for the first time in ^{64}Se, fifteen in ^{64}As, eleven in ^{63}Ge and eight in ^{66}Se. The case of ^{66}As decay was the only one where no γ-rays were observed, suggesting that this decay only populates the ground state in ^{66}Ge.

After identify those γ-ray belongings to each decay conditions over the γ-γ coincidences were applied in order to determine possible γ-ray cascades to construct the level scheme. Nine new excited states were observed for ^{64}Se decay, moreover, six are proton emitters and one corresponds to an excited state in ^{63}Ge. In ^{64}As decay, four states were previously reported in literature while other sixteen were identified for the first time in this work and six are proton emitters. For ^{66}Se decay seven excited states were observed in this thesis, where five of them observed for the firt time in this work.

At the moment of this thesis, no experimental measurements for the mass excess of ^{64}Se and ^{64}As have been performed. Moreover, mass excess for these nuclei are known only by extrapolations from lighter nuclei. In this work we use the Isobaric Mass Multiplet Equation (IMME) in the $A = 64$ multiplet together with the measured energies for protons and γ-rays, and the mass excess of ^{64}Ga and ^{64}Zn to determine the mass excess for ^{64}As from our data. $\mathbf{-39597(44)\ keV}$ was obtained for the ground state of ^{64}As. Then, using the IMME curve to evaluate the mass excess for ^{64}Se we obtained $\mathbf{-27429(88)\ keV}$.

Part I

Introduction

Motivation

Each atomic nucleus is formed by a set of neutrons and protons bound by the *strong force*. Ignoring, to a first approximation, the electric charge, protons and neutrons are very similar and are often considered to be two states of the same particle: the *nucleon*. This analogy can be extended in the same way as the quantum angular momentum, giving arise to the *isospin* formalism, a quantum number that is useful in describing nuclear properties in nuclei with similar numbers of protons and neutrons. The third component of nuclear isospin is defined as $T_z = (N - Z)/2$. Thus a nucleus with equal numbers of protons and neutrons has $T_z = 0$. Two nuclei are said to be mirror nuclei if they have the same mass number A, but the proton and neutron numbers are exchanged. For example ${}^{66}_{34}\mathrm{Se}_{32}$ and ${}^{66}_{32}\mathrm{Ge}_{34}$ are mirror nuclei. If a nucleus is transformed into its mirror partner it is expected to be almost identical in structure from the point of view of the strong interaction. This is the so-called *mirror symmetry* which is the main subject of study of this thesis [FRG11].

This symmetry can be extended to mirror processes such as β^+ and β^- decay, where a proton turns to a neutron (β^+ decay) or vice versa a neutron turns to a proton (β^- decay) with the emission of a positron and a neutrino, or an electron and an anti-neutrino, respectively. Both β^+ and β^- are called *mirror processes*. Isobars where these two processes can be observed both in proton-rich and neutron-rich mirror nuclei, are whose one can seek to test the mirror symmetry. These kind

of isobars can be observed up to nuclei with $A < 40$, where the stability line turns to the neutron-rich nuclei because of increasing the influence of the Coulomb energy, and the β^- decay is no longer available to perform this analysis. Nevertheless, there are so-called *charge exchange reactions* (CE), in which a proton or neutron of the projectile is exchanged with a neutron or proton of the target nucleus. This type of reaction can be categorized into β^- type ((p,n)-like reactions) and β^+ type ((n,p)-like reactions). It was only after 2001 that the (^{3}He$,t$) reaction ((p,n)-like) [Fuj01] could be studied in high resolution at RCNP in OSAKA (Japan), so that the mirror comparison using both β^+ and CE reactions became useful in the medium mass region.

From all mirror pairs, the easiest case to study is the $T_z = \pm 1$ case, where both the β^+ decay and the CE reaction end up in the same daughter nucleus. With this idea in mind we started a campaign of experiments at GSI to study the mirror nuclei using both β^+ decay and charge exchange reactions [Mol11, MRF+15].

This kind of study has to overcome several experimental difficulties. In this region of nuclei, the beta decay is dominated by an allowed Fermi transition, in consequence the half-life becomes very short. In order to produce and measure nuclei with such small half-lives, the experiments have to be carried out at *in-flight* facilities, such as the FRS at GSI [Mol11], BigRIPS at RIBF [F+13, K+12] or LISE3 at GANIL. In this kind of experiment, the elapsed time from the production of the nuclei of interest up to their implantation in an active stopper is very small. In the experiments at GSI and GANIL we have covered $T_z = -1$ and $T_z = -2$ nuclei up to ^{56}Zn, using a beam of ^{58}Ni [ORA+14, ORF+14, ORF+16]. Heavier nuclei, such as $T_z = -1, -2$ Ge and Se nuclei, cannot be produced with a ^{58}Ni beam. One possibility is to use a ^{78}Kr beam. But this nucleus lies further away from the $N = Z$ line than

^{58}Ni and in consequence, the production cross section decreases dramatically. This can be compensated by having an intense primary beam, as can be produced at the RIKEN Nishina Center.

In this context, this thesis is the continuation of this systematic study started in 2006, in which we present studies of the beta decays for the $T_z = -2$ ^{64}Se decay and the $T_z = -1$ ^{66}Se decay measured at RIKEN. Indeed the ^{64}Se decay, is the last nucleus that can be compared with the CE reaction, since higher $T_z = -2$ nuclei do not have the corresponding stable $T_z = +2$ partner. This is a challenging case, since for the ^{64}Se and its daughter nucleus ^{64}As there is no previous experimental information such as the energies of excited states and half-lives. Q_β values are known only from mass extrapolations.

This thesis is divided into five parts, and ten chapters. Part I starts with an introduction to the beta decay process. Then the concept of isospin is discussed and its relation to beta decay. Then the charge exchange reactions are discussed, to make the connection to the beta decay through the isospin symmetry. In Part II the experimental details are presented, starting with the description of the Facility and how the nuclei of interest ^{64}Se and ^{66}Se were produced. Then the active stopper named WAS3ABi, and the γ-ray spectrometer EURICA are described as well as their calibrations. Also the data handling is discussed. Part III explains the analysis. Starting with an overview of the correlation analysis, the procedure to obtain the intensities for both beta (β), proton (p), and γ-rays is explained. Then the analysis is discussed. As this is the first experimental work on the decay of ^{64}Se, which is a candidate for beta-delayed p-emission as shown in Fig. 1a, we proceeded as follows, Firstly we studied the daughter nuclei, ^{64}As and ^{63}Ge. This was done in order to identify the gamma radiation correlated with ^{64}Se that belonged to ^{64}As or ^{63}Ge.

Because the short half-lives are of comparable magnitude, decay radiation belonging to the ^{64}As decay and ^{63}Ge decay may be present in the decay of ^{64}Se. Then, the same logic is applied to the decay of ^{66}Se, showing first the analysis of its daughter nuclide ^{66}As. In Chapter IV, the intensities and half-lives measured for the nuclei of interest are presented, including the beta decay probability to states in the daughter nucleus. At the end of the Chapter the results are compared with the mirror charge exchange process measured at Osaka RCNP. Finally in Part V a summary of the conclusions is presented.

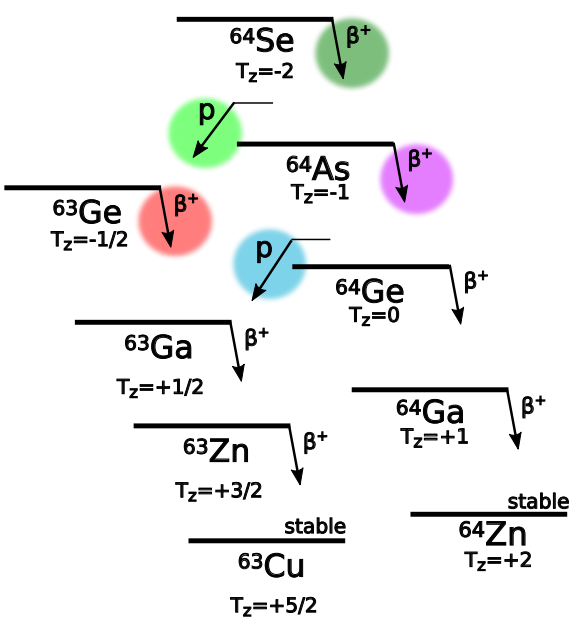

(a) ^{64}Se decay diagram.

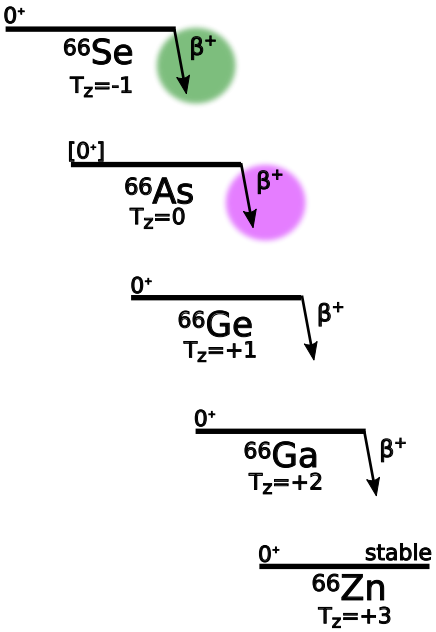

(b) ^{66}Se decay diagram.

Figure 1: Decay scheme of the isobaric multiplet ^{64}Se and ^{66}Se for the nuclei of interest. Nuclei populated in its decay are also shown. Colour is used to indicate decays with comparable half-lives that may overlap in both beta and γ-ray spectra.

Chapter 1

Beta Decay in Proton Rich Nuclei

Radioactivity was discovered in 1986 by Henri Becquerel [Bec96]. Since then, the common types of radiation such as α, and β were identified. In 1899 and 1900 the beta radiation was first identified. Beta decay from the physics point of view present an inherent difficulty which corresponds to its three-body nature. Chadwick in 1914 [Cha14], using a magnetic spectrometer, discovered the continuous spectrum of the β particles. This was considered a feature of the β decay in contrast to the other radiations such as α and γ radiation that were understood as discrete transitions between nuclear states. It was not until 1930 where Pauli [Pau33] introduces the idea of neutrino and its simultaneous emission with the beta particle (electron) in a *three body* process. Then in 1934 Fermi presented his theory based on the relativistic formalism with the underlying idea of the *Weak Interaction* [Fer34]. In 1934 the emission of *positive electrons* and β^+ decay was discovered and explained by Irene and Frédéric Joliot-Curie. This was the first observation of artificial radioactivity, then in 1936 the theory of beta decay transitions in nuclei was completed by Gamow and Teller.

1.1. Beta decay

The actual concept of beta decay involves two types of emission processes, the β^+ decay and the β^- decay:

> β^- **decay:** In this decay mode, a neutron n from the nucleus turns to a proton p due to the *Weak Interaction*, emitting an electron e^- and an anti-neutrino $\bar{\nu}$:
>
> $$n \longrightarrow p + e^- + \bar{\nu} \ .$$
>
> β^+ **decay:** In this decay mode, a proton p from the nucleus turns to a neutron n due to the *Weak Interaction*, emitting a position e^+ and a neutrino ν:
>
> $$p \longrightarrow n + e^+ + \nu \ .$$

Another similar process was observed in 1938 by Alvarez, where the decay takes place via the interaction with an electron in the inner atomic shell:

> **EC Electron Capture:** In this decay mode, an electron e^- from the inner shell of the atom is captured by the nucleus, transforming a proton p into a neutron n, emitting a neutrino ν:
>
> $$p + e^- \longrightarrow n + \nu \ .$$

With the Standard model, beta decay can be understood as the transformation of one quark type in another via exchange of a charged weak currents ($W^\pm$ bosons) as shown in Fig. 1.1.

From the point of view of the whole system, the maximum energy released by the β^+ decay is given by the Q-value. It depends on the mass of the mother

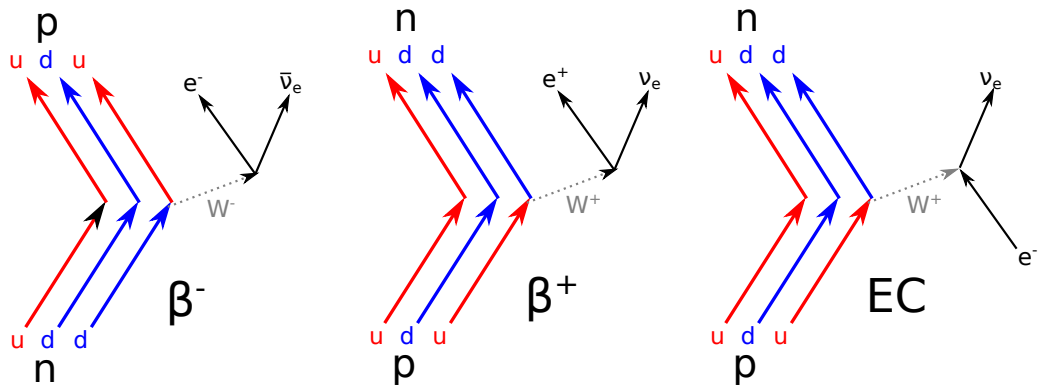

Figure 1.1: The beta decay process from the Weak interaction point of view.

nucleus $M(Z, A)$ and the daughter nucleus $M(Z-1, A)$, the electron mass m_e, and the speed of light c,

$$Q_{\beta^+} = M\left(Z, A\right) c^2 - M\left(Z-1, A\right) c^2 - 2m_e c^2 \ , \tag{1.1}$$

and for the EC process the Q-value can be written as:

$$Q_{\mathrm{EC}} = M\left(Z, A\right) c^2 - M\left(Z-1, A\right) c^2 - B \ , \tag{1.2}$$

where B is the binding energy of the electron removed from the atomic shell.

As stated earlier, beta decay is a three body problem. Depending on the energy carried by the neutrino, the energy measured by the electron or positron is continuous, and the maximum energy transferable corresponds to the Q_β value. This will be clarified in Section 1.1.1.

This energy constraints also limits the energy of excited states that can be populated in the beta decay. In other words, a beta decay can populate states in the daughter nuclide with excitation energy (E_{ex}) lower than the Q_β value $E_{\mathrm{ex}} \leq Q_\beta$. Nevertheless this is from the energy point of view only, other constrains for the population of states in the daughter nucleus will come from the conservation of the

angular momentum.

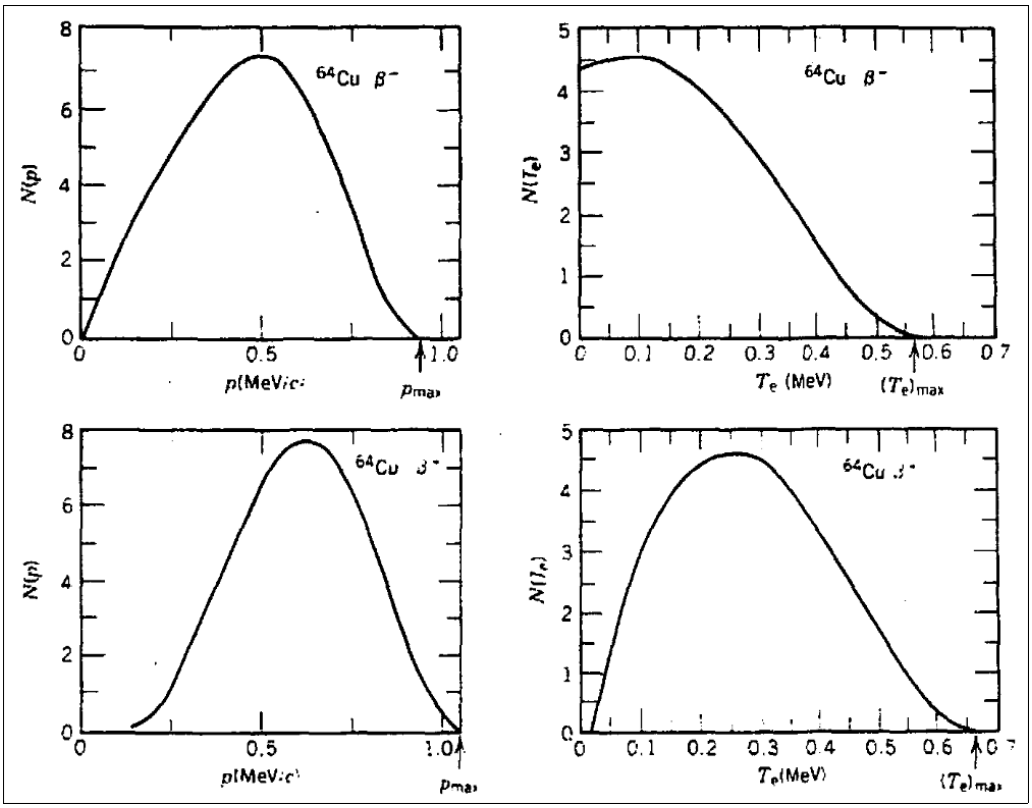

Figure 1.2: Example of the energy distribution and the momentum distribution for ^{64}Cu β^+ decay, and the ^{64}Cu β^- decay, from Kenneth S. Krane [Kra87]. The main difference resides in the electromagnetic interaction.

1.1.1. Fermi Theory of Beta Decay

In 1934, Fermi [Fer34] developed its theory about the β decay taking into account a third particle the anti-neutrino, and that the interaction was point like. Fermi consider the nuclear potential $V(\vec{x})$, and introduce the interaction responsible for the transition as a small perturbation $v_\beta(\vec{x}, t)$. Then the perturbed potential $V'(\vec{x}, t) = V(\vec{x}) + v_\beta(\vec{x}, t)$ can be used to obtain the transition rate λ as,

$$\lambda = \frac{2\pi}{\hbar} \left| \langle \psi_f^* | H_{\text{inte}} | \psi_i \rangle \right|^2 \rho(E_f) \ , \tag{1.3}$$

where $\rho(E_f) = dn/dE_f$ is the density of final states. Fermi did not know the form of the interaction $\left|\langle\psi_f^*|H_{\text{inte}}|\psi_i\rangle\right|^2$. It took twenty years to obtain the correct form of the interaction. The initial state corresponds to the wave function of the mother state ψ_i, while the final state consists of the wave function of the daughter nucleus ψ_f, together with the wave function of the electron ϕ_e, and the anti-neutrino $\phi_{\bar{\nu}}$. Then, the

$$\langle\psi_f \left| H^{\beta}_{\text{inte}} \right| \psi_i\rangle \ = \sum_x g_x \int [\psi_f^* \phi_e^* \phi_{\bar{\nu}}^*] O_x \psi_i \ d\vec{x} \ . \tag{1.4}$$

where g_x corresponds to the strength associated with the operator O_x. Fermi did not know the proper form of the O_x operator. It took almost twenty years in obtain the proper form of these operators [Hey99, RG09, Kra87]. For the moment, we will work with the electron and anti-neutrino wave functions, which can be approximated by plane waves with momentum $\vec{p}_e$ and $\vec{p}_{\bar{\nu}}$ in the volume V,

$$\phi_e = \frac{1}{\sqrt{V}} e^{i\vec{p}_e\cdot\vec{x}/\hbar} \approx \frac{1}{\sqrt{V}} \left(1 + i\frac{\vec{p}_e\cdot\vec{x}}{\hbar} - \left(\frac{\vec{p}_e\cdot\vec{x}}{\hbar}\right)^2 + \mathcal{O}\{3\}\right) \tag{1.5}$$

$$\phi_{\bar{\nu}} = \frac{1}{\sqrt{V}} e^{i\vec{p}_{\bar{\nu}}\cdot\vec{x}/\hbar} \approx \frac{1}{\sqrt{V}} \left(1 + i\frac{\vec{p}_{\bar{\nu}}\cdot\vec{x}}{\hbar} - \left(\frac{\vec{p}_{\bar{\nu}}\cdot\vec{x}}{\hbar}\right)^2 + \mathcal{O}\{3\}\right) \tag{1.6}$$

The *allowed* approximation corresponds to taking the first order in the expansion $\phi \sim 1/\sqrt{V}$. This means that the angular momentum carried by both the electron and anti-neutrino is zero [RG09]. In this approximation, the matrix element for the interaction would be written as:

$$\langle\psi_f \left| H^{\beta}_{\text{inte}} \right| \psi_i\rangle = \frac{1}{V} \ M_{fi} \ , \tag{1.7}$$

where,

$$M_{fi} = \sum_x g_x \int \psi_f^* O_x \psi_i \ d\vec{x} \ . \tag{1.8}$$

In order to produce a more realistic approximation for the electron, the

wave function at the origin must be modified taking into account the electrostatic distortion produced by the daughter nucleus with Z_D protons as [Hey99],

$$|\phi_e^*(0, Z_D)|^2 \approx \frac{1}{V} F(Z_D, p) \approx \frac{1}{V} \frac{2\pi\eta}{1 - e^{2\pi\eta}} \ , \tag{1.9}$$

where $F(Z_D, p)$ corresponds to the so-called *Fermi function* and

$$\eta = \pm \frac{Ze^2}{4\pi\varepsilon_0 h} \frac{\sqrt{m_e^2 + p^2/c^2}}{p} \ , \quad \text{for } \beta^{\mp} \text{ decay} \ , \tag{1.10}$$

where h is the Planck constant, c is the speed of light, ε_0 is the vacuum permittivity, and e and m_e the charge and the mass of the electron respectively.

The density of the states $\rho(E_f)$ corresponds to the number of states with the electron dn_e and the anti-neutrino $dn_{\bar{\nu}_E}$,

$$dn_e = \frac{4\pi V}{h^3} p_e^2 dp_e \ , \tag{1.11}$$

$$dn_{\bar{\nu}} = \frac{4\pi V}{h^3} p_{\bar{\nu}}^2 dp_{\bar{\nu}} \ , \tag{1.12}$$

and the number of states with simultaneously electron and anti-neutrino states ($dn(e^-, \bar{\nu})$):

$$dn(e, \bar{\nu}) = \frac{(4\pi)^2 V^2}{h^6} p_e^2 p_{\bar{\nu}}^2 dp_e dp_{\bar{\nu}} \ , \tag{1.13}$$

then the density of states is obtained as,

$$\rho(E_f) dp_e = \frac{dn}{dE_f}(e^-, \bar{\nu}) = \frac{(4\pi)^2 V^2}{h^6} p_e^2 p_{\bar{\nu}}^2 dp_e \frac{dp_{\bar{\nu}}}{dE_f} \ . \tag{1.14}$$

The total energy E (historically called Q) corresponds to the energy of the electron E_e, the energy of the anti-neutrino $E_{\bar{\nu}}$, and the recoil E_Y of the daughter nucleus, this is $E = E_e + E_{\bar{\nu}} + E_Y$. Neglecting the small recoil energy, so the electron anti-neutrino energy is $E_{\bar{\nu}} = E - E_e$. For the relativistic form the energy takes the

form $E^2 = p^2c^2 + m^2c^4$ and thus $dp/dE = E/(pc^2)$:

$$\rho(E_f)dp_e = \frac{(4\pi)^2 V^2}{h^6 c^3} p_e^2 (E - E_e)^2 \sqrt{1 - \frac{m_{\bar{\nu}} c^4}{(E - E_e)^2}}\, dp_e \tag{1.15}$$

Taking into account the density of states in (1.15), and the matrix element M_{fi} in (1.4), the transition rate in (1.3) could be expressed, integrating over all possible electron momentum up to $p_e^{\max}$, as,

$$\lambda = \frac{|M_{fi}|^2}{2\pi^3 \hbar^7 c^3} \cdot \int_0^{p_e^{\max}} F(Z_D, p_e) p_e^2 (E - E_e)^2 \, dp_e \ . \tag{1.16}$$

The integral corresponds to the so-called *Fermi integral* $f(E, Z_D)$, and must be evaluated numerically. Expressing the transition ratio in terms of the partial half-life $\lambda = \ln 2/t$,

$$ft = \frac{2\pi^3 \hbar^7 \ln 2}{m_e^5 c^4 \ |M_{fi}|^2} \tag{1.17}$$

The $\log ft$ value, often called *comparative half-life*, allows one to compare the β-decay probability in different nucleus [RG09]. They are tabulated in Table 1.1, together with the change in orbital angular momentum and parity associated with each one.

Transition	$\log ft$ range	L	$\Delta\pi$
Super-allowed	2.9 - 3.7	0	No
Allowed	4.4 - 6.0	0	No
First Forbidden	6 - 10	1	Yes
Second Forbidden	10 - 13	2	No
Third Forbidden	>13	3	Yes

Table 1.1: Classification of β decays according to the change in the orbital angular momentum L and parity. The change in the nuclear parity is related to $\pi_M = \pi_D(-1)^L$ [Hey99]. The range of log ft values for each class of transition is also given.

1.1.2. Beta Decay of Fermi and Gamow-Teller transitions

In a beta decay, the electron and anti-neutrino carry angular momentum L. Also the spin S of these particles must be considered, in this sense, the change in the nuclear angular momentum I_i to I_f in daughter nucleus will be coupled as:

$$\vec{I}_i = \vec{I}_f + \vec{L} + \vec{S} \ . \tag{1.18}$$

As the spin of the electron is $s_e = 1/2$, and the spin of the anti-neutrino is $s_{\bar{\nu}} = 1/2$, then the total spin carried by the electron and the anti-neutrino could take the values $S = 0$ (anti-parallel), or $S \pm 1$ (parallel). In the allowed approximation, $L = 0$ by definition, then the change in allowed approximation $\Delta I = 0, \pm 1$, giving arise to the Fermi and Gamow-Teller transitions.

The original Fermi assumption was $S = 0$, leading to a total nuclear spin change $\Delta I = 0$, and was called Fermi decay (F). On the other side, the $S = \pm 1$ case corresponds to Gamow-Teller decay (GT), and leads to a total nuclear spin change of $\Delta I = 0, \pm 1$, where the case $0 \to 0$ is not possible by the (1.18) [RG09].

1.1.3. Strength in Beta Decay

Returning to the discussion of the matrix element M_{fi} in (1.4), the Fermi strength $B(F)$ and Gamow-Teller strength $B(GT)$ can be defined as,

$$B(F) = |\langle \psi_f | \tau | \psi_i \rangle|^2 \ , \tag{1.19}$$

$$B(GT) = |\langle \psi_f | \tau\sigma | \psi_i \rangle|^2 \ , \tag{1.20}$$

this is, Fermi decay is governed by the τ operator, while the Gamow-Teller decay is governed by the $\tau\sigma$ operator [FRG11]. With this definitions, the matrix element

M_{fi} in (1.8) can be rewritten as:

$$M_{fi}^2 = g_V^2 B(F) + g_A^2 B(GT) \ . \tag{1.21}$$

then, using this definition the comparative half-life ft in (1.17) could be rewritten as,

$$ft = \frac{K}{B(F) + \lambda^2 B(GT)} \ , \ \text{with} \, K = \frac{2\pi^3 \hbar^7}{g_V^2 m_e^5 c^4} \ , \ \text{and} \ \lambda = \frac{g_A^2}{g_V^2} \ , \tag{1.22}$$

where these constants are known to be $K = 6289.6(27)$ from [HT15], and $\lambda = -1.27139(19)$ from [AAB+02].

It can be calculated[1] that in general the Fermi strength corresponds to the difference of the neutron number (N) and the atomic number (Z), this is $B(F) = |N-Z|$, allowing one to obtain the g_V^2 constant from the measured ft-values in nuclei with $N = Z$, and $N - Z = -2$, isospin $T = 1$ (explained in next section) [TH15]. This allows us to determine the strength in cases of pure $B(F)$ or pure $B(GT)$

$$B(F)^{l \to m} = \frac{K}{f^{l \to m} \cdot t_m} \tag{1.23}$$

$$B(GT)^{l \to m} = \frac{K}{\lambda^2 \cdot f^{l \to m} \cdot t_m} \tag{1.24}$$

The previous equations can be expressed in terms of the half-life of the nuclide $T_{1/2}$ and intensity of the transition I_m from the state l in the mother nucleus to the state m in the daughter nucleus, replacing the partial half-life as $t_m = T_{1/2}/I_m$,

$$B(F)^{l \to m} = \frac{K \cdot I_m}{f^{l \to m} \cdot T_{1/2}} \tag{1.25}$$

$$B(GT)^{l \to m} = \frac{K \cdot I_m}{\lambda^2 \cdot f^{l \to m} \cdot T_{1/2}} \tag{1.26}$$

[1] Using the Isospin algebra, for example see [RG09].

1.2. Isospin in Beta Decay

Proton and neutrons are often treated as if they are two states of the same particle: the nucleon. To take into account this symmetry, the atomic wave functions described by a spatial part $\psi(\mathbf{r})$ and a spin part χ_{spin}, must also include an isospin component ξ_{isospin}:

$$\Psi = \psi(\mathbf{r})\, \chi_{\text{spin}}\, \xi_{\text{isospin}} \ .$$

In order to reach a formalism to describe nuclear behavior, the isospin is introduced in analogy with the angular momentum formalism. In this formalism the proton is defined as the $+1/2$ state and the neutron is the $-1/2$ state for the third component of the isospin t_z. Then the third component of the nuclear isospin can be expressed (in units of $\hbar$):

$$T_z = \frac{(N-Z)}{2} \ ,$$

Isobars with opposite values of the third component of isospin correspond to the so-called *mirror nuclei*. The $T_z = 0$ nuclei corresponds to those nuclei with the same number of neutrons and protons. These nuclei can be visualized with a yellow line in Fig. 1.3, where the light/medium mass region with $20 \leq Z \leq 36$ and $21 \leq N \leq 44$ is shown.

From the point of view of the isospin, mirror nuclei processes such as β^+ decay and a (p,n)-like *charge exchange* reaction are mirror processes, populating analogue states in the daughter nuclei and with the same strength. Charge exchange reactions will be described in next section.

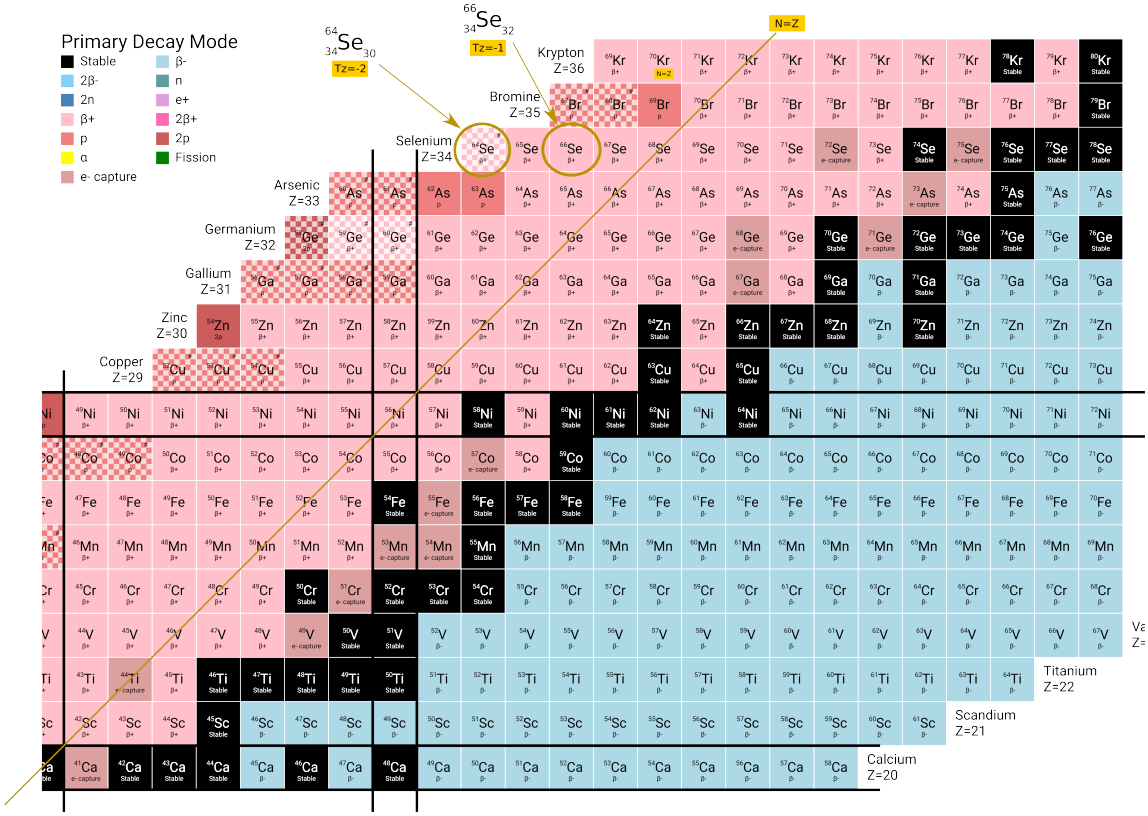

Figure 1.3: Nuclear chart around ^{64}Se and ^{66}Se from [Sim19]. A yellow line is drawn through nuclei with $T_z = 0$ (N=Z). Chequered pattern represents nuclei known only from theoretical extrapolations.

1.3. Charge Exchange Reactions

In the CE reactions such as (p, n) or $(^3\text{He}, t)$, it is known that at intermediate beam energies ($E > 100$MeV/nucleon) the cross section measured at small angles, including 0°, is proportional to the Gamow-Teller strength B(GT) [FRG11],

$$\frac{d\sigma_{\text{GT}}}{d\Omega}(0°) \propto K(\omega) N_{\sigma\tau} \left| J_{\sigma\tau}(q) \right|^2 B(GT) \tag{1.27}$$

$$= \hat{\sigma}_{\text{GT}}(q, \omega) B(GT) \tag{1.28}$$

where the $J_{\sigma\tau}(q)$ is the volume integral of the effective interaction $V_{\sigma\tau}$ at momentum transfer q, $K(\omega)$ is the kinematic factor and $\omega = E_x - Q_{\text{g.s}-\text{g.s.}}$, $N_{\sigma\tau}$ is a distortion

factor, and $\hat{\sigma}_{\mathrm{GT}}(q,\omega)$ is a unit (differential) cross-section for the GT transition.

The resolution for this kind of reaction depends on the masses of the projectile/ejectile involved. For instance, in Fig. 1.4 (p,n)-like reactions such as (p,n) and $(^3\mathrm{He},t)$ have very different resolution. Before the $(^3\mathrm{He},t)$ reaction was available, comparing the β decay with (p,n) reactions was not attractive since it was not possible to study the strength to a single state.

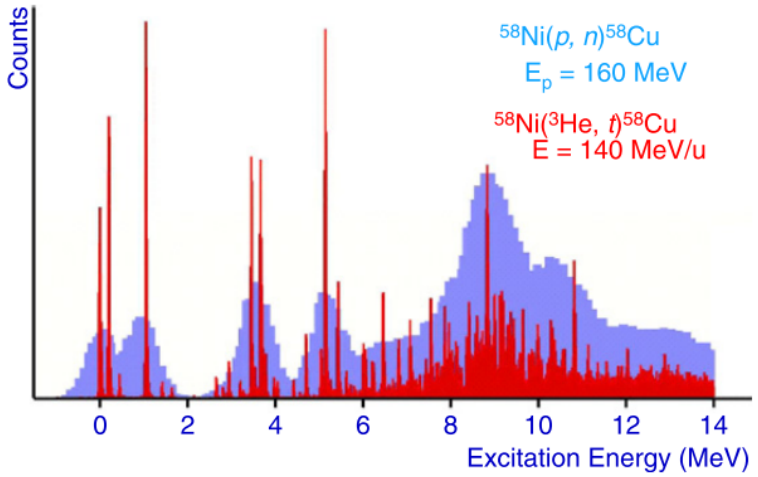

Figure 1.4: Charge exchange comparison between the $^{58}\mathrm{Ni}(p,n)^{58}\mathrm{Cu}$, and the $^{58}\mathrm{Ni}(^3\mathrm{He},t)^{58}\mathrm{Cu}$ reactions, from Fujita et al. [FRG11]. The improvement in resolution using the $(^3\mathrm{He},t)$ reaction is one of the key aspects that allows this kind of mirror comparison.

1.4. Isospin Symmetry: Comparison Mirror Nuclei

The systematic study of the mirror symmetry by comparing the β decay with the corresponding CE reaction started in 2006 [Mol11, MRF+15] with the study of the mirror nuclei with $T_z = \pm 1$, for ^{42}Ti, ^{46}Cr, ^{50}Fe, and ^{54}Ni, comparing it with the corresponding CE reaction in the ^{42}Ca, ^{46}Ti, ^{50}Cr, and ^{54}Fe (see Fig. 1.3).

As stated earlier, nuclei with opposite T_z values are mirror. Indeed the

CE reactions such as (p,n), or $(^3\mathrm{He},t)$ go from ${}^{A}_{Z-1}Z_{N+1} \xrightarrow{\mathrm{CE}} {}^{A}_{Z}Y_{N}$, and the inverse transition for the β^+ decay is ${}^{A}_{Z+1}X_{N-1} \xrightarrow{\beta^+} {}^{A}_{Z}Y_{N}$. In a clearer way, as example for the case of $|T_z| \leq 1$ ss ,

$$ {}^{A}_{Z+1}X_{N-1} \xrightarrow{\beta^+} {}^{A}_{Z}Y_{N} \xleftarrow[(p,n)-\mathrm{type}]{\mathrm{CE}} {}^{A}_{Z-1}\bar{X}_{N+1} \ . \tag{1.29} $$

If isospin is a good quantum number, the CE reaction populates the same states in the daughter nuclei the β^+ decay, and with the same strength. This kind of comparison gained more relevance when the $(^3\mathrm{He},t)$ CE improved the standard (p,n)-type CE, as can be seen in Fig. 1.4 taken from Fujita et al. [FRG11].

In Fig. 1.5 [MRF+15] a diagram for the isobaric multiplets for $A = 50$ and $A = 54$ is shown [FRG11]. In this diagram the Coulomb interaction was subtracted. As the β decay is governed by the τ and $\sigma\tau$ operators, the total change in nuclear spin could be $\Delta I = 0, 1$. Considering that the $T_z = -1$ g.s. is a 0^+ state, beta decay could populate directly only states with $I = 0^+, 1^+$. Also a similar rule appears in the isospin side, since in beta decay the mother state is a $T = 1$, the beta decay may populate states with $\Delta T = 0, 1$. Indeed beta decay can populate states with excitation energy below the Q_β value window.

The $T_z = \pm 2$ case is very similar to the $T_z = \pm 1$ case, but the daughter nuclide is not the same in the CE reaction and in the β decay. In Fig. 1.6, a diagram of the comparison for the $A = 52$ isobaric multiplet is shown, taken from Fujita et. al. [FRG11]. The ^{52}Ni g.s. is a 0^+, and the beta decay can populate only $I^\pi = 0^+, 1^+$ states only.

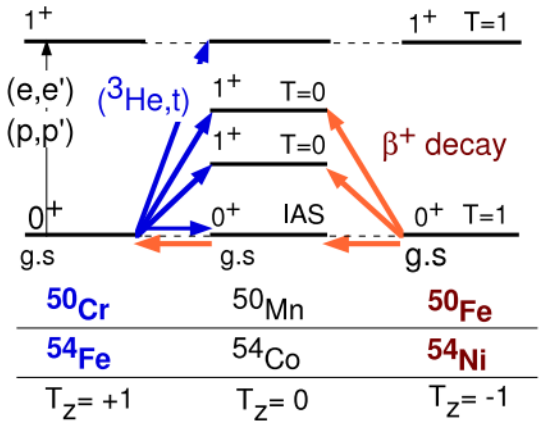

Figure 1.5: Isobaric $A = 50$ and $A = 54$ multiplet diagrams taken from Fujita et al. [FRG11]. These systems were analyzed using both CE reactions and β^+ decay. Due to the Q_β value window, states below this value could be populated in β decay, while in the CE reaction there is no such energy restriction.

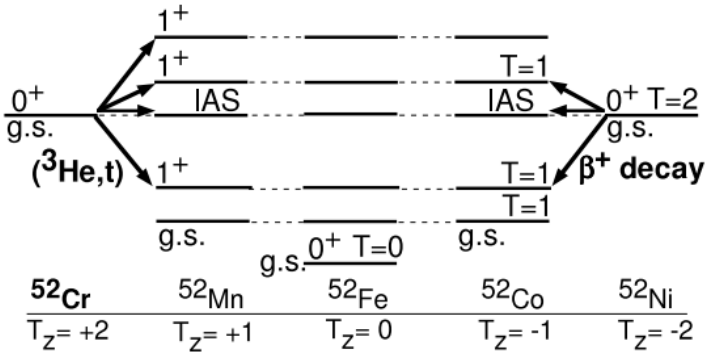

Figure 1.6: Isobaric $A = 52$ multiplet diagram taken from Fujita et al. [FRG11]. Here, where the $T_z = \pm 2$ members of the multiplet are studied one is comparing the corresponding transitions to states in the $T_z = \pm 1$ nuclei.

Part II

The NP1112-RIBF82 Experiment at RIBF (RIKEN)

Chapter 2

The RIBF facility at RIKEN

The $T_z = -2$ and $T_z = -1$ Se isotopes of interest were produced at the RIKEN Nishina Center (see Fig. 2.1) using the fragmentation of a 345 MeV/nucleon ^{78}Kr beam with unprecedented intensity (up to 300 particle nA) on a $^{m}athrmnat$Be target. The fragments were separated in flight using the BigRIPS separator [F^{+}13, K^{+}12] and implanted in three 1 mm thick WAS3ABi double-sided Si strip detectors (DSSSD) [NLXW13] each of them having an active area of 60×40 mm^2 segmented into 60 vertical by 40 horizontal strips. The implantation setup was surrounded by the EUROBALL-RIKEN Cluster Array (EURICA) [SND^{+}13], 12 CLUSTER-detectors of Euroball type, each one consisting of seven tapered hexagonal HPGe crystals at a nominal distance of 22 cm from the center of WAS3ABi. In this chapter all pieces of equipment used during the experiment will be described as well as their calibration.

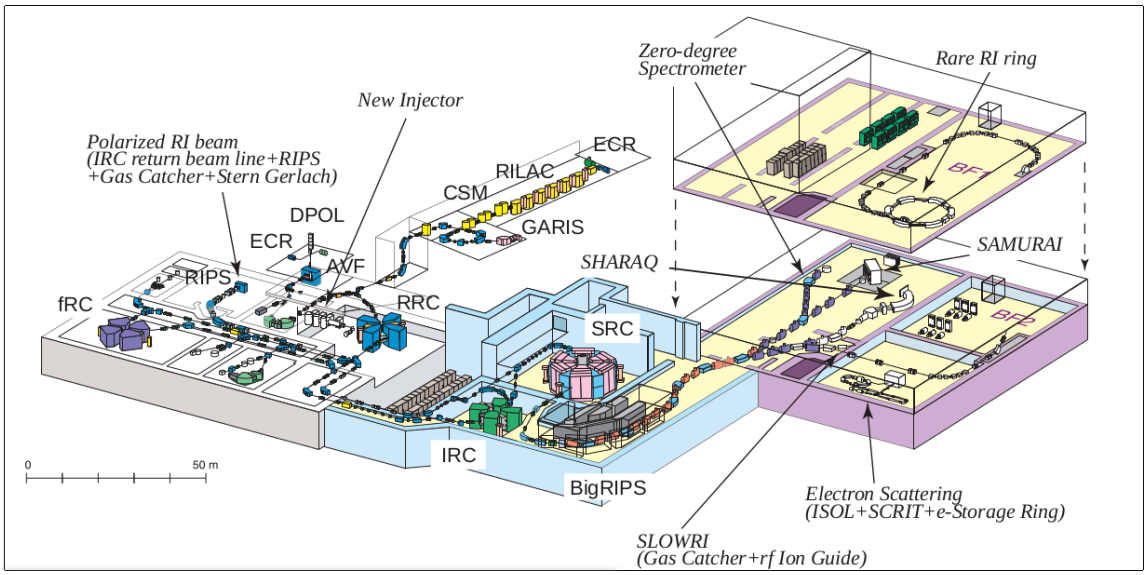

Figure 2.1: Scheme of RIBF. The facility is divided in three parts: acceleration section (grey), identification stage (light blue), and the experimental zones (purple).

2.1. Production of Isotopes

The study of exotic nuclei demands very intense beams, and the more exotic the nuclide, the more intensity is required. There are not many facilities in the world that can reach enough intensity to perform this study, with the **R**adioactive **I**on **B**eam **F**acility (**RIBF**) in RIKEN Nishina Center (see Figure 2.1) the facility that can produce the most intense beams in the world at present. In this facility, the specific isotope is produced via nuclear reactions with a ^{nat}Be target, together with many others that must be separated from the isotope of interest.

In the present work the production of isotopes was carried out by fragmentation of ^{78}Kr on a ^{nat}Be target. The primary beam of ^{78}Kr was produced for the first time in this experimental campaign with enough intensity to allow beta decay experiments to be carried out using the chain of accelerators and cyclotrons available at RIBF.

In Figure 2.1 a diagram of RIBF is shown, first stage (primary beam acceleration) painted in gray and white. Starting with an ion source (ECR) and linear accelerator RILAC2 [Kam17] (see Fig. 2.3a) as shown in Fig. 2.2, the beam is injected successively in four main cyclotrons the RRC (see 2.3b), followed by fRC (see 2.3c), then IRC (see 2.3d), and then SRC (see 2.3e) before being conducted to the target. The last cyclotron in the acceleration stage is the **S**uperconducting **R**ing **C**yclotron (SRC).

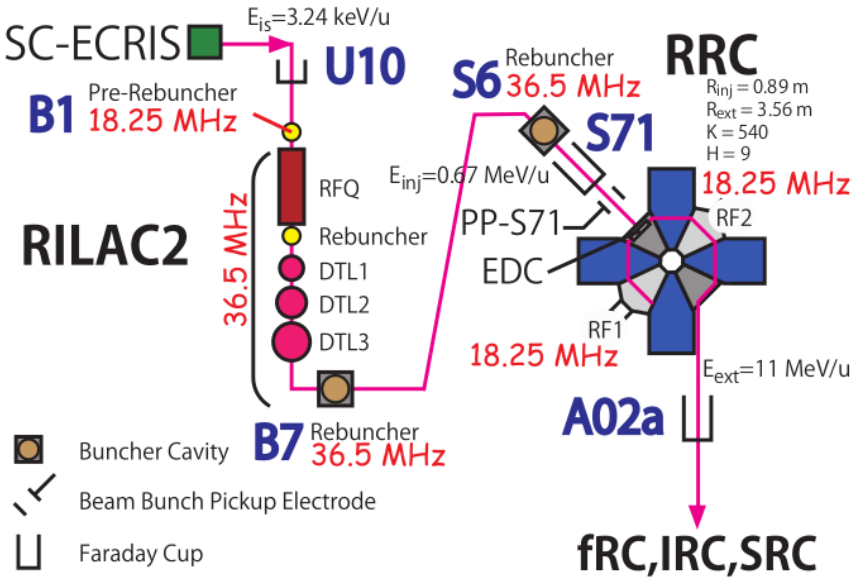

Figure 2.2: Scheme of the injector stage at RIBF, obtained from [SFF+14].

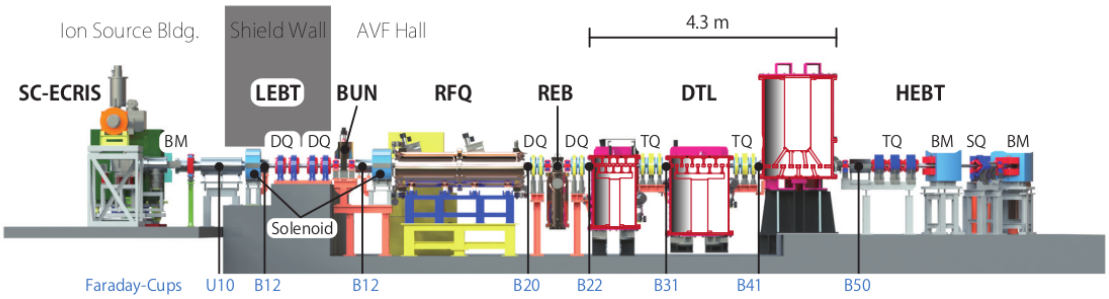

(a) RILAC2 diagram, obtained from [Kam17].

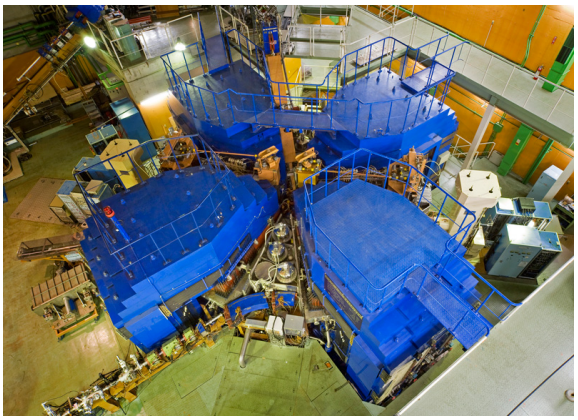

(b) RRC cyclotron.

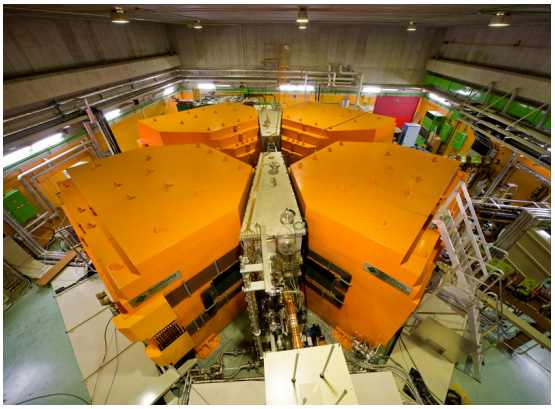

(c) fRC cyclotron.

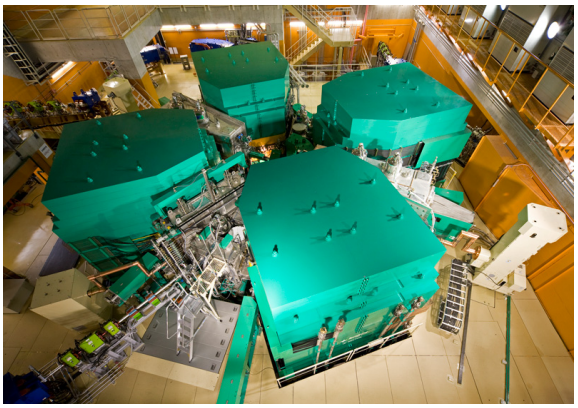

(d) IRC cyclotron.

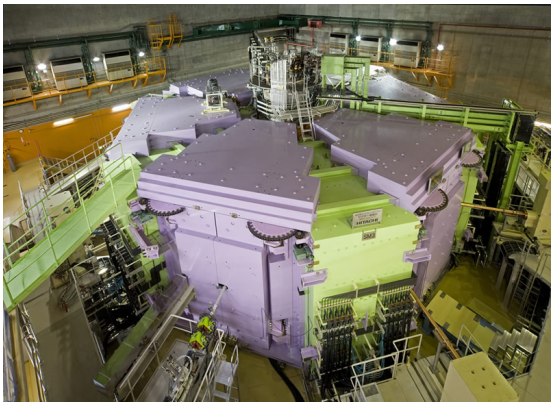

(e) SRC cyclotron.

Figure 2.3: Linear accelerator and cyclotrons used in RIBF (RIKEN) to produce the primary the beam of ^{78}Kr for this work.

2.2. The BigRIPS separator

The ^{78}Kr beam was accelerated and impinged on a ^{nat}Be target of 7 mm thickness. In this fragmentation reaction, many nuclear species were produced and the nuclei of interest must be identified and separated before being studied. The beam is injected into BigRIPS, an on-line fragment separator placed after the SRC cyclotron (see Figure 2.4). Using dipoles (to select the magnetic ridigity of the ions) and quadrupoles (to spatially focalize different ion species) the nuclei of interest were conducted to the last focal plane where an active stopper (WAS3ABi) was placed.

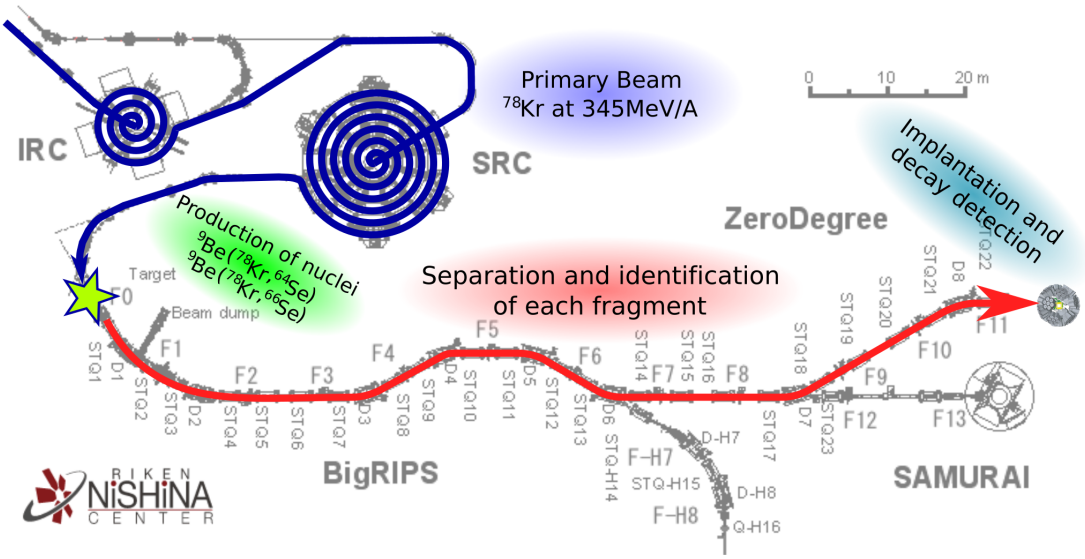

Figure 2.4: Scheme of BigRIPS at RIBF. In blue the last two cyclotrons deliver the primary beam to the target placed at F0. After nuclear reactions, the fragments are separated and identified by the BigRIPS fragment separator (red) before being implanted in the active stopper placed at the last focal plane.

Fragments were identified using the mass-over-charge ratio (A/Q) and proton number (Z), obtained using measurements of Time of fight (TOF), magnetic rigidity ($B\rho$), and energy loss (ΔE) measurements (TOF $-$ $B\rho$ $-$ ΔE method [F$^+$13, K$^+$12]). To use the TOF $-$ $B\rho$ $-$ ΔE method, a knowledge of the trajectory

and velocity is necessary for each fragment. This can be done using plastic scintillator and Parallel Plate Avalanche Counters (PPACs) [KOF+13] to reconstruct the trajectory parameters, and MUlti-Sampling Ionization Chamber [C+15] (MUSICs) to measure the energy loss (see Section 2.3).

PPACs are gas-filled [KOF+13] detectors consisting of cathode-anode-cathode stripped layers connected to a multi-tapped delay (see Fig. 2.5a). When a charged particle passes through the PPAC detector, the signal is collected by both sides of the delay line, and the position is then determined by measuring the time difference between signals appearing at the two ends. This allows us to determine the X-Y position, where the charged particle passes through the PPAC. In BigRIPS, double PPACs are used allowing us to determine the incident angle.

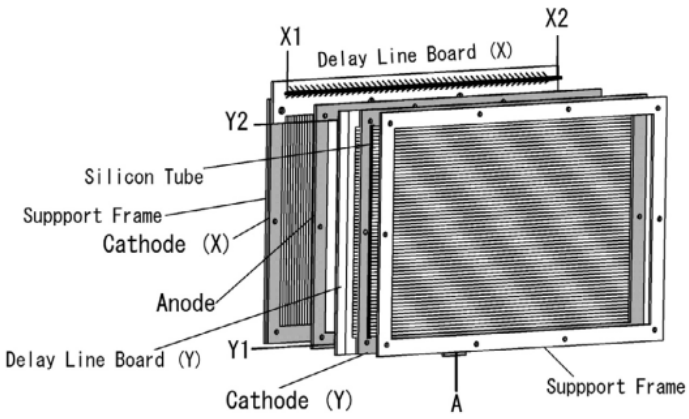

(a) PPAC diagram, divided in two layers measuring the X and Y position.

(b) Picture of a PPAC.

Figure 2.5: PPAC figures from [KOF+13]

MUSIC is another type of gas filled detector used to determine the charge of the particle passing through. It consists of several cathode-anode layers (see Fig. 2.6b) collecting the charge deposited in the gas by the charged particle. The ionization produced in the gas is proportional to the charge of the particle, allowing

one to use the charge from the signals collected by the electrodes to measure the charge of the particle.

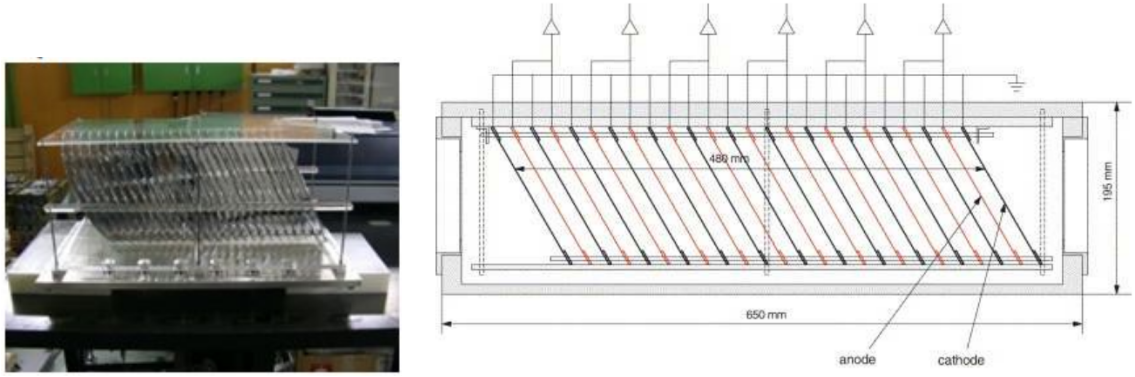

(a) **(b)**

Figure 2.6: MUSIC chamber [C+15] used to measure the charge of ions.

Plastic detectors used in this work have an active area of 120 mm(or 100 mm) x 100 mm (240 mm x 100 mm at F5), and available thickness of 0.1 mm, 0.2 mm, 1 mm, and 3 mm [Tea19].

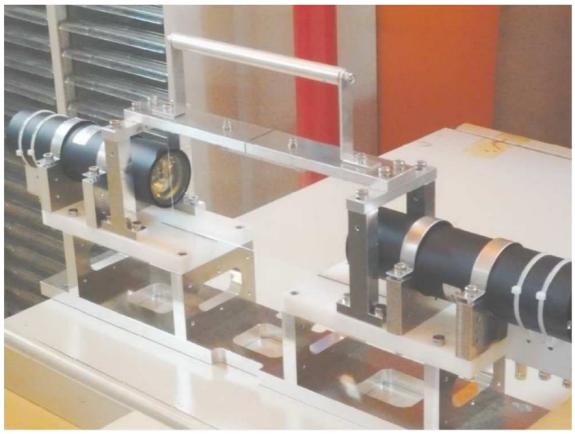

Figure 2.7: Plastic scintillator picture from [Tea19]. Each plastic detector used in BigRIPS has two photomultipliers attached on the edges.

2.3. Separation and identification in BigRIPS

In a fragmentation facility such RIBF at RIKEN it is possible to individually identify each ion passing through the separator after the fragmentation reaction, including the implantation at the active stopper. In this section the procedure to select and identify nuclei of interest from the other nuclear species produced using electric and magnetic fields will be explained. Those fields are generated in RIBF by dipole magnets (D1 up to D8 in Fig. 2.8) and superconducting triplet quadrupole magnets (STQ1 to STQ22 in Fig. 2.8). Also velocity and positional selectors such as slits, wedges (at F5), and degraders (at F11), are used to guide the nuclei of interest to the experimental zone (in this work, the active stopper) with minimum contribution from other nuclear species. In Fig. 2.8 a diagram of the separation and identification process is shown.

The strategy to separate fragments consists in the use of magnetic fields to achieve curved trajectories according to the mass-over-charge ratio (A/Q) of each individual fragment immersed on it. In the following lines this will be explained in detail.

If the reaction fragments are fully electron stripped[1] and the ratio between the mass $m = Au$, expressed in terms of the atomic mass unit u and the charge Q of each fragment determines the trajectory in the magnetic field $\vec{B}$ inside the dipoles. A particle moving at velocity $\vec{v}$ in a magnetic field $\vec{B}$ results in the magnetic Lorentz force $Q(\vec{v} \times \vec{B})$ resulting in a circular movement of radius ρ. The magnetic Lorentz force is then balanced by the centripetal force taking into account the relativistic momentum $p = \beta\gamma Auc$ [K$^+$12, F$^+$13, Mol11, Goi17], where $\beta = v/c$,

[1] Meaning that the total charge Q of the nucleus correspond to the atomic number Z times the charge of the electron e ($Q = eZ$).

and $\gamma = \sqrt{1/(1-\beta^2)}$ corresponds to the relativistic terms for the velocity and the Lorentz factor, respectively. Thus

$$B\rho = \beta\gamma uc\frac{\mathrm{A}}{\mathrm{Q}} \ , \tag{2.1}$$

relating the mass over charge ratio to the trajectory of the nucleus. The term $B\rho$ is known as *magnetic rigidity*, representing the reference value for the central trajectory inside the dipoles[2]. The angular spread produced during fragmentation reactions implies that not all nuclei follow the central trajectory, resulting in some deviations. A precise $B\rho$ measurement requires the trajectory reconstruction combined with the ion-optical transfer matrix from experimental data [K+12, F+13]. Eq. (2.1) for the magnetic rigidity shows that nuclei with different A/Q values follows different trajectories in the separator that can be filtered using slits[3]. However nuclear species with the same A/Q value cannot be separated unless the beam is conducted through a degrader[4]. The energy loss (per unit of length) of a charged particle when passing through a material is proportional to the atomic number $\check{Z}$, mass $\check{A}$, density ρ, and mean excitation energy I of the material, and is known as the Bethe-Bloch equation:

$$-\frac{dE}{dx} = \frac{4\pi}{m_e c^2}\frac{\check{Z}N_a\check{\rho}Z^2}{\check{A}\beta^2}\left(\frac{e^2}{4\pi\epsilon_0}\right)^2\left[\ln\left(\frac{2m_e c^2\beta}{I(1-\beta^2)}\right)-\beta^2\right] \ , \tag{2.2}$$

where m_e is the electron mass, c is the speed of light, and N_a is the Avogadro constant. This shows that nuclei with different Z values lose different amounts of energy in a degrader, allowing one to separate nuclei with similar A/Q values.

As said before, nuclear species are characterized by the atomic number Z and the mass over charge ratio A/Q. These values can be measured using the TOF-$B\rho$-ΔE method [F+13], where the Z and A/Q are deduced from the TOF, $B\rho$, and

[2] During the experiment their values were between 3 Tm and 6 Tm.
[3] Piece of material used to stop some excentric ion trajectories, placed after dipole magnets.
[4] Piece of material used to produce the energy lose of the ion while passing through it.

ΔE measurements. The atomic number Z can be obtained using the energy loss measured by MUSIC either in F7 and F11 (see Fig. 2.8). The ratio A/Q can be obtained measuring the magnetic rigidity $B\rho$ at every dipole magnet and the velocity of the fragment β. This velocity can be obtained by using TOF measurements with plastic scintillators between two focal planes and then relating its to the length of trajectory L,

$$\beta c = \frac{L}{\mathrm{TOF}} \ . \tag{2.3}$$

With these elements the fragment can be characterized by their measured Z and A/Q values.

In BigRIPS a degrader is placed in F5. As the velocity of the fragment changes, the TOF measured between F3 and F7 is related to the flight path length between F3-F5 L_{35} and F5-F7 L_{57}. This could be seen in Fig. 2.8. Then, together with the respective fragment velocities β_{35} and β_{57},

$$\mathrm{TOF}_{37} = \frac{L_{35}}{\beta_{35}c} + \frac{L_{57}}{\beta_{57}c} \ . \tag{2.4}$$

Taking into account this velocity difference, the equation (2.1) can be written for these two segments F3-F5 and F5-F7, as

$$\left(\frac{\mathrm{A}}{\mathrm{Q}}\right)_{35} = \frac{B\rho_{35}}{\beta_{35}\gamma_{35}uc} \ , \tag{2.5}$$

$$\left(\frac{\mathrm{A}}{\mathrm{Q}}\right)_{57} = \frac{B\rho_{57}}{\beta_{57}\gamma_{57}uc} \ , \tag{2.6}$$

If no change in the A/Q value is produced in the degrader[5], the previous relations lead to

$$\frac{\beta_{35}\gamma_{35}}{\beta_{57}\gamma_{57}} = \frac{B\rho_{35}}{B\rho_{57}} \ . \tag{2.7}$$

[5]Nuclear reactions may occur inside the degrader, leading to a change in the A/Q ratio.

This relation together with (2.4) allows one to determine the fragment velocities β_{35} and β_{57} using the measured values for the TOF_{37}, $B\rho_{35}$, and $B\rho_{57}$, leading to an unambiguous A/Q measurement.

The above identification procedure was performed using ANAROOT [gro13, Iso13], a software toolkit based in ROOT for the online/offline analysis of RIBF experiments. This allows one to process easily the BigRIPS identification information and condense into a ROOT file with data from detectors together with the identification.

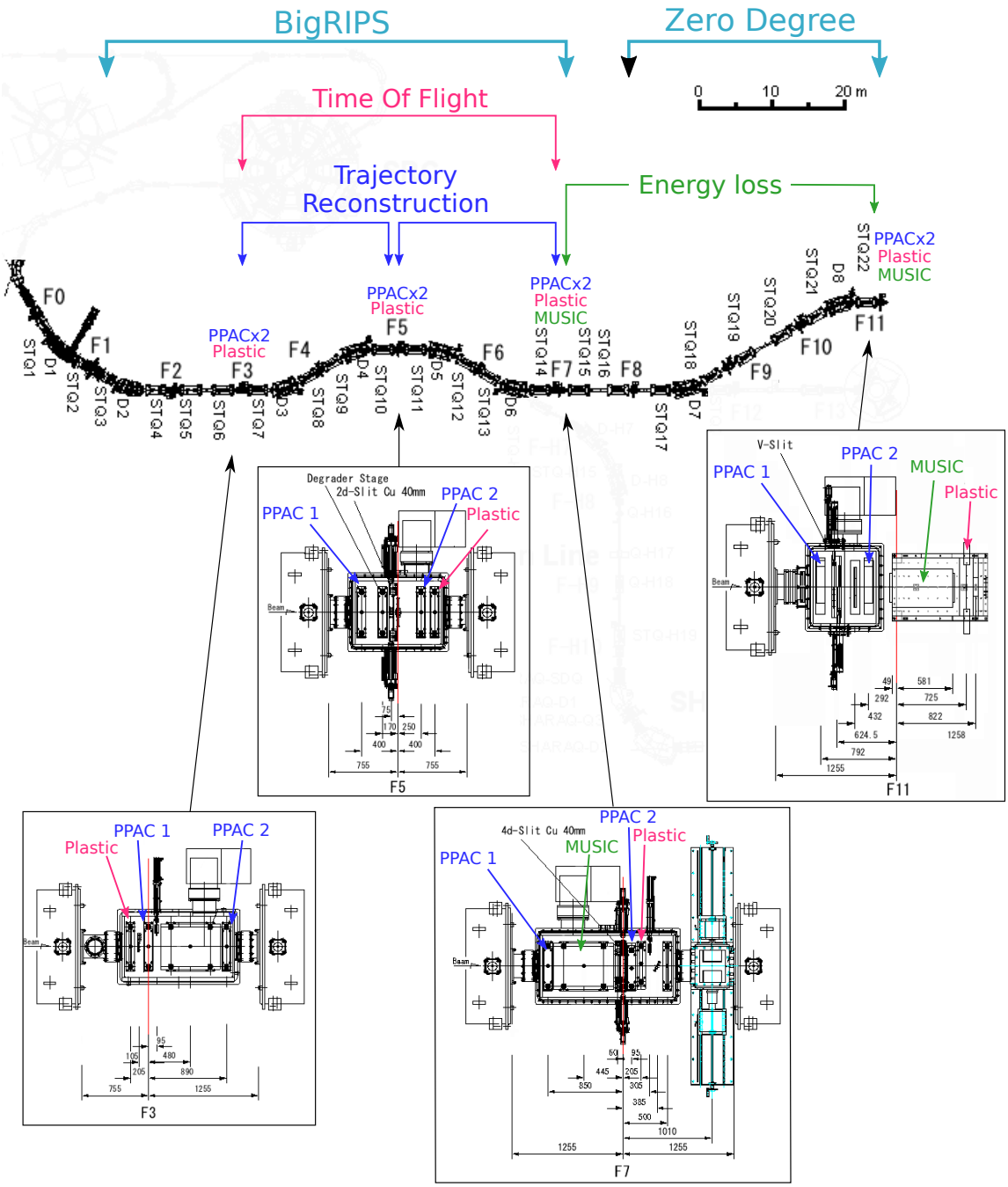

Figure 2.8: BigRIPS standard diagram (obtained from [Tea19]) of the electronics involved in the identification process. Detectors are identified with colours (PPAC in blue, Plastic scintillator in red, and the MUSIC in green). Also a zoom is shown for the F3, F5, F7, and F11 focal planes which are directly related to the identification procedure.

2.3.1. Particle Identification for each BigRIPS configuration

In the NP1112-RIBF82 experiment the BigRIPS fragment separator was configured in order to adjust the depth of the implantation position for each nucleus of interest. The whole experimental campaign comprised four experiments, three of them related to this work. During each experiment, the nuclei produced and their implantation position was controlled by changing the BigRIPS configuration and the final adjustment was made by the insertion of a metal foil of varying thickness before implantation in WAS3ABi. The settings used are summarised in Table D.1.

In Table D.2 the number of ions is shown after applying a cleaning condition for each setting, and particle identification plots (PIDs) for each setting (see Tab. D.1) are shown in Fig. 2.9.

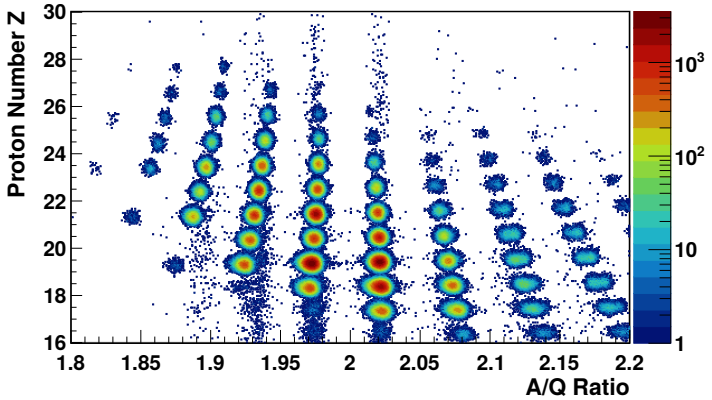

(a) BigRIPS calibration setting optimized to separate ^{58}Ni.

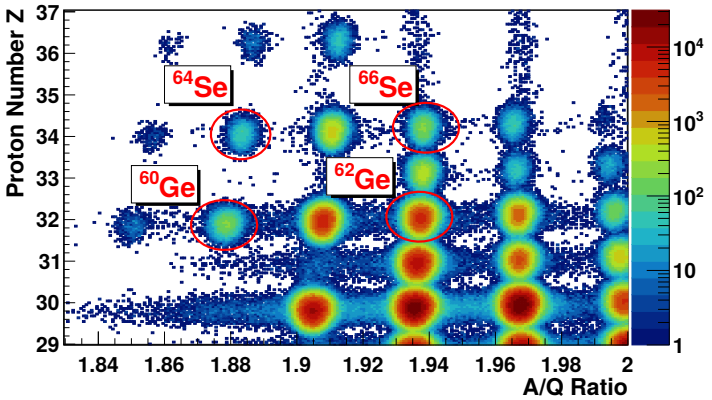

(b) Second BigRIPS configuration setting, optimized to separate ^{65}Br.

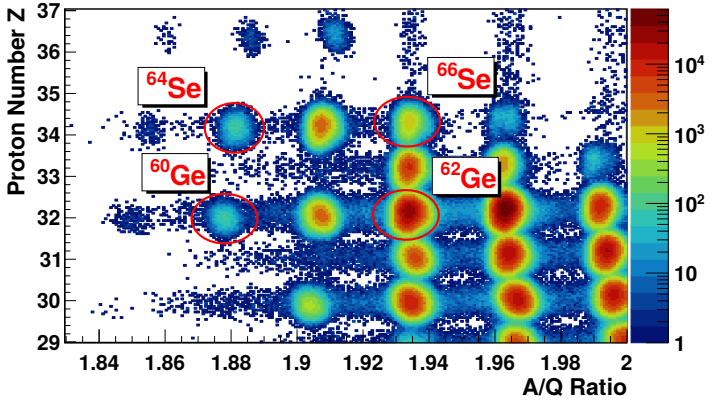

(c) Third BigRIPS configuration setting, optimized to separate either ^{60}Ge and ^{64}Se.

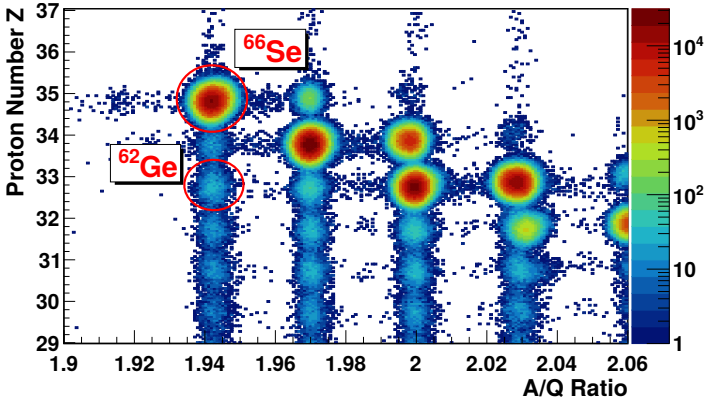

(d) Fourth BigRIPS configuration setting, optimized to separate ^{66}Se.

Figure 2.9: Particle identification plot (PID) for each configuration setting of BigRIPS used during the experimental campaign NP1112-RIBF82.

Chapter 3

The Zero Degree experimental line at RIBF

3.1. Wide-range Active Silicon-Strip Stopper Array for Beta and Ion detection (WAS3ABi)

After separation in BigRIPS, nuclei may reach up to an energy of 345 MeV/u, and are stopped in an active stopper named WAS3ABi (see Fig. 3.1). WAS3ABi [Nis12] consists of three layers of **D**ouble **S**ided **S**ilicon **S**trip **D**etector (DSSSD) (model Canberra PF-60CT-40CD-40x60), with dimensions of 60 mm x 40 mm x 1.2 mm (see Fig. 3.1). When a charged particle travels through a DSSSD, it creates electron-hole pairs as it ionises the semiconductor. The number of electron-hole pairs is proportional to the amount of energy deposited in the material. Each side of the DSSSD has an area of 60 mm x 40 mm with 60 vertical strips (X-side) and 40 horizontal strips (Y-side) acting as electrodes when a bias voltage is applied to the Y-side, with the X-side grounded. This allows one to determine the position where the charge was produced inside the DSSSD. Since each strip has 1 mm width, the intersection of X-strip and Y-strips together define pixels of 1 mm x 1 mm x 1.2 mm

volume.

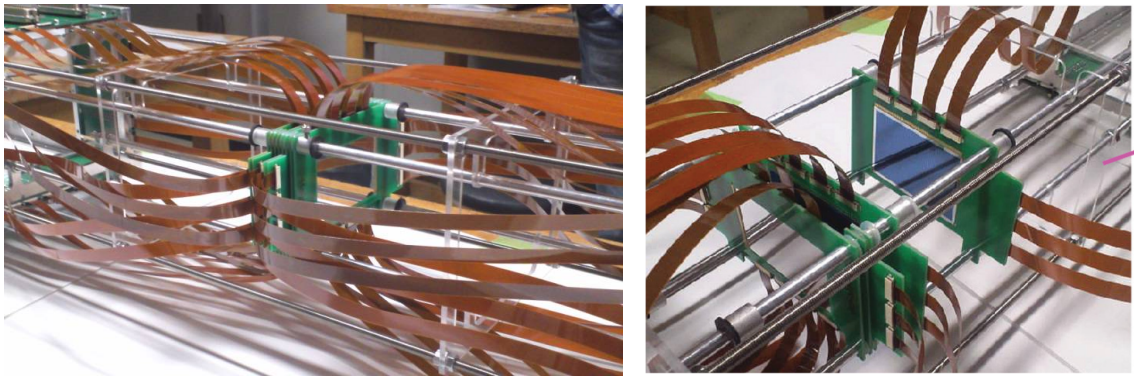

(a) **(b)**

Figure 3.1: Picture of WAS3ABi DSSSDs without the aluminum cover. Each side of the DSSSD, the X and Y sides, is compared of strips. The end of each strip is connected to a HUB that it was connected to the pre-amplifier.

An implantation in the last DSSSD is difficult to determine. For this purpose, two plastic (Q-beta plastic and Veto plastic) scintillators were placed after the last DSSSD. Signals in these plastics were used to differentiate between those nuclei passing through the DSSSDs and not stopped inside. In Fig. 3.2 the plastic scintillators are shown together with a diagram of their position relative to WAS3ABi.

The DSSSDs shown in Fig. 3.1b, were placed inside an aluminium box of 1 mm thickness, as shown in Fig. 3.3, and kept at an uniform temperature of 10 °C using gaseous N_2. The Y-side of each DSSSD was polarized to 250 V (MHV-4 Mesytec, see Fig. 3.4a) while the X-side was grounded. Starting from F11 to the active stopper, DSSSDs were spaced at 0.5 mm and placed in alternate Ground-Bias (DSSSD 1), Bias-Ground (DSSSD 2), Ground-Bias (DSSSD 3) configurations.

To collect the signal produced in WAS3ABi when charged particles pass through a DSSSD, electronic instruments were configured as shown in Fig. 3.4b. The charge in the DSSSD was collected by a charge sensitive preamplifier model

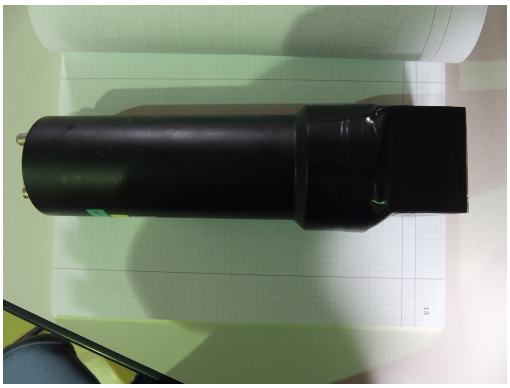

(a) Q-beta plastic scintillator detector with its photomultiplier.

(b) Final plastic scintillator used as Veto of particles.

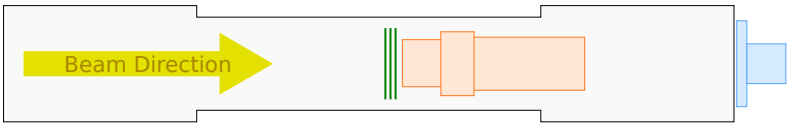

(c) Positions relative to WAS3ABi (gray) of the DSSSDs (green), the Q-beta plastic (orange), and the Veto plastic (blue).

Figure 3.2: Q-beta plastic and Veto plastic detectors used in the experiment to identify nuclei not fully stopped in WAS3ABi DSSSDs. A diagram for relative position is shown, Q-beta plastic was placed after DSSSDs, while Veto plastic was placed outside WAS3ABi.

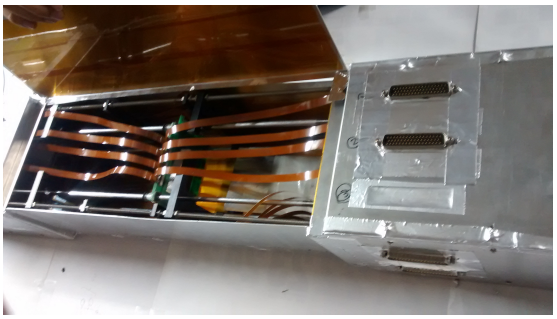

(a)

(b)

Figure 3.3: WAS3ABi DSSSDs inside the aluminium cover, thath helps to maintain the cooling of the DSSSDs at 10 °C with gaseous N_2.

KPA-10 10ch C.S. preamp. (see Fig. 3.4c) and shaped by CAEN amplifiers model N568B (see Fig. 3.4e). The X and Y-sides of the DSSSDs have different ranges in order to mantain sensitivity to low energy and at the same time measure high energy protons. The X-side was left with short range and low thresholds while Y-side was left with high range and high thresholds. In Table 3.1 the DSSSD ranges are tabulated together with the hardware and software threshold applied to remove events triggered by electronic noise.

DSSSD	Side	Range	Thresh. (Hard.)	Thresh. (Soft.)
0	X	6 MeV	45 keV	55 keV
	Y	10 MeV	115 keV	133 keV
1	X	4 MeV	55 keV	55 keV
	Y	10 MeV	130 keV	133 keV
2	X	4 MeV	45 keV	55 keV
	Y	10 MeV	133 keV	133 keV

Table 3.1: WAS3ABi amplification parameters.

After the signal is amplified, it is fed into two different branches, an energy branch and a time branch. The energy branch consist of two types of 12-bit ADCs a model CAEN V785 and an MADC-32 (see Fig. 3.4d) with 4086 channels. The time branch consists of a chain of leading-edge discriminators, namely LeCroy 3412 model (see Fig. 3.4f) and a TDC CAEN V775 model (see Fig. 3.4d). A second output was extracted from the discriminators and used to send the trigger signal together with the F11 plastic signal. Only the X-side was used as a trigger since it has a low threshold.

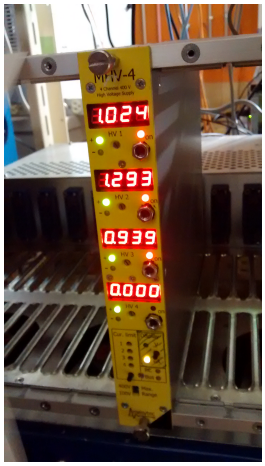

(a) High voltage unit model MHV-4 Mesytec, used in WAS3ABi.

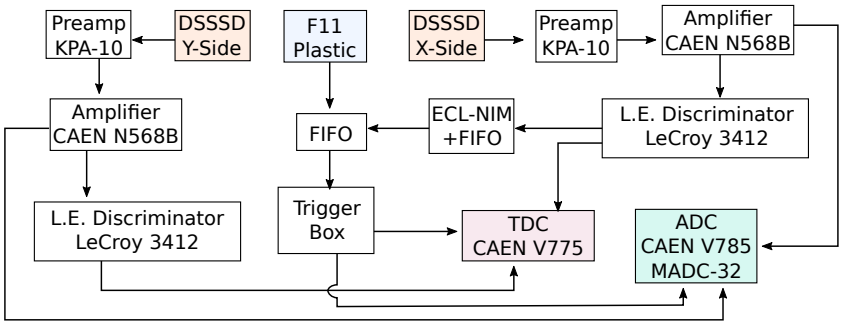

(b) Scheme for WAS3ABi electronics signals.

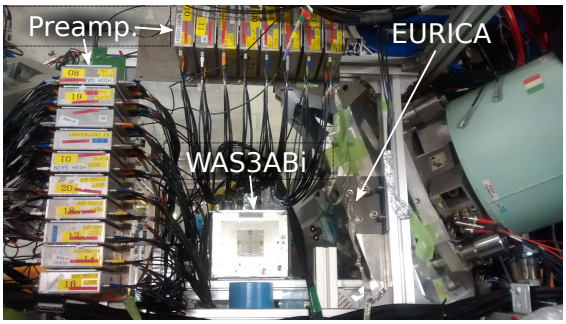

(c) Preamps. model KPA-10 10ch C.S., mounted next to WAS3ABi.

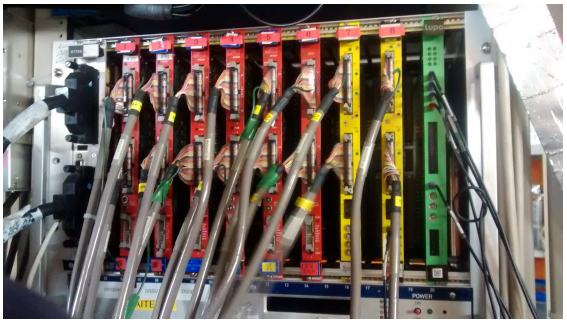

(d) TDCs model CAEN mod. V775, and ADCs model CAEN V785 and MADC-32, used in WAS3ABi.

(e) Shaping CAEN amplifiers model N568B used in WAS3ABi.

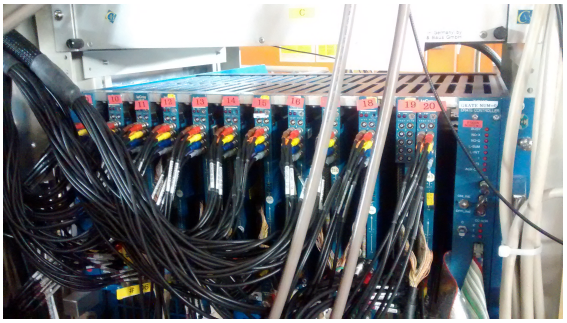

(f) Leading-edge discriminators model LeCroy 3412 used in WAS3ABi.

Figure 3.4: Overview of the electronics of WAS3ABi described in the text.

3.1.1. WAS3ABi detector energy calibration

In section 3.1 it was explained that the purpose of WAS3ABi is to measure the position of each implantation together with that of the decay particles either betas or protons emitted at a later time. This means that it is necessary to obtain an energy calibration for every strip of WAS3ABi. Two methods are available to obtain the energy references to perform the calibration. One of them is a ^{207}Bi source, and the other requires the use of proton-emitting nucleus produced during the experiment, namely ^{57}Zn, and ^{61}Ge.

The ^{207}Bi source emits conversion electrons with energies below 1 MeV. In order to obtain good statistics for all strips, the source was placed at five positions in front of each DSSSD, separated by about 5 mm from the DSSSD, to cover most of the strips.

(a) Lateral picture of position of the calibration source placed in front of one DSSSD.

(b) Diagram showing the frontal positions where the ^{207}Bi calibration source was placed.

Figure 3.5: ^{207}Bi calibration source position during the WAS3ABi energy calibration.

The ^{207}Bi source provides calibration points up to 1.2 MeV. To obtain

experimental points at higher energies, the ^{57}Zn decay (see App. F.2) [J^{+}02, B^{+}07], ^{61}Ge decay (see App. F.1) [H^{+}87, B^{+}07], and ^{65}Se decay (see App. F.3) [RGL^{+}11, Goi17], which are produced in the experiment and reported to be proton emitters, were used.

3.2. EURICA HPGe array

EURICA (Euroball at RIKEN Cluster Array) [Nis12] is a γ-ray array formed by twelve clusters of HPGe detectors (see Fig. 3.6a), each one divided in seven independent crystals (see Fig. 3.6b and 3.6c). EURICA was previously used in 2007 in the active stopper experimental campaign at GSI, under the name of RISING [Mol11, Mor11, MRF^{+}15] providing high resolution spectroscopy to measure the γ-rays emitted during the decay of implanted nuclei. Each crystal has two outputs, the first one is sent to Digital-Gamma-Finder (DGF) modules, and the second one is sent to analogue timing modules. The digital branch had a 25 ns/ch time resolution and 100 μs range, while analogue branch was fed into the 2 types of **T**ime to **D**igital **C**onverter (TDC), the short-range TDCs had 0.31 ns/ch and 1 μs range, while the long-range one had 0.73 ns/ch and 800 μs range. The EURICA data acquisition was triggered only by the F7/F11 plastic detectors of BigRIPS or by WAS3ABi.

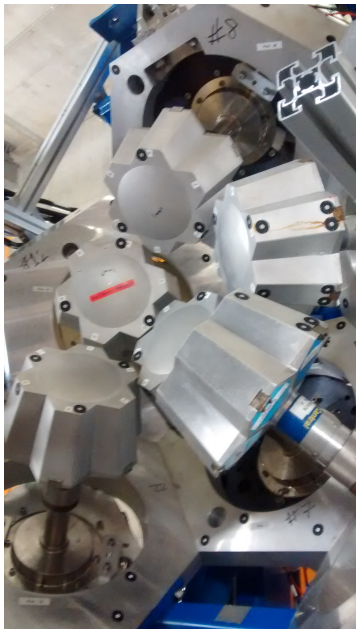

(a) EURICA cluster array hemisphere (half of the array).

(b) Overview of an individual cluster with dewar.

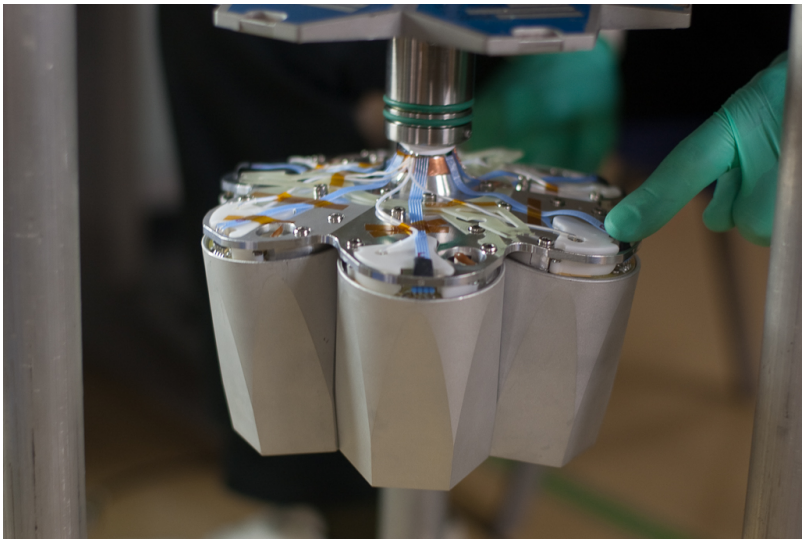

(c) An EURICA cluster with seven crystals.

Figure 3.6: Pictures of EURICA placed at the last focal plane of BigRIPS, taken during the EURICA commissioning.

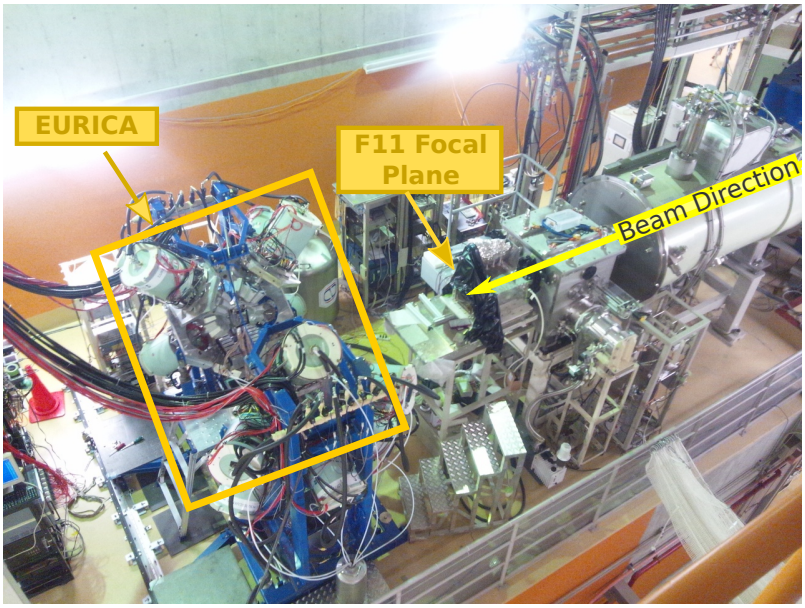

(a) Overview of the last focal plane of BigRIPS.

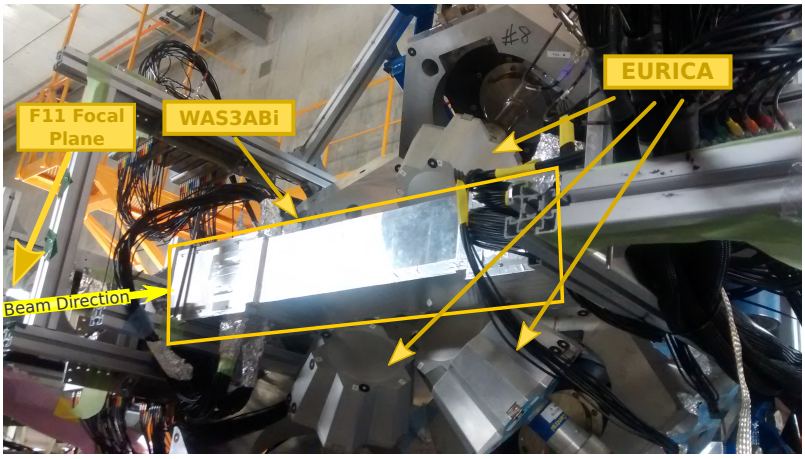

(b) Active stopper (WAS3ABi) and EURICA cluster array.

Figure 3.7: Picture of EURICA, the HPGe cluster array surrounding WAS3ABi, that was used to detect the γ-ray for each decay.

3.2.1. EURICA energy and efficiency calibration

For the efficiency calibration, in order to measure the γ-rays emitted during decays, EURICA was calibrated using ^{152}Eu and ^{133}Ba. A 100 kHz pulser was used to trigger the acquisition of EURICA during calibration measurements to obtain the spectra for both sources. In Appendix C, the calibration results are shown for both sources.

Each peak in the calibration spectra was fitted to obtain the net number of counts $C(E_\gamma)$ for each γ-ray. This value is proportional to the detection efficiency $\varepsilon(E_\gamma)$, which depends on the γ-ray intensity I_γ, source activity A_{source}, size (T_{gate}) and the number of triggers N_{triggers} during the measurement:

$$\epsilon_\gamma(E_\gamma) = \frac{C(E_\gamma)}{A_{\text{source}} \cdot I(E_\gamma) \cdot N_{triggers} \cdot T_{gate}} \ . \tag{3.1}$$

and this allows us to obtain ε_γ experimentally as a function of the energy of the γ-ray. The most intense peaks of the calibration sources of ^{152}Eu and ^{133}Ba were used to measure the ε_γ. In Appendix C the efficiency measurements are summarised.

The efficiency curve was obtained by adjusting the RADWARE [Rad00] equation to the measured points for the calibration sources,

$$\varepsilon_\gamma(E_\gamma) = \exp\left\{ \left(\left[A + BX + CX^2\right]^{-G} + \left[D + EY + FY^2\right]^{-G} \right)^{-1/G} \right\} \ ; \tag{3.2}$$

$$X(E_\gamma) = \ln\left(\frac{E_\gamma}{E_1}\right) \quad ; \quad Y(E_\gamma) = \ln\left(\frac{E_\gamma}{E_2}\right) \ ; \tag{3.3}$$

obtaining the parameters A, B, C, D, E, F, and G, using E_1=100 keV, and E_2=1 MeV. In Table 3.2 all of the parameters are summarised corresponding to the γ-ray efficiency calibration. In Fig. 3.8, the measured efficiency points are

shown together with the fitted efficiency curve.

	A	B	C	D	E	F	G
Value	16.3396	6.75877	-2.67803	3.8662	-0.899682	0.0767614	0.572096

Table 3.2: Optimal RADWARE parameters obtained by fitting Eqs. (3.2) and (3.3) to the measured γ-ray efficiency for EURICA using ^{152}Eu and ^{152}Ba sources.

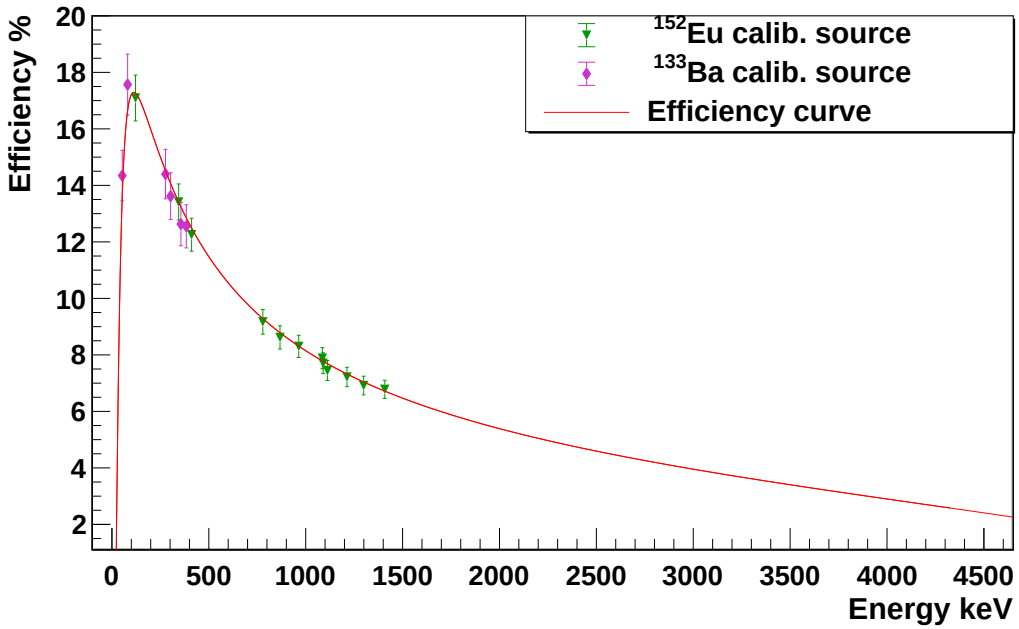

Figure 3.8: EURICA efficiency curve obtained using the measured efficiency points from the ^{152}Eu, and ^{133}Ba calibration sources. The efficiency was obtained adjusting the RADWARE curve to the measured points from the calibration source.

Chapter 4

Data reconstruction for implantation and decays using data from BigRIPs, WAS3ABI, and EURICA

In previous sections, the experimental setup was described. All of these instruments record experimental information that must be interpreted in order to understand the physics involved. In this experiment, there are two event types, implantation and decay events, corresponding to two different phenomena. The first corresponds to an ion traveling through BigRIPS, and being stopped in WAS3ABi. The latter corresponds to a subsequent decay of the heavy ion inside WAS3ABi. In this section the criteria used to identify these two phenomena from the information given by BigRIPS, WAS3ABi, and EURICA detectors, will be explained.

4.1. Implantation event reconstruction for WAS3ABi detector

An implantation event corresponds to an ion produced in the fragmentation reaction travelling through the BigRIPS separator, reaching the last focal plane and being implanted in the WAS3ABi active stopper detector. During its journey the ion creates signals in all the detectors across BigRIPS upto the implantation position. To ensure that these signals correspond to an ion, specific conditions in all detectors must be met for both BigRIPS and WAS3ABi.

As explained in section 2.2, BigRIPS was used both to separate and for identify the nuclei of interest from the cocktail beam produced in the fragmentation reactions of the ^{78}Kr primary beam and the ^{nat}Be target. The so-called *minimal conditions* on BigRIPS data were applied on the **P**article **ID**entification plot (PID),

$$1 \leq \frac{A}{Q} \leq 3 \tag{4.1}$$

$$1 \leq Z \leq 50 \tag{4.2}$$

rejecting all ion events that at some point in the passage through BigRIPS leads to an incorrect identification. In addition a condition was applied to the signals from the plastic scintillator detector placed at the F11 focal plane, which is associated with the acquisition trigger. For this plastic scintillator at F11, both of its photomultipliers[1] must have a valid signal.

Once the ion is identified at the F11 focal plane of BigRIPS, another condition related to strip signal overflows, must be included in order to ensure the implantation took place at the WAS3ABi active stopper. The implantation condition

[1]Plastic scintillators have a photomultiplier at each ends, see Fig. 2.7.

is explained below.

In section 3.1, the WAS3ABi active stopper was described including its electronics, and in section 3.1.1 its calibration was explained. Once each strip of a DSSSD are energy calibrated, the DSSSD could be used as a 'non-strip' detector, by constructing a beta decay energy spectrum allowing more than one strip fired by the decay event. This is suitable for decay events that deposit a few MeV over the strips. However, as the implantation events deposit energies of the order of GeV over a few strips (typically three strips overflow) and the available linear pre-amplifiers[2] of WAS3ABi are saturated with high energy signals, making it impossible to measure the energy of the ion and hence determine the implantation position. This problem was solved in previous work [Xu15, Tap15, Goi17] by making use of the strip implantation time signal instead of the strip implantation energy signal. When an implantation takes place, the strip with the maximum amount of energy is also the strip which gives a signal that reaches a given threshold first. This recovery of information is possible because leading-edge discriminator electronics were used for each strip signal in WAS3ABi [Xu15, Tap15, Goi17]. In Fig. 4.1 is shown the time from the TDC with the condition of a minimum time in strip 30 (X-side) and in strip 20 (Y-side). Then a signal can be considered produced by an ion (implantation signal) if the strip has an overflow in the energy branch and the TDC module for that strip records a signal time. Thus, the X-Y position of an implanted ion or an ion that traverses the detector corresponds to the X and Y strips with the fastest TDC time signal (see scheme at Fig. 4.2).

To determine the implantation depth[3] in the WAS3ABi active stopper detector, the DSSSDs and veto detectors were examined consecutively looking for an

[2]Model KPA-10 10ch C.S. pre-amplifiers, explained in section 3.1.

[3]In this analysis, depth means in which detector the particle was implanted: DSSSD1, DSSSD2, DSSSD3, or Veto detectors.

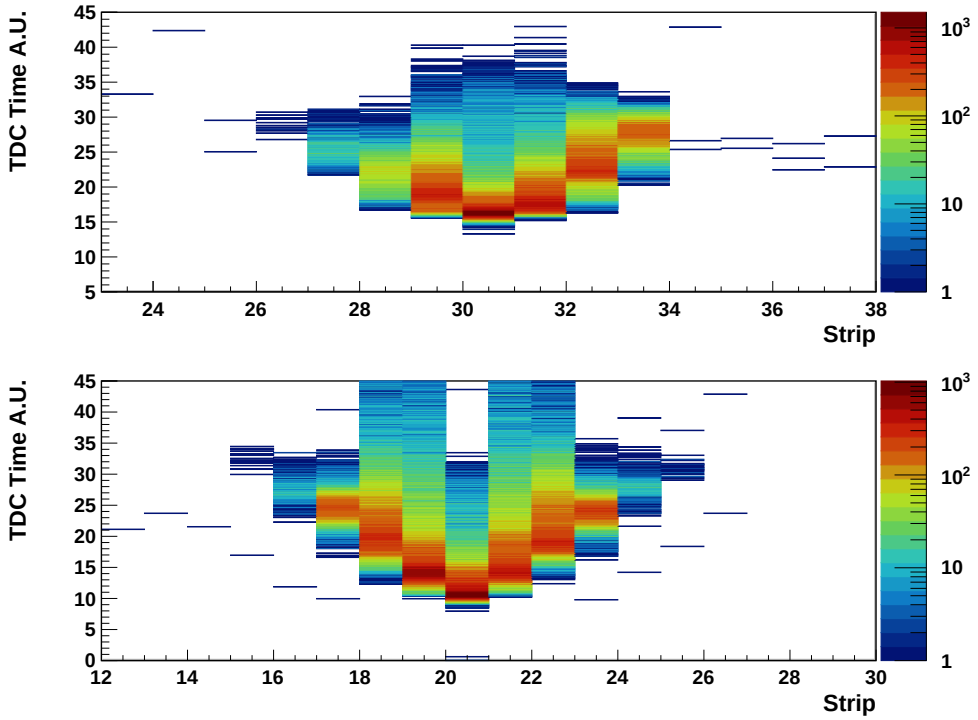

Figure 4.1: Time of the WAS3ABi TDC requiring implantation in strip 30 (X-side) and strip 20 (Y-side).

implantation signal. In Tab. 4.1 the implantation depth criteria are summarised. The criteria are evaluated from the first detector (DSSSD 1) to the last one (Veto plastic) and the implantation depth is determined by the first detector that fulfills the condition.

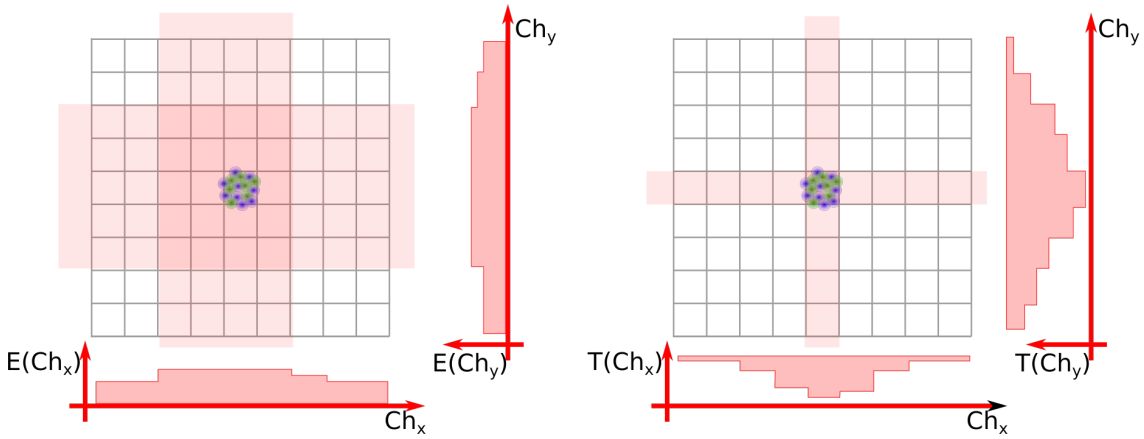

(a) Diagram for energy branch on an implantation event example.

(b) Diagram for time branch on an implantation event example.

Figure 4.2: Implantation position reconstruction diagram. An implantation deposits energies of the order of GeV order, making it impossible to determine the energy of the implantation using the available electronics. This problem was solved in previous work by assigning the implantation to the pixel where the X-side and Y-side strips have the minimum time (see Fig. 4.1).

Implant Depth	DSSSD			Q-beta pl.	Veto pl.
	1	2	3		
DSSSD 1	Of	!Of	-	-	-
DSSSD 2	-	Of	!Of	-	-
DSSSD 3	-	-	Of	!Of	-
Q-beta pl.	-	-	-	Of	-
Veto pl.	-	-	-	-	Si

Table 4.1: Summary of implantation depth criteria. The overflowsignal in WAS3ABi is shown with "Of", and non-overflow signal is shown by "!Of". The signal in veto plastic is shown with "Si". A dash (-) indicates that no requirement was demanded for that detector. The implantation depth is checked from the first strip detector (DSSSD 1) until the Veto plastic detector. Then the depth is assigned to the first detector that fulfills this criterion.

4.2. Decay event reconstruction from the WAS3ABi detector

A decay event corresponds to a signal deposited by a charged particle emitted during the decay of an ion implanted in the DSSSD. This kind of event requires, just as for the implantation events explained in Section 4.1, at least one valid signal from both sides of the DSSSDto conform a pixel.

In this work, decay event if conformed with every pixel that rise a signal during the event. In Fig. 5.4 a diagram of a decay event is show to visualize different implant-decay distance conditions used during this work.

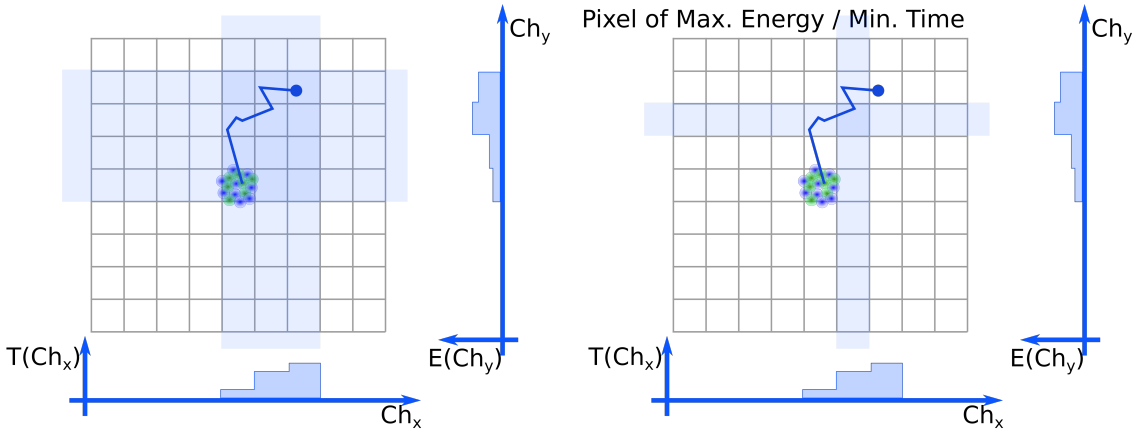

(a) A decay-type event deposits energy in several strips as the particle travel across the DSSSDs.

(b) the energy of the event is given by Y-side strip with the maximum energy and X-side minimum time.

Figure 4.3: Decay position reconstruction diagram. In this work the decay event is not restricted to only one pixel, in order to maximize the correlation beta efficiency, a beta event is treated using all pixels with signals, characterized with the Y-side energy of the maximum energy pixel.

Energy deposition per strip is different depending on the path followed and implantation position. In this work, a decay event in the DSSSD could be of two

different types: a positron from a beta decay or a proton from the beta-delayed proton emission process. Beta particles deposit energy in several strips. On the contrary protons can deposits all of its energy in one strip, as it is discussed in Appendix I. The proton position is easily obtained, since it normally corresponds to the strip where the maximum energy is detected. However the beta particles can travel through several strips and deposit only a fraction of their energy in each strip. To take these facts into account decay events are assigned to all pixels with signals within the event.

In Section 3.1 it was explained that the X-sides of DSSSDs have a shorter energy range than the Y-sides, due to the low gain settings of the amplifiers at the beginning of the experiment. In order to detect high energy protons, X-side overflows are allowed as a valid decay event. Energies were taken from the Y-side, and times were taken from the X-side of DSSSD.

4.3. Data Merging from BigRIPS, WAS3ABI, and EURICA

In Chapter 2.1 the production of isotopes was explained. During the experiment, several types of nuclei were implanted in WAS3ABi. In order to measure precisely the decay radiation such as β decay, β-delayed proton emission, and γ-rays, the experimental data is acquired and processed using three different data acquisition systems that must be synchronized in the off-line analysis. The process that synchronises the BigRIPS, WAS3ABi, and EURICA data signals is called *data merging*.

Each of the three data acquisition systems has its own clock with a resolu-

tion of 0.1 ns. These clocks are synchronized using a **L**ogic **U**nit for **P**rogrammable **O**peration (LUPO) unit, developed at RIKEN [B+10, B+15], giving a common time stamp. A diagram for the synchronization process is shown in Fig. 4.4, where the three DACQs are synchronized using the WAS3ABi time stamp. In Fig. 4.5 the time stamp of WAS3ABi was compared with the closest event in the BigRIPS and EURICA DACQ. Fig. 4.5a shows the coincidence between events within −6 ns to 6 ns. Events outside that window may correspond to random coincidence with BigRIPS events where the ion did not reach WAS3ABi.

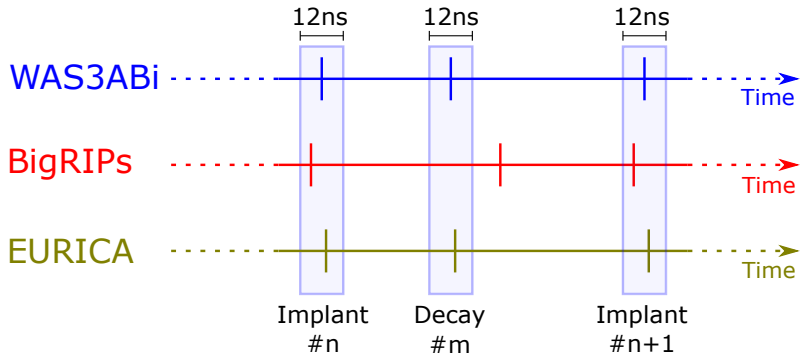

Figure 4.4: Diagram for the event coincidence between time stamp DACQs. WAS3ABi and BigRIPs data are used to identify implantation and decay events.

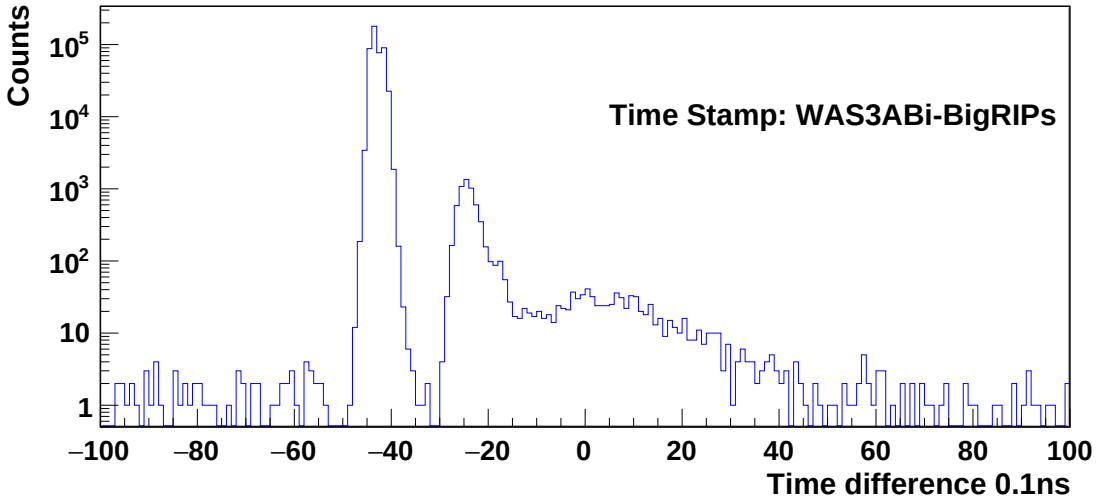

(a) Time stamp difference between WAS3ABi and BigRIPS, during run 2106.

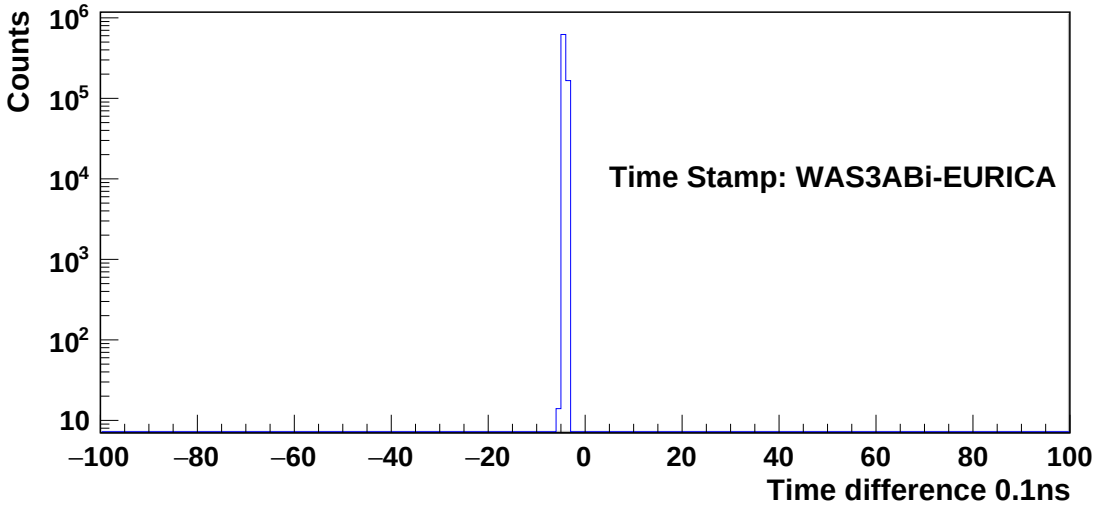

(b) Time stamp difference between WAS3ABi and EURICA, during run 2106.

Figure 4.5: Time stamp differences for the three DACQ involved in the experiment. Differences between WAS3ABi and EURICA are stable at -0.5 ns. In BigRIPS these may exist ions that are lost after firing a trigger but before reaching the WAS3ABi active stopper. Then, some random coincidences may exist as shown in Fig. 4.5a. Then, the coincidence windows between the BigRIPs and WAS3ABi was set within -6 ns to 6 ns.

Part III

Analysis and Results

Chapter 5

Analysis Overview

In Part II the experimental procedures for producing, measuring and storing the data for the nuclei of interest were explained, and two types of event were identified: implantation and decay events. In this chapter the procedures and the criteria used to construct the implant-decay correlations will be described. Then the beta, proton, and gamma-ray spectra for each nucleus analysed will be obtained.

Keeping in mind the chart of nuclei, the nuclei of interest in the present work, $^{64}_{34}Se_{30}$ and $^{66}_{34}Se_{30}$ are located near the proton drip-line. Prior to this experiment their decay properties were not known. Both nuclei are very far from stability and consequently difficult to produce. One possible production method is by fragmentation of a ^{78}Kr beam. Unfortunately the reaction cross section is very small and the only way to compensate for that is by using very intense beams such as those available at RIKEN. Indeed the further from stability that these nuclei are, the lower the production cross sections. Accordingly the only place in the world at this moment where one can find such an intense beam of ^{78}Kr is RIKEN. This work represents the first experimental study of the beta decay of these nuclei. In addition one of the most challenging aspects of beta decay studies in fragmentation

reactions lies in the stochastic nature of the nuclear decay process, which means that we require suitable detectors, electronics and data acquisition systems to collect data which can be correlated in completely different time scales from milliseconds to several hours. As reported in the literature the half-lives of the nuclei of interest in the present work are of the order of dozens of milliseconds similar to the half-lives of their daughter nuclei. This represents another difficulty because of the incomplete informationeither for half-lives or level schemes.

The decay chain for ^{64}Se and ^{66}Se are shown in Figs. 5.1a and 5.1b respectively. Nuclei with half-lives of the order of milliseconds are marked with coloured circles. Because of the short half-life, the radiation from the decay of the nuclei ^{64}As, ^{63}Ge, and ^{66}As will overlap in time and space with the decay of ^{64}Se and ^{66}Se. To take into account this overlap, the strategy followed in this work was first to analyse the daughter nuclei ^{64}As, ^{63}Ge, and ^{66}As, followed by the analysis of the decay of the nuclei of interest ^{64}Se and ^{66}Se.

In Part II the distinction between implantation and decay events was explained in detail. Since it is not possible to know which implantation produced a decay signal, a correlation analysis was performed and is explained in Section 5.1. The time correlation analysis includes all implantation-decay pairs and in consequence some pairs will correspond to real implantation-decay events while others, wrongly assigned, will contribute to the random correlation background. Since beta decay follows an exponential time distribution while random correlations have no time correlation distribution, it is possible to obtain the total number of correct correlations without knowing which couples are true correlations. Following this philosophy, it was possible to obtain the decay spectra for each nucleus of interest, as will be explained in Section 5.2.

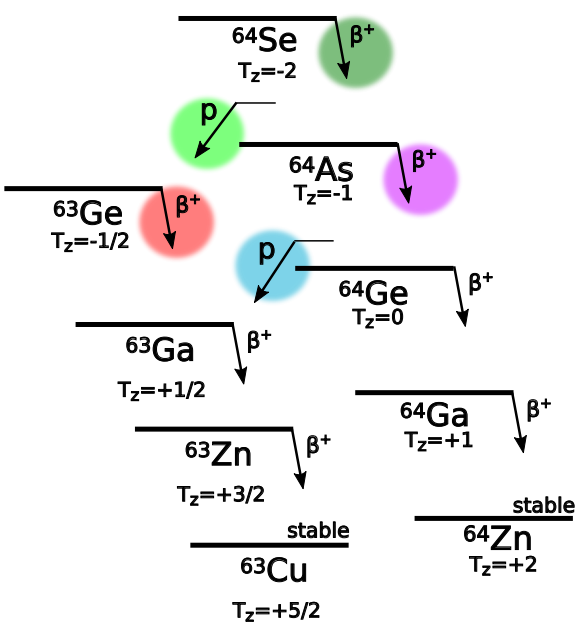

(a) ^{64}Se decay diagram.

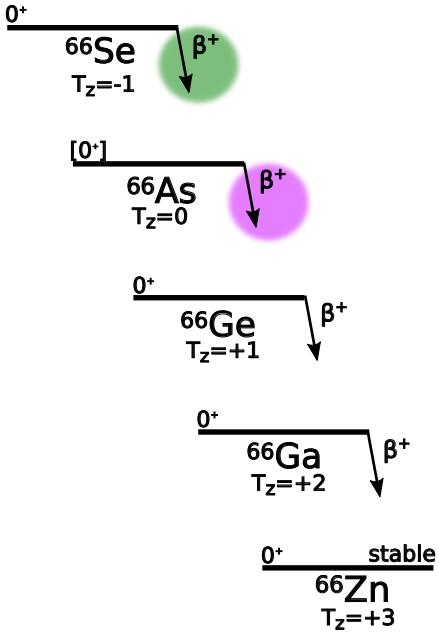

(b) ^{66}Se decay diagram.

Figure 5.1: The decay schemes for the isobaric multiplets of the nuclei of interest.

5.1. Correlation procedure for implantation and decays

After the merging process explained in Part II, two types of events are constructed for further analysis, namely implantation-type and decay-type events. Since nuclear decay is a stochastic process, obtaining the correct decay spectrum for each nuclear species is not a trivial task, and correlation analysis must be performed. The methodology used in this work consists in taking into account all possible implant-decay correlations, spatially and temporarily constrained. The criteria considered in constraining the correlations will be explained in the following subsections.

5.1.1. Time correlation conditions

Each implantation and decay event has a unique timestamp value given by the event acquisition trigger. To ensure that the true correlation is collected for each implant, the correlation should be performed over several hours. Since each implantation is correlated with many decays, the correlation process involves a duplication of decay data size several times in the offline analysis. To reduce this, the correlations are performed in suitable time windows that are adjusted to correlate properly the implanted ion with its decay particles.

Since the half-lives of the nuclei of interest are shorter than one second,in this work time correlations were performed within a forward and backward time window of ± 10 s. In Fig. 5.2 a time correlation diagram is shown for ^{63}Ge beta decay. However, this time correlation windows could be reduced, if needed, to improve the analysis cleaning conditions. For a detailed explanation the reader is referred to Appendix G, Section G.1.

In this work the correlation time is defined as $T_{\text{corr.}} = T_{\text{decay}} - T_{\text{implant}}$. Positive correlation times corresponds to either true correlations or random correlations. On the other hand, negative correlation times correspond to an event where a decay was recorded *before* an implant. This kind of event can only correspond to random and non-physical correlations [DAA+07, MRF+15, Mol11]. If a symmetrical correlation background is assumed, backward correlations can be used to subtract the number of random correlations in the forward direction [MRF+15, Mol11]. In Fig. 5.2b, the backward correlation times were reflected to forward times assuming that the number of backward correlations are statistically the same as the number of forward correlations.

To simplify the notation in this work, a time interval from t_i to t_f is written as $[t_i, t_f]$. When a non-continuous interval is used, the $\oplus$ symbol is used to denote inclusion, and the $\ominus$ denote the subtraction. For example, the correlation window C_w within the intervals t_a to t_b and t_c to t_d with background subtraction window in the interval within t_f to t_g will be written as:

$$C_w = [t_a, t_b] \oplus [t_c, t_d] \ominus [t_f, t_g] \ . \tag{5.1}$$

If an asymmetric subtracting window is used, the subtracted events are weighted by the correlation time window size:

$$W = \frac{\Delta(\text{size of the positive region})}{\Delta(\text{size of the negative region})} \ . \tag{5.2}$$

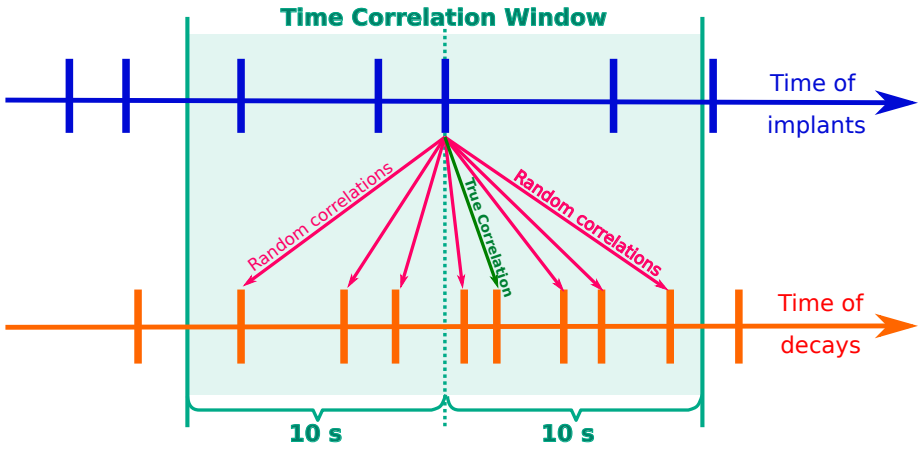

(a) Correlation diagram between implants and decays events. Events are represented as vertical lines both for implants and decays. The diagram shows the correlation for one implant, that implantation produced only one decay (indicated with a True Correlation). All other possible correlations are drawn with magenta arrows and will be random coincidences for that implant.

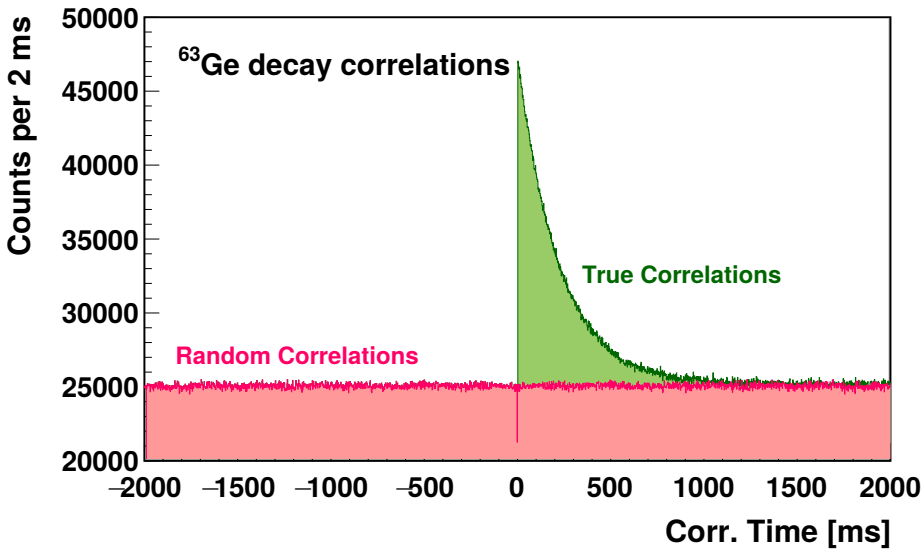

(b) An example for the correlation time distribution obtained for the ^{63}Ge decay (see Sec. 6.1.7). Forward background was drawn as a reflection of backward correlations (see text for details).

Figure 5.2: Diagram for the time correlation procedure. In Fig. 5.2a the time correlation method is shown. In Fig. 5.2b the temporary distribution obtained for ^{63}Ge decay using this method is shown. A detailed analysis for ^{63}Ge will be shown in Sec. 6.1.

5.1.2. Spatial conditions for correlations

Time correlation conditions are important in order to obtain decay chain time distributions and afterwards the half-life of the nuclei of interest. For this reason imposing spatial conditions between implantation and decays helps to reduce the number of random correlations. When a decay takes place, the radiation emitted ionises atoms of the silicon detector in the same pixel where the implantation event took place. True non-neighbouring events would correspond to events where the decay occurred near the surface of the DSSSD and after scattering returned to another pixel. This kind of event may occur, but with such small probability that it becomes better to ignore them in order to avoid random correlations.

To construct the implantation-decay correlations, we require that the distance between the implanting position (i_X, i_Y) and any of the strips associated with the decay event (d_X^j, d_Y^k) cannot be larger than one, that is:

$$\left|i_X - d_X^j\right| \leq 1 \quad \wedge \quad \left|i_Y - d_Y^k\right| \leq 1 \ , \tag{5.3}$$

where d_X^j and d_Y^k represent the closest decay strips to the implantation strip. This represents the condition that a correlation must fulfill in order to be used in the subsequent analysis. In Fig. 5.3 is shown an example for this minimum condition for the implantation-decay correlation distance. Nevertheless, the spatial condition can be refined by including or reducing the number of neighbouring decay pixels according to their distance in strips from the implantation.

An implantation may produce a decay event within the same pixel or in a neighbouring one. As discussed in Section 3.1, the decay event can leave signals in several pixels depositing comparable amounts of energy ΔE, making it difficult to know where the decay took place. In this work the concept of a *pixel distance*

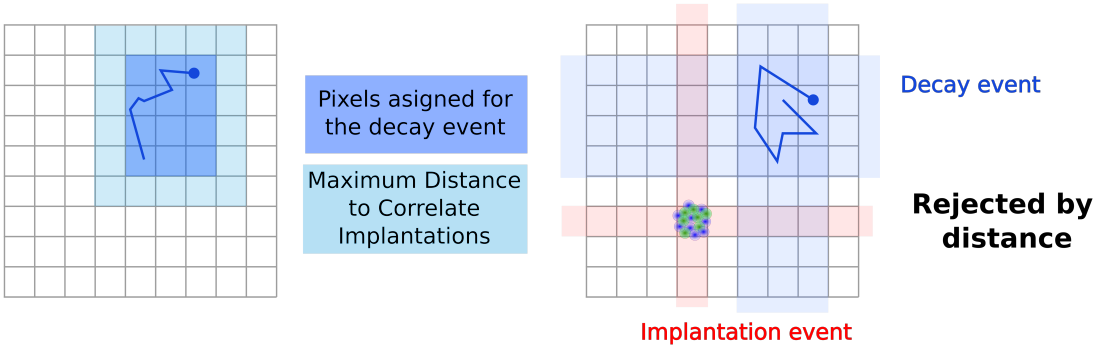

(a) Correlation were performed up to one strip of distance between decay and implantation events, independently for X and Y side.

(b) Example of a rejected correlation due distance. Implantation pixels non-neighbouring to a decay pixel hardly will be true correlations.

Figure 5.3: Example for the spatial correlation conditions. An implantation is correlated to a decay event only if they are neighbouring pixels. Subsequent analysis was performed using only events fulfilling this minimal distance condition.

of correlation was included. This distance is measured independently in terms of numbers of pixels on the X and Y sides of the DSSSD. Implantation events are assigned to the pixel with the fastest strips on the X and Y sides. The position of the decay event is assigned to the pixel with the fastest strip on the X-side and the highest energy on the Y-side. If an implantation has the position (X_i, Y_i) in DSSSD number Z_i, and the decay event is in position (X_d, Y_d) in DSSSD number Z_d, then the distance will be written as $D(|X_i - X_d|, |Y_i - Y_d|, |Z_i - Z_d|)$. In Fig. 5.4 a schematic diagram for distance conditions is shown. The D000 condition (see Fig. 5.4a) corresponds to decay and implantation detected within the same pixel; the D110 condition (see Fig. 5.4b) corresponds to events where the implantation was detected including a neighbouring strip in the same DSSSD as the decay; and the D111 is analogous to the D110 condition but including the equivalent pixels in the neighboring DSSSDs.

The conditions D000 and D110 are very suitable for p emission where the detection takes place in the same pixel where it was emitted due to the short range[1] of protons in silicon as will be shown in Appendix I. Beta particles are much lighter than protons and can travel through several pixels before being stopped, depositing only a ΔE fraction of their energy in each strip making it difficult to identify the emission position. In order to correlate most of the β decays, the NMD condition (No Maximum Distance, Fig. 5.4c) and NMDSIP condition (No Maximum Distance with Signal in the Implantation Pixel, Fig. 5.4d) were used.

The effect of the spatial correlation on the beta or proton spectrum is shown in Fig. 5.5, which will be discussed in detail in Appendix F.2.2. The proton spectrum for the ^{57}Zn β-delayed p-spectrum was constructed using the D000, D110 and NMD conditions. The D000 condition gave a better spectrum shape for the proton spectrum and was used to define the peak positions, however the ε_β is smaller. EURICA was triggered by WAS3ABi, so in order to measure the γ-delayed beta decay we need to correlate most of the betas. The NMDSIP condition increases the number of true beta correlations, and was used to measure the γ-delayed beta decay. The ^{64}As decay, that will be treated in Section 6.2, is an example of why the D000 was used in addition to the NMD condition. In ^{64}As decay, the D000 condition gave a better p-spectrum shape than the NMD condition as explained in Section 6.2.3, since most of that decay goes through β decay, the tail of the beta energy distribution is dominant up to 1.4 keV. As a consequence, the low intensity protons overlap with the betas. The D000 condition reduces the overlapping since it has lower beta efficiency than the D110 or D111 conditions.

[1]Maximum path length before being stopped.

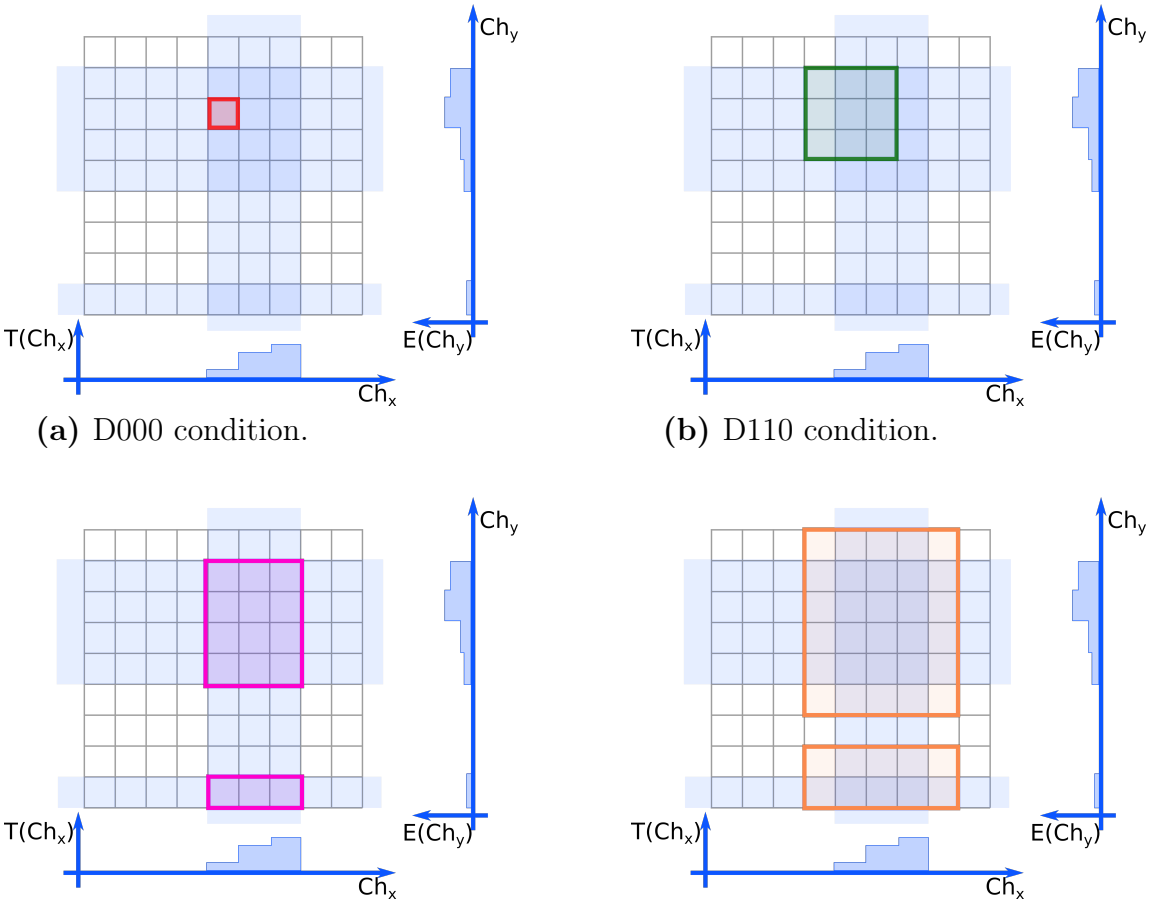

(a) D000 condition.

(b) D110 condition.

(c) NMDSIP condition

(d) NMD condition.

Figure 5.4: Examples of the spatial conditions used in the implant-decay correlation in a DSSSD. The figure shows the signal for a decay event and implantation pixels fulfilling the spatial conditions.

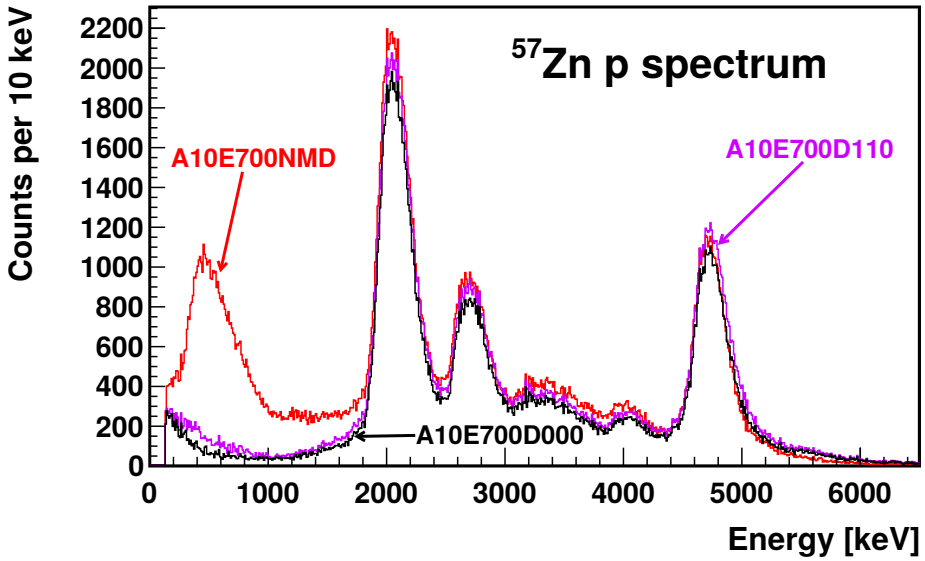

Figure 5.5: Implantation-decay distance conditions for the ^{57}Zn decay. Three cases are shown when the correlation distance is varied: in same pixel (D000, black), one neighbouring pixel (D110, purple), and close to one fired pixel only (NMD, red). The A10E700 reconstruction algorithm will be explained in Section 5.1.3. Detailed analysis for this spectrum can be found in Appendix F.2.2.

5.1.3. Energy reconstruction for DSSSD events

The distance correlation conditions such as NMD, D110, and D000, affect directly the detection efficiency for decay events. However, the quality of the proton peaks is another important factor to take into account during reconstruction. The proton range for decays occurring inside a DSSSD is discussed in Appendix I. The proton range is short enough to allow the capture of the proton in the same strip as the implantation most of the time, but there are some cases where the proton reaches the strip border and escapes into another strip, depositing part of its energy in both strips. When the beta event is labelled using only the strip with the highest recovered energy, such proton events are recorded with a lower energy than the true energy, thus distorting the shape of the peak. This reconstruction was improved by adding the energy of the strip with the maximum energy deposition and the energy of the neighbouring strip if its energy is above a threshold of 700 keV, as will be explained in Appendix F. However only one neighboring strip can be added, corresponding to the neighboring strip with the highest energy. In Fig. 5.6 a diagram of this reconstruction is shown. The minimum time (X-side) and maximum energy pixel (Y-side) is shown with a red box, normal reconstruction would assign $E_y^{(1)}$ as the energy for this event. To recover the energy of proton events the energies in neighbouring strips ($E_y^{(2)}$ and $E_y^{(3)}$ only) are compared, the highest among them ($E_y^{(2)}$ in this diagram) is added to the event energy if its energy is above an energy threshold. If this condition is fulfilled, then the energy of the event is defined as $E_{\text{event}} = E_y^{(1)} + E_y^{(2)}$.

The reason to define an energy threshold to reconstruct the proton energy is that in beta-delayed proton decay, protons are always emitted in coincidence with a beta particle. Adding the ΔE deposited in the strip of DSSSD by the beta particle

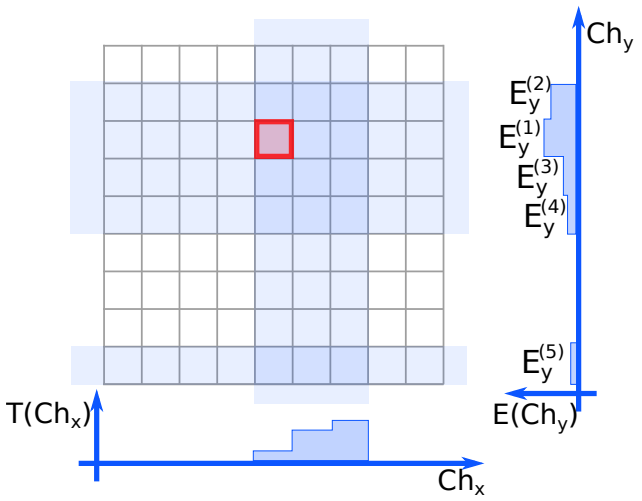

Figure 5.6: Energy adding diagram for DSSSD events. Events are labelled with the maximum energy of strips in the Y-side. To improve the resolution of the proton peaks, the energy can be added to the strip with maximum energy deposition if it is above some threshold (700 keV in this work), and if it is one of the two directly neighbouring strips.

will worsen the proton peak resolution. However, considering that the beta particles generally deposits less than 1 MeV, avoiding signals below 700 keV recovers most of the incomplete proton signals. In order to set the best energy threshold for the reconstruction, the proton spectrum from ^{61}Ge decay was used. This nucleus is a beta-delayed proton emitter, and is analysed in Appendix F.1. In Fig. 5.7 the proton spectrum for ^{61}Ge decay is reconstructed varying the energy threshold.

The energy threshold was set to 700 keV taking into account the improvement in resolution when the events with incomplete energy are recovered. The complete discussion can be found in Appendix F.1.1. In the next section this reconstruction will be labeled as **A10E700**, meaning **A**dding **1** Y-side strip at distance of **0** DSSSD (same DSSSD for maximum energy and the added strip), with an **E**nergy threshold of **700** keV.

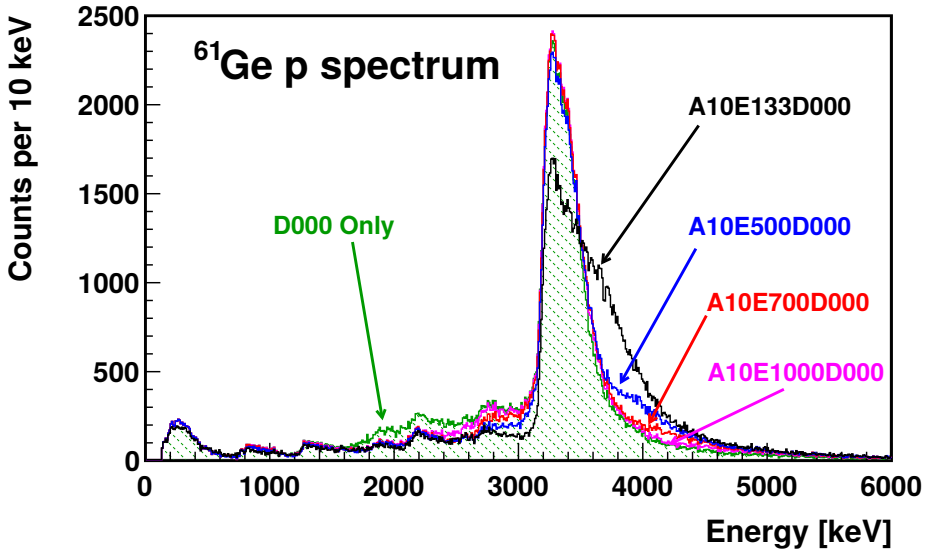

Figure 5.7: Reconstruction of the charged particle spectrum for the decay of ^{61}Ge, adding to the maximum energy deposition in one strip, the energy of the neighbouring strip with different threshold conditions: no-addition in green, 133 keV threshold in black, 500 keV threshold in blue, 700 keV threshold in red, and 1000 keV threshold in purple. A detailed analysis of this proton spectrum can be found in the Appendix F.1.1.

5.2. Beta, proton, and gamma-ray spectra from implant-decay correlations

In previous sections the time (see Section 5.1.1) and spatial (see Section 5.1.2) conditions that implantations and decays must fulfil to be correlated were explained. A correlation event between an implantation and a decay implies treating the decay as if it actually was[2] produced by the implant, allowing us to use the β, γ-ray, and time information to construct the spectra for each nuclear species.

[2]A correlation can be a true correlation if the implantation did indeed produce the decay, or a random correlation if not.

5.2.1. Parametric function to fit β spectra

A particle deposits part of its kinetic energy passing through the DSSSD. Depending on the mean free path, the particle can escape the pixel depositing only part of the energy in the corresponding strip, or can be completely stopped depositing all of its kinetic energy. This deposition also depends on the relative position inside the DSSSD. Protons usually deposit all their energy in one strip, while β particles (electrons or positrons) deposit only part of their energy (typically 2 MeV in WAS3ABi strip geometry). To adjust the spectrum produced by β particles a parametric function was defined, as described in Appendix E.

5.2.2. Obtaining gamma, proton and beta intensities from experimental data.

To obtain the intensity of a transition $I_{\beta,p}$, the number of counts $C(E_{\beta,p})$ obtained in the corresponding spectrum was normalized to the number of ions implanted N_{implants}, corrected by dead-time during the data acquisition DT, the width of the correlation time window C_w, and by the detection efficiency $\varepsilon_{\beta,p}(E_{\beta,p})$. This is summarized as,

$$I_{\beta,p}(E_{\beta,p}) = \frac{C(E_{\beta,p})}{(1-DT)\cdot C_w \cdot \varepsilon_{\beta,p}(E_{\beta,p}) \cdot N_{\text{implants}}} \tag{5.4}$$

The correction for the correlation time window size C_w is given by,

$$C_w = \frac{\int_{t_a}^{t_b} dt\, e^{-\lambda\cdot t}}{\int_0^{\infty} dt\, e^{-\lambda\cdot t}}\ , \tag{5.5}$$

and can be obtained by comparing the number of decays within the correlation window $[t_a, t_b]$ with the total number of possible decays,

In Appendix G, the total number of betas, and protons were analysed for

^{64}Se using different correlation window sizes. The optimal size of correlation time windows was obtained for seven half-lives of the mother isotope. Following this criterion, the correlation windows were chosen within 1 ms and $7{\cdot}T_{1/2}^{(\mathrm{mother})}$ ms in order to maximize the number of mother nuclei without including too many contributions from the daughter.

Dead-time correction was obtained by using scalers in the WAS3ABi acquisition electronics. The registered dead-time depends on the counting rate of implantation events, which in our experimental campaign depends on the setup of the BigRIPS separator. For this reason, a weighted value of dead-time was calculated for each nuclear species. In Appendix D.2, a weighted DT was obtained for each nuclide averaging dead-time at implantation time for each ion.

The normalization for γ-ray intensities is slightly different from β and p normalization because EURICA was not self triggered, it requires a trigger in WAS3ABi to allow its acquisition as explained in Section 3.2. In this case:

$$I_\gamma(E_\gamma) = \frac{C(E_\gamma)}{(1-DT)\cdot C_w \cdot \varepsilon_{\beta,p}(E_{\beta,p})\cdot \varepsilon_\gamma(E_\gamma)\cdot N_{\mathrm{implants}}} \ , \tag{5.6}$$

This ensures that it is not only the ε_γ efficiency that is involved in obtaining the intensity, but also the $\varepsilon_{\beta/p}$ efficiency.

Chapter 6

Analysis of the nuclei of interest

In the following sections of this chapter, the analysis of the decay of the nuclei of interest ^{64}Se and ^{66}Se is presented. However, as explained earlier, there is no previous experimental information on the beta decay properties of ^{64}Se in the literature, so it is necessary to study all daughter nuclei involved in the decay, first starting with the closest to stability and then climbing to the more exotic cases.

The main objective of this work is to obtain the beta decay strength to excited states in the daughter nucleus. To do this it is necessary to measure the half-life $T_{1/2}$ of the mother nuclei, the intensity of the transition from the ground state (g.s.) of the mother nucleus to the ground and excited states in the daughter nucleus including the excitation energies of these states (beta feeding), and the mass difference between the mother and daughter nucleus (Q_β value). From this experiment it is only possible to obtain the $T_{1/2}$ and the beta feeding. To measure the Q_β value it is necessary to carry out a different experiment with a completely different experimental setup such as a storage ring or an ion trap mass experiment. As will be explained in Section 6.3, there is no such experimental information for ^{64}Se decay. Because of the very small proton binding energy in the daughter nucleus

^{64}As, beta-delayed proton emission is expected. This represents an extra difficulty if we want to obtain the transition intensities, since protons are not detected with as good resolution as γ-rays. In order to be able to reconstruct the decay scheme for ^{64}Se, it is better to study first the proton-daughter ^{63}Ge, and the beta-daughter ^{64}As, the two nuclei in the decay chain with the shortest half-lives. This will allow us to identify and distinguish the γ-rays belonging to the mother decay and those belonging to the following daughter decay. For this reason, the analysis will be presented starting with ^{63}Ge, followed by ^{64}As, and ending with the nucleus of interest ^{64}Se. The ^{66}Se decay analysis follows the same logic, first analyzing the decay of the daughter nucleus ^{66}As, before analysing the nucleus of interest ^{66}Se decay.

6.1. ^{63}Ge decay analysis

In the study of the decay properties of ^{64}Se, ^{63}Ge is produced as the grand-daughter activity after the beta decay of ^{64}Se to ^{64}As and the subsequent proton decay as shown in Fig. 6.1. Fortunately, ^{63}Ge is produced directly in our experiment and stopped mainly in the central DSSSD. In order to identify γ-rays corresponding to this decay, we have studied the decay of ^{63}Ge independently. In the next section we will describe what is known in the literature for this decay and the results of our study.

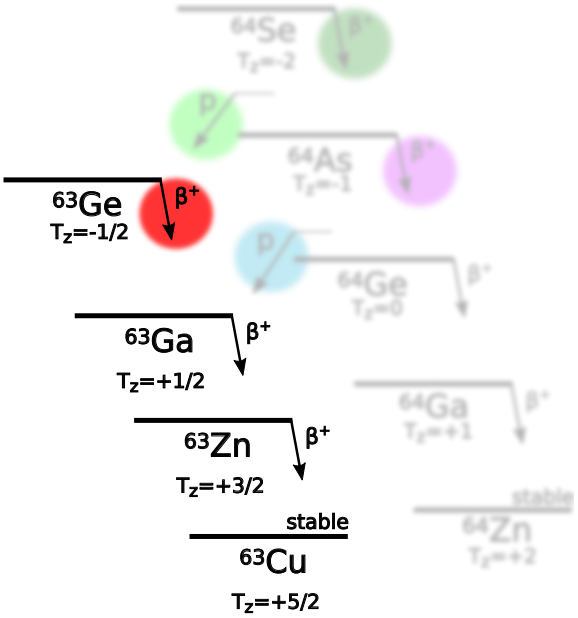

Figure 6.1: Diagram for ^{63}Ge decay, as a necessary ingredient in the study of the nucleus of interest ^{64}Se. Half-lives comparable to that of ^{64}Se are marked with color circles.

6.1.1. Previous knowledge of the excited states of ^{63}Ga: beta decay daughter of ^{63}Ge

The decay of ^{63}Ge was not known prior to our experiment. Previous knowledge of the excited states of ^{63}Ga, the daughter nucleus of ^{63}Ge, comes from the in-beam study by Balamuth et al. [B$^+$91] using the ^{40}Ca(^{28}Si,αp), the ^{40}Ca(^{32}Si,2αp), and the ^{40}Ca(^{29}Si,2αpn) reactions at the University of Pennsylvania. The level scheme they propose can be seen in Fig. 6.2a. Also Weiszflog et al. [W$^+$01] studied the states in ^{63}Ga using the ^{32}Si+^{40}Ca reaction at LNL. In Fig. 6.2b the level scheme proposed by Weiszflog is shown. These two works gave inconsistent results, which will be discussed in Section 7.1.

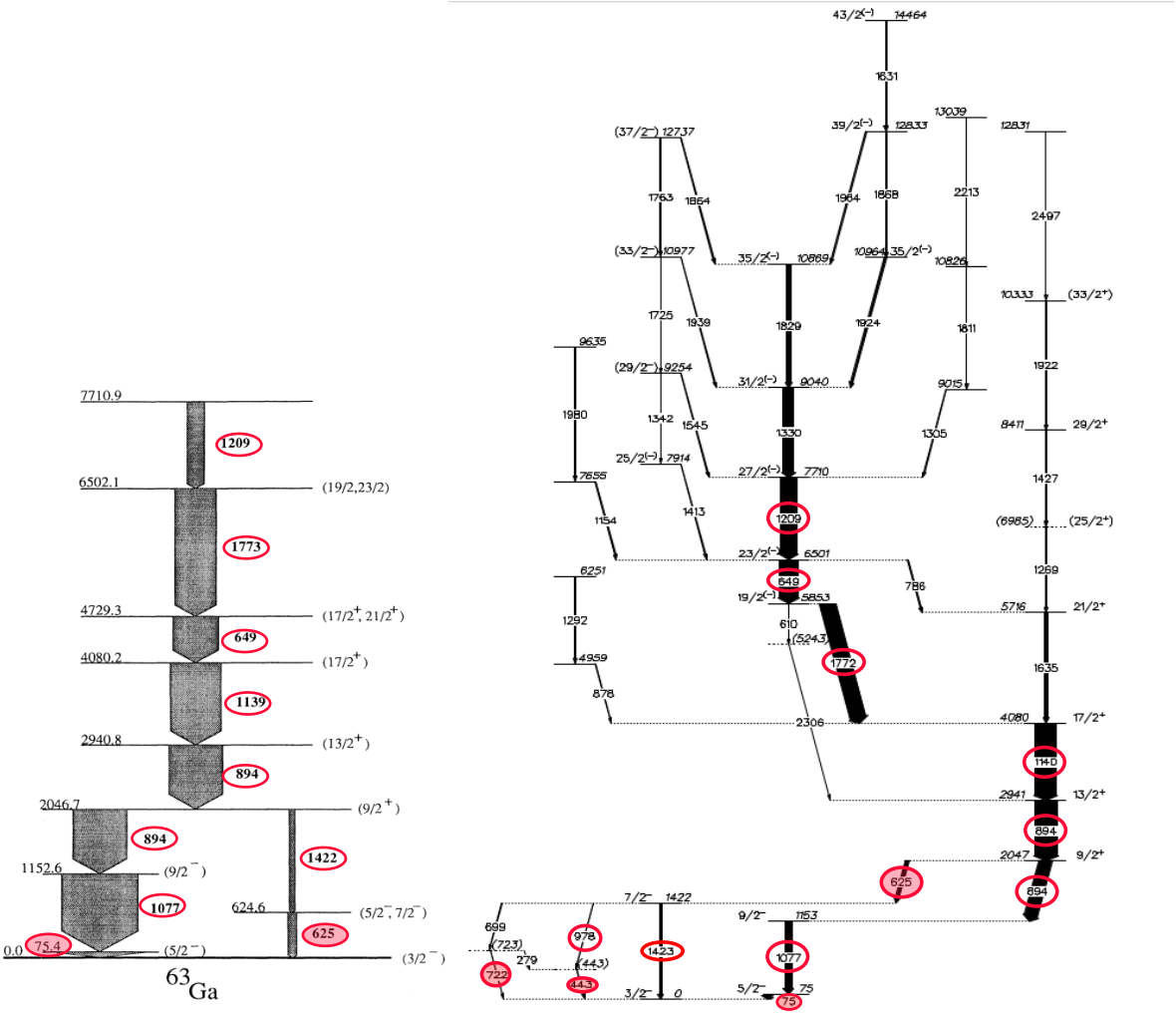

(a) Balamuth et al. [B+91] **(b)** Weiszflog et al. [W+01]

Figure 6.2: Level scheme for ^{63}Ga from previous works by (a) Balamuth et al. [B+91] and (b) Weiszflog et al. [W+01]. Gamma-rays observed in the present work were marked with a red ellipse, and those observed also in Balamuth et. al and in Weizflog et. al are marked with filled red ellipses.

6.1.2. Implantation-decay correlation for ^{63}Ge decay

The previously reported half-life for ^{63}Ge decay is 142(8) ms [AKW+17]. In the present work we used the criteria used throughout this thesis of choosing a time-range for the correlations of seven half-lives (see Appendix G). For this decay the

correlation time window corresponds to $[-1050\ \text{ms}, 1050\ \text{ms}]$, avoiding symmetrically the first millisecond of correlation. In Fig. 6.3 a plot of the implantation-decay correlations within a wider time correlation window of 10 s is shown to clarify that after the seven half-life interval (in green), most of the correlations would correspond to random coincidences (in red). Then, the green region corresponds to the seven half-lives correlation window that will be used in the following sections to construct the beta and γ-ray spectra for this decay.

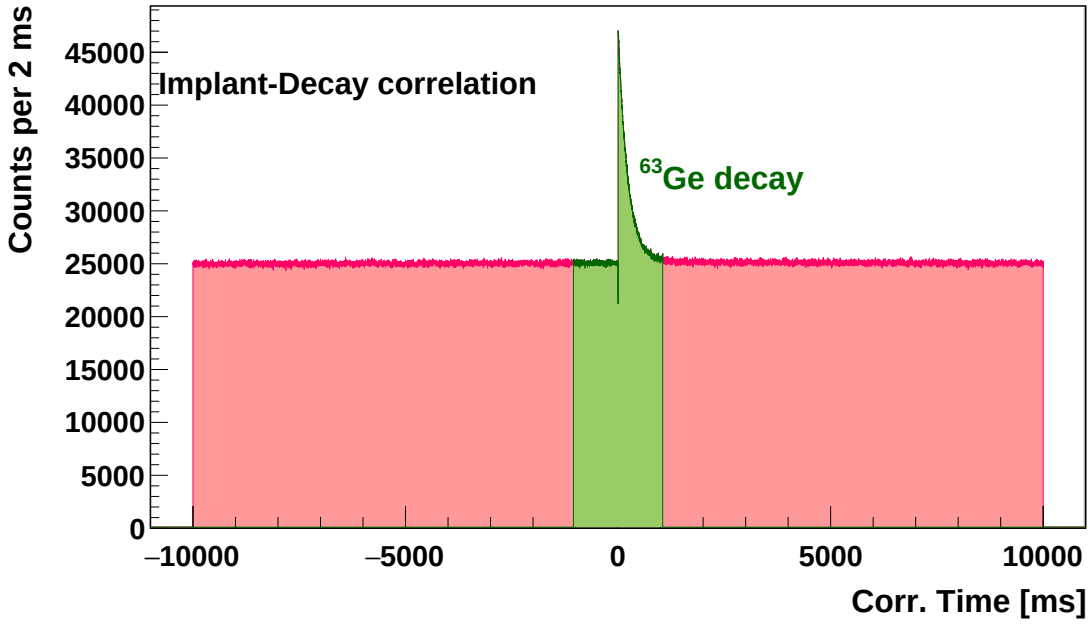

Figure 6.3: Implantation-decay correlation for ^{63}Ge. Correlations were made up to 10 s symmetrically forward and backwards, however to obtain the beta and γ-ray spectra for this decay, the time correlation window was constrained to 1050 ms (seven mother half-lives), shown in green.

6.1.3. Beta spectrum for ^{63}Ge decay

The beta spectrum was obtained by correlating implantation and decays within the 1 ms to 1050 ms correlation time window. The beta spectrum correspond-

ing to the background of random correlations was subtracted using the symmetrically negative implantation-decay correlation times within the −1050 ms to −1 ms correlation time window. Decay events were reconstructed using the A10E700NMD condition explained in Section 4.2, which allows one to obtain a higher beta efficiency than the more common condition A10E700D110 which uses nine pixels of spatial correlation. In Fig. 6.4, the beta spectrum is shown as the fitted function using the parametric beta function described in Appendix E. This fit allows one to identify two components corresponding to the the energy deposited by the beta particle in one strip.

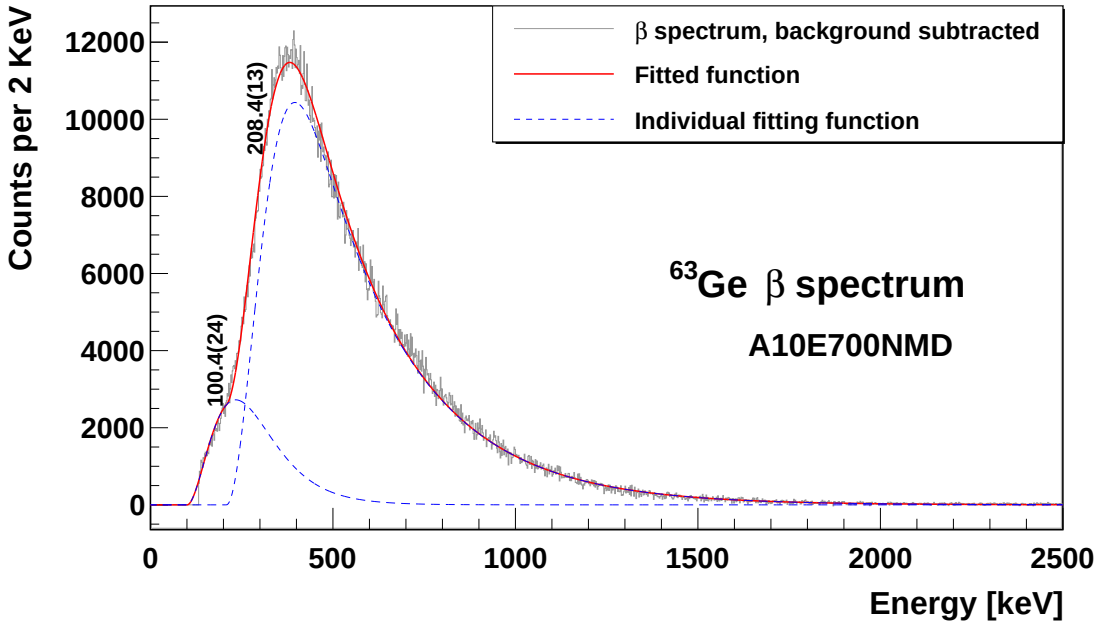

Figure 6.4: Beta spectrum for ^{63}Ge decay within the $C_w = [1, 1050] \ominus [-1050, -1]$ ms implantation-decay correlation window. The spectrum was fitted using the parametric beta function detailed in Appendix E. Fit results can be found in Table 6.4.

X_0	Amplitude	CRaise	BTail	χ^2/NDF
208(1)	2.16(2)E6	139(2)	264(1)	1112.2/901
100(2)	3.1(2)E5	182(30)	88(10)	

Table 6.1: The results of the fits for ^{63}Ge beta spectrum shown in Fig. 6.4. The parameters and functions used are described in Appendix E.

6.1.4. Gamma spectrum for ^{63}Ge decay

The γ-ray spectrum for the ^{63}Ge decay was constructed using the same implant-decay correlation window $C_w = [1, 1050] \ominus [-1050, -1]$ ms described in Section 6.1.2. Fig. 6.5 shows a scatter plot of the EURICA DGF (Digital Gamma Finder) digitalizer energy -Y axis- and time -X axis- signals. In this figure the γ-prompts corresponds to the γ-rays emitted in coincidence with the beta particle, that is, the γ-rays emitted in the beta decay, indicated between red lines in Fig. 6.5. The 100 μs time window used for the EURICA array acquisition, allows one to detect both the prompt γ-ray emitted during the beta decay and the background γ-ray radiation. To remove the background γ-rays, a γ-prompt condition was set in $[0, 0.8] \ominus [-80, -40]$ μs in the EURICA DGF-time, as marked in Fig. 6.5 with red lines.

The ^{63}Ge decay γ-prompt spectrum can be seen in Fig. 6.6. Thirty eight γ-rays were observed, including lead fluorescence x-rays, the positron annihilation photo-peak, and fifteen γ-rays identified as belonging to the ^{63}Ge decay:

- The 367.5 keV, 373.1 keV, 442.8 keV, 482.4 keV, 627.0 keV, 641.1 keV, 647.1 keV, 709.1 keV, 722.2 keV, 925.0 keV, 954.2 keV, 1363.6 keV, 2485.4 keV, and 2765.1 keV γ-rays energies were identified as being in the ^{63}Ge decay.

Pb x-rays The 72.9 keV, 75.0 keV, and the 84.9 keV peaks correspond to

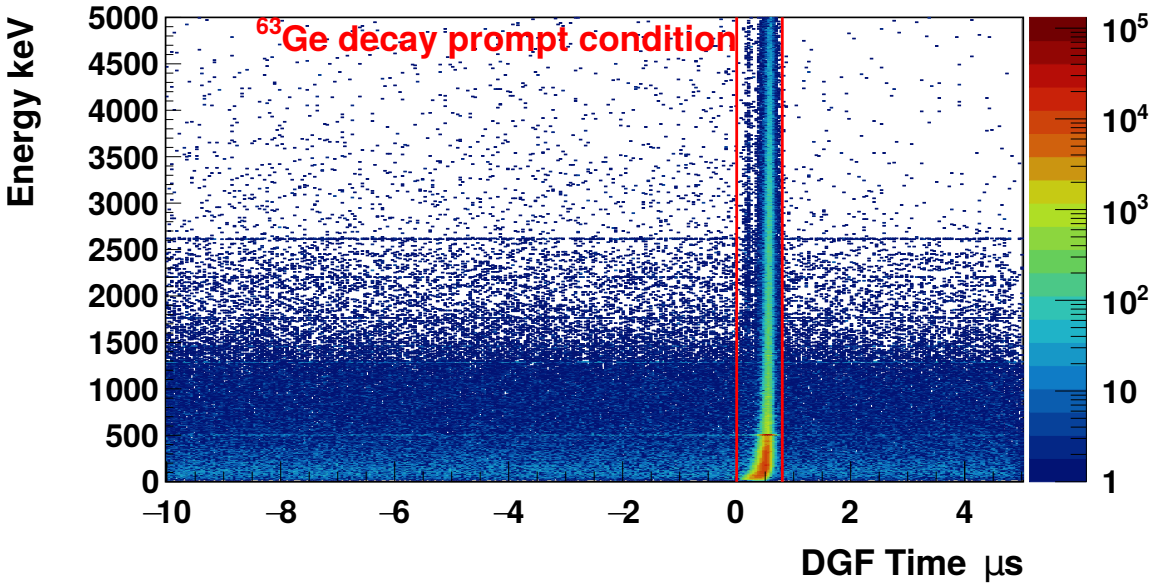

Figure 6.5: γ-ray energy-time scatter plot, requiring the implantation of ^{63}Ge condition over the PID plot. The γ-prompt condition is shown between two red lines (0.8 μs width) and corresponds to γ-rays emitted promptly in ^{63}Ge decay.

the lead fluorescence x-rays $k_{\alpha 1}$, $k_{\alpha 2}$, and $k_{\beta 1}$ respectively.

♦ The 72.9 has an intensity higher than expected from x-ray fluorescence and it is suspected of being in the ^{63}Ge decay.

Ann. The 510.9 keV γ-ray energy corresponds to the peak observed in positron annihilation.

□ The 636.3 keV, 637.7 keV, 650.7 keV, 670.4 keV, 794.5 keV, 911.5 keV, 921.1 keV, 1065.8 keV, 1332.9 keV, 1350.0 keV, 1395.3 keV, 1495.1 keV, 1498.2 keV, 1505.1 keV, 1690.6 keV, 1887.1 keV, 1936.8 keV, 2409.3 keV, 2971.4 keV, and the 3365.7 keV γ-rays remain as unplaced γ radiation.

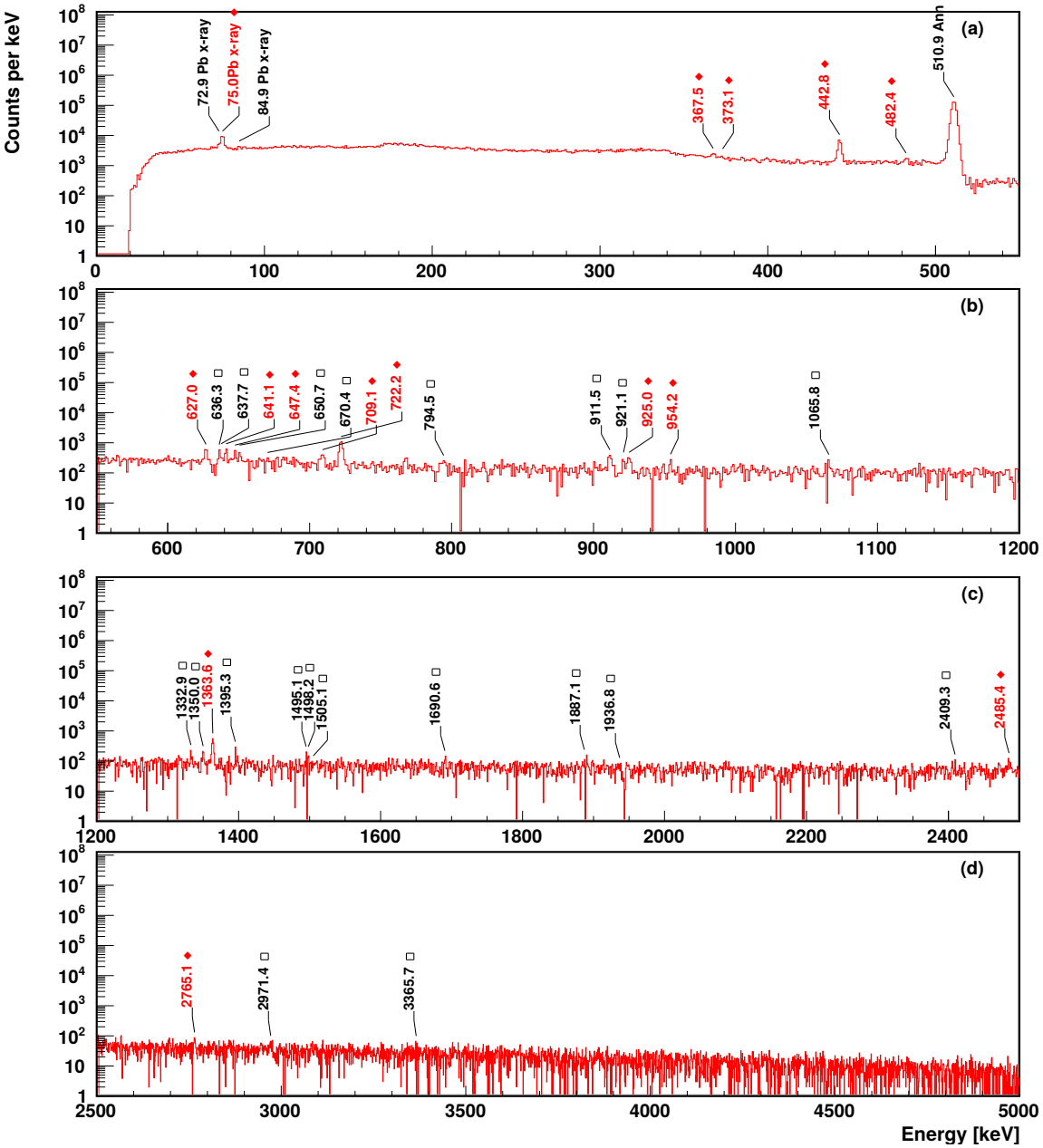

Figure 6.6: Gamma spectrum for ^{63}Ge decay with a $C_w = [1, 1050] \ominus [-1050, -1]$ ms implant-decay correlation window, and a 0.8 μs width β-γ coincidence window. Unplaced γ-rays are marked with $\square$ together with the Pb x-ray and the e^+ annihilation γ. The γ-rays identifed in ^{63}Ge beta decay are marked with ♦.

Energy keV	FWHM keV	Counts (C_γ)	Efficiency (ε_γ)	Intensity ($C_\gamma/\varepsilon_\gamma$)	Comments
72.90(5)	1.750(3)	2242(100)	0.161(6)	1.39(9)E4	Pb x-ray $k_{\alpha 2} + k_{\alpha 3}$
74.98(1)	1.750(3)	1.26(2)E4	0.163(6)	7.7(3)E4	Pb x-ray $k_{\alpha 1}$ and ^{63}Ge decay
84.89(8)	1.750(3)	909(100)	0.168(6)	5402(700)	Pb x-ray $k_{\beta 1} + k_{\beta 3}$
367.49(7)	2.7(2)	2114(200)	0.131(5)	1.6(1)E4	^{63}Ge decay
373.08(3)	2.7(2)	568(100)	0.130(5)	4369(900)	^{63}Ge decay
442.81(1)	1.95(2)	1.33(1)E4	0.121(4)	1.10(4)E5	^{63}Ge decay
482.42(8)	2.1(2)	1136(90)	0.117(4)	9747(800)	^{63}Ge decay
510.95(0)	3.089(4)	4.457(7)E5	0.114(4)	3.9(1)E6	$e^- + e^+$
627.01(4)	1.7(1)	925(40)	0.103(4)	8956(500)	^{63}Ge decay
636.32(7)	1.75(1)	664(50)	0.103(4)	6471(600)	-
637.7(1)	1.75(1)	266(50)	0.102(4)	2592(500)	-
641.15(4)	1.75(1)	847(40)	0.102(4)	8287(500)	^{63}Ge decay
647.40(6)	1.75(1)	593(40)	0.102(4)	5826(400)	^{63}Ge decay
650.68(6)	1.75(1)	504(30)	0.102(4)	4963(400)	-
670.3(1)	1.75(4)	208(30)	0.100(4)	2077(300)	-
709.08(8)	2.36(5)	645(40)	0.097(3)	6630(500)	^{63}Ge decay
722.18(3)	2.36(5)	2584(60)	0.096(3)	2.7(1)E4	^{63}Ge decay
794.4(2)	3.1(5)	339(40)	0.092(3)	3686(500)	-
911.53(5)	2.14(9)	700(40)	0.086(3)	8179(500)	-
921.08(8)	2.14(9)	364(30)	0.085(3)	4275(400)	-
925.03(7)	2.14(9)	547(30)	0.085(3)	6442(500)	^{63}Ge decay
954.21(8)	1.75(3)	269(20)	0.084(3)	3225(300)	^{63}Ge decay
1065.8(1)	1.75(8)	199(20)	0.079(3)	2532(300)	-
1332.9(1)	2.4(2)	271(30)	0.069(2)	3907(400)	(^{63}Ge decay)
1350.0(1)	2.49(8)	345(30)	0.069(2)	5015(400)	-
1363.59(4)	2.49(8)	1317(40)	0.068(2)	1.92(9)E4	^{63}Ge decay
1395.33(6)	1.75(2)	299(20)	0.068(2)	4431(400)	-
1495.07(7)	1.75(1)	204(20)	0.065(2)	3150(300)	-
1498.2(1)	1.75(1)	129(20)	0.065(2)	1998(300)	-
1505.10(9)	1.75(1)	31(10)	0.065(3)	486(200)	-
1690.6(2)	2.2(2)	150(20)	0.060(3)	2488(400)	-
1887.1(1)	1.75(3)	93(20)	0.056(3)	1663(300)	-
1936.8(2)	3(1)	43(20)	0.055(3)	775(400)	-
2409.3(1)	1.75(4)	67(10)	0.047(2)	1420(300)	-
2485.4(3)	4.4(6)	220(30)	0.046(2)	4756(700)	^{63}Ge decay
2765.1(2)	3.5(4)	177(20)	0.042(2)	4165(500)	^{63}Ge decay
2971.4(5)	5.2(2)	147(20)	0.040(2)	3686(600)	-
3365.7(5)	5(2)	105(20)	0.035(2)	2959(600)	-

Table 6.2: Results for the ^{63}Ge decay γ-ray prompt spectrum shown in Fig. 6.6. The intensity shown in the fifth column corresponds to the number of counts corrected by the γ-ray efficiency.

6.1.5. Gamma-gamma coincidence spectra for ^{63}Ge decay

From the γ-ray spectrum of the ^{63}Ge decay in Fig. 6.6, the energies and intensities of each γ-ray transition were obtained. From them each γ-ray corresponds to a transition between two levels in the daughter nucleus ^{63}Ga, however, only four were previously reported in Balamuth et. al [B$^+$91] and Weiszflog et. al [W$^+$01]. To obtain the energies of the excited states from which these γ-rays are emitted and determine which ones are emitted in cascade, the γ-γ coincidence projection spectra were constructed by gating on several γ-rays observed in the γ-spectrum for the ^{63}Ge decay shown in Fig. 6.6.

For each γ-ray observed in Fig. 6.6 an energy coincidence window was defined. Since some background γ-rays are also present in this region, a neighbouring region was used to subtract the background coincidences. In Fig. 6.7 the 442 keV γ-ray energy window is shown as an example. The blue interval indicates the γ-coincidence window, while the red interval denotes the neighbouring coincidence window used to subtract the background coincidences.

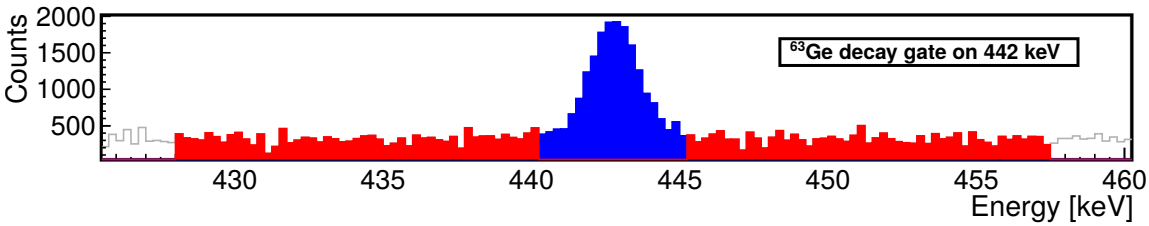

Figure 6.7: Energy window used in the γ-γ coincidence projection spectrum for the 442 keV γ-ray emitted in the ^{63}Ge decay. The coincidence window is shown in blue, while the background subtraction windows are shown in red. Events within the red intervals are weighted by the width of the energy region selected for this peak.

In Figs. 6.8 to 6.10, the γ-γ coincidence projection spectra gating on several

γ-rays observed and identified as belonging to ^{63}Ge beta decay in Fig. 6.6 are shown. The coincidence analysis will be discussed in Section 7.1.

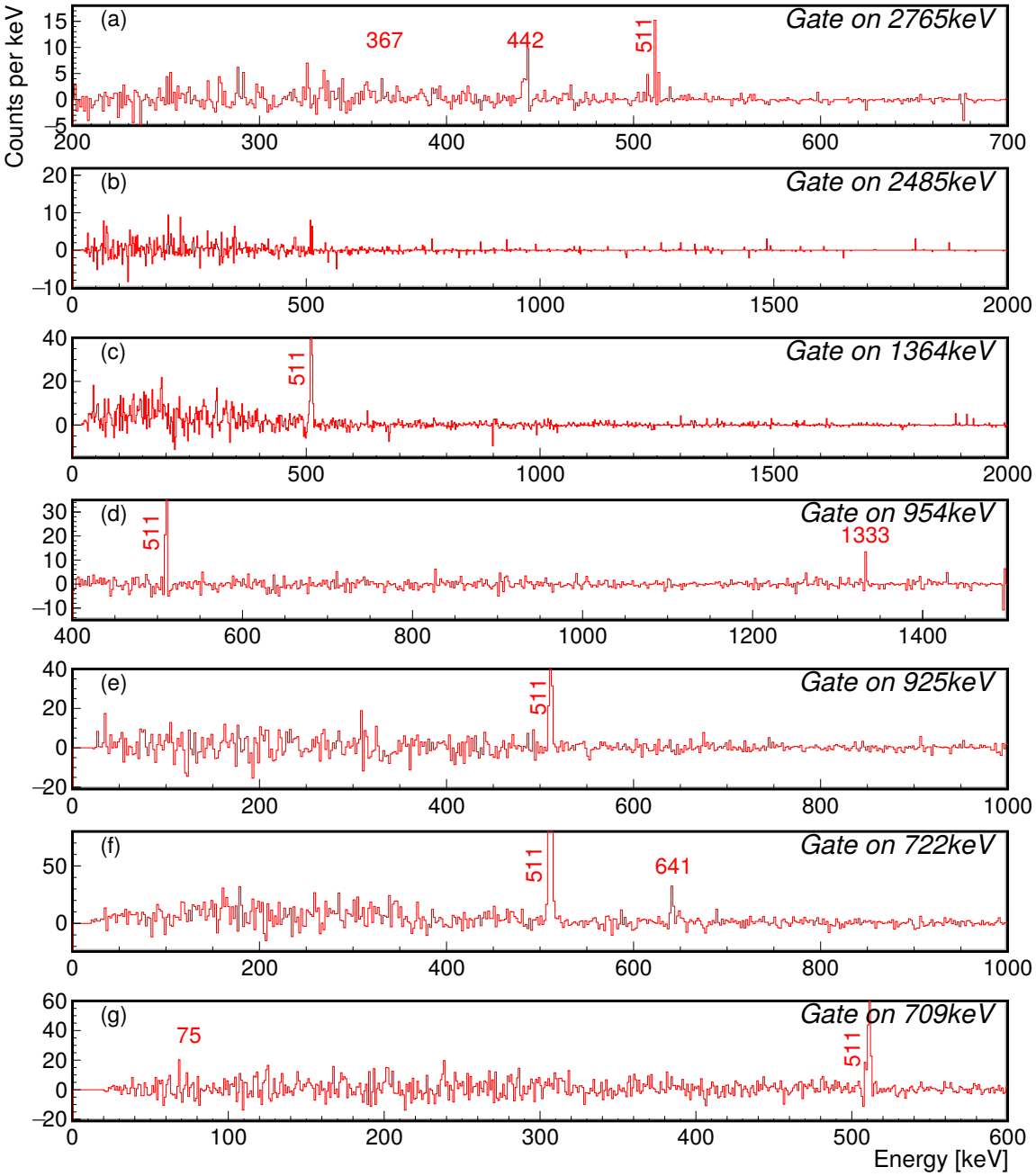

Figure 6.8: γ-γ background subtracted coincidence spectra for the ^{63}Ge decay, constructed imposing 0.8 μs coincidence window for γ-rays, for: (a) 2765 keV, (b) 2485 keV, (c) 1364 keV, (d) 954 keV, (e) 925 keV, (f) 722 keV, (g) 709 keV γ-ray energy (continues on next page).

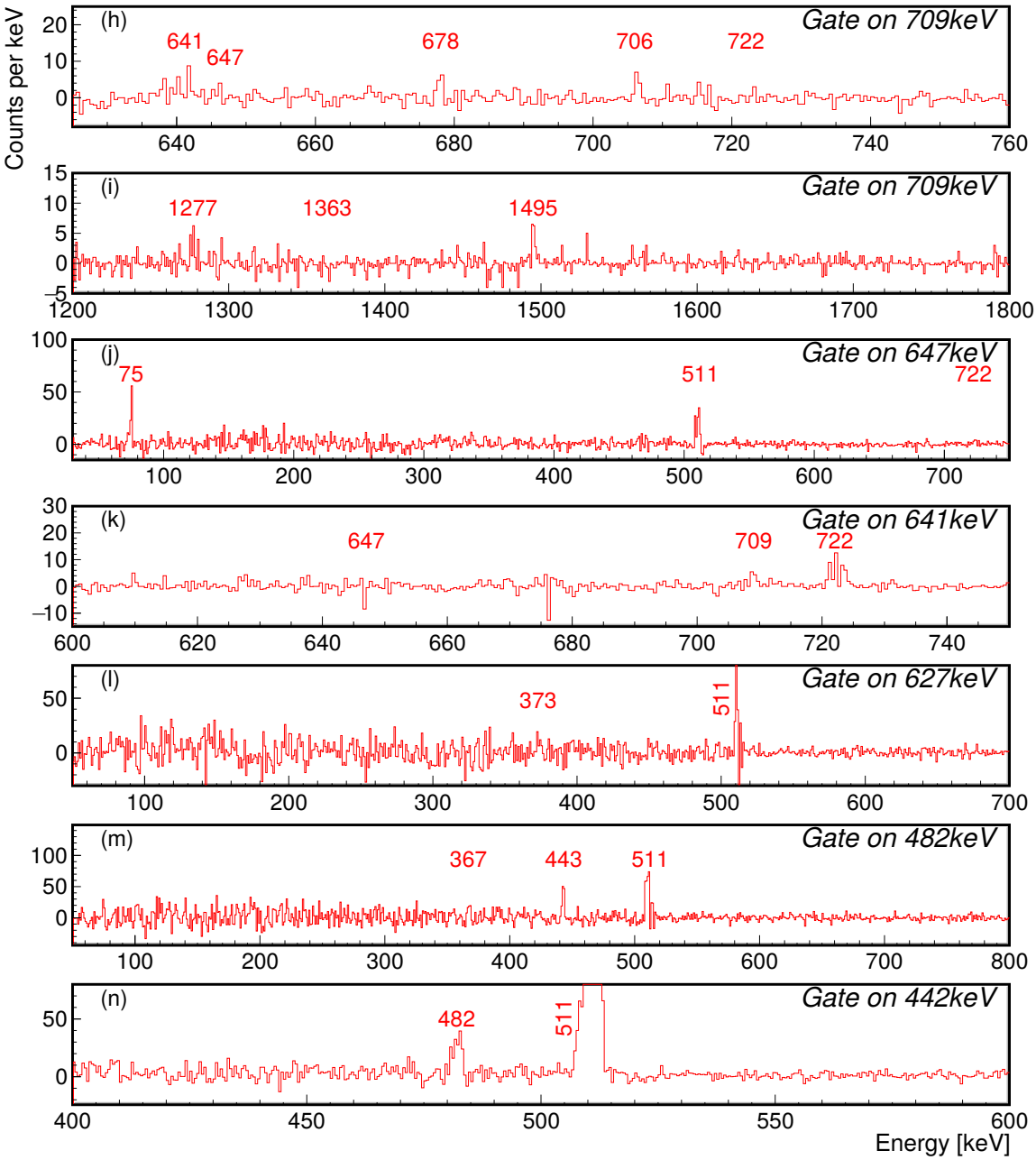

Figure 6.9: (continuation) (h) 709 keV continuation, (i) 709 keV continuation, (j) 647 keV, (k) 641 keV, (l) 627 keV, (m) 482 keV, (n) 442 keV γ-ray energy (continues on next page).

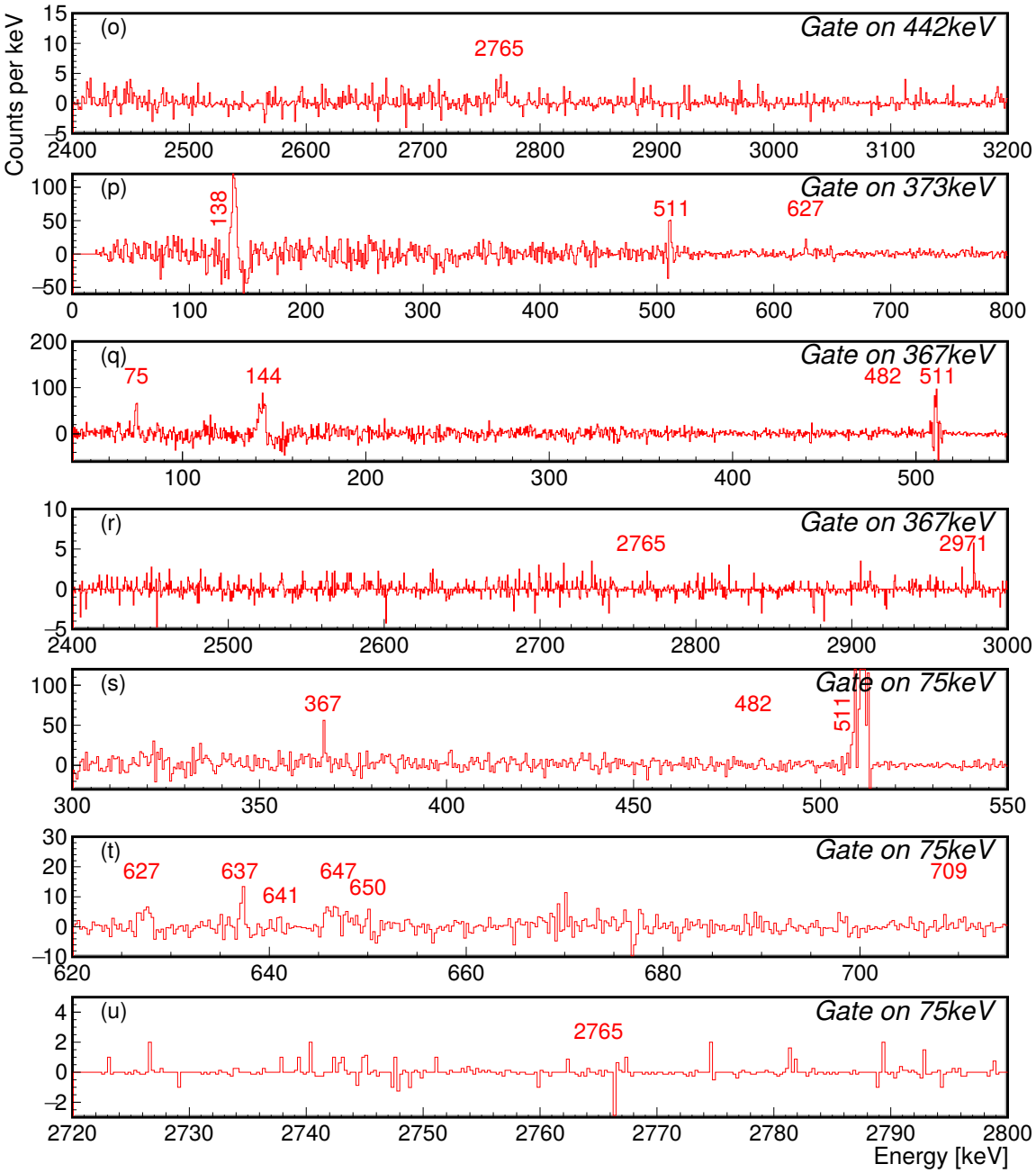

Figure 6.10: (continuation) (o) 442 keV continuation, (p) 373 keV, (q) 367 keV, (r) 367 keV continuation, (s) 75 keV, (t) 75 keV continuation, (u) 75 keV continuation.

6.1.6. ^{63}Ge half-life determination using the 442 keV γ-ray

The 443 keV γ-ray is assigned to the ^{63}Ge decay by Weiszflog et. al [W$^+$01]. Since this γ-ray is exclusive to the ^{63}Ge decay, it can be used in order to avoid the daughter nuclei contributions to the implantation-decay correlation involved in the analysis using the betas, measuring a more accurate half-life value by imposing a β-delayed γ-ray energy window. A time condition of the coincidence window within $[0, 0.8] \ominus [-80, -40]$ms, and an energy coincidence window within $[440.521, 445.159] \ominus [428.923, 440.521] \ominus [445.159, 456.757]$ keV were used to select the β-γ coincidences for the 442 keV γ-ray. The correlation spectrum is shown in Fig. 6.11. Implantation-decay correlations were fitted using the solution of the Bateman equation corresponding to the mother decay only $A_0(t;^{63}\,\mathrm{Ge})$ described in Appendix H, and a linear background $a_0 + a_1 t$ within 10 s of the implantation-decay correlation window. The function used to fit the implantation-decay correlations was,

$$A(t) = a_0 + a_1\, t + (1 - DT)\, \varepsilon_{\beta\gamma}\, A_0(t;^{63}\,\mathrm{Ge}) \tag{6.1}$$

where $DT = 17.7(2)\%$ corresponds to the measured dead time discussed in Appendix D, and $\varepsilon_{\beta\gamma} = \varepsilon_\beta\, \varepsilon_{442\,keV}$ corresponds to the detection efficiency of the γ-gated correlations. The results of the fit can be seen in Fig. 6.11 and Table 6.3.

Nucl.	N_0	$T_{1/2}$	$\varepsilon_{\beta\gamma}$	DT
^{63}Ge	3620209	152.7(28)ms	$4.054(52) \times 10^{-3}$	0.176922
^{63}Ga	0	32400ms	0	0.176922
^{63}Zn	0	2308200ms	0	0.176922

(a) Fitted parameters corresponding to the Bateman equations.

Parameter	Comment
a_0	10.04(11)
a_1	$-0.50(19) \times 10^{-4}$
χ^2_i/NDF	1968/1995
Fit Method	RMIELN

(b) Statistics and background fitted parameters.

Table 6.3: The results of the fits for ^{63}Ge decay in coincidence with the $E_\gamma =$ 442 keV shown in Fig. 6.11.

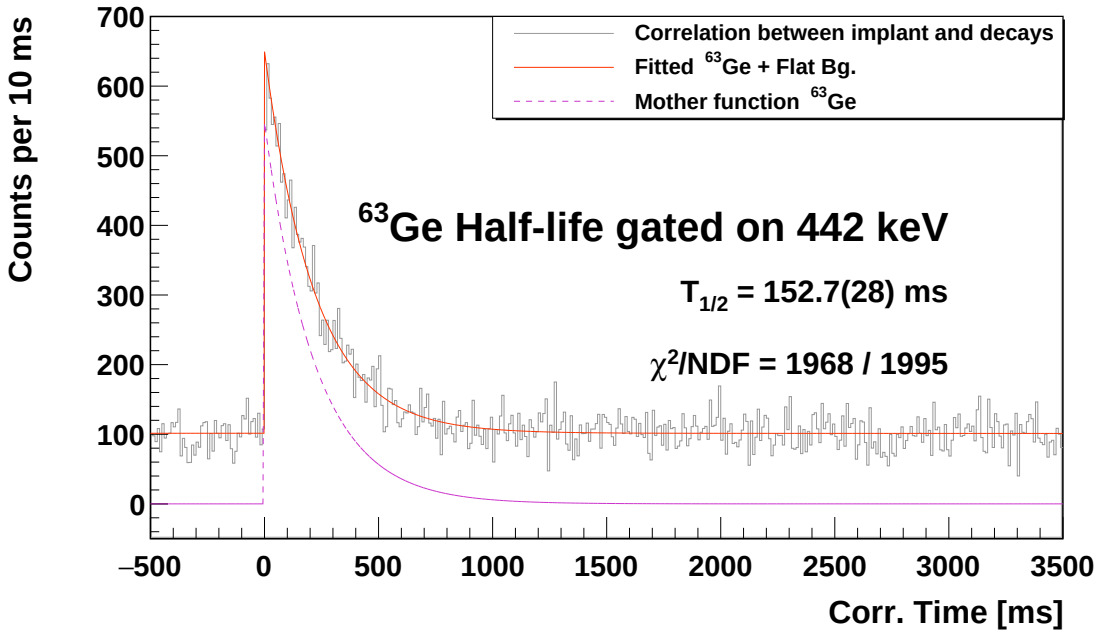

Figure 6.11: Correlation time distribution for ^{63}Ge decay in coincidence with $E_\gamma = 442$ keV.

6.1.7. ^{63}Ge half-life determination using all decay members

Although the half-life measured by using the γ-ray coincidence condition is more accurate that when it is not imposed, it also decreases the statistics associated with $\varepsilon_\gamma(442\text{ keV})$. In this section, the half-life for ^{63}Ge will be measured taking into account all decay members. The details are discussed in Appendix H.

The implantation-decay time correlation for ^{63}Ge was obtained correlating implantations of ^{63}Ge in the central DSSSD of the WAS3ABi active stopper with all decays within the $[0, 10]$ s$\ominus[-10, 0]$ s time window. The implantation-decay correlation were fitted considering the activity of ^{63}Ge $A_0(t;^{63}\text{Ge})$, the beta decay daughter ^{63}Ga $A_1(t;^{63}\text{Ga})$, the beta decay granddaughter ^{63}Zn $A_2(t;^{63}\text{Zn})$, and a linear back-

ground $a_0 + a_1\, t$. The function used to fit the implantation-decay correlations was,

$$A(t) = a_0 + a_1\, t + (1 - DT)\, \left(\varepsilon_\beta\, A_0(t;^{63}\,\mathrm{Ge}) + \varepsilon_\beta\, A_1(t;^{63}\,\mathrm{Ga}) + \varepsilon_\beta\, A_2(t;^{63}\,\mathrm{Zn})\right) \quad (6.2)$$

where ε_β corresponds to the beta efficiency and $DT = 17.7(2)\%$ is the measured dead-time. The half-lives of the daughter nuclei were known prior to this work [WAK+17], and were fixed during the fit. The results of the fitting for the implantation-decay correlation for ^{63}Ge can be seen in Fig. 6.12, while the fitted parameters are shown in Table 6.4.

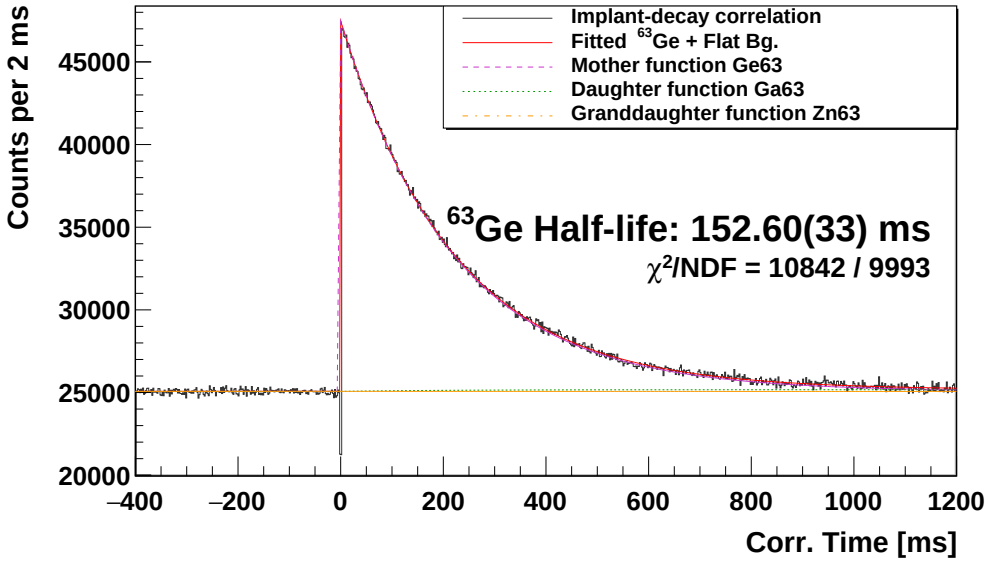

Figure 6.12: Half-life measurement for ^{63}Ge decay, using all decay members. The daughter half-lives were fixed according to reported values [WAK+17, AKW+17].

Iso.	N_0	$T_{1/2}$	ε_β	DT
^{63}Ge	3620209	152.60(33)ms	0.8277(12)	0.176922
^{63}Ga	0	32400ms	0.8277(12)	0.176922
^{63}Zn	0	2308200ms	0.8277(12)	0.176922

(a) Fitted parameters corresponding to Bateman equations.

Parameter	Comment
A_0	12535.067(35)
A_1	$-4.5344(70) \times 10^{-3}$
χ^2_i/NDF	10842/9993
Fit Method	RMIELN

(b) Fitted statistics and background adjusted parameters.

Table 6.4: The results of the fits for ^{63}Ge decay using all decay members as shown in Fig. 6.12.

6.1.8. Correction for the 75 keV γ-ray

In Balamuth et al. [B+91] and in Weiszflog et al. [W+01], the 75 keV γ-ray appears in the level scheme of excited states in ^{63}Ga. Also the γ-γ spectra in Figs. 6.10(s) - 6.10(u) exhibit γ-ray coincidences belonging to the ^{63}Ge decay as will be discussed in Section 7.1, indicating that this peak corresponds to a mix of lead x-ray fluorescence and ^{63}Ge decay γ-rays.

The contribution from the Pb x-ray as detailed in Appendix K, corresponds to the $k_{\alpha 2}$ and $k_{\alpha 3}$ for the 72.9 keV and to $k_{\alpha 1}$ for the 75.0 keV γ-ray as can be found in Table K.1 where the fluorescence lead x-rays are tabulated per 100 K-shell vacancies. To quantify the number of counts in the 75 keV peak corresponding to the decay of ^{63}Ge, the 72.9 keV line was used to estimate the number of counts produced by the x-ray contribution to the 75 keV peak. Using the Eq. 5.4 the expected number of counts in the γ-peak can be expressed as:

$$C_\gamma(75\text{ keV}) = \left(I_{\text{xray}}(75\text{ keV}) + I_\gamma(75\text{ keV})\right)\varepsilon_\gamma(75\text{ keV}) \cdot (1 - DT) C_w \varepsilon_\beta N_{imp}\ , \tag{6.3}$$

where $C_\gamma(75\text{ keV})$ corresponds to the number of counts observed in the photo-peak, $I_{\text{xray}}(75\text{ keV})$ corresponds to the x-ray intensity of the 75 keV peak, $I_\gamma(75\text{ keV})$ cor-

responds to the intensity of the 75 keV from the ^{63}Ga γ-ray, ε_γ is the γ-ray efficiency for 75 keV, DT is the measured dead-time for the implant events, ε_β is the beta efficiency, C_w is the correction for the correlation window length and N_{imp} is the number of implantations.

In order to obtain the x-rays contribution $I_{\text{xray}}(75\text{ keV})$ we can use the ratio between lead K_α lines. The ratio between intensities for peaks placed around 72.9 keV and 75.0 keV due to only x-rays is,

$$\begin{aligned} R &= \frac{I_{\text{xray}}(72\text{ keV})}{I_{\text{xray}}(75\text{ keV})}\ , \\ R &= \frac{I(k_{\alpha 2}) + I(k_{\alpha 3})}{I(k_{\alpha 1})}\ , \\ R &= 0.600_{17}\ . \end{aligned} \tag{6.4}$$

Using this ratio we can estimate the x-ray contribution in 75 keV γ-ray peak by using the intensity of the 72 keV peak, $I_{\text{xray}}(75\text{ keV}) = I_{\text{xray}}(72\text{ keV})/R$. Then the intensity in 75 keV due to x-ray can be written as,

$$I_{\text{xray}}(75\text{ keV}) = \frac{1}{R} \cdot \frac{C(72)}{\varepsilon_\gamma(72\text{ keV}) \cdot (1 - DT) C_w \varepsilon_\beta N_{imp}}\ . \tag{6.5}$$

Moreover, the total intensity of the transition between the state at **75 keV** corresponds to a mixing of γ-ray transition and conversion electron emission. The conversion electrons are not being detected by the WAS3ABi active stopper since the energy threshold for beta particles are setted to 133 keV for each strip. Even if they were above the threshold, it is not clear that they could be distinguished from the beta decay spectrum. For this reason we estimate the conversion electron contribution in the 75 keV intensity using the α_{tot} coefficient $\alpha_{\text{tot}} = 0.28$ for this case

as proposed by Balamuth et al. [B+91] and the γ-ray intensity of 75 keV,

$$I_{\text{decay}} = (1 + \alpha_{\text{tot}}) \cdot I_{\gamma}(75 \text{ keV}) \ . \tag{6.6}$$

Taking into account the correction for conversion electrons in Eq. 6.6 and our estimation of the x-rays contribution to the γ-ray peak in Eq. 6.5 to obtain the 75 keV transition from Eq. 6.3,

$$I_{\text{decay}} = \frac{(1 + \alpha_{\text{tot}})}{(1 - DT) C_w \varepsilon_\beta N_{imp}} \cdot \left(\frac{C_\gamma(75\text{keV})}{\varepsilon_\gamma(75 \text{ keV})} - \frac{C_\gamma(72\text{keV})}{\varepsilon_\gamma(72\text{keV}) \cdot R} \right) . \tag{6.7}$$

6.2. ^{64}As decay Analysis

The ^{64}As decay analysis is the second step before studying the nucleus of interest ^{64}Se. As the ^{64}Se beta decay will populate excited states in ^{64}As, and since their half-lives are comparable, γ-rays will be mixed in the spectrum. In addition to this, previous knowledge of excited states in ^{64}Ge came only from in-beam experiments [ELG+91, FEA+03]. All of this suggests that it is necessary to characterize all new γ-rays observed in this beta decay before studying the mother nucleus. A diagram of the expected decay for this nucleus is shown in Fig. 6.13.

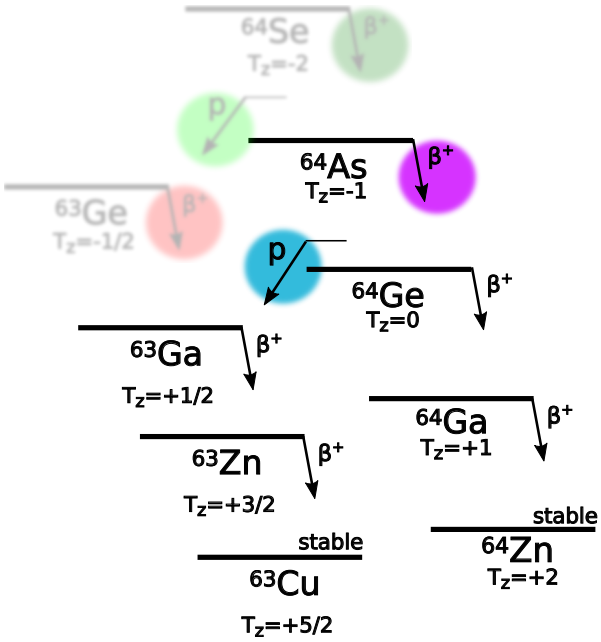

Figure 6.13: Diagram for the ^{64}As decay, as a necessary ingredient in the study of the nucleus of interest ^{64}Se. Half-lives comparable to that of ^{64}Se are marked with coloured circles.

Another interesting fact for this decay that will be discussed in Section 6.3.4, is that this nucleus is a beta-delayed proton emitter. This proton emission may also populate excited states in the ^{63}Ga and this gives additional information about the structure of ^{63}Ga.

6.2.1. Previous knowledge of the excited states in ^{64}Ge: The beta decay daughter of ^{64}As

This nucleus was studied in in-beam experiments by Ennis et al. [ELG+91], and the level scheme proposed is shown in Fig. 6.14a. Another in-beam study was performed by Farnea et al. at LNL [FEA+03], and its level scheme is shown in Fig. 6.14. The γ-rays observed in both studies are marked with red ellipses, and the γ-rays also observed in the present study are marked with red filled ellipses. In Section 7.2 we shall return to this discussion.

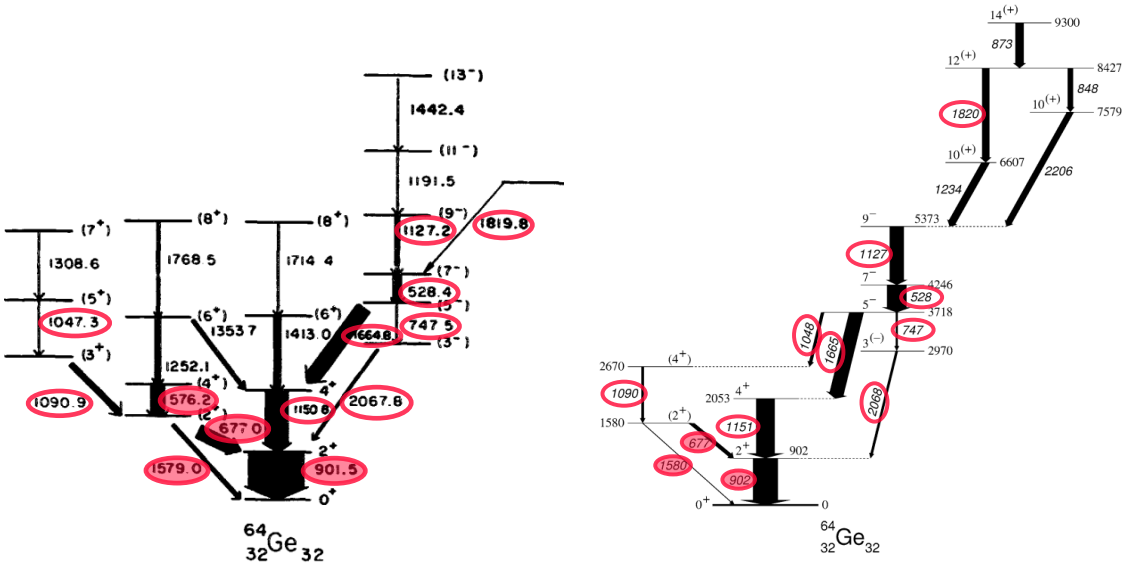

(a) Ennis et al. [ELG+91]. **(b)** Farnea et al. [FEA+03].

Figure 6.14: Level scheme of ^{64}Ge reported in previous works [ELG+91, FEA+03]. Gamma-rays observed in both works are marked with red ellipses, γ-rays observed in this work are marked with a red filled ellipse.

6.2.2. Implant-decay correlation for ^{64}As decay

The previously reported value for the ^{64}As decay half-life is 40(30) ms [AKW+17]. For the present work a common criterion of seven half-lives of the mother nucleus was established (see Appendix G). For the present case, the time correlation window is $[-440, 440]$ ms, avoiding symmetrically the first millisecond. Nevertheless in Fig. 6.15 a plot of the implantation-decay correlations within a wider time correlation window of 10 s is shown to clarify that after the seven half-life interval (in green), most of the correlations would correspond to random coincidences (in red). Then the green region corresponding to the seven half-lives interval will be used in the following sections to construct the beta, proton, and γ-ray spectra for this decay.

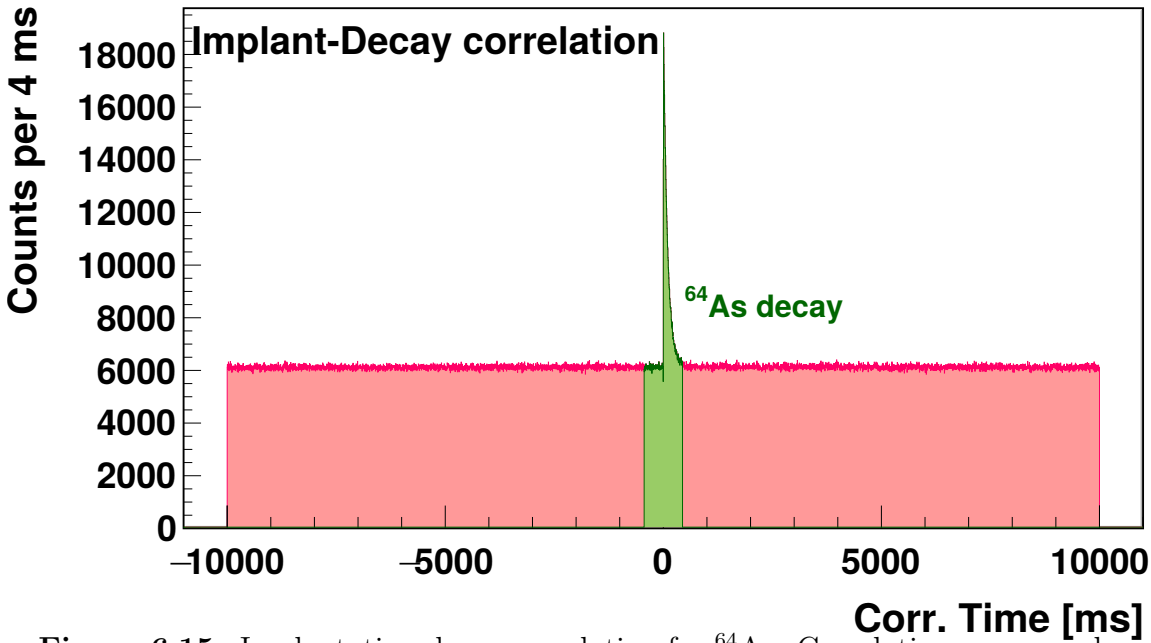

Figure 6.15: Implantation-decay correlation for ^{64}As. Correlations were made up to 10 s forward and backward, but to obtain the proton and γ-ray spectra the implantation-decay correlations were constrained to the 440 ms time window (seven mother half-lives) shown in green.

6.2.3. Beta-delayed proton spectrum for ^{64}As decay

The proton spectrum was constructed using a correlation window between the implantation and decays within the $C_w = [1, 440] \ominus [-440, -1]$ms time window. In Fig. 6.16 and Table 6.5 the two proton spectra were obtained using the A10E700D110 condition (implantations next to the maximum energy beta pixel), and A10E700NMD condition (implantations next to any beta pixel).

The spectrum constructed using the A10E700D110 condition (see Fig. 6.16a) has much better resolution for the proton peaks and was used to define the proton peak energies. On the other hand, the spectrum constructed with the A10E700NMD condition in Fig. 6.16b and Table 6.6 has higher beta efficiency and was used to construct the γ-ray spectrum in prompt coincidence with betas[1].

$E^{Obs.}$ [keV]	E^{p} [keV]	Width	Amplitude	Integral
1493(10)	1363(29)	70.0(17)	529(39)	2064(130)
1846.5(76)	1716(28)	70.0(17)	918(40)	3579(190)
2224(11)	2094(29)	70.0(17)	839(62)	3272(200)
2464.0(98)	2334(29)	70.0(17)	920(63)	3588(220)
2847(14)	2717(30)	70.0(17)	366(27)	1425(90)
3203(29)	3073(40)	70.0(17)	169(32)	660(76)
3453(30)	3323(40)	70.0(17)	189(47)	737(110)
3701(27)	3571(38)	70.0(17)	234(41)	911(100)
4067(29)	3937(40)	70.0(17)	181(23)	704(61)
4505(29)	4375(40)	70.0(17)	142(14)	553(40)
5161(26)	5031(38)	70.0(17)	50.5(80)	197(20)

Table 6.5: The results of fitting for the proton spectrum shown in Fig. 6.16a of the ^{64}As decay using the A10E700D110 condition. The proton energy E^{p} was obtained by subtracting from the observed energy E^{obs}, an energy shift of 130(27) keV due to the deformation produced as an effect of the summing of the proton particles with the ΔE of the betas happening at the same time. The width and amplitude are related to the characterisation of the proton function that can be found in Appendix E.

[1] As explained in Section 3.2, the EURICA GeHP array was triggered by the active stopper WAS3ABi.

$E^{Obs.}$ [keV]	E^{p} [keV]	Width	Amplitude	Integral
1505.0(15)	1375(27)	68.3(26)	560.2(0)	2218(100)
1825.0(22)	1695(27)	68.3(26)	907.1(0)	3591(160)
2205(26)	2075(38)	68.3(26)	836.8(0)	3313(150)
2464.4(72)	2334(28)	68.3(26)	922.5(0)	3652(170)
2841(13)	2711(30)	68.3(26)	364.1(0)	1441(66)
3204(30)	3074(40)	68.3(26)	162.5(0)	643(29)
3472(40)	3342(48)	68.3(26)	187.9(0)	744(34)
3703(30)	3573(40)	68.3(26)	235.1(0)	931(43)
4081(32)	3951(42)	68.3(26)	179.5(0)	711(33)
4524(28)	4394(39)	68.3(26)	142.4(0)	564(26)
5145(39)	5015(48)	68.3(26)	50.9(0)	201.6(92)

Table 6.6: The results of the fits for the proton spectrum following ^{64}As decay using the A10E700NMD condition in Fig. 6.16b. The proton energy E^{p} was obtained by subtracting the observed energy E^{obs}, the energy shift (130(27) keV), due to the coincidence with the beta particle. The width and amplitude are related to the characterisation of the proton function that can be found in Appendix E. In this case, the amplitude parameters were fixed at the value obtained in the A10E700D110 fit.

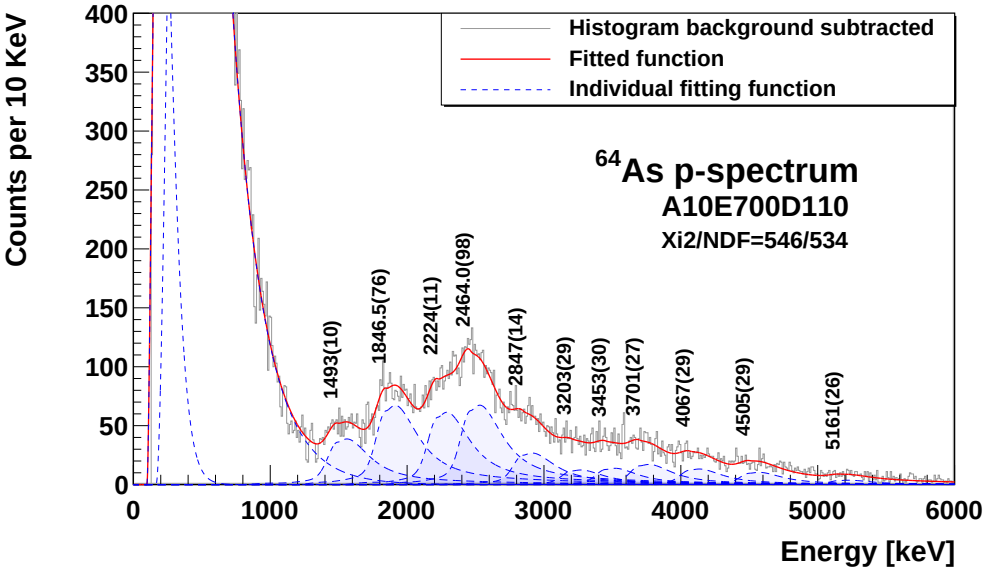

(a) Proton spectrum for the ^{64}As decay using the A10E700D110 condition.

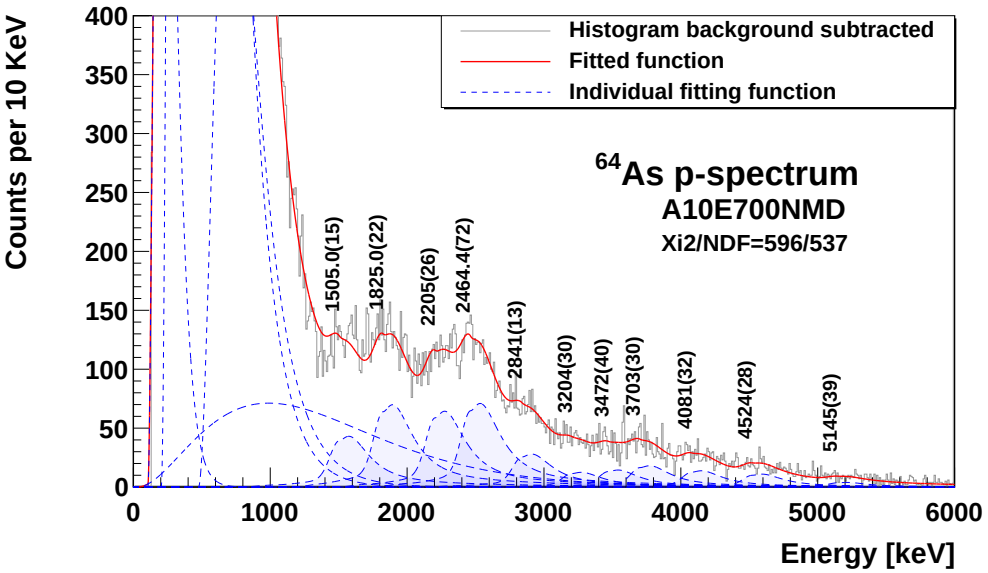

(b) Proton spectrum for the ^{64}As decay using the A10E700NMD condition.

Figure 6.16: Proton spectrum for ^{64}As decay, using both A10E700D110 and A10E700NMD conditions, described in Section 5.1.2, within an implant-decay correlation window of $C_w = [1, 440] \ominus [-440, -1]$ms. Proton peaks are filled in blue, while the beta spectrum contribution is drawn with a dashed blue line.

6.2.4. Gamma spectrum for ^{64}As decay

To obtain the γ-ray spectrum for ^{64}As decay, implantation-decay correlations were looked at within the $C_w = [1, 440] \ominus [-440, -1]$ms time correlation window as discussed in Section 6.2.2. Fig. 6.17 shows a scatter plot of the EURICA DGF (Digital Gamma Finder) digitalizer energy -Y axis- and time -X axis- signals. In this figure the γ-prompt condition was imposed within the $[0, 0.8] \ominus [-80, -40]\mu$s β-γ coincidence window, indicated between the red lines. In addition, the A10E700NMD condition was used in the implantation-decay coincidences as explained in Section 6.2.3. The γ-ray spectrum is shown in Fig. 6.18 where the γ-rays identified as transitions in ^{64}As decay are marked with ♣.

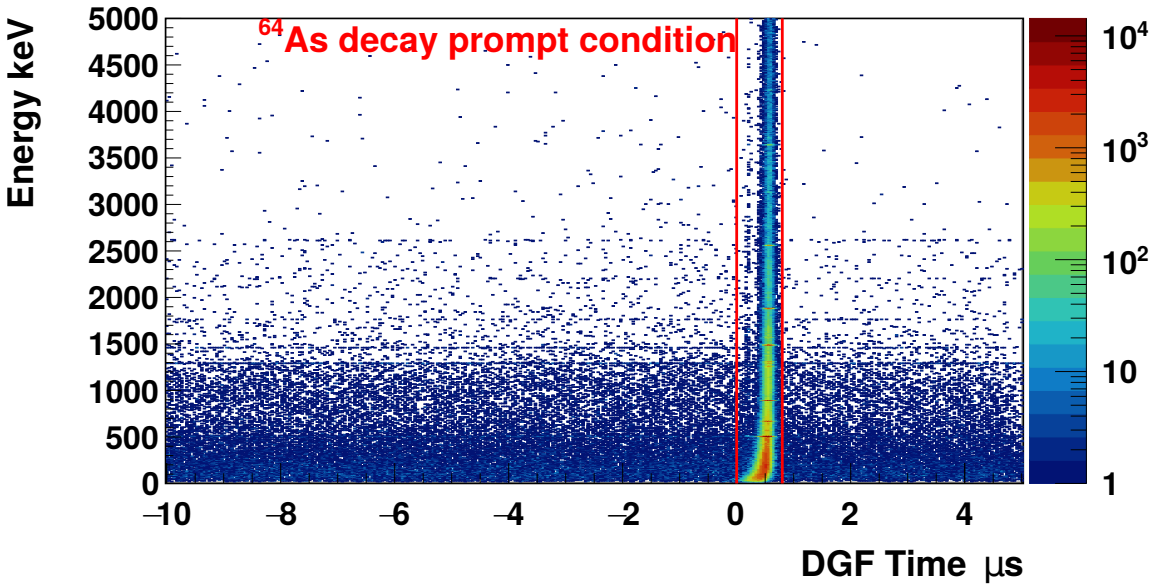

Figure 6.17: ^{64}As decay energy-time of γ-ray spectrum, requiring the implantation of ^{64}As condition over the PID plot. The γ-prompt condition is shown between two red lines (0.8 μs width) and corresponds to γ-rays emitted in ^{64}As decay.

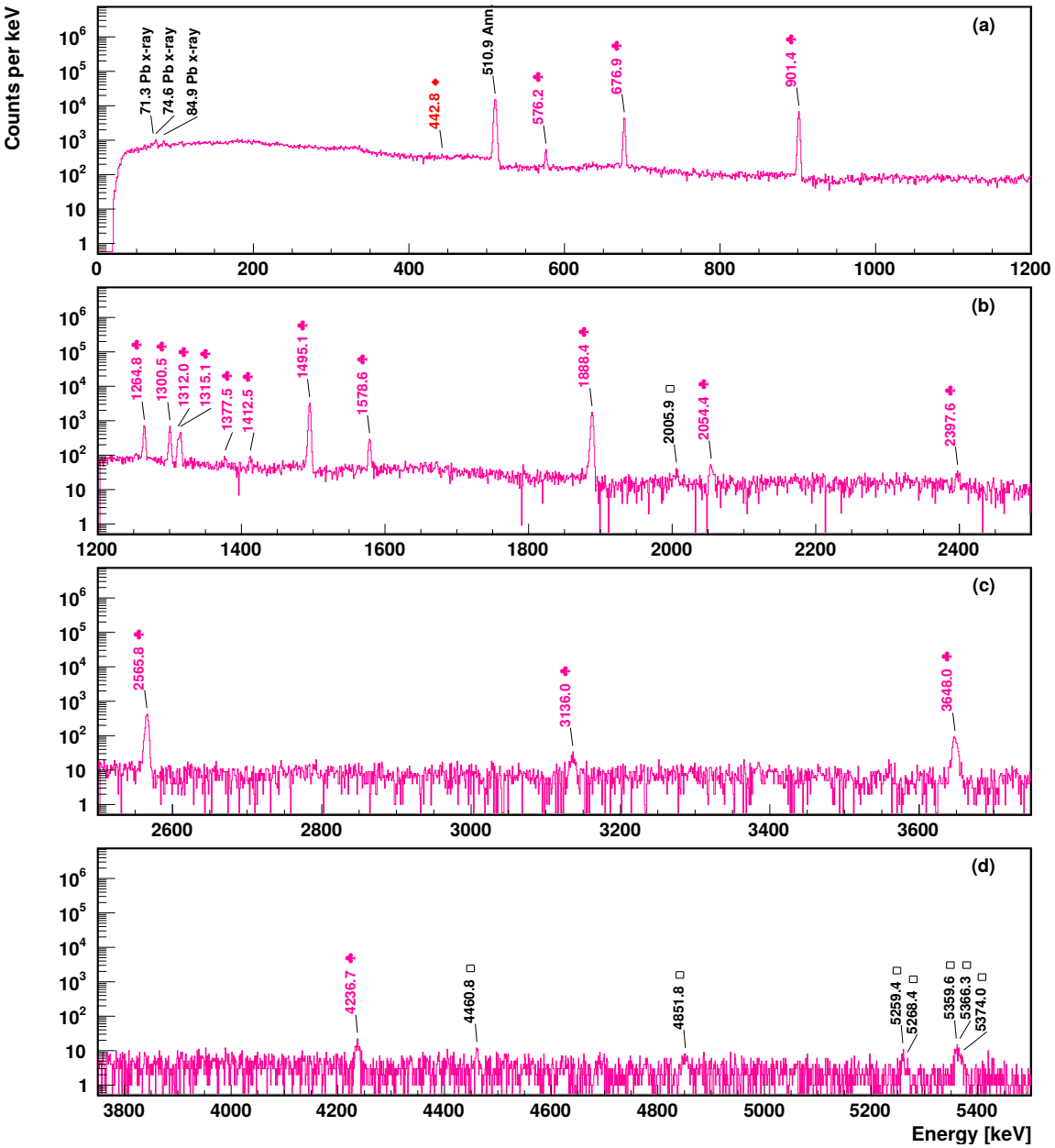

Figure 6.18: Gamma spectrum for ^{64}As decay imposing the β-γ coincidence window $G_w = [0, 0.8] \ominus [-80, -40]$ μs, and the implant-decay correlation window $C_w = [1, 440] \ominus [-440, -1]$ ms. Unplaced γ-rays are shown in black marked with $\square$, together with the lead x-ray and the positron annihilation peak. The γ-rays assigned to ^{64}As β decay are shown in pink and marked with $\clubsuit$. Also the γ-rays assigned to ^{63}Ge decay are shown in red and marked with $\diamond$.

Each peak in the γ-ray spectrum in Fig. 6.18 was fitted and tabulated in Table 6.7, where the energy, width and counts are presented together with the γ-ray intensity obtained using the efficiency correction given in Equation (3.1).

Twenty four peaks were observed in the γ-ray spectrum in Fig. 6.18 in coincidence with the ^{64}As beta decay. This included lead fluorescence x-rays, the positron annihilation peak, and fourteen γ-rays identified in the ^{64}As beta decay:

Pb xrays The 71.3 keV, 74.6 keV, and 84.9 keV γ-ray energies correspond to the $k_{\alpha 2}$ plus $k_{\alpha 3}$, $k_{\alpha 1}$, and $k_{\beta 1}$ plus $k_{\beta 3}$ lead x-rays respectively.

♣ The 576.2 keV, 676.9 keV, 901.4 keV, 1264.8 keV, 1300.5 keV, 1312.0 keV, 1315.1 keV, 1495.1 keV, 1578.6 keV, 1888.4 keV, 2054.4 keV, 2565.8 keV, 3136.0 keV, and 3648.0 keV peaks were identified as belonging to the ^{64}As decay.

♢ The 442.8 keV peak was identified in the decay of ^{63}Ge.

□ The 608.6 keV, 1377.5 keV, 1692.4 keV, 4236.7 keV, and 4851.8 keV peaks remain as unplaced γ-rays.

Energy keV	FWHM keV	Counts	Efficiency (ε_γ)	Intensity	Comments
71.3(2)	2.5(2)	369(60)	0.160(6)	2305(400)	Pb x-ray $k_{\alpha 2} + k_{\alpha 3}$
74.63(9)	2.5(2)	923(70)	0.163(6)	5673(500)	Pb x-ray $k_{\alpha 1}$
84.9(1)	2.5(2)	621(70)	0.168(6)	3688(400)	Pb x-ray $k_{\beta 1} + k_{\beta 3}$
442.8(1)	1.75(6)	169(30)	0.121(4)	1398(300)	^{63}Ge decay
510.95(1)	3.08(1)	5.16(2)E4	0.114(4)	4.5(2)E5	$e^- + e^+$
576.20(5)	2.0(1)	843(40)	0.108(4)	7838(500)	^{64}As decay
676.90(1)	2.24(2)	1.13(1)E4	0.100(4)	1.13(4)E5	^{64}As decay
901.42(1)	2.43(2)	1.75(1)E4	0.086(3)	2.03(7)E5	^{64}As decay
1264.85(3)	2.70(7)	1906(50)	0.072(3)	2.7(1)E4	^{64}As decay
1300.47(3)	2.68(5)	1773(50)	0.070(2)	2.5(1)E4	^{64}As decay
1311.97(8)	2.68(5)	690(40)	0.070(2)	9853(600)	^{64}As decay
1315.14(5)	2.68(5)	1151(40)	0.070(2)	1.65(9)E4	^{64}As decay
1377.5(2)	3.3(5)	146(20)	0.068(2)	2150(300)	^{64}As decay
1412.5(2)	3.3(4)	177(20)	0.067(2)	2640(400)	^{64}As decay
1495.07(1)	3.00(3)	1.01(1)E4	0.065(2)	1.56(6)E5	^{64}As decay
1578.60(6)	3.2(1)	893(30)	0.063(3)	1.42(9)E4	^{64}As decay
1888.41(2)	3.49(4)	6397(80)	0.056(3)	1.14(6)E5	^{64}As decay
2005.9(5)	5(2)	93(20)	0.054(3)	1725(300)	-
2054.4(3)	4.9(5)	189(20)	0.053(3)	3562(400)	^{64}As decay
2397.6(4)	4.8(6)	87(10)	0.047(2)	1836(300)	^{64}As decay
2565.77(4)	4.69(8)	1996(40)	0.045(2)	4.4(2)E4	^{64}As decay
3136.0(4)	5.2(1)	116(10)	0.038(2)	3052(400)	^{64}As decay
3648.0(1)	5.20(1)	564(30)	0.033(2)	1.7(1)E4	^{64}As decay
4236.7(4)	5.20(9)	99(10)	0.027(1)	3716(500)	^{64}As decay
4460.8(4)	3.5(8)	33(8)	0.024(1)	1357(300)	-
4852(2)	5.2(3)	27(8)	0.021(1)	1312(400)	-
5259.4(5)	4.8(9)	34(8)	0.0160(8)	2150(500)	-
5268(3)	4.8(9)	10(5)	0.0159(8)	632(300)	-
5359.6(6)	5.2(1)	63(10)	0.0147(7)	4296(800)	-
5366.3(9)	5.2(1)	41(9)	0.0146(7)	2824(600)	-
5374.0(6)	5.2(1)	12(6)	0.0145(7)	859(400)	-

Table 6.7: The result of the fitting for ^{64}As decay γ-ray prompt spectrum shown in Fig. 6.18. Intensity shown in the fifth column corresponds to the number of counts corrected by the γ-ray efficiency.

6.2.5. Gamma-gamma coincidence spectra for ^{64}As decay

From the γ-ray spectrum of the ^{64}As decay in Fig. 6.18, the energy and intensity were obtained for each γ-ray. Nevertheless, only four of the γ-rays were previously reported by Ennis et. al [ELG+91] and by Farnea et. al [FEA+03]. To obtain the energies of the levels from which these γ-rays are emitted and hence those which are emitted in cascade, the γ-γ coincidence projection spectra were constructed by gating on several γ-rays observed in the γ-spectrum for ^{64}As decay in Fig. 6.18.

For each γ-ray observed in Fig. 6.18 an energy coincidence window was defined. An example of these coincidence windows is shown in Fig. 6.19 for the $E_\gamma = 576$ keV peak, where the blue region corresponds to the γ-coincidence window, while the red region corresponds to the interval used to remove the γ-γ coincidence background.

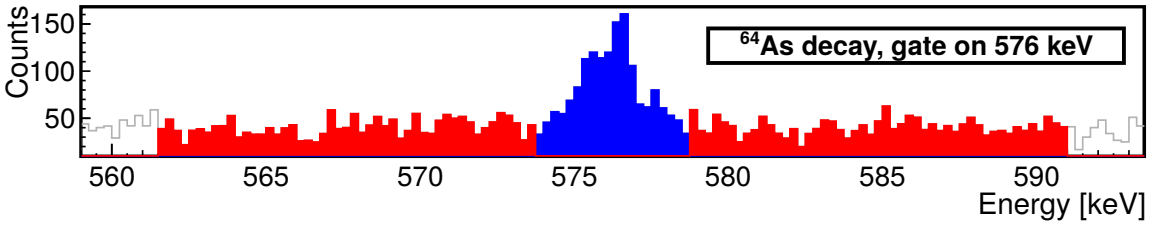

Figure 6.19: Energy window used in the γ-γ coincidence projection spectrum for the 576 keV γ-ray energy emitted in ^{64}As decay. The coincidence window is shown in blue, while the γ-γ background subtraction windows are shown in red, normalized to the width of the energy region selected for this peak.

In Figs. 6.20-6.23 the γ-γ coincidence projection spectra gating on several γ-rays assigned to ^{64}As decay in Fig. 6.18 are shown. The γ-coincidence analysis will be discussed in Section 7.2.

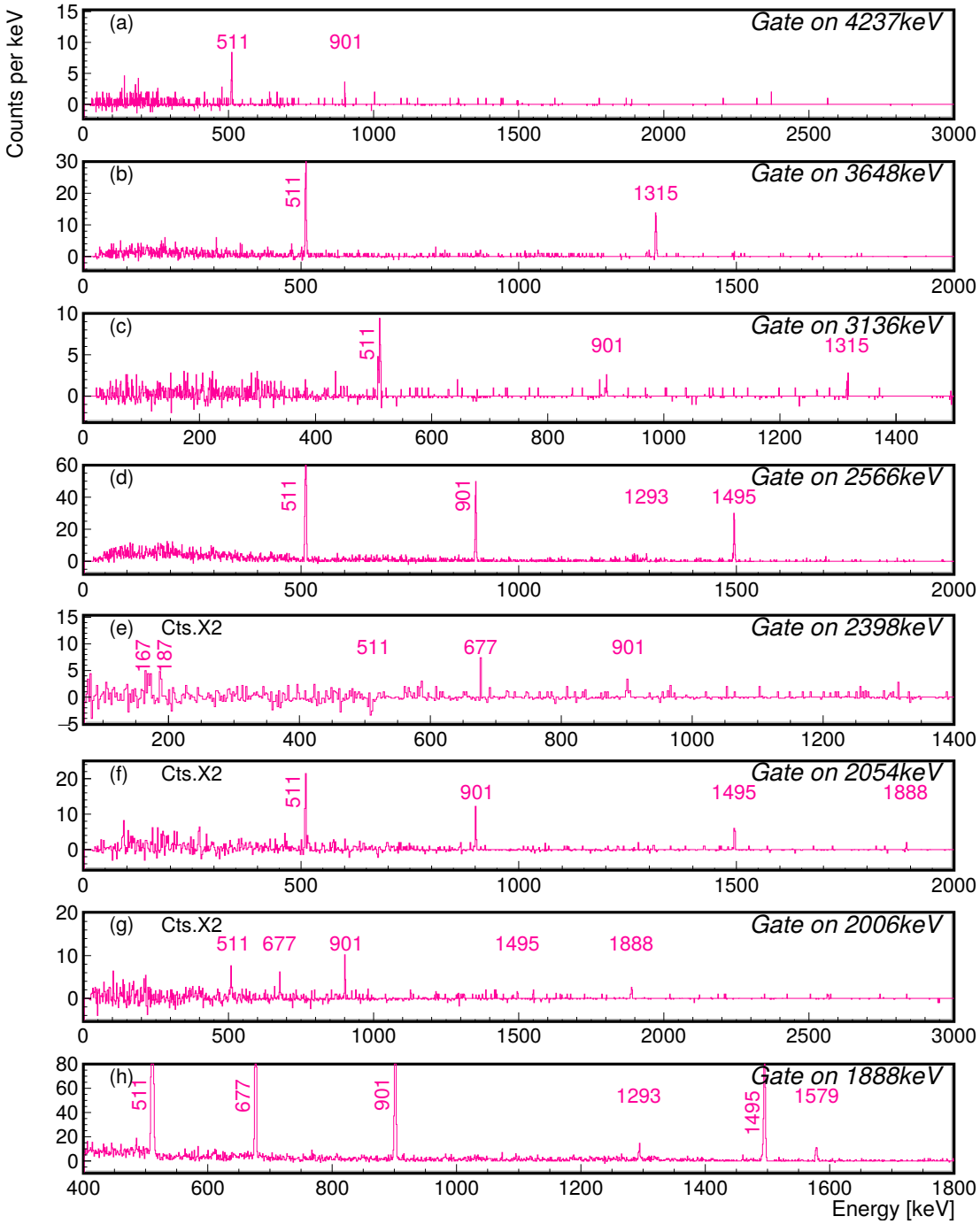

Figure 6.20: Gamma-Gamma coincidence spectra with background subtracted for ^{64}As decay, requiring coincidence for: (a) 4237 keV, (b) 3648 keV, (c) 3136 keV, (d) 2566 keV, (e) 2398 keV, (f) 2054 keV, (g) 2006 keV, (h) 1888 keV. (continued on next page).

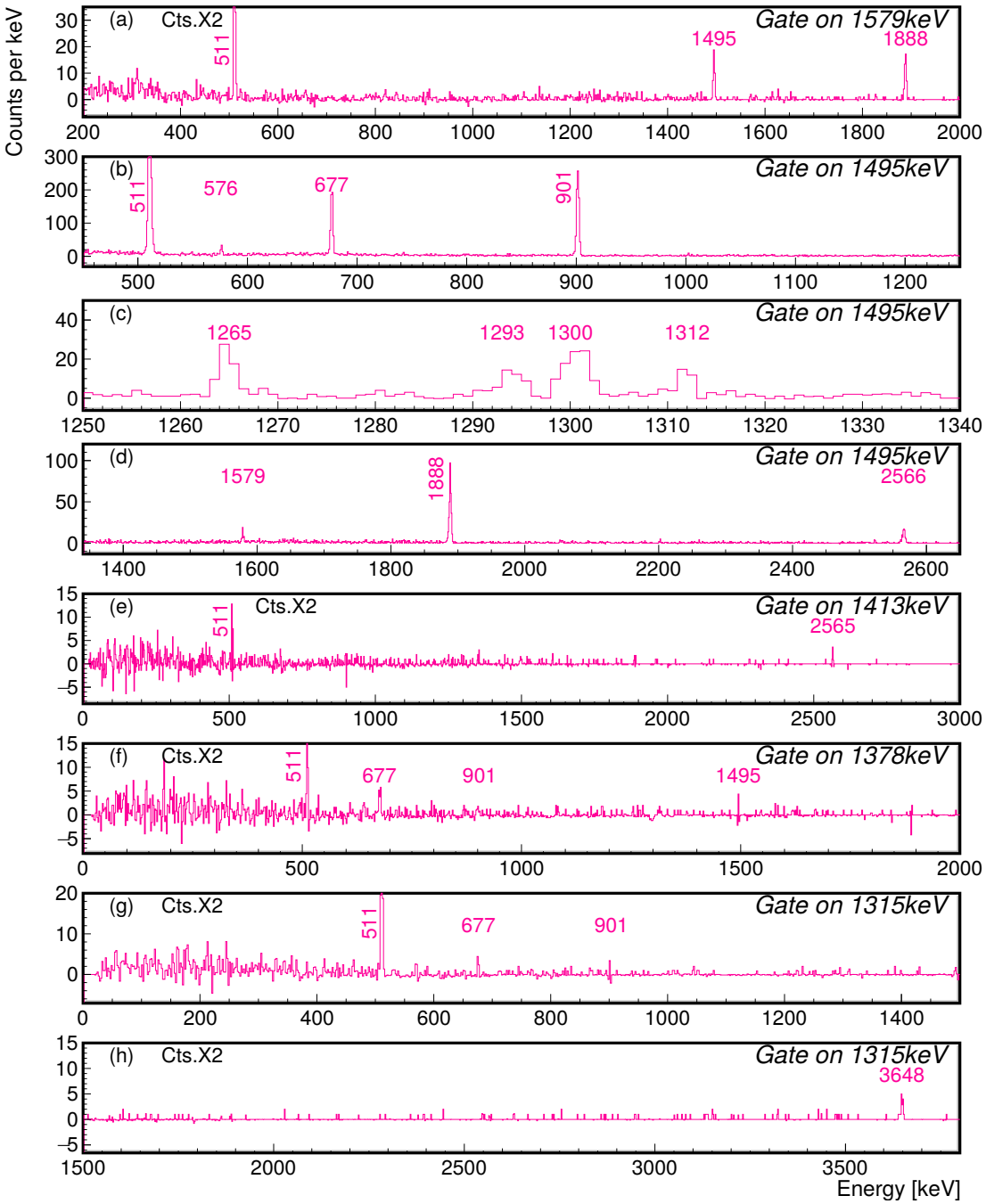

Figure 6.21: (a) 1579 keV, (b) 1495 keV, (c) 1495 keV(continuation), (d) 1495 keV(continuation), (e) 1413 keV, (f) 1378 keV, (g) 1315 keV, (h) 1315 keV(continuation), (continued on next page).

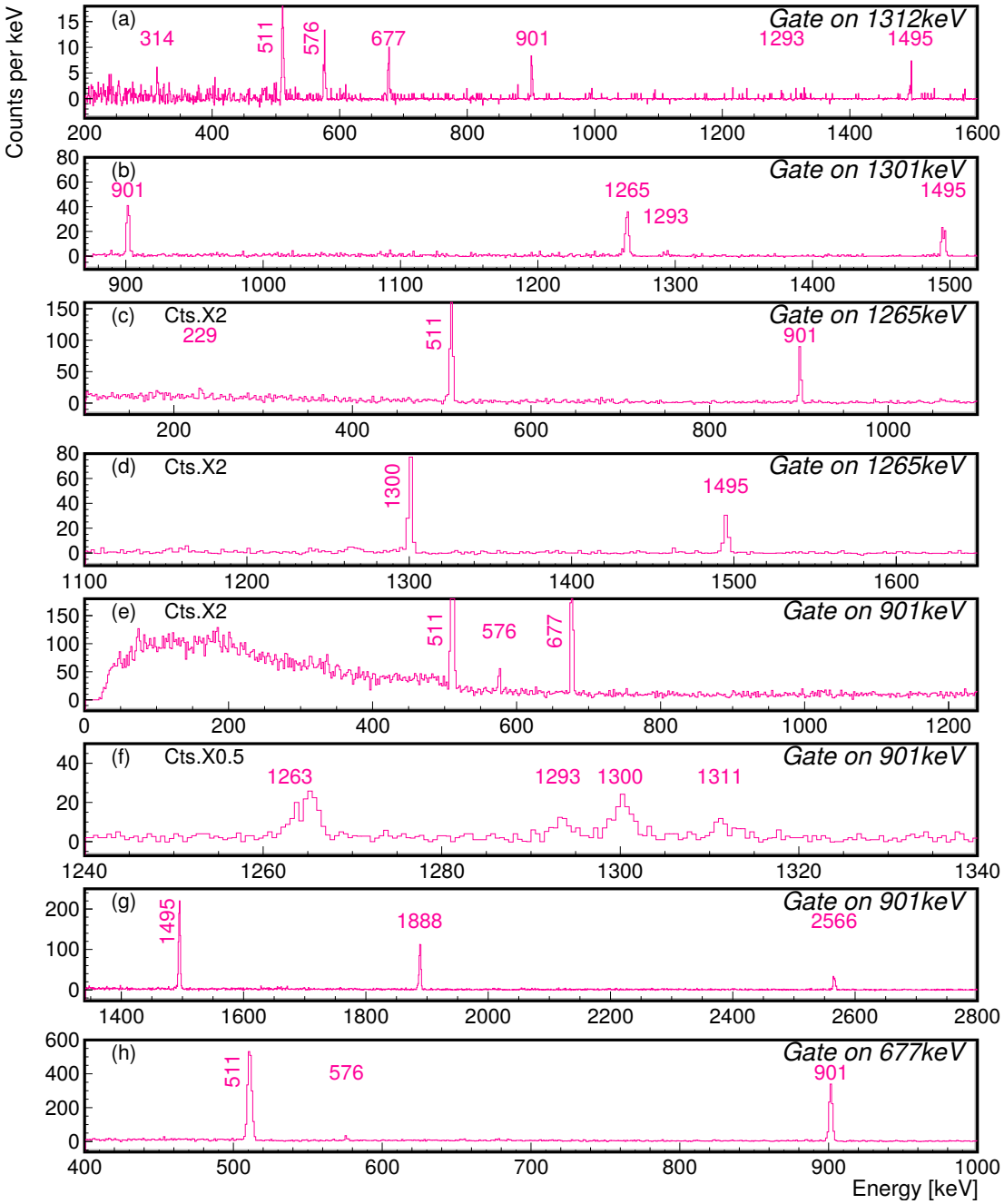

Figure 6.22: (a) 1312 keV, (b) 1301 keV, (c) 1265 keV, (d) 1265 keV (continuation), (e) 901 keV, (f) 901 keV (continuation), (g) 901 keV (continuation), (h) 677 keV. (continue on next page).

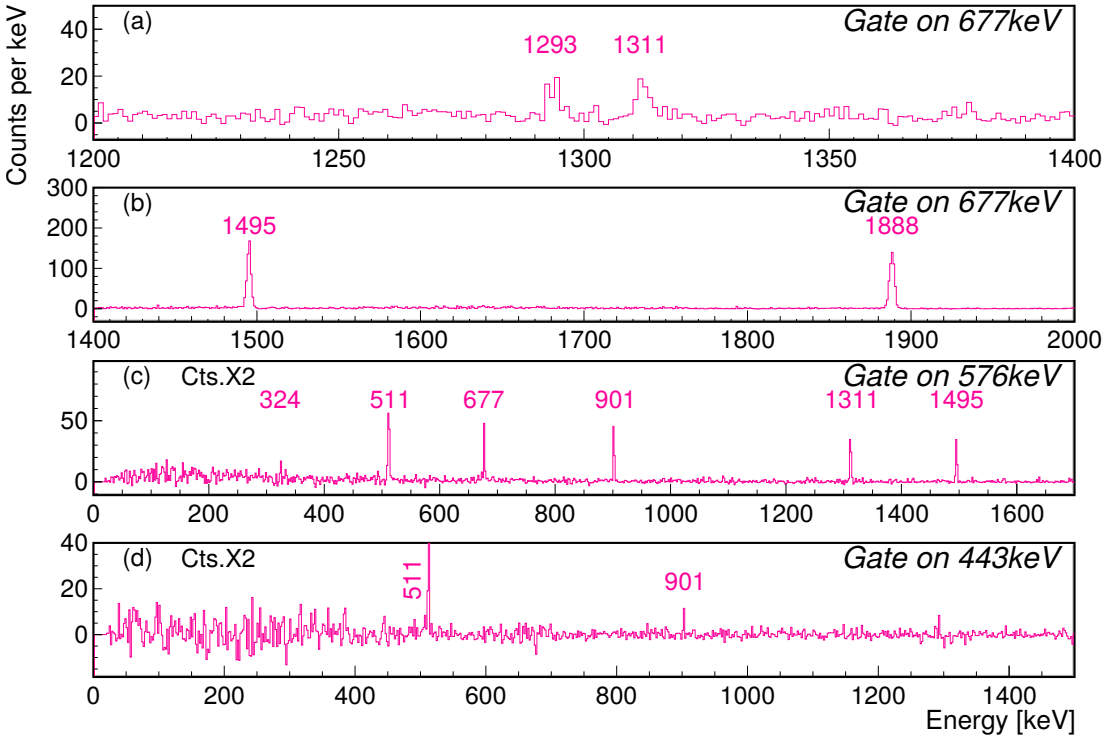

Figure 6.23: (a) 677 keV (continuation), (b) 677 keV (continuation), (c) 576 keV, (d) 443 keV.

6.2.6. Gamma-proton coincidences for ^{64}As decay

As discussed in Section 6.2.3, ^{64}As is a beta-delayed proton emitter. After the beta decay, if ^{64}Ge was populated in a state above the proton separation energy $S(p) = 5057_4$ keV [WAK+17], then a proton will be emitted and the remaining ^{63}Ga could be either in the g.s. or in an excited state. If an excited state in ^{63}Ga is populated, γ-rays may be emitted in coincidence with the proton. In order to identify any p-γ coincidences that may exist, gates on the energy of the proton decay event were defined. The p-gated γ-ray spectra for ^{64}As are shown in Fig. 6.24.

In Fig. 6.24(a) the first spectrum shown corresponds to events with energies between 135 keV to 1282 keV where the major part of these events should correspond to β-decay events only. Thus it represents β-γ coincidences. In Fig. 6.24(b) p-γ coincidences for events with energies above 1282 keV are shown corresponding to β-delayed proton emission events. These p-γ coincidences were used to build the level scheme in Section 7.2.

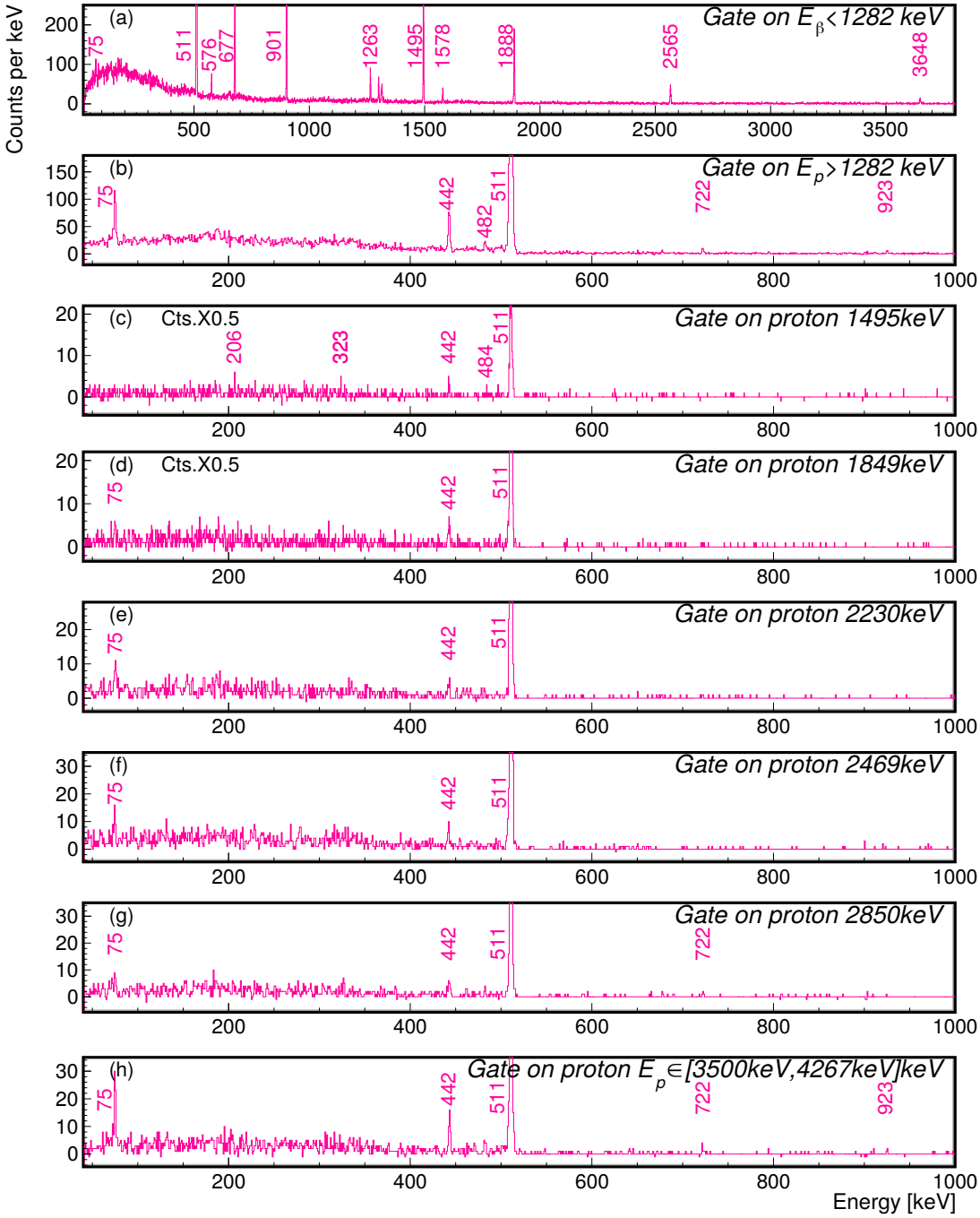

Figure 6.24: Proton-Gamma and Beta-Gamma coincidences for the ^{64}As decay, using different gates on the energy of the p or β event detected in the DSSSD. (a) β events, (b) p events, (c) $Ep = 1495$ keV, (d) $Ep = 1849$ keV, (e) $Ep = 2230$ keV, (f) $Ep = 2469$ keV, (g) $Ep = 2850$ keV and (h) $Ep > 3500$ keV.

6.2.7. ^{64}As half-life determination using a beta-proton coincidence condition

As the ^{64}As is a β-delayed proton emitter, protons can be used to measure the half-life of the mother nucleus, without the influence of daughter activities, since as shown in Fig. 6.25, the daughter nuclei ^{63}Ga and ^{63}Ge are not proton emitters and will be removed by the gate on the energies of decay events.

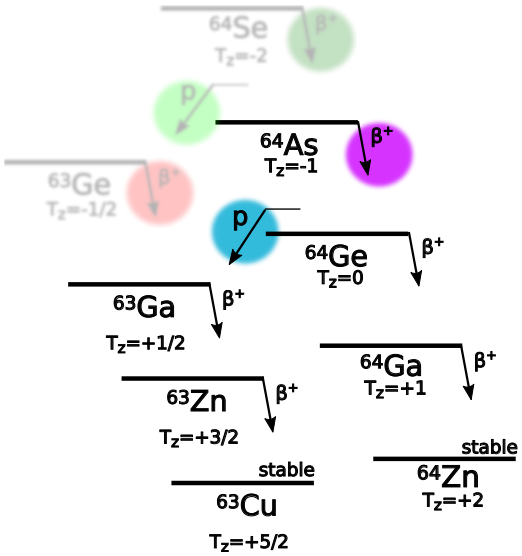

Figure 6.25: Diagram showing ^{64}As decay and its relation to the nuclei that follow it in the decay chain of ^{64}Se.

Protons were selected by placing a proton energy window of $E_p \in [1254, 6000]$ keV on the decay events, using the A10E700D111 in Fig. 6.16. The adjustment for the implantation-decay time correlation can be seen in Fig. 6.26. In this case, the number of ^{64}As implantations was fixed, while its half-life $T_{1/2}$ and proton branching ratio $Bp(^{64}\text{As})$ were adjusted. Implantation-decay correlations were fitted using the solution of the Bateman equation corresponding to the mother decay only $A_0(t;^{64}\text{As})$ described in Appendix H, and a constant background a_0 within 10 s of the implantation-decay correlation window. Then function used to fit the implantation-

decay correlations was,

$$A(t) = a_0 + (1 - DT)\,\varepsilon_p\,Bp(^{64}\mathrm{As})\,A_0(t;^{64}\mathrm{As}) \tag{6.8}$$

where $DT = 17.8(23)\%$ corresponds to the measured dead-time discussed in Appendix D, and ε_p is the proton detection efficiency assumed to be 100%. In Table 6.8 the results of the fitting can be found.

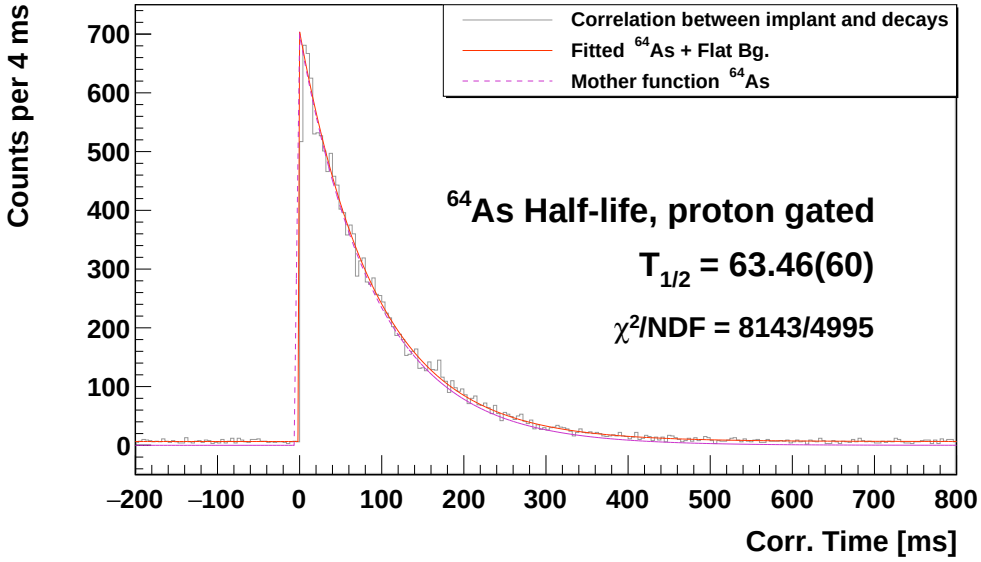

Figure 6.26: Half-life fit for the ^{64}As with the proton-coincidence condition in the window $[1254, 6000]$ keV. The implant-decay were correlated in 10 s forward and backward. The first millisecond in positive and negative times was avoided.

Isotope	N_0	$T_{1/2}$	$\varepsilon_\beta/\varepsilon_p$	Br_β/Br_p	DT
^{64}As	442.489	$63,46_{60}$ms	0/1	$0,95608_{36}/0.04392$	0, 178265
^{64}Ge	0	63.700ms	0/−	1/−	0, 178265
^{64}Ga	0	32.400ms	0/−	1/−	0, 178265

(a) Fitted parameters corresponding to Bateman equations.

Parameter	Comment
a_0	$6,471_{36}$
χ^2_i/NDF	8143/4995
Fit Method	RMIELN

(b) Fitted statistics and background adjusted parameters.

Table 6.8: Fit results for the proton gated spectrum in Fig. 6.26, parameters fixed during the fit are shown in black, and fitted parameters are shown in blue.

6.2.8. ^{64}As half-life determination using the whole decay chain

In this section the half-life for ^{64}As decay will be determined including all nuclei in the decay chain. To measure the half-life for ^{64}As using all of its decay descendants, a more accurate adjustment could be made if the proton branching ratio which already was determined in Section 6.2.8 ($B_\beta = 0.95608/B_p = 0.04392$) is fixed during this fit. Indeed, fixing the proton branching ratio allows one to measure the beta efficiency since both are related to the daughter activity obtained in the Bateman equation. Implantation-decay correlations were fitted using the solution of the Bateman equation corresponding to the mother decay only $A_0(t;^{64}\,\mathrm{As})$ described in Appendix H, and a constant background a_0 within 10 s of the implantation-decay correlation window. The function used to fit the implantation-decay correlations was,

$$\begin{aligned} A(t) = a_0 + a_1\,t + (1-DT)\,\big[&(\varepsilon_p\,Bp(^{64}\mathrm{As}) + \varepsilon_\beta(1-Bp(^{64}\mathrm{As})))\,A_0(t;^{64}\,\mathrm{As}) \\ &+ \varepsilon_\beta\,Bp(^{64}\mathrm{As})\,\big(A_1(t;^{63}\,\mathrm{Ga}) + A_2(t;^{63}\,\mathrm{Zn})\big) \\ &+ \varepsilon_\beta(1-Bp(^{64}\mathrm{As}))\,\big(A_1(t;^{64}\,\mathrm{Ge}) + A_2(t;^{64}\,\mathrm{Ga})\big)\big] \end{aligned} \tag{6.9}$$

where $DT = 17.8(23)\%$ corresponds to the measured dead-time discussed in Appendix D, ε_p is the proton detection efficiency assumed to be 100%, and ε_β is the beta detection efficiency.

In Fig.6.27 the fit to the implant-decay correlations can be shown. This fit was performed with an up to 10 s correlation window, symmetrically forward and backward. These fit results are shown in Fig. 6.27 and Table 6.9.

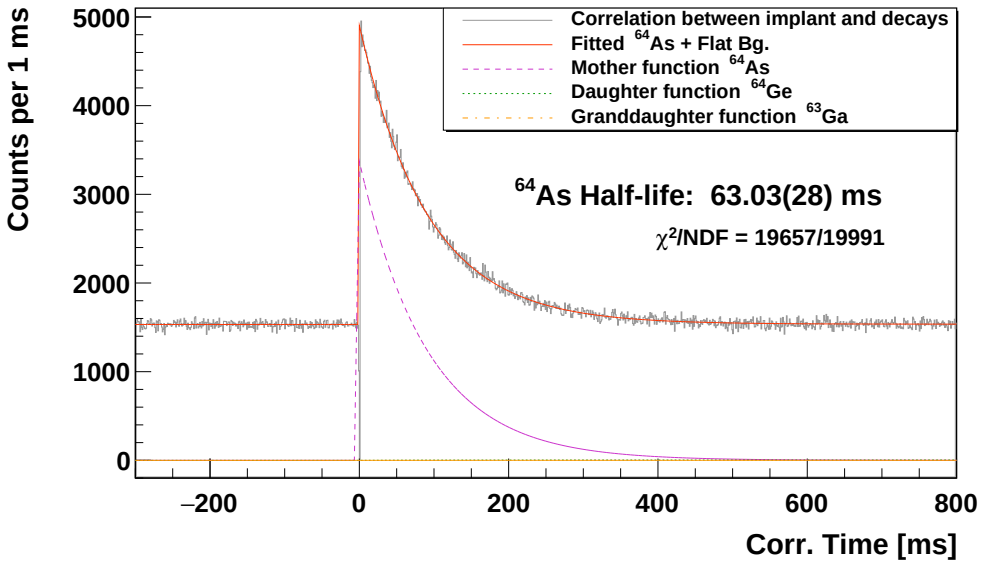

Figure 6.27: Half-life fit for ^{64}As. The implant-decay correlation window was $C_w = [0, 10000] \ominus [-10000, 0]$ ms (see Eq. 5.1).

Nucl.	N_0	$T_{1/2}$	$\varepsilon_\beta/\varepsilon_p$	Br_β/Br_p	DT
^{64}As	442.489	$63,03_{29}$ms	$0.8358_{28}/1$	0,95608/0.04392	0,178265
^{64}Ge	0	63.700ms	$0.8358_{28}/0$	1/0	0,178265
^{64}Ga	0	157.620ms	$0.8358_{28}/0$	1/0	0,178265
^{63}Ga	0	32.400ms	$0.8358_{28}/0$	1/0	0,178265
^{63}Zn	0	2.308.200ms	$0.8358_{28}/0$	1/0	0,178265

(a) Fitted parameters corresponding to Bateman equations.

Parameter	Comment
a_0	$1.532,44_{60}$
a_1	$-0,00054_{12}$
χ^2_i/NDF	19.657/19.991
Fit Method	RMIELN

(b) Fitted statistics and background adjusted parameters.

Table 6.9: The result of the fitting of ^{64}As decay (see Fig. 6.27). Parameters fixed during the fit are shown in black, and fitted parameters are shown in blue.

6.2.9. ^{64}As half-life determination using different beta-gamma coincidence conditions

In ^{64}As decay, there are at least four γ-rays corresponding to transitions between states in ^{64}Ge with enough intensity to measure the half-life by imposing a β-delayed γ-ray energy window. Their energies are 676.9 keV, 901.4 keV, 1495.1 keV, and 1888.4 keV and they can be seen in Fig. 6.18, in Section 6.2.4. The number of implants N_0, the dead-time $DT = 17.8(23)\%$, and the proton branching ratio $Bp(^{64}\text{As})$ were fixed, where the proton branching ratio was extracted from the p-β half-life fit in Section 6.2.7.

Implantation-decay correlations were fitted using the solution of the Bateman equation corresponding to the mother decay only $A_0(t;^{64}\,\text{As})$ described in Appendix H, and a constant background a_0 within 10 s of the implantation-decay correlation window. The function used to fit the implantation-decay correlations was,

$$A(t) = a_0 + (1 - DT)\,\varepsilon_\beta\,(1 - Bp(^{64}\text{As}))\,A_0(t;^{64}\,\text{As})\,. \tag{6.10}$$

The results of fitting the half-life obtained using each γ-ray are summarised in Table 6.10. The half-lives values will be discussed in Part V.

Parameter/Energy	676.9 keV	901.4 keV	1495.1 keV	1888.4 keV
N_0		4424890		
$T_{1/2}(^{64}\text{As})$ms	61.39(72)	63.31(67)	62.15(86)	61.6(11)
Dead-time		0.178265		
$\tilde{\varepsilon_\beta}(^{64}\text{As})$	0.02867(31)	0.04344(39)	0.02451(29)	0.01521(23)
$B_\beta(^{64}\text{As})$		0.95608		
$\varepsilon_p(^{64}\text{As})$	0.02867(31)	0.04344(39)	0.02451(29)	0.01521(23)
$B_p(^{64}\text{As})$		0.04392		
a_0 (bg.)	6.182(56)	20.10(10)	10.086(72)	6.064(56)
χ^2_i/NDF	2243/1996	2147/1996	2304/1996	2563/1996
Fit Method		RMIELN		
Range ms		$[-10000, 10000] \ominus [-2, 2]$		

Table 6.10: The result of the fits of γ-gated spectrum (see Fig. 6.18). Parameters fixed during the fit are shown in black, and fitted parameters are shown in blue. Parameters common to all fits are shown in the centre of the row.

6.3. ^{64}Se decay Analysis

^{64}Se is the most exotic nucleus studied in this work and the last nucleus in the nuclide chart that can be compared with its counterpart in charge exchange to examine mirror symmetry. For this isotope only an upper limit for its half-life was previously reported [SBF+05].

From the point of view of mirror symmetry studies using beta decay and charge exchange experiments, the isobaric multiplet $A = 64$ is the highest mass that can be studied in terms of the mirror symmetry, since higher masses do not have stable isotopes that can be used as targets in CE reactions [FRG11] to perform the charge exchange reaction. Further evidences must await developments in radioactive ion beams.

As can be seen in Fig. 6.28, the daughter nuclei ^{64}As and ^{63}Ga also decay by β^+ emission. Fortunately, both nuclei were also separated and identified by BigRIPS, and implanted in the same DSSSD of WAS3ABi as ^{64}Se, allowing us to

gain information prior to this analysis. From Section 6.3.3 on, the analysis for ^{64}Se decay will be presented.

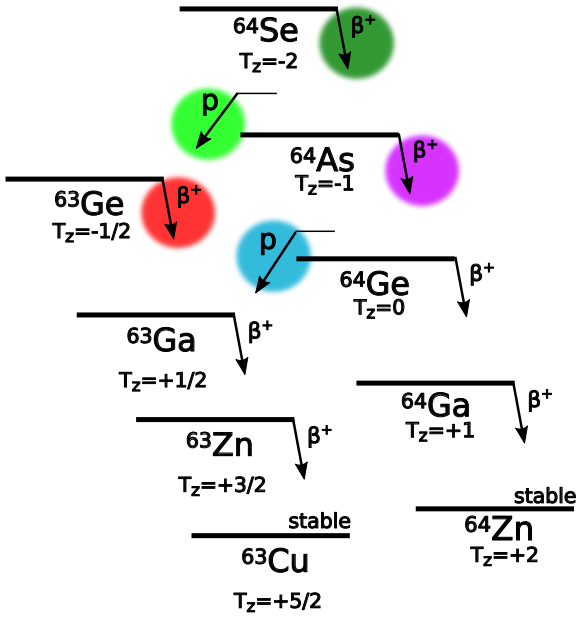

Figure 6.28: Diagram for the decay of the nuclide of interest ^{64}Se. The main contributors to the implantation-decay correlation are those with comparable half-lives, which are marked with coloured circles.

6.3.1. Previous knowledge of the excited states of ^{64}As: The beta decay daughter of ^{64}Se

The nucleus ^{64}Se was first observed in 2005 at the NCSL Laboratory [SBF+05] using a ^{78}Kr beam.Only four nuclei of ^{64}Se were produced and separated during 32 h of beam-time with an average primary beam current of 13.5pnA and energy 140 MeV/nucleon. There is no more experimental knowledge for this decay that can be used, beyond the decay of the daughter nuclei ^{64}As and ^{63}Ge analyzed Section 6.1 and 6.2. In our experiment 10308 ions produced, separated, and identified as ^{64}Se were implanted in WAS3ABi with an average primary beam current of 200pnA and energy 345 MeV/nucleon.

6.3.2. Analogue mirror transitions observed for ^{64}Zn(^{3}He,t)^{64}Ga charge exchange reaction experiment at RCNP

The analogue of the beta decay of ^{64}Se to levels in ^{64}As is the CE reaction $^{64}\mathrm{Zn}(^{3}\mathrm{He}, t)^{64}\mathrm{Ga}$. This particular CE reaction was studied in 2015 in an experimental campaign at RCNP facilities at Osaka (Japan) and it was part of the Master-thesis of F. Diel [Die15, DFF+19] from the University of Cologne. In Fig.6.29 we see the results for the $^{64}\mathrm{Zn}(^{3}\mathrm{He}, t)^{64}\mathrm{Ga}$ CE reaction. The states identified with $\Delta L = 0$ correspond to Gamow-Teller transitions from the mother nucleus ^{64}Zn with $T_z = +2$ into the daughter nucleus ^{64}Ga with $T_z = +1$. These transitions correspond to analogue transitions in the isobaric multiplet beta decay from the $T_z = -2$ ^{64}Se to the $T_z = -1$ ^{64}As [FRG11]. In Section 9.1 we shall return to this discussion.

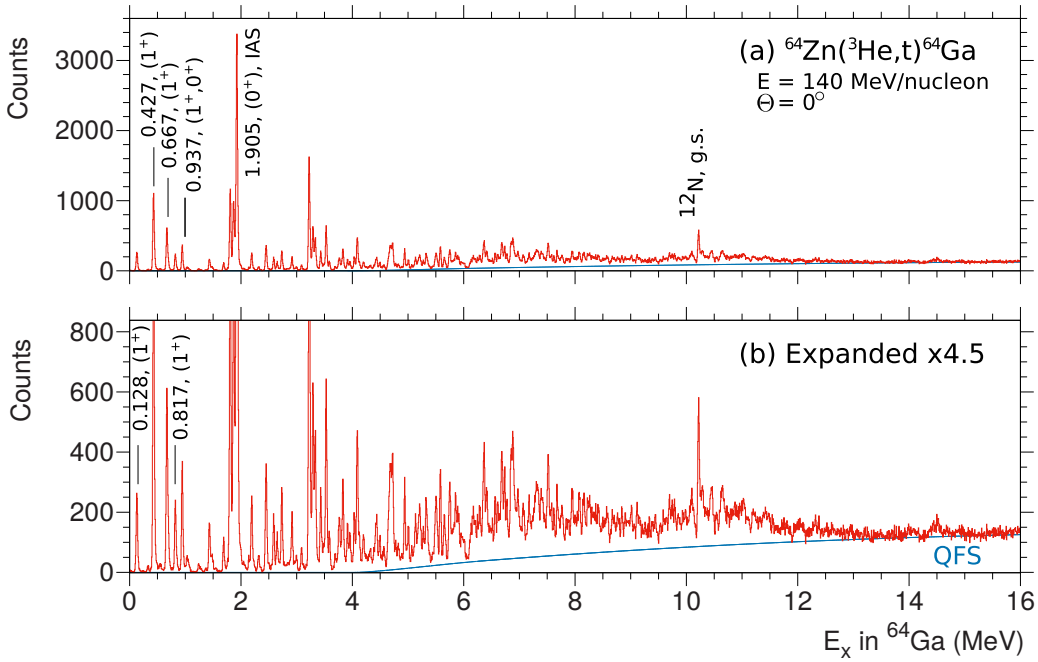

Figure 6.29: Triton spectrum measured in charge exchange reaction by F. Diel [DFF+19] at the high resolution facility of the Research Center for Nuclear Physics (RCNP) in Osaka, Japan.

6.3.3. Implant-decay correlation for ^{64}Se decay

The reported value for the ^{64}Se decay half-life is 30# ms obtained from theoretical extrapolations [AKW+17], while a lower limit of $T_{1/2}$ >180 ns was previously measured at the NCSL Laboratory [SBF+05]. Following the same criteria that we imposed in the analysis of its daughter nuclei 63Ge and 64As, the correlation window size was established in seven times the half-life of mother nuclei (see Appendix G for details). This window corresponds to $[-170, 170]$ ms for this decay, avoiding symmetrically the first millisecond $[-1, 1]$ ms. Nevertheless in Fig. 6.30 a plot of the implantation-decay correlations within a wider time correlation window of 10 s is shown to clarify that after the seven half-life interval (in green), most of the correlations would correspond to random coincidences (in red). Then the green region corresponding to the seven half-lives will be used in the following sections to construct the beta, proton, and γ-ray spectra for this decay.

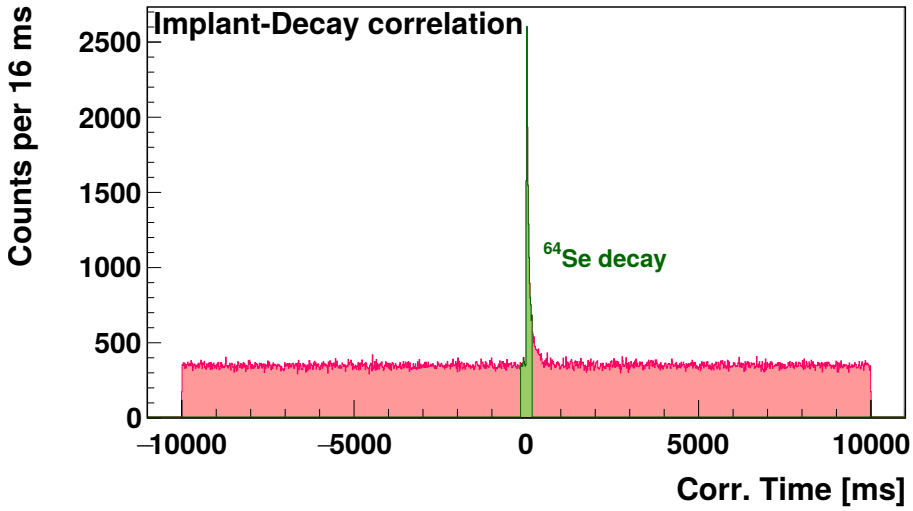

Figure 6.30: Implantation-decay correlation for ^{64}Se. Correlations were made up to 10 s forward and backward, but to obtain the spectra the implantation-decay correlations were constrained to the 170 ms window (seven mother half-lives) shown in green.

6.3.4. Beta-delayed proton spectrum for ^{64}Se decay

The proton spectrum for ^{64}Se was constructed within 1 ms to 170 ms implantation -decay correlation times, corresponding approximately to seven half-lives of the mother nucleus as discussed in Appendix G.2. Background correlations were subtracted using negative correlation times within −170 ms to −1 ms. In Fig. 6.31 the proton spectrum was obtained using two different conditions: the A10E700D110 condition corresponding to implantations next to the maximum energy beta pixel (see Fig. 6.31a), and the A10E700NMD condition corresponding to implantations next to any beta pixel (see Fig. 6.31b). Both methods were explained in Section 4.2. The A10E700D110 condition has lower beta efficiency than the A10E700NMD, but gave better proton peak definition. This condition was used to find and adjust the proton peaks. Nevertheless the A10E700NMD has higher beta efficiency and will be used to construct the γ-ray spectra and analyse γ-γ coincidence.

In Fig. 6.31 the proton spectrum for ^{64}Se is presented together with the fit of beta and proton spectrum. The proton spectrum was fitted using the parametric functions detailed in Appendix E, and fit results can be found in Tables 6.11 and 6.12. Fitted proton energies are shown above each proton peak, corresponding to the proton energy plus the $\Delta E = 130$ keV of the β particle as will be discussed in Sections F.1 and F.2 in the Appendix F.

$E^{Obs.}$ [keV]	E^{p} [keV]	Width	Amplitude	Integral
1711(12)	1581(29)	66.0(42)	231(22)	874(66)
2114.6(70)	1985(28)	66.0(42)	386(15)	1462(83)
1249(29)	1119(39)	66.0(42)	20(15)	74(33)
3139(30)	3009(40)	66.0(42)	33.9(90)	129(20)
3390(29)	3260(39)	66.0(42)	58.7(95)	223(24)
3855(29)	3725(40)	66.0(42)	14.7(66)	56(14)
4140(22)	4010(35)	66.0(42)	14.4(56)	55(12)
4813(29)	4683(39)	66.0(42)	16.9(37)	64.2(86)

Table 6.11: The result of the fitting for the ^{64}Se β-delayed proton spectrum, using the A10E700D110 condition. The parametric proton function is characterised by the proton energy E^{obs}, the width, and the amplitude. The proton energy E^{p} was obtained by subtracting to the observed energy E^{obs}, the energy shift (130(27) keV) due to the coincidence with the beta particle. The Integral value corresponds to the total number of proton events.

$E^{Obs.}$ [keV]	E^{p} [keV]	Width	Amplitude	Integral
1712.2(96)	1582(29)	61.9(40)	230.5(0)	913(23)
2111.7(65)	1982(28)	61.9(40)	385.7(0)	1527(38)
1269(40)	1139(48)	61.9(40)	19.6(0)	77.5(19)
3124(25)	2994(37)	61.9(40)	33.9(0)	134.2(34)
3375(21)	3245(34)	61.9(40)	58.7(0)	232.5(58)
3835(40)	3705(48)	61.9(40)	14.7(0)	58.2(15)
4120(38)	3990(47)	61.9(40)	14.4(0)	57.2(14)
4793(29)	4663(40)	61.9(40)	16.9(0)	67.1(17)

Table 6.12: Fit results for ^{64}Se β-delayed proton spectrum, using the A10E700NMD condition. The parametric proton function is characterised by the proton energy E^{obs}, the width, and the amplitude. The Integral value corresponds to the total number of proton events.

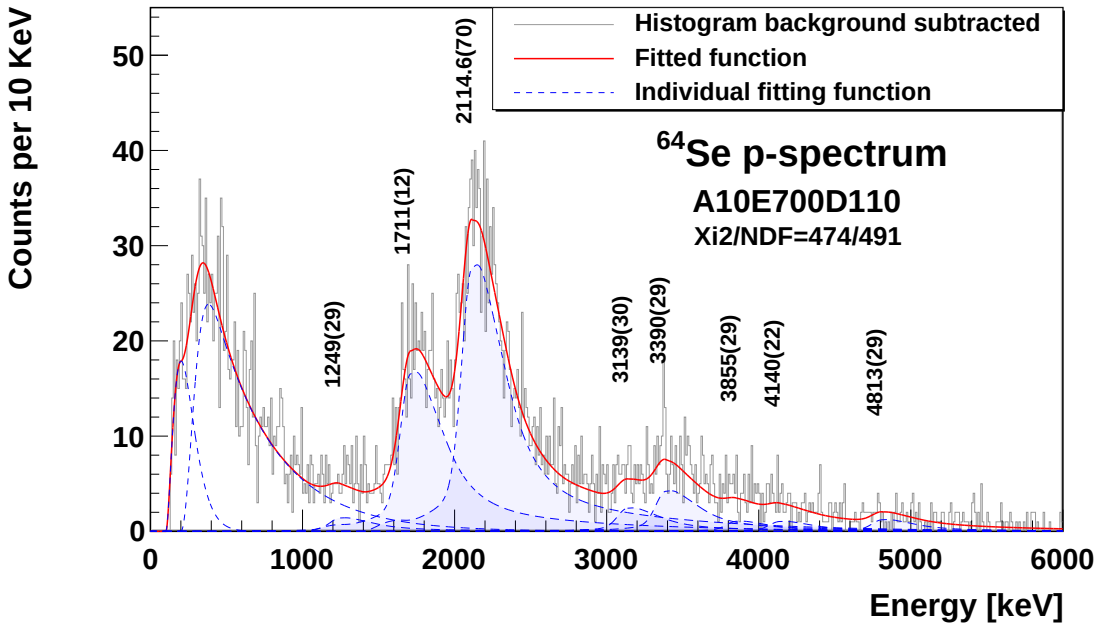

(a) The A10E700D110 condition.

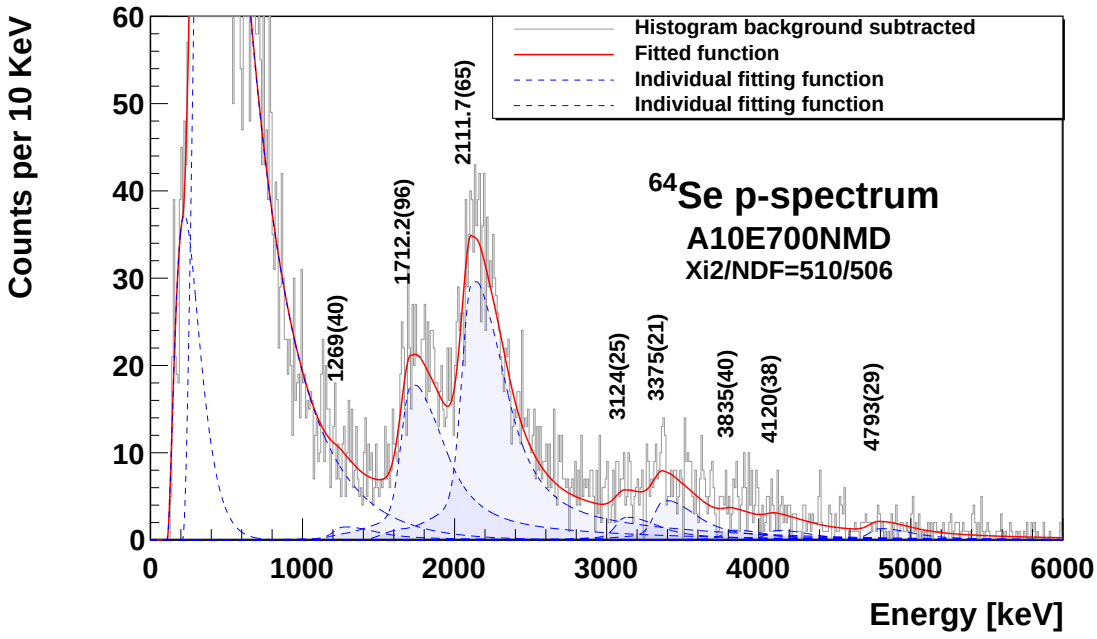

(b) The A10E700NMD condition.

Figure 6.31: Proton spectrum for ^{64}Se constructed within the $[1, 170] \ominus [-170, -1]$ms correlation window. The spectrum was fitted using the parametric beta function described in Appendix E.

6.3.5. Gamma spectrum for ^{64}Se decay

The γ-ray spectrum for ^{64}Se was constructed using the $C_w = [1, 170] \ominus [-170, -1]$ ms implantation-decay correlation window, and the A10E700NMD condition for decay events as described in Section 5.1.2. Fig. 6.5 shows a scatter plot of the EURICA DGF (Digital Gamma Finder) digitalizer energy -Y axis- and time -X axis- signals. In this figure the γ-prompt coincidence window was taken to be $[0, 0.8] \ominus [-80, -40]$ μs to select γ-rays emitted during the beta decay of ^{64}Se, indicated between red lines. Then the γ-ray spectrum for ^{64}Se decay was obtained and can be seen in Fig. 6.33.

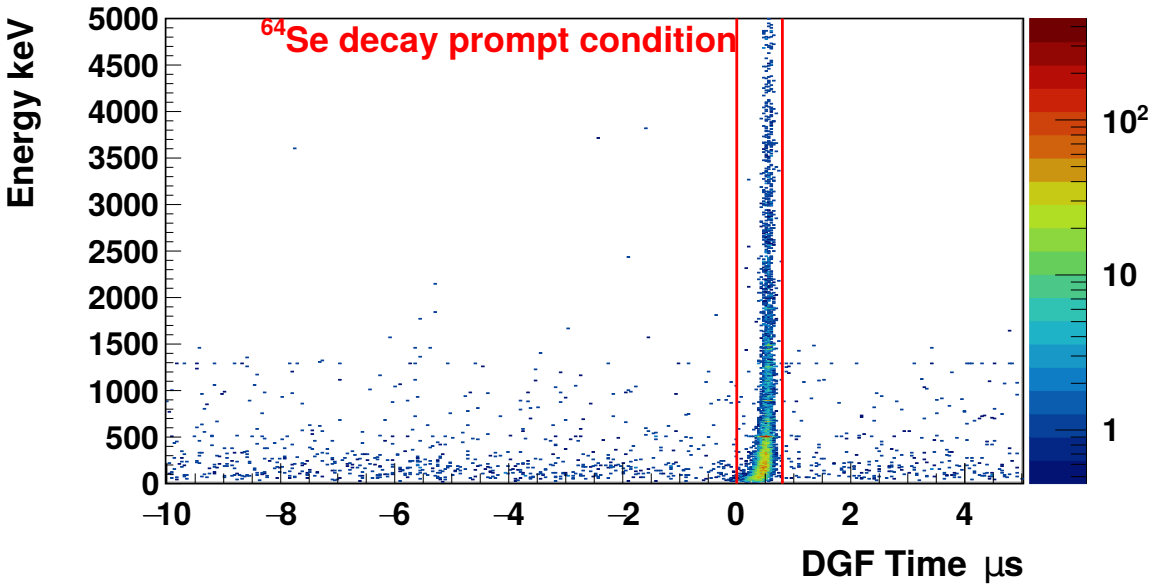

Figure 6.32: ^{64}Se decay energy-time plot for the γ-ray spectrum, requiring the implantation of ^{64}Se condition over the PID plot. The γ-prompt condition is shown between two red lines (0.8 μs width) and corresponds to γ-rays emitted in the ^{64}Se decay.

Each peak in the γ-ray spectrum of ^{64}Se decay was fitted and the energy, FWHM, and number of counts were obtained. These results could be found in Table 6.13. Also the γ-ray efficiency correction in Equation 3.2 was obtained for each γ-ray

transition and shown in the fourth column. This efficiency value was used to obtain the corrected number of counts in the fifth column of Table 6.13.

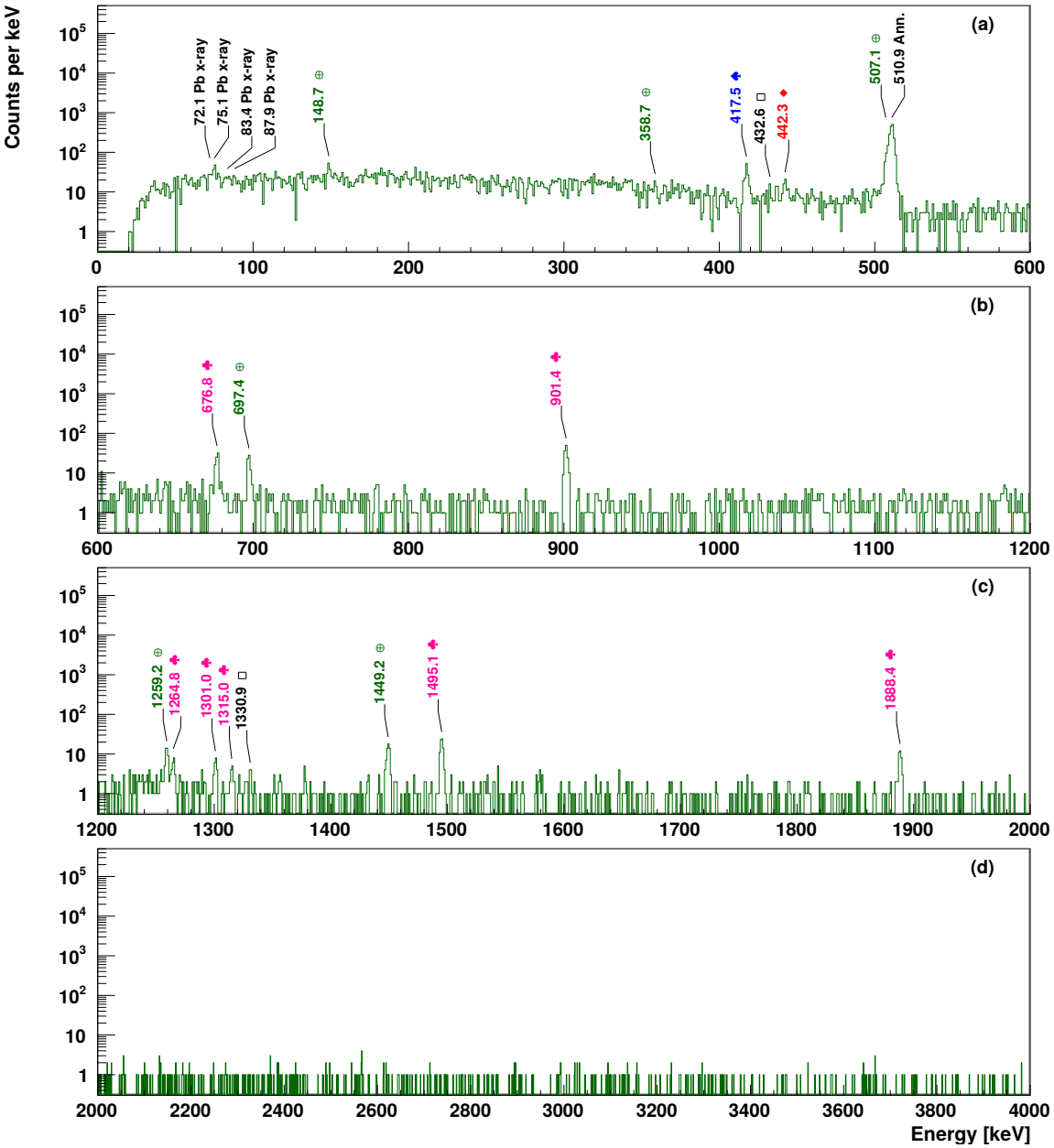

Figure 6.33: The γ-ray spectrum for ^{64}Se decay. The γ-rays assigned to ^{64}Se decay are shown in green with $\oplus$, and those assigned to ^{64}Se p-delayed β decay is shown in blue with ♠. The γ-rays assigned to ^{64}As decay are shown in pink with ♣. The γ-rays assigned to ^{63}Ge decay are shown in red with $\diamond$. Unassigned, annihilation, or x-rays are shown in black marked with □.

Energy keV	FWHM keV	Counts	Efficiency (ε_γ)	Intensity	Comments
72.1(3)	1.7(2)	22(9)	0.161(6)	136(60)	Pb x-ray $k_{\alpha 2} + k_{\alpha 3}$
75.1(2)	1.7(2)	54(10)	0.163(6)	333(70)	Pb x-ray $k_{\alpha 1}$
83(1)	1.7(2)	9(9)	0.168(6)	55(50)	Pb x-ray $k_{\beta 3} + k_{\beta 1}$
88(1)	1.7(2)	11(8)	0.169(6)	64(50)	Pb x-ray $k_{\beta 2}$
148.7(2)	2(3)	56(10)	0.169(6)	333(70)	^{64}Se decay
358.7(3)	1.7(4)	16(7)	0.132(5)	120(50)	^{64}Se decay
417.5(1)	2.5(3)	103(10)	0.124(4)	829(100)	^{64}Se p-delayed β decay
432.6(3)	1.7(3)	10(5)	0.122(4)	80(40)	-
442.3(2)	1.7(3)	29(7)	0.121(4)	237(60)	^{63}Ge decay
507.13(3)	3.09(8)	185(20)	0.114(4)	1619(200)	^{64}Se decay
510.92(4)	3.09(8)	1658(40)	0.114(4)	1.46(6)E4	$e^- + e^+$
676.8(1)	2.2(3)	72(10)	0.100(4)	728(100)	^{64}As decay
697.4(1)	2.2(3)	61(9)	0.098(3)	624(90)	^{64}Se decay
901.39(9)	2.3(2)	123(10)	0.086(3)	1430(100)	^{64}As decay
1259.2(2)	2.4(3)	39(7)	0.072(3)	540(100)	^{64}Se decay
1264.8(4)	2.4(3)	17(5)	0.072(3)	231(70)	^{64}As decay
1301.0(3)	2.3(5)	18(5)	0.070(2)	260(70)	^{64}As decay
1315.0(4)	2(2)	9(6)	0.070(2)	132(90)	^{64}As decay
1331(2)	1.7(7)	6(3)	0.069(2)	91(40)	-
1449.2(2)	2.8(3)	56(8)	0.066(2)	842(100)	^{64}Se decay
1495.1(1)	2.6(3)	74(9)	0.065(2)	1139(100)	^{64}As decay
1888.4(2)	2.9(5)	36(6)	0.056(3)	644(100)	^{64}As decay

Table 6.13: The result of fitting the prompt γ-ray spectrum from ^{64}Se decay shown in Fig. 6.33. Intensity shown in the fifth column corresponds to the number of counts corrected by the γ-ray efficiency.

The gamma-ray spectrum for ^{64}Se contains γ-rays emitted in transitions between states in ^{64}As, and others emitted in the granddaughter nuclei ^{64}Ge and ^{63}Ga. Since the γ-ray spectra for the daughter nuclei were studied in Sections 6.1.4 and 6.2.4, some of these γ-rays were also recognized in the ^{64}Se decay γ-ray spectrum, shown in Fig. 6.33, and marked with ♠ and ♦ corresponding to ^{63}Ge decay and ^{64}As decay, respectively. A summary of the identified and unidentified γ-ray peaks in the spectrum is shown in Fig. 6.33:

Pb x-rays The 72.1 keV, 75.1 keV, 83 keV, and 88 keV x-ray energies correspond to the $k_{\alpha 2}$ plus $k_{\alpha 3}$, $k_{\alpha 1}$, $k_{\beta 3}$ plus $k_{\beta 1}$, and $k_{\beta 2}$ Lead x-rays respectively.

$\oplus$ The γ-rays with energies 148.7 keV, 358.7 keV, 697.4 keV, 1259.2 keV, 1449.2 keV were assigned to the ^{64}Se β decay to ^{64}As.

♠ The 417.5 keV peak was identified in the ^{64}Se p-delayed β decay to the ^{63}Ge.

♣ The γ-rays with energies 676.8 keV, 901.4 keV, 1264.8 keV, 1301.0 keV, 1315.0 keV, 1495.1 keV, and 1888.4 keV were identified in the ^{64}As decay (see Sec. 6.2.4).

$\diamond$ The 442.3 keV γ-ray energy was identified in the ^{63}Ge β decay (see Sec. 6.1.4).

$\square$ The 432.6 keV, and 1331 keV γ-ray energy peaks are unplaced.

6.3.6. Gamma-gamma coincidence spectra for ^{64}Se decay

From the γ-ray spectrum for the ^{64}Se decay in Fig. 6.33, energies and intensities of the γ-rays were obtained. As this is the first beta decay experiment in this region of the nuclear chart, there is no reported γ-ray, or daughter level information. The γ-rays in ^{64}As were identified in Section 6.3 comparing the γ-ray spectrum obtained for the ^{64}Se decay with the corresponding ones in ^{64}As decay and the ^{63}Ge decay shown in Sections 6.2.4 and 6.1.4, respectively. In this section, the γ-γ coincidence projection spectra will be constructed for all γ-rays in this decay, in order to find γ-ray cascades that may exist in ^{64}As.

In Fig. 6.34 the γ-γ coincidence projection spectra were obtained by gating on several γ-rays observed in the γ-ray spectrum in Fig. 6.33. The prompt condition was imposed using the same coincidence window of 0.8 μs as the in γ-ray spectrum,

and the same implantation-decay correlation window $[-170, 170]$ ms as in the proton spectrum. The γ-γ coincidences will be discussed in Section 7.3.

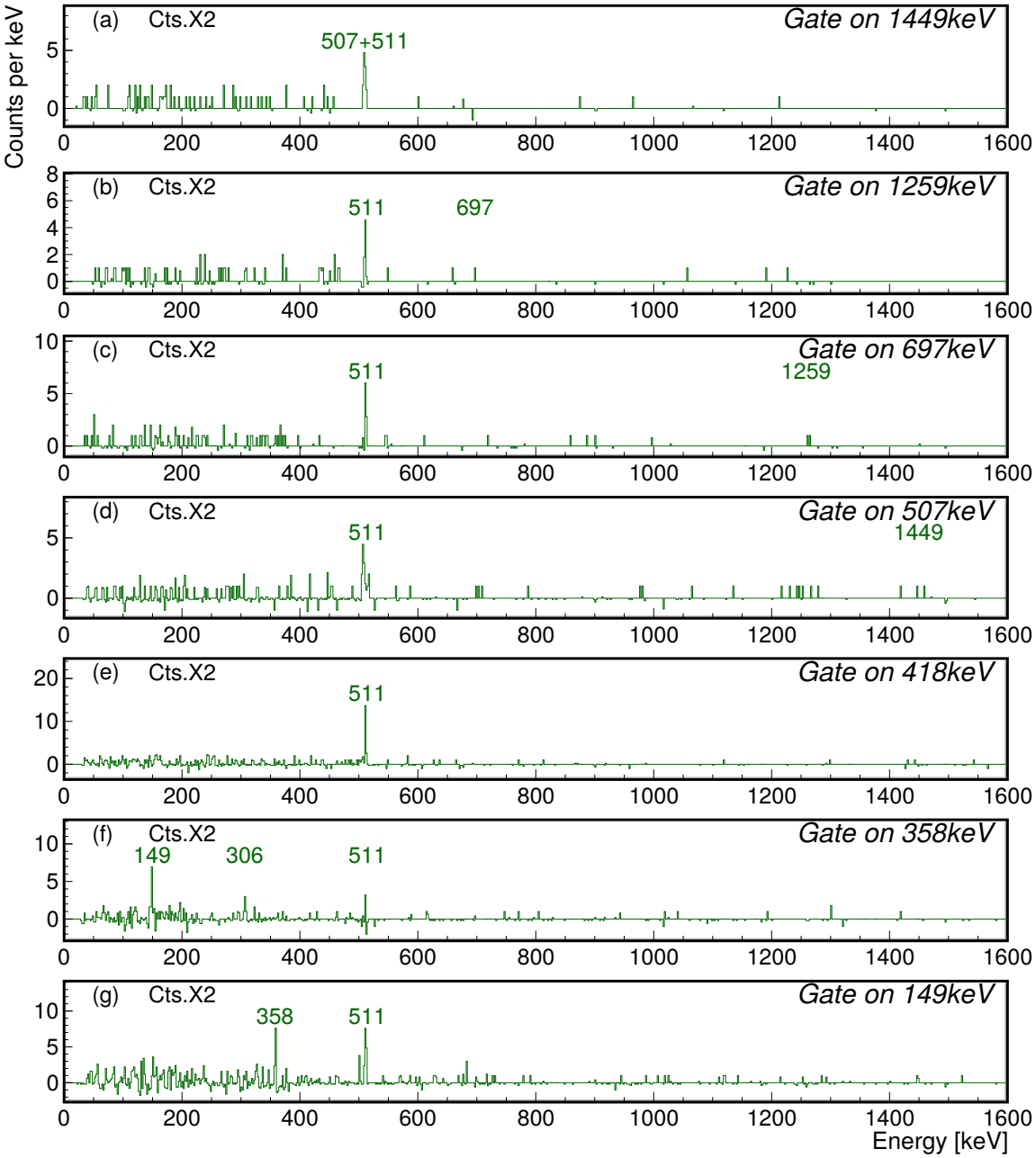

Figure 6.34: γ-γ coincidence spectra for ^{64}Se decay, requiring a γ-prompt condition within $[0\ \mu s, 0.8\ \mu s] \ominus [-80\ \mu s, -40\ \mu s]$, and coincidence for the γ-rays: (a) 1449 keV, (b) 1259 keV, (c) 697 keV, (d) 507 keV, (e) 418 keV, (f) 358 keV, (g) 149 keV.

6.3.7. Gamma-proton coincidences for ^{64}Se decay

The proton emission may occur when beta decay from ^{64}Se populates a state above the proton separation energy $S(p) = -100\#(200)$ keV [WAK+17] in ^{64}As. When a proton is emitted, the ^{63}Ge may be populated either in the g.s. or an excited state, and some γ-rays may be observed in coincidence. In this section, the proton spectrum will be obtained including the γ-ray coincidence energy window for each γ-ray in ^{64}Se decay.

In Fig. 6.35 the γ-p coincidences were obtained for the 75 keV, 148 keV, 358 keV, and 417 keV peaks continuing in Fig. 6.36 for the 697 keV, 1259 keV, and 1449 keV peaks. The 417 keV windows in Fig 6.35(d) shows coincidences with proton energies of 1716 keV. On the other hand, the 1449 keV in Fig 6.35(c) is an example of γ-rays in coincidence only with beta particles. These γ-p coincidences will be discussed in Section 7.3.

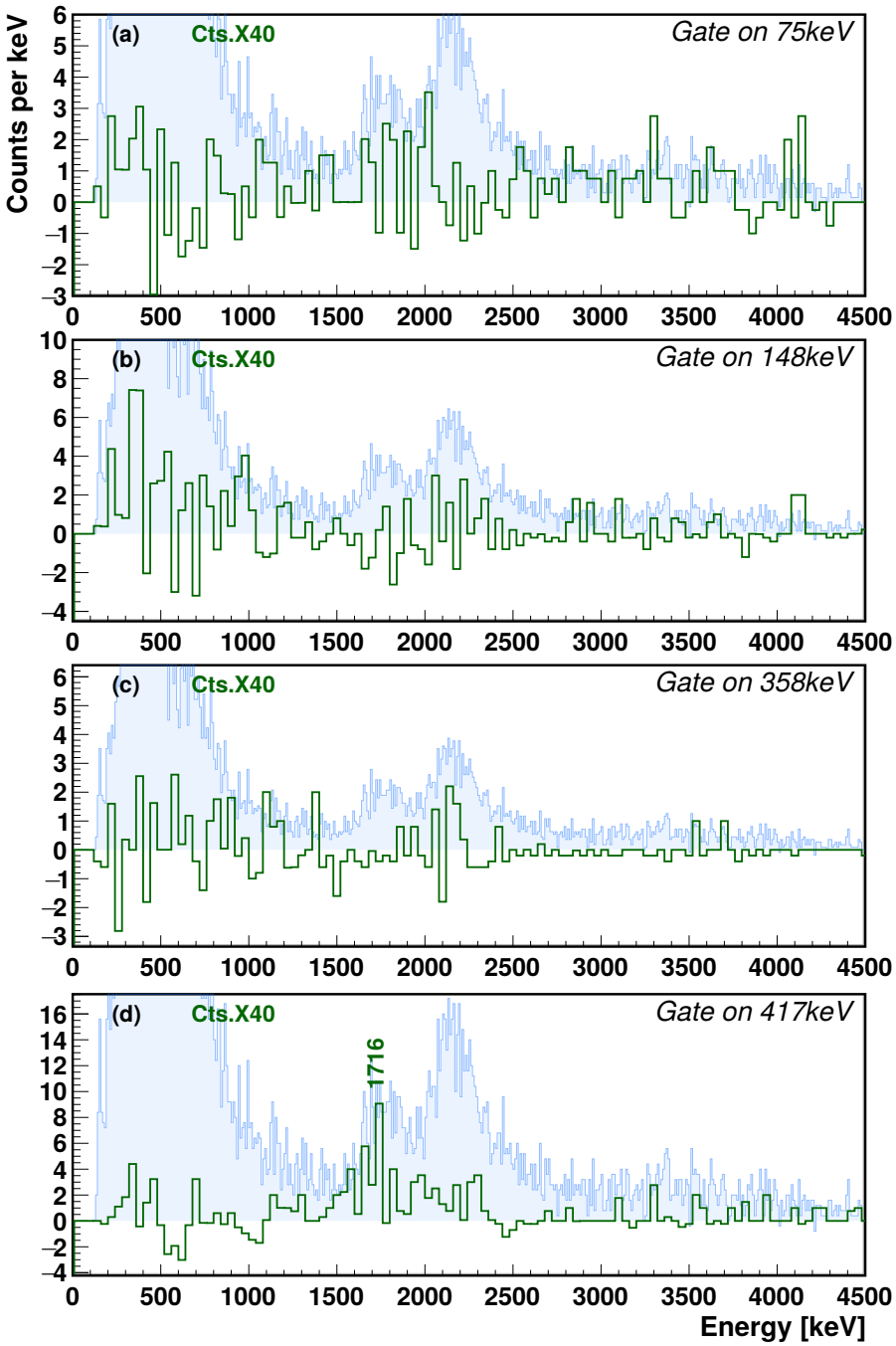

Figure 6.35: γ-p coincidence spectra for ^{64}Se decay. The γ-gated spectra are shown in green, while the p-spectrum (see Fig. 6.31) was scaled and draw in blue for each gate as a reference. γ-prompt condition within $[0\ \mu s, 0.8\ \mu s] \ominus [-80\ \mu s, -40\ \mu s]$ was required together with the energy condition for each γ-rays: (a) 75 keV, (b) 148 keV, (c) 358 keV. (d) 417 keV. (Continues on following page)

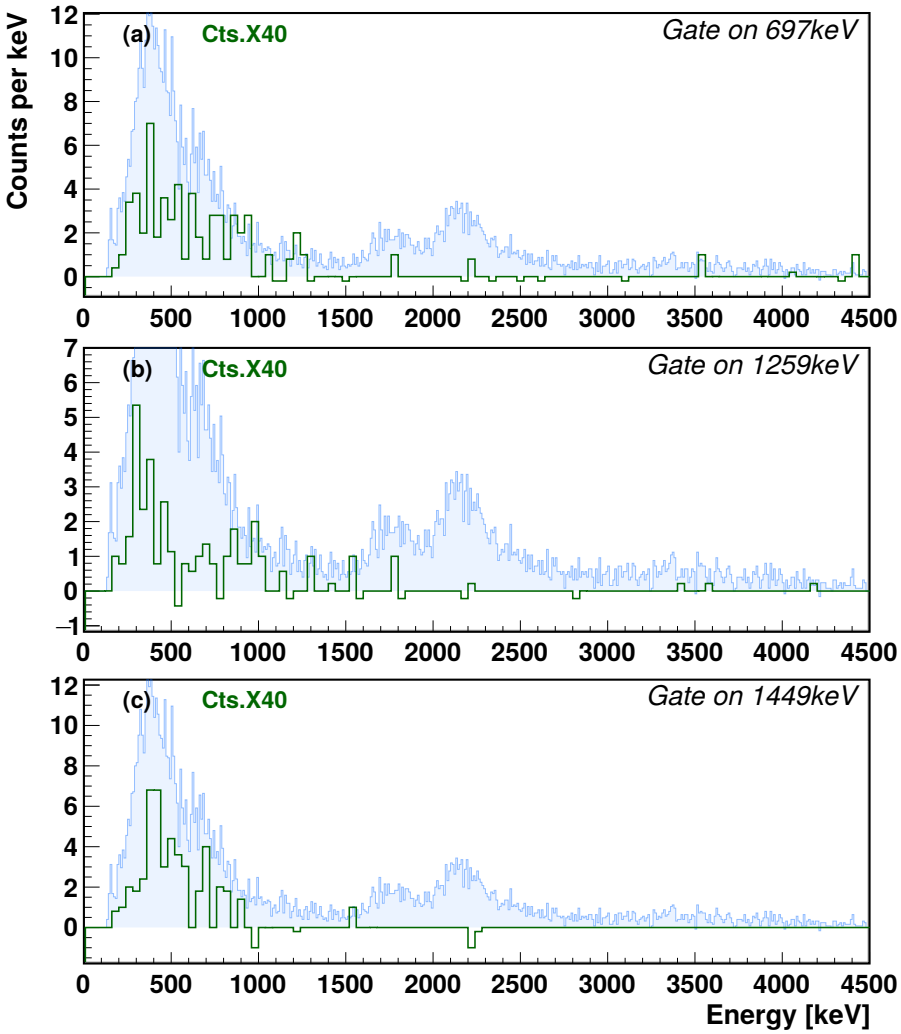

Figure 6.36: The proton spectrum gated with γ-rays: (a) 697 keV, (b) 1259 keV, (c) 1449 keV.

6.3.8. ^{64}Se half-life determination using a beta-proton coincidence condition

The ^{64}Se decay populates daughter nuclei with comparable half-lives, in this case 63.03(28) ms for ^{64}As and 152.60(33) ms for ^{63}Ge, as measured in Sections 6.2.8 and 6.1.7, respectively. As can be seen from the diagram in Fig. 6.28, we could remove the implantation-decay correlations corresponding to ^{63}Ge decay and most of ^{64}As decay by imposing a proton coincidence condition within $E_p \in [1420, 10000]$ keV in the proton spectrum in the Fig. 6.31b.

Implantation-decay correlations were fitted using the solution of the Bateman equation corresponding to the mother decay $A_0(t;^{64}\,\mathrm{Se})$ and daughter decay $A_1(t;^{64}\,\mathrm{As})$ described in Appendix H and a linear background $a_0 + a_1\,t$ within 10 s of the implantation-decay correlation window. Then function used to fit the implantation-decay correlations was,

$$\begin{aligned} A(t) =& a_0 + a_1\,t + (1 - DT)\,\varepsilon_p\,\big[Bp(^{64}\mathrm{Se})\,A_0(t;^{64}\,\mathrm{Se}) \\ &+ (1 - Bp(^{64}\mathrm{Se}))\,Bp(^{64}\mathrm{As})\,A_1(t;^{64}\,\mathrm{As})\big] \end{aligned} \tag{6.11}$$

where $DT = 22.5(46)\%$ corresponds to the measured dead-time discussed in Appendix D, ε_p is the proton detection efficiency assumed to be 100%. In Table 6.14 results of the fits are summarised, where we obtained $T_{1/2} = 23.32(62)$ for the ^{64}Se decay.

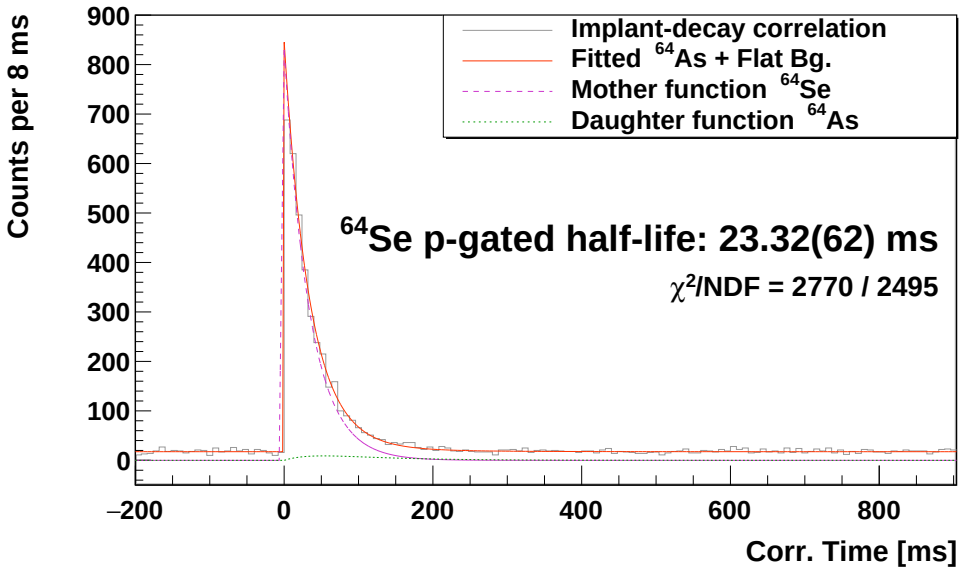

Figure 6.37: ^{64}Se half-life measurement using the β-p coincidence condition. Free parameters in the fitting process are shown in Table 6.14 in blue. The $E_\beta \in [1420, 10000]$ coincidence condition was required in the A10E700NMD proton spectrum in Fig. 6.31.

Nucl.	N_0	$T_{1/2}$	$\varepsilon_\beta/\varepsilon_p$	Br_β/Br_p	DT
^{64}Se	71952	23.32(62)ms	0/1	0, 5198(89)/0.4802(89)	0, 225186
^{64}As	0	63.03ms	0/1	0.95608/0.04392	0, 225186
^{63}Ge	0	152.60ms	0/1	1/-	0, 225186
^{64}Ge	0	63700ms	0/1	1/-	0, 225186
^{63}Ga	0	32400ms	0/1	1/-	0, 225186

(a) Fitted parameters corresponding to Bateman equations.

Parameter	Comment
a_0	17.51(17)
a_1	$-2.8(29) \times 10^{-5}$
Bins/ms	0.125
χ^2_i/NDF	2770/2494
Fit Method	RMIELN

(b) Fitted statistics and background adjusted parameters.

Table 6.14: The result of the fitting for ^{64}Se decay using the β-p coincidence condition in Fig. 6.37. Parameters fixed during the fit are shown in black, while fitted parameters are shown in blue (N_0 and A_0 value must be multiplied by the binning factor).

6.3.9. ^{64}Se half-life determination using beta-gamma coincidence conditions

As in the previous section, imposing a condition on the γ-ray energy we may remove the major part of the implant-decay correlations corresponding to the daughter nuclei. However, the γ-ray efficiency ε_γ dramatically reduces the already low statistics for this decay. The β-delayed γ-ray energy window was imposed by using the sum of spectra gated on three γ-rays. They were the 697 keV, 1259 keV, and 1449 keV γ-rays. Then, the β-delayed γ-ray energy window was,

$$\begin{aligned} E_\gamma \in\, & [694.6, 700.1] \ominus [680.9, 694.6] \ominus [700.1, 713.9] \\ & \oplus [1256.1, 1261.7] \ominus [1240.5, 1256.1] \ominus [1267.9, 1277.9] \\ & \oplus [1445.7, 1452.7] \ominus [1428.1, 1445.7] \ominus [1452.7, 1470.3] \text{ keV} \,. \end{aligned} \tag{6.12}$$

As in the γ-ray spectrum in Fig. 6.33, the prompt condition was imposed within $[0, 0.8] \ominus [-80, -40]$ ms in the EURICA GeHP DGF-times.

Implantation-decay correlations were fitted using the solution of the Bateman equation corresponding to the mother decay only $A_0(t;^{64}\,\mathrm{Se})$ described in Appendix H, and a constant background a_0 within 10 s of the implantation-decay correlation window. The function used to fit the implantation-decay correlations was,

$$A(t) = a_0 + (1 - DT)\,\varepsilon_{\beta\gamma}\,(1 - Bp(^{64}\mathrm{Se}))\,A_0(t;^{64}\,\mathrm{Se})\,. \tag{6.13}$$

In Fig. 6.38 the γ-gated implantation-decay time correlation is shown as well as the fit to the Bateman equation. In Table 6.15 results of the fits can be seen.

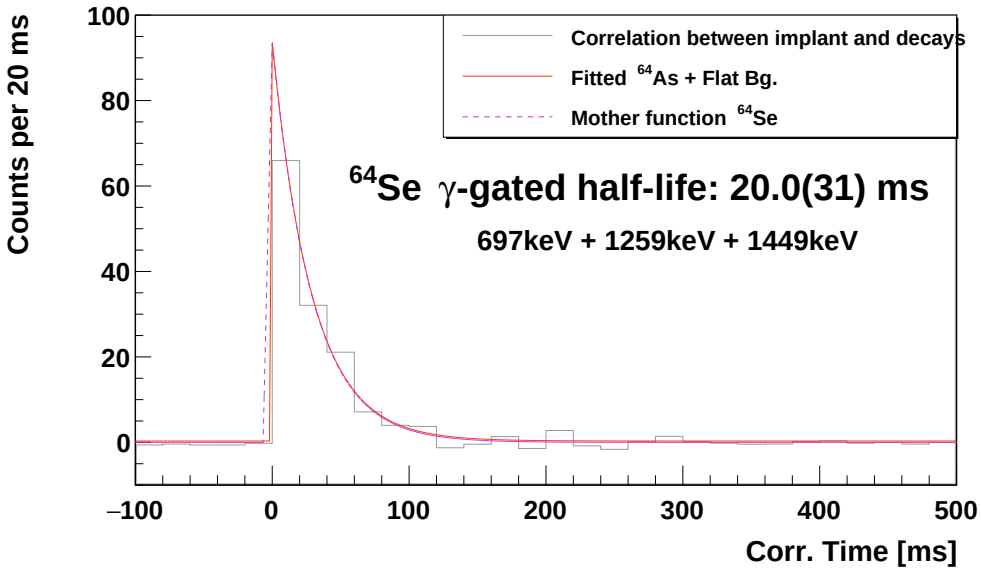

Figure 6.38: ^{64}Se half-life fit using the γ coincidence condition. Free parameters in the fitting process are shown in Tab. 6.15 in blue. To obtain this spectrum the following three γ-rays were used, 697 keV, 1259 keV, and 1449 keV (see Fig. 6.33).

Nucl.	N_0	$T_{1/2}$	$\varepsilon_{\beta\gamma}$	Br_β/Br_p	DT
^{64}Se	179880	20.0(31)ms	0.0372(58)	0, 5198(89)/0.4802(89)	0, 225186
^{64}As	0	63.03ms	0	0.95608/0.04392	0, 225186
^{63}Ge	0	152.60ms	0	1/-	0, 225186

(a) Fitted parameters corresponding to Bateman equations.

Parameter	Comment
a_0	0.316(18)
Bins/ms	0.05
χ^2_i/NDF	186150/996
Fit Method	RMIELN

(b) Fitted statistics and background adjusted parameters.

Table 6.15: The result of the fitting for ^{64}Se decay using the γ coincidence condition (see Fig. 6.33 and Eq. 6.12). Parameters fixed during the fit are shown in black, while fitted parameters are shown in blue (The N_0 and A_0 values must be multiplied by the binning factor).

6.3.10. ^{64}Se half-life determination using all decay members

The half-life for ^{64}Se can be obtained more accurately using the proton branching ratio $Br(p) = 0.4802(89)$ measured in Section 6.3.8 using the β-p coincidence condition.

Implantation-decay correlations were fitted using the solution of the Bateman equation corresponding to the ^{64}Se mother decay $A_0(t;^{64}\,\mathrm{Se})$, the ^{64}As beta decay daughter nucleus $A_1(t;^{64}\,\mathrm{As})$, the ^{63}Ge beta-delayed proton emission $A_1(t;^{63}\,\mathrm{Ge})$. As the daughter ^{64}As also decays by beta-delayed proton emission, its daughter nuclei (granddaughter for ^{64}Se) ^{64}Ge and ^{63}Ga were also included $A_2(t;^{64}\,\mathrm{Ge})$ and $A_2(t;^{63}\,\mathrm{Ga})$. Their contributions to the total activity $A(t)$ are discussed in Appendix H. Also a linear background $a_0 + a_1\,t$ was included corresponding to the random coincidence background.

The implantation-decay time correlations for ^{64}Se decay can be seen in Fig. 6.3.10. Taking into account the half-lives measured for ^{64}As and for ^{63}Ge reported in Sections 6.2.8 and 6.1.7, respectively, the half-life for ^{64}Se was obtained by adjusting the Bateman equations, which are discussed in Appendix H, for this decay with the result $T_{1/2} = 22.47(60)$ms. In Table 6.16 the parameters obtained can be found.

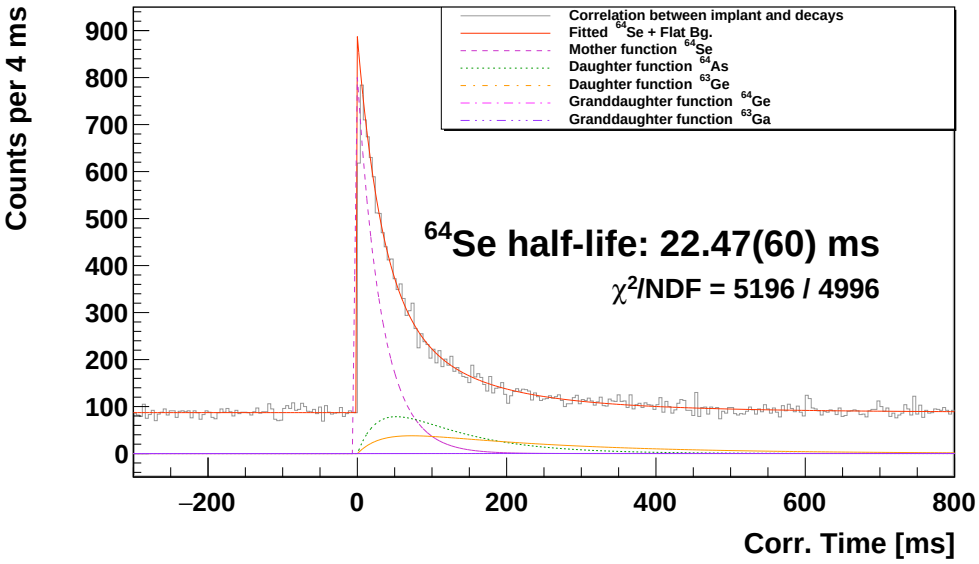

Figure 6.39: ^{64}Se decay half-life measurement using the whole decay chain.

Nucl.	N_0	$T_{1/2}$	$\varepsilon_\beta/\ \varepsilon_p$	Br_β/Br_p	DT
^{64}Se	71952	22.47(60)ms	0.867(15)/1	0, 5198/0.4802	0, 225186
^{64}As	0	63.03ms	0.867(15)/1	0.95608/0.04392	0, 225186
^{63}Ge	0	152.60ms	0.867(15)/-	1/-	0, 225186
^{64}Ge	0	63700ms	0.867(15)/-	1/-	0, 225186
^{63}Ga	0	32400ms	0.867(15)/-	1/-	0, 225186

(a) Fitted parameters corresponding to Bateman equations.

Parameter	Comment
a_0	175.38(56)
a_1	$-1.52(94) \times 10^{-4}$
Bins/ms	0.125
χ^2_i/NDF	2575/2494
Fit Method	RMIELN

(b) Fitted statistics and background adjusted parameters.

Table 6.16: The result of the fitting using all decay members for the ^{64}Se decay. Parameters fixed during the fit are shown in black, while fitted parameters are shown in blue (The N_0 and A_0 values must be multiplied by the binning factor).

6.4. ^{66}As decay analysis

The $A = 66$ mass nuclei analysed in this work correspond to ^{66}As and ^{66}Se. As in the $A = 64$ case, it is convenient to analyse the decay of its daughter nucleus ^{66}As prior to the decay of ^{66}Se, in order to be able to identify the decay radiation belongings to the decay activity of the daughter.

The nucleus $^{66}_{33}As_{33}$ is an odd-odd nucleus and decays by β^+ emission to ^{66}Ge. This nucleus was also produced, separated, and identified by BigRIPs and fortunately it was also implanted in the second DSSSD of the WAS3ABi active stopper.

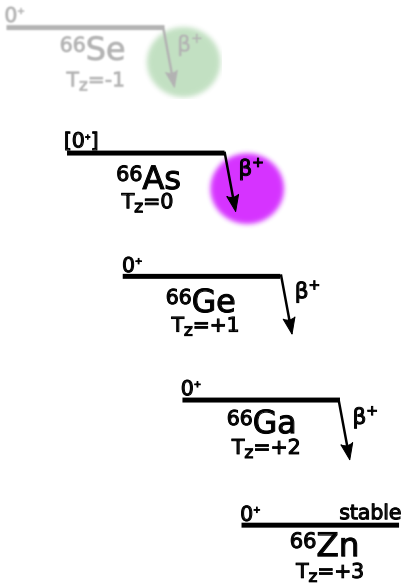

Figure 6.40: Diagram for ^{66}As decay. The main contributors to the implantation-decay correlation are those with comparable half-lives, which are marked with coloured circles.

6.4.1. Implant-decay correlation for ^{66}As decay

The previously reported value for the half-life of ^{66}As corresponds to $T_{1/2} = 95.77(23)$ms [AKW+17]. For this work a common criterion of seven half-lives of the mother nucleus was established (see Appendix G). For this nucleus the time correlation window corresponds to $[-670, 670]$ ms, avoiding symmetrically the first millisecond. Nevertheless in Fig. 6.41 a plot of the implantation-decay time correlations within a wider time correlation window of 10 s is shown to clarify that after the seven half-life interval (in green), most of the correlations would correspond to random coincidences (in red). Then, the green region corresponds to the seven half-lives interval that will be used in the following sections to construct both the beta, and the γ-ray spectra for this decay.

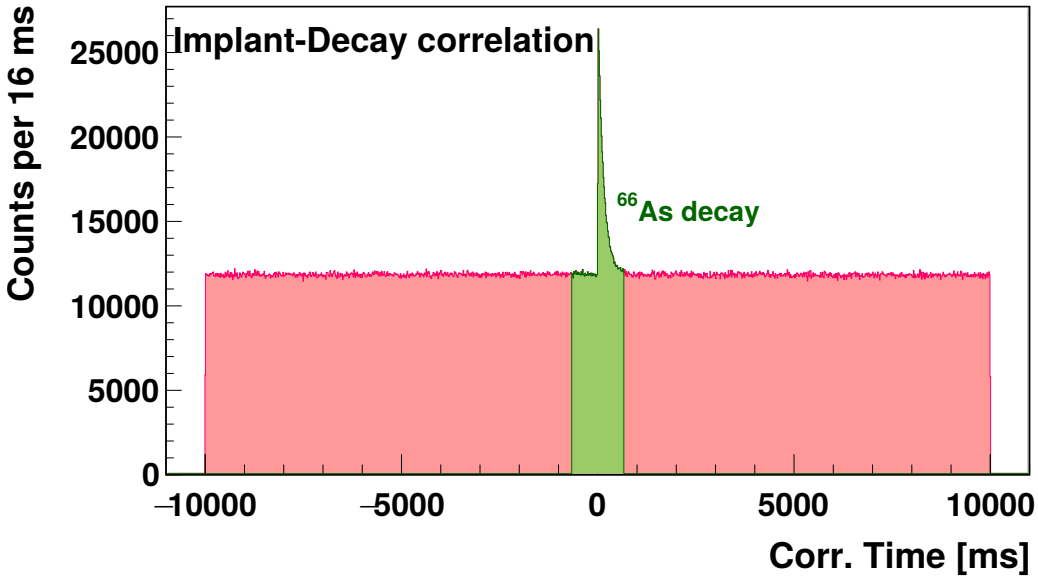

Figure 6.41: Implant-decay correlation for ^{66}As. Correlations were made up to 10 s forward and backward, but to obtain the spectra the implant-decay correlations were constrained to the 670 ms window (seven mother halflives) shown in green.

6.4.2. Beta spectrum for ^{66}As decay

The beta spectrum for ^{66}As decay was obtained using time correlations between implantation and decays within a 1 ms to 670 ms time window. The random correlation background was subtracted using the symmetrically negative implantation-decay time correlations within −670 ms to −1 ms. Decay events were reconstructed using the A10E700NMD condition explained in Section 4.2, which allows one to obtain a higher beta efficiency than the condition A10E700D110 which uses nine pixels of spatial correlation. In Fig. 6.48 the β spectrum is shown, fitted using the parametric beta function described in Appendix E. This fit allows one to identify two components corresponding to the the energy deposited by the beta particle in one strip.

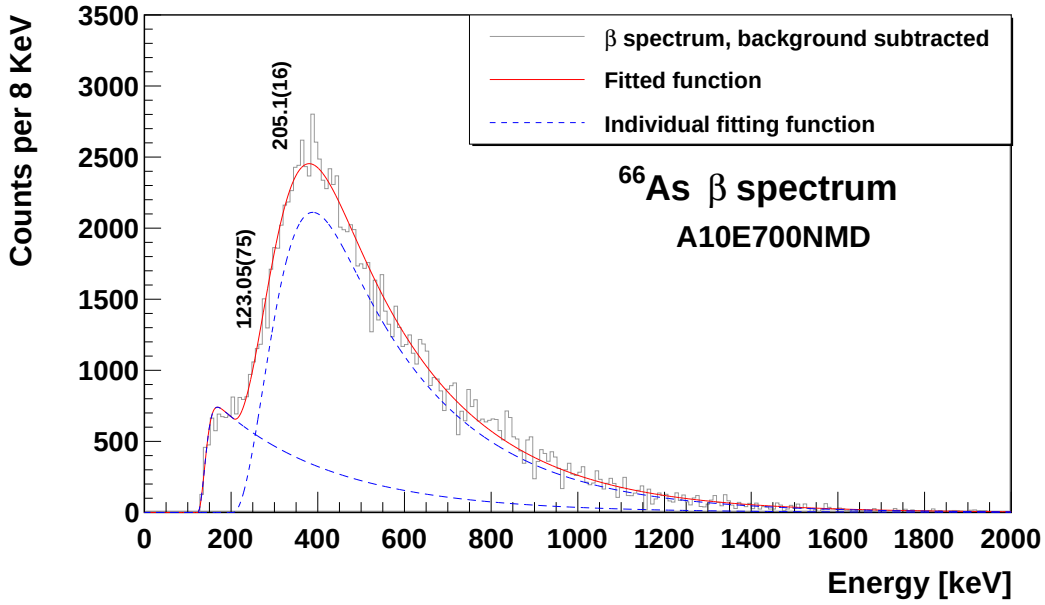

Figure 6.42: Beta spectrum for ^{66}As decay within the $C_w = [1, 670] \ominus [-670, -1]$ ms implantation-decay correlation window. The spectrum was fitted using the parametric beta function detailed in Appendix E. The results of the fits can be seen in Table 6.17.

X_0	Amplitude	CRaise	BTail
123.1(8)	2.8(1)E4	23(2)	272(10)
205(2)	1.05(1)E5	138(2)	253(2)

Table 6.17: The result for the fitting of the ^{66}As beta spectrum shown in Fig. 6.42. The parameters and functions used are described in the Appendix E.

6.4.3. Gamma spectrum for ^{66}As decay

The γ-ray spectrum for ^{66}As was obtained using the same implantation-decay correlation window $C_w = [1, 670]$ ms$\ominus[-670, -1]$ ms as for the beta spectrum. The γ-rays emitted in coincidence with the β^- decay were selected using a prompt condition for $[0, 0.8] \ominus [-80, -40]$ ms in the EURICA GeHP array DGF-times.

The ^{66}As decay γ-ray spectrum can be seen in Fig. 6.43. Apart from the positron annihilation peak at 511 keV, no other γ-ray was observed.

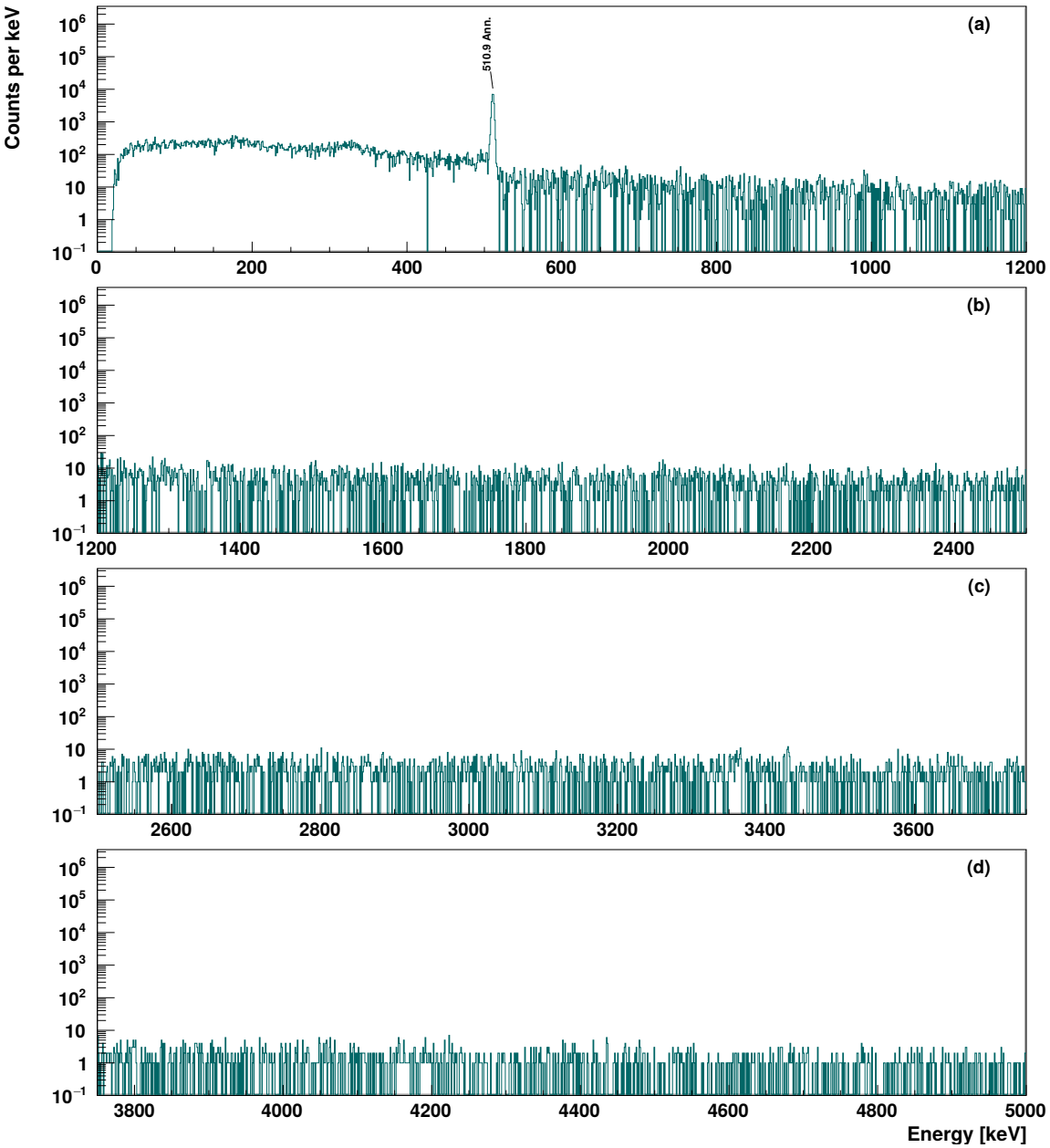

Figure 6.43: Gamma spectrum for ^{66}As decay. In this case no γ-rays were observed.

6.4.4. ^{66}As half-life determination using all decay members

In this section, the half-life for the decay of ^{66}As will be obtained including all the decay members in the Bateman equations, which are discussed in Appendix H. The implantation-decay time correlation distribution was obtained as explained in Section 6.4.1, using a symmetrical time window from -670 ms to 670 ms, avoiding the first millisecond. The implantation-decay correlation were fitted considering the activity of ^{66}As $A_0(t;^{66}\,\mathrm{As})$, the beta decay daughter ^{66}Ge $A_1(t;^{66}\,\mathrm{Ge})$, the beta dacay granddaughter ^{66}Ga $A_2(t;^{66}\,\mathrm{Ga})$, and a linear background $a_0+a_1\,t$. The function used to fit the implantation-decay correlations was,

$$A(t) = a_0 + a_1\,t + (1-DT)\,\varepsilon_\beta\,\varepsilon_\beta\,\left(A_0(t;^{66}\,\mathrm{As}) + A_1(t;^{66}\,\mathrm{Ge}) + A_2(t;^{66}\,\mathrm{Ga})\right) \quad (6.14)$$

where ε_β corresponds to the beta efficiency and $DT = 16.5(11)\%$ is the measured dead-time. The results of the fitting can be seen in Table 6.18 and Fig. 6.44.

Nucl.	N_0	$T_{1/2}$	ε_β	DT
^{66}As	885944	95.31(77)ms	0.7654(43)	0.16499739
^{66}Ge	0	135600ms	0.7654(43)	0.16499739
^{66}Ga	0	34164000ms	0.7654(43)	0.16499739

(a) Fitted parameters corresponding to Bateman equations.

Parameter	Comment
A_0	2964.8(16)
A_1	$-1.0(3)\times10^{-3}$
Bins/ms	0.25
χ^2_i/NDF	5220.4/4995
Fit Method	RMIELN

(b) Fitted statistics and background adjusted parameters.

Table 6.18: The results for the implantation-decay time correlation fit for ^{66}As shown in Fig. 6.44. The parameters obtained are shown in blue. Parameters that were fixed during the fit are shown in black. The number of implantations, N_0 and the background constant A_0 value must be multiplied by the binning factor.

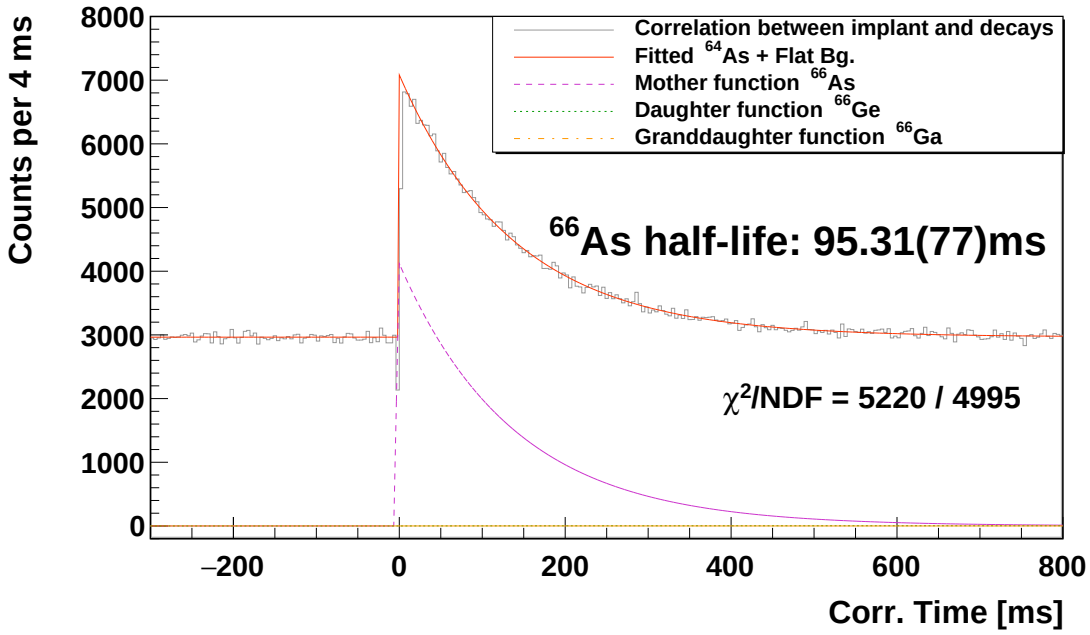

Figure 6.44: Half-life measurement for ^{66}As decay, using all decay members. Daughter half-lives were fixed according to reported values [WAK+17,AKW+17].

6.5. ^{66}Se decay analysis

The nucleus $^{66}_{34}Se_{32}$ has $T_z = -1$. A decay scheme for this nucleus can be seen in Fig. 6.45. It represents the end of the mirror symmetry comparison with charge exchange reactions, since its mirror nucleus, ^{66}Ge, is not stable, until the development of suitable radioactive ion beams.

In Section 6.4 the beta decay daughter ^{66}As was studied, and no γ·ray was observed in the γ-ray spectrum. This is very important since it implies that in the γ-ray spectrum for ^{66}Se decay there will only be γ-rays from the excited states of ^{66}As. In the following sections, the implantation-decay time correlations will be used to obtain both the beta and γ-ray spectra for the ^{66}Se decay.

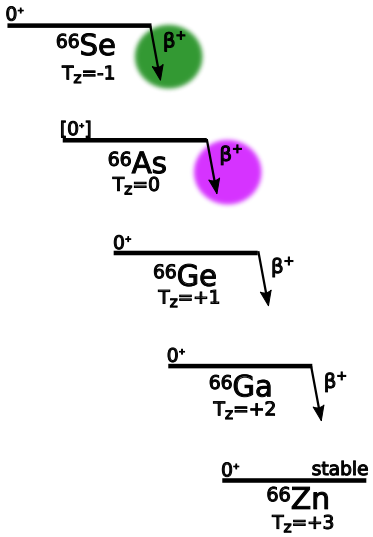

Figure 6.45: Decay scheme for ^{66}Se. The daughter decay, which has a comparable half-life, is coloured, corresponding to ^{66}As decay.

6.5.1. Previous knowledge of the excited states of ^{66}As: The beta decay daughter of ^{66}Se

Excited states in ^{66}As have been studied *in-beam* by Grzywacz et al. at GANIL [G+95, G+98] and at ORNL [G+01]. The level scheme reported in these works is shown in Fig. 6.46. In the level scheme in Fig. 6.46a there are only two tentative 1^+ states while in 6.46b there is only one, the 837 keV. Since the ^{66}Se is tentatively assigned 0^+, the rest of the excited states in ^{66}As seen by Grzywacz et. al. could not be directly populated in the ^{66}Se beta decay. In Section 7.5 we will return to this discussion.

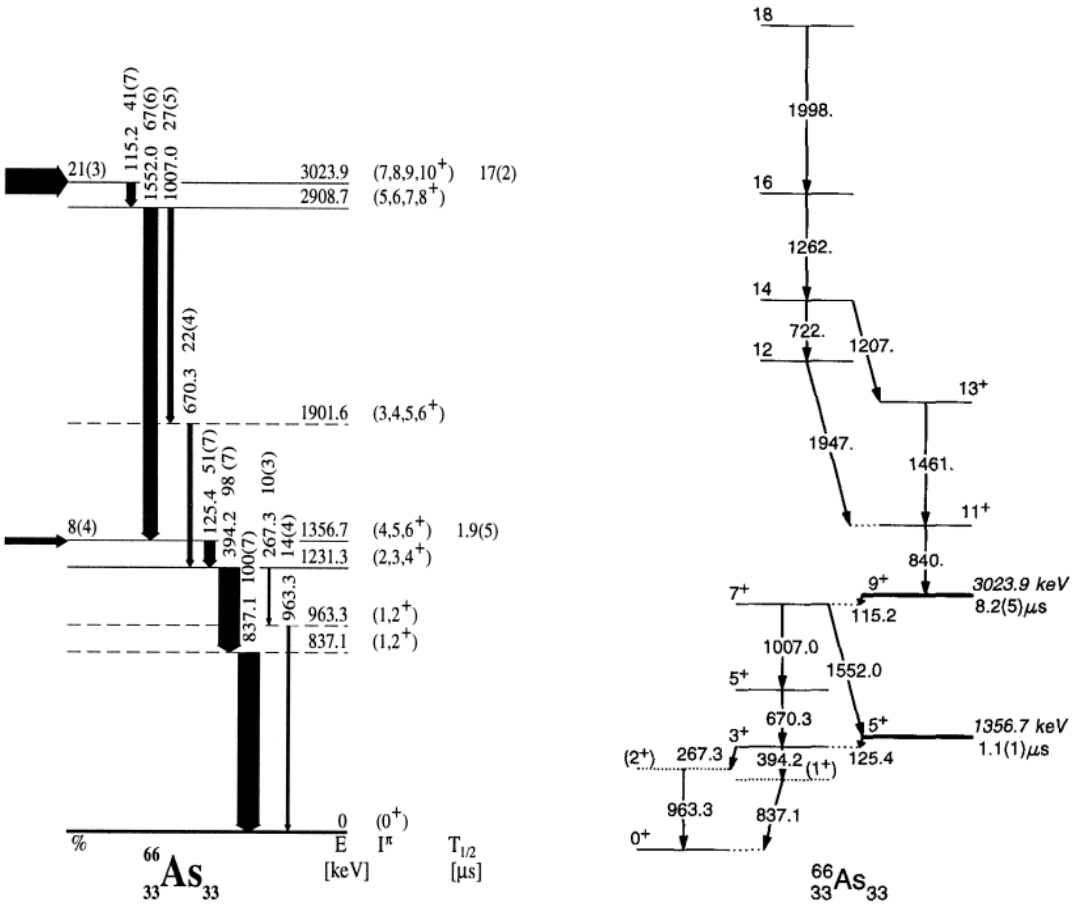

(a) Grzywacz et al. (1998) [G+98]. **(b)** Grzywacz et al. (2001) [G+01].

Figure 6.46: Level scheme for ^{66}As reported by Grzywacz et. al. [G+98, G+01].

6.5.2. Implant-decay correlation for ^{66}Se decay

The previously reported half-life for ^{66}Se decay is 33(12) ms [AKW+17]. In this work a common criterion of seven half-lives of the mother nucleus was established (see Appendix G). For this decay the correlation time window corresponds to $[-400, 400]$ ms, avoiding symmetrically the first millisecond of correlation. In Fig. 6.47 a plot of the implantation-decay correlations within a wider time correlation window of 10 s is shown to clarify that after the seven half-life interval (in green), most of the correlations would correspond to random coincidences (in red). Then,

the green region corresponds to the seven half-lives correlation window that will be used in the following sections to construct the beta and γ-ray spectra for this decay.

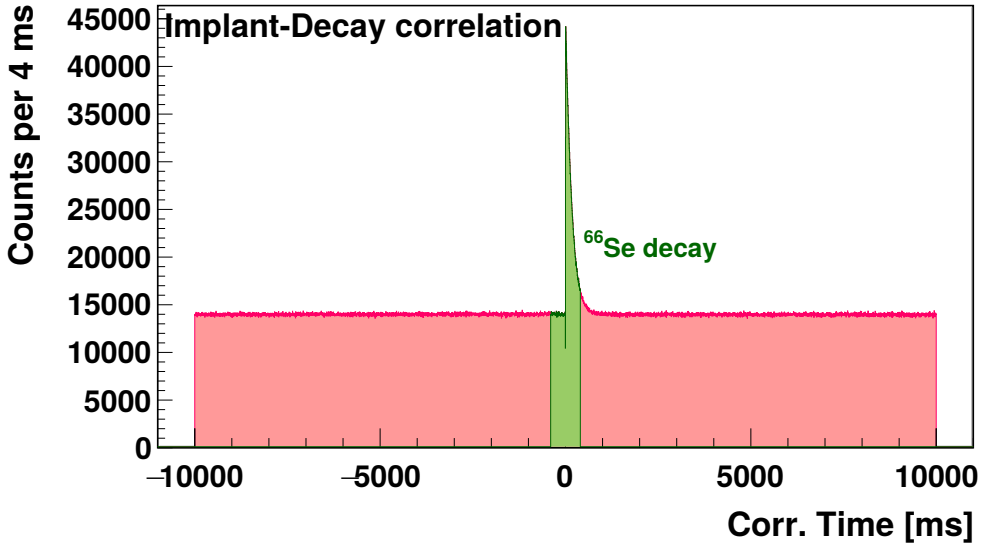

Figure 6.47: Implantation-decay correlation for ^{66}Se. Correlations were made up to 10 s symmetrically forward and backward, however to obtain the beta and γ-ray spectra for this decay, the time correlation window was constrained to 400 ms (seven mother half-lives), shown in green.

6.5.3. Beta spectrum for ^{66}Se decay

The beta spectrum was obtained by correlating implantations and decays within the 1 ms to 400 ms correlation window. The random correlations background was subtracted using the symmetrically negative implantation-decay correlation times within the −1050 ms to −1 ms correlation time window. For the decay events, the A10E700NMD condition described in Section 4.2 was used to obtain the beta spectrum since it offers a higher detection efficiency than the A10E700D110 condition. In Fig. 6.48 the β spectrum is shown, and it was fitted using the parametric beta function detailed in Appendix E.4. This fit allows one to identify three components corresponding to the energy deposited by the beta particle in one strip.

In this case a small component has to be added between 500 keV and 1000 keV which has not been completely understood.

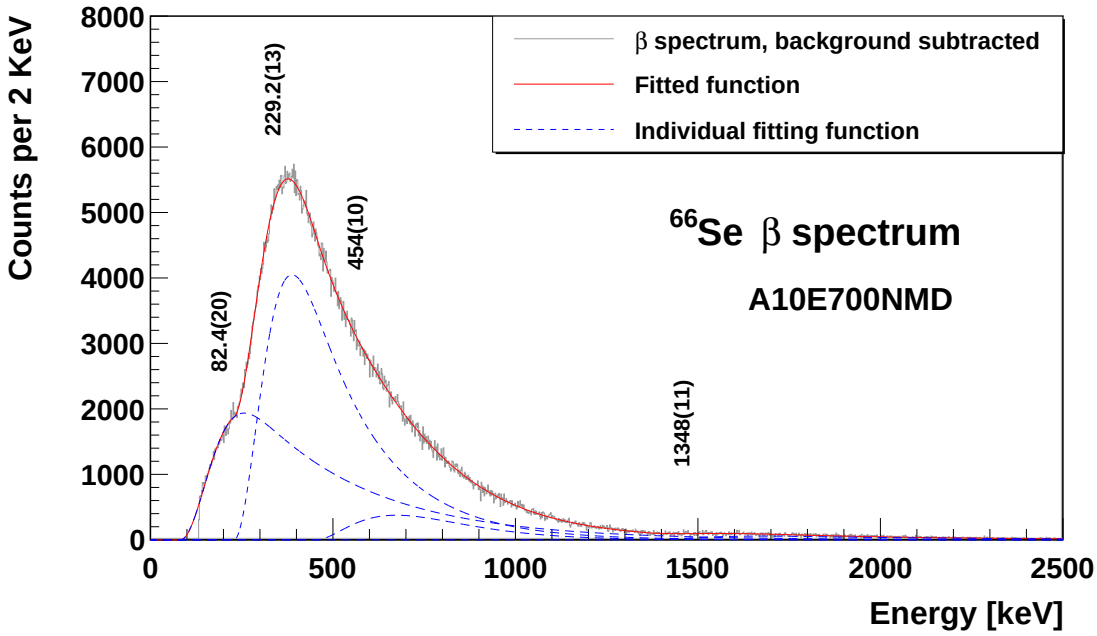

Figure 6.48: Beta spectrum for ^{66}Se decay within the $C_w = [1, 400] \ominus [-400, -1]$ ms implantation-decay correlation window. The spectrum was fitted using the parametric beta function described in Appendix E.4.

X_0	Amplitude	CRaise	BTail
82(2)	4.39(5)E5	117(6)	319(8)
229(1)	6.45(7)E5	129(3)	187(1)
454(10)	7.6(3)E4	3000(3000)	110(3)
1348(10)	2.26(7)E4	222(10)	544(10)

Table 6.19: The result of the fitting for ^{66}Se beta spectrum shown in Fig. 6.48. The parameters and functions used are described in Appendix E.

6.5.4. Gamma spectrum for ^{66}Se decay

The γ-ray spectrum for ^{66}Se decay was constructed using the same implantation-decay correlation window $C_w = [1, 400] \ominus [-400, -1]$ ms described in Section 6.5.2.

Fig. 6.5 shows a scatter plot of the EURICA DGF (Digital Gamma Finder) digitalizer energy -Y axis- and time -X axis- signals. In this figure the γ-prompt condition was imposed within $[0, 0.8] \ominus [-80, -40]$ μs in the EURICA GeHP array, indicated between red lines in Fig. 6.49.

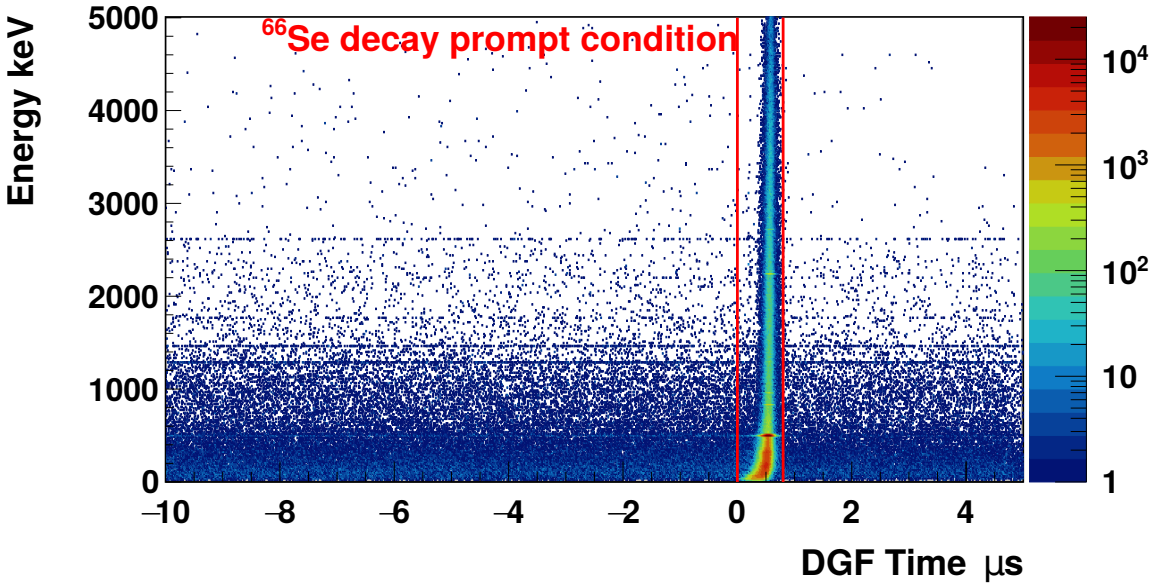

Figure 6.49: A plot of decay energy versus time for the ^{66}Se γ-ray spectrum under the condition that a ^{66}Se nucleus was implanted. The γ-prompt condition is shown between two red lines (0.8 μs width) and corresponds to γ-rays emitted in ^{66}Se decay.

The γ-ray spectrum obtained for ^{66}Se decay can be seen in Fig. 6.50. Each peak in the γ-ray spectrum was fitted in order to obtain the energy, width, and number of counts. The results of the fits are summarised in Table 6.20.

Thirty eight peaks were observed in the γ-ray spectrum of ^{66}Se decay, including the lead fluorescence x-rays, the positron annihilation photo-peak, and nine γ-rays identified in the ^{66}Se decay:

- The 836.9 keV, 963.6 keV, 1309.4 keV, 1765.8 keV, 2249.9 keV, 2273.8 keV, 2725.9 keV, 2730.6 keV, and 3117.8 keV γ-rays were assigned to ^{66}Se decay.

Pb x-rays The 72.8 keV, 74.9 keV, 84.8 keV, and the 86.7 keV lines correspond to Lead fluorescence x-rays $k_{\alpha 2} + k_{\alpha 3}$, $k_{\alpha 1}$, $k_{\beta 1} + k_{\beta 3}$, and $k_{\beta 2}$, respectively (see Appendix K).

Ann. The 511.0 keV γ-ray energy corresponds to the positron annihilation peak.

□ The 114.9 keV, 649.4 keV, 808.6 keV, 919.2 keV, 1681.6 keV, 1705.5 keV, 1737.8 keV, 1743.8 keV, 2000.8 keV, 2216.8 keV, 2228 keV, 2305 keV, 2314.2 keV, 2319.7 keV, 2375.6 keV, 2854.3 keV, 2862.4 keV, 3366.5 keV, 3371.5 keV photo-peaks were considered to be too weak to be assigned to ^{66}Se decay.

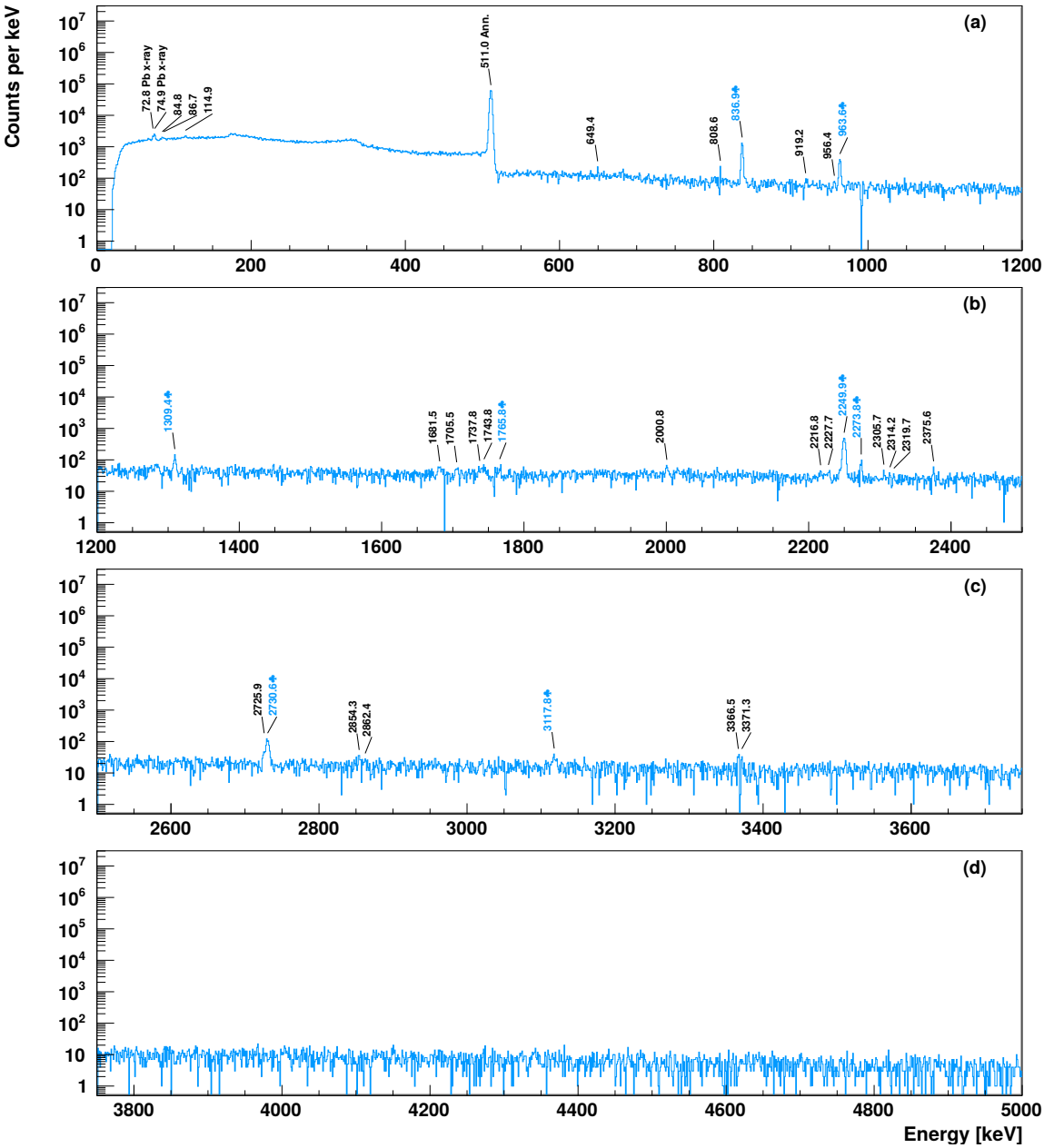

Figure 6.50: Gamma ray spectrum for ^{66}Se decay constructed within the $[0, 0.8] \ominus [-80, -40]$ μs β-γ coincidence window. Gamma rays as belongings to ^{66}Se are marked with ♣. Unplaced γ-ray radiation is marked with □, together with the lead fluorescence x-rays, and the positron annihilation peak.

Energy keV	FWHM keV	Counts	Efficiency (ε_γ)	Intensity	Comments
72.8(9)	1.8(2)	953(90)	0.161(6)	5905(600)	Pb x-ray $k_{\alpha 2} + k_{\alpha 3}$
74.9(6)	1.8(2)	1732(100)	0.163(6)	1.06(7)E4	Pb x-ray $k_{\alpha 1}$
84.8(2)	1.8(2)	524(80)	0.168(6)	3113(500)	Pb x-ray $k_{\beta 3} + k_{\beta 1}$
86.7(6)	1.8(2)	277(80)	0.169(6)	1638(500)	Pb x-ray $k_{\beta 2}$
114.9(1)	2.5(4)	914(100)	0.173(6)	5286(800)	-
510.97(0)	3.143(5)	2.138(5)E5	0.114(4)	1.88(7)E6	$e^+ + e^-$
649.4(1)	1.75(4)	170(20)	0.102(4)	1670(200)	-
808.6(8)	1.75(1)	146(20)	0.091(3)	1598(200)	-
836.9(2)	2.36(4)	3335(60)	0.090(3)	3.7(1)E4	^{66}Se decay
919.2(2)	1.75(7)	75(20)	0.085(3)	882(200)	-
956.4(3)	2.47(9)	68(20)	0.083(3)	815(200)	-
963.6(4)	2.47(9)	997(40)	0.083(3)	1.20(6)E4	^{66}Se decay
1309.4(1)	2.9(3)	300(30)	0.070(2)	4277(400)	^{66}Se decay
1681.6(4)	4.7(5)	146(20)	0.060(3)	2422(400)	-
1705.5(4)	4.7(5)	97(20)	0.060(3)	1625(300)	-
1737.8(6)	4.7(5)	95(20)	0.059(3)	1606(400)	-
1743.8(5)	4.7(5)	136(20)	0.059(3)	2303(400)	-
1765.8(5)	4.7(5)	106(20)	0.058(3)	1817(400)	^{66}Se decay
2000.8(3)	2.8(6)	81(20)	0.054(3)	1504(300)	-
2216.8(5)	4.09(9)	57(20)	0.050(3)	1140(300)	-
2228(1)	4.09(9)	59(20)	0.050(3)	1177(300)	-
2249.9(4)	4.09(9)	2136(50)	0.050(2)	4.3(2)E4	^{66}Se decay
2273.8(2)	4.09(9)	201(20)	0.049(2)	4070(500)	^{66}Se decay
2305.7(2)	1.7(1)	42(10)	0.049(2)	854(200)	-
2314.2(3)	1.7(1)	28(10)	0.049(2)	567(200)	-
2319.7(4)	1.7(1)	21(10)	0.049(2)	425(200)	-
2375.6(2)	1.7(2)	64(10)	0.048(2)	1349(300)	-
2725.9(5)	4.3(3)	90(20)	0.043(2)	2098(500)	^{66}Se decay
2730.6(1)	4.3(3)	456(30)	0.043(2)	1.07(8)E4	^{66}Se decay
2854.3(2)	1.8(5)	47(10)	0.041(2)	1143(300)	-
2862.4(2)	1.8(5)	27(9)	0.041(2)	649(200)	-
3117.8(4)	5(3)	100(20)	0.038(2)	2615(400)	^{66}Se decay
3366.5(2)	1.8(3)	59(10)	0.035(2)	1670(300)	-
3371.3(2)	1.8(3)	42(9)	0.035(2)	1180(300)	-

Table 6.20: Results of the fitting of the ^{66}Se decay γ-ray prompt spectrum shown in Fig. 6.50. The intensities shown in the fifth column correspond to the number of counts corrected by the γ-ray efficiency.

6.5.5. Gamma-gamma coincidence spectra for ^{66}Se decay

From the γ-ray spectrum for ^{66}Se decay in Fig. 6.50, the energies and intensities were obtained for each γ-ray transition. Only two γ-rays were previously reported by Grzywacz et. al. in [G$^+$98, G$^+$01]. Thus, in order to obtain the energies of the excited states in ^{66}As from which each γ-ray was emitted, the γ-γ coincidence projection spectra were constructed in Figs. 6.51 to 6.54 by gating on several γ-rays observed in the γ-spectrum for ^{66}Se decay in Fig. 6.50. The γ-γ coincidence analysis for ^{66}Se will be discussed in Section 7.5 during the decay scheme construction.

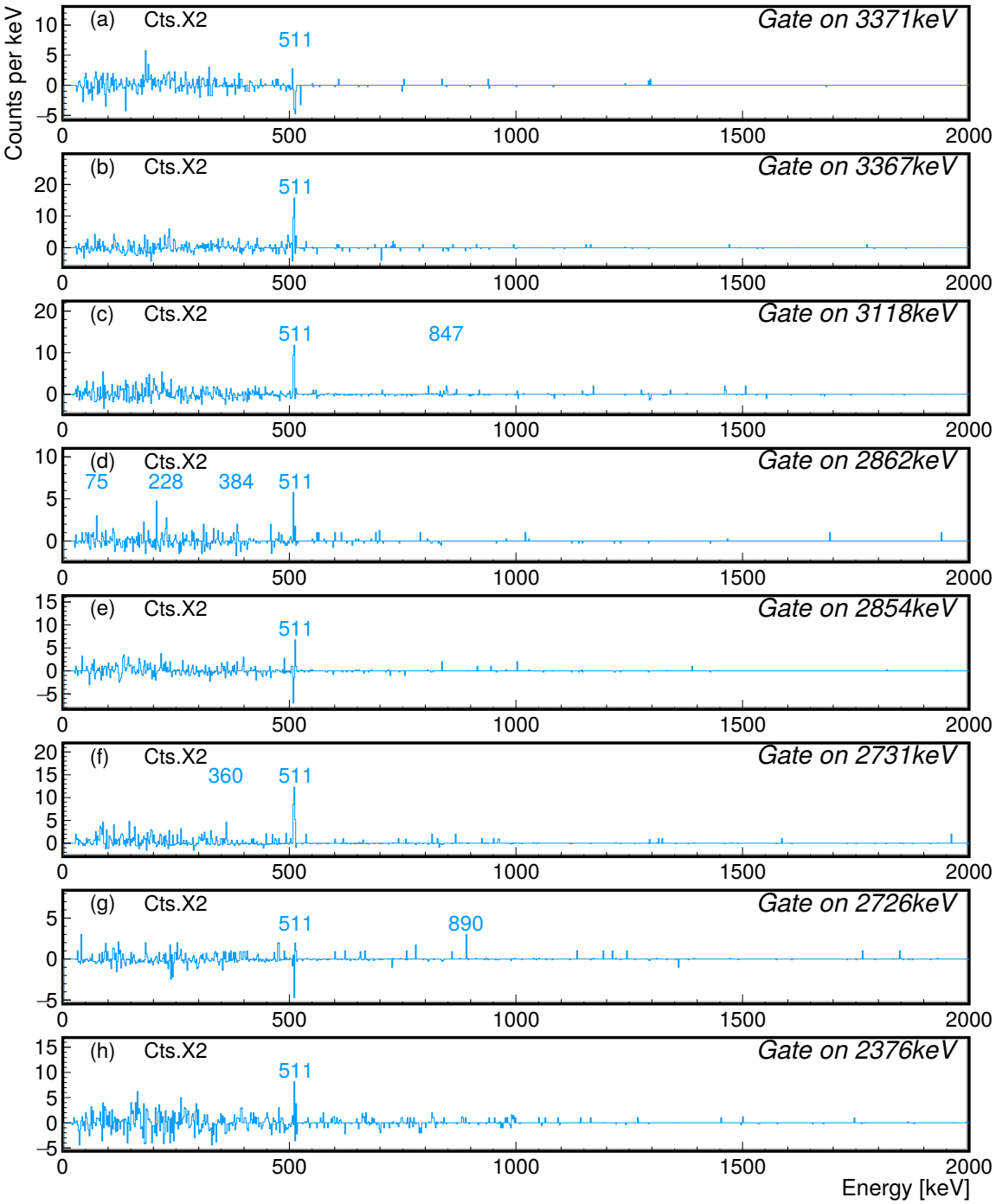

Figure 6.51: γ-γ background subtracted coincidence spectra for the ^{66}Se decay, requiring coincidences with: (a) 3371 keV, (b) 3367 keV, (c) 3118 keV, (d) 2862 keV, (e) 2854 keV, (f) 2731 keV, (g) 2726 keV and (h) 2376 keV.

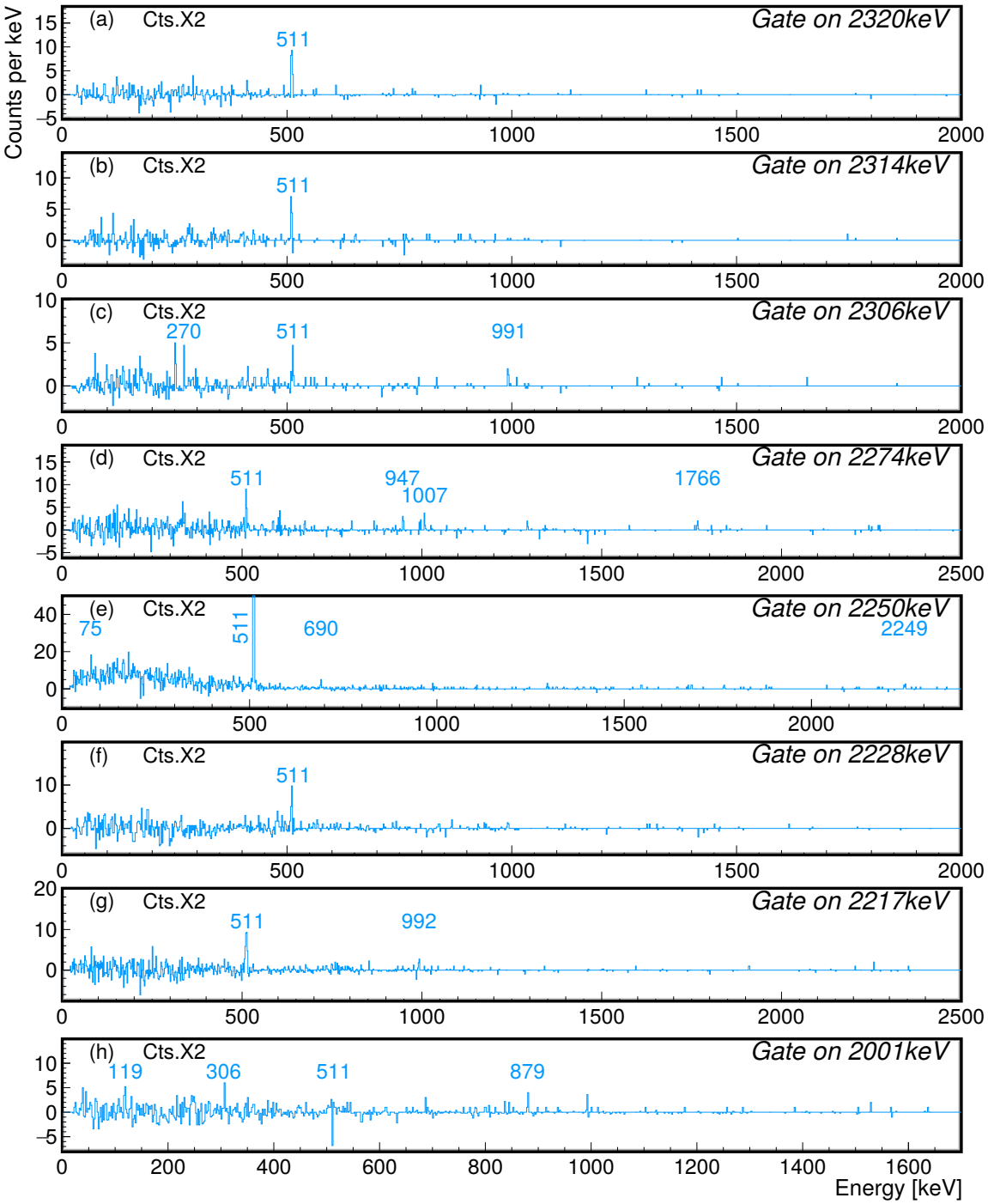

Figure 6.52: γ-γ background subtracted coincidence spectra for the ^{66}Se decay, requiring coincidences with: (a) 2320 keV, (b) 2314 keV, (c) 2306 keV, (d) 2274 keV, (e) 2250 keV, (f) 2228 keV, (g) 2217 keV and (h) 2001 keV.

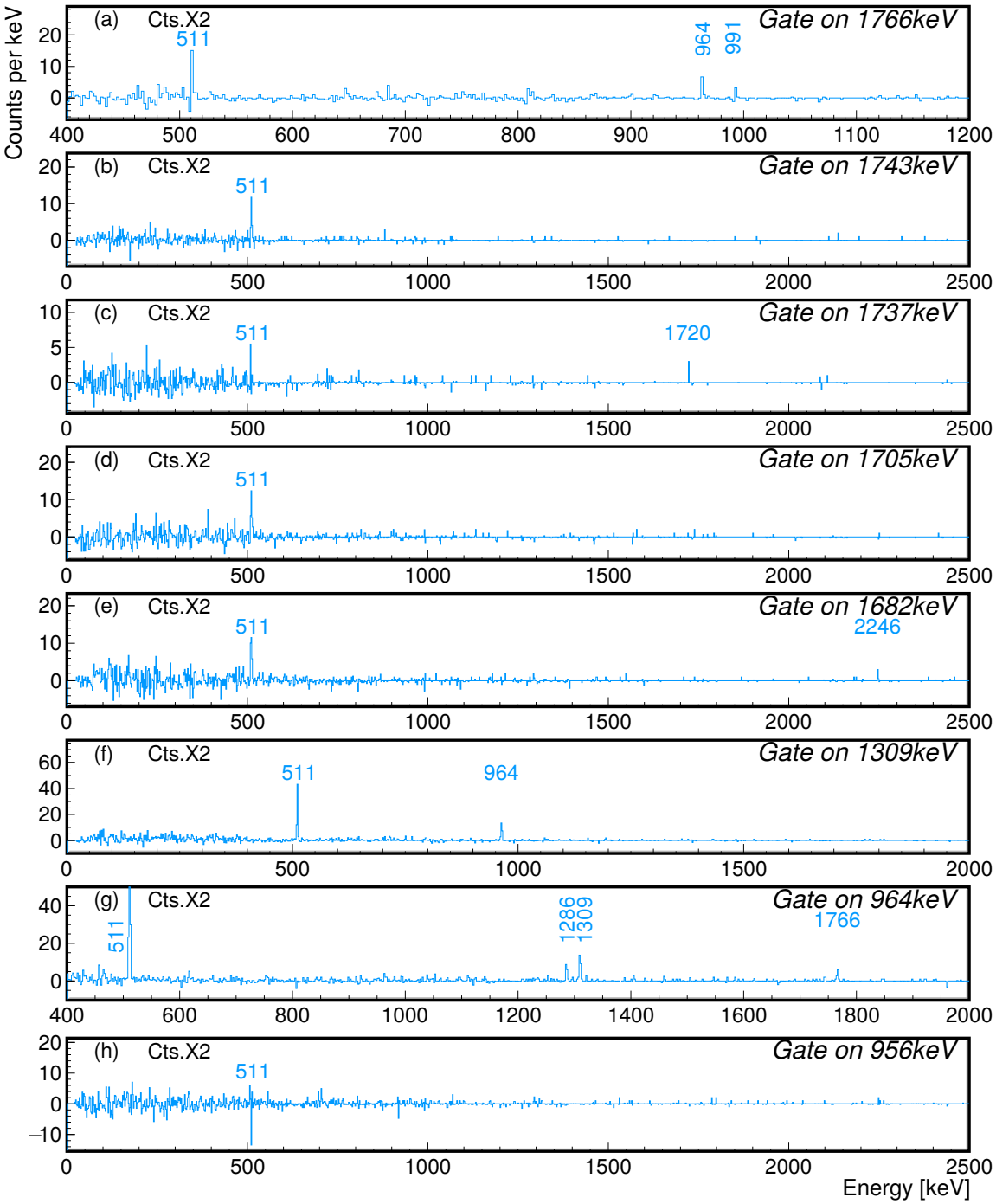

Figure 6.53: γ-γ background subtracted coincidence spectra for the ^{66}Se decay, requiring coincidences with: (a) 1766 keV, (b) 1743 keV, (c) 1737 keV, (d) 1705 keV, (e) 1682 keV, (f) 1309 keV, (g) 964 keV and (h) 956 keV.

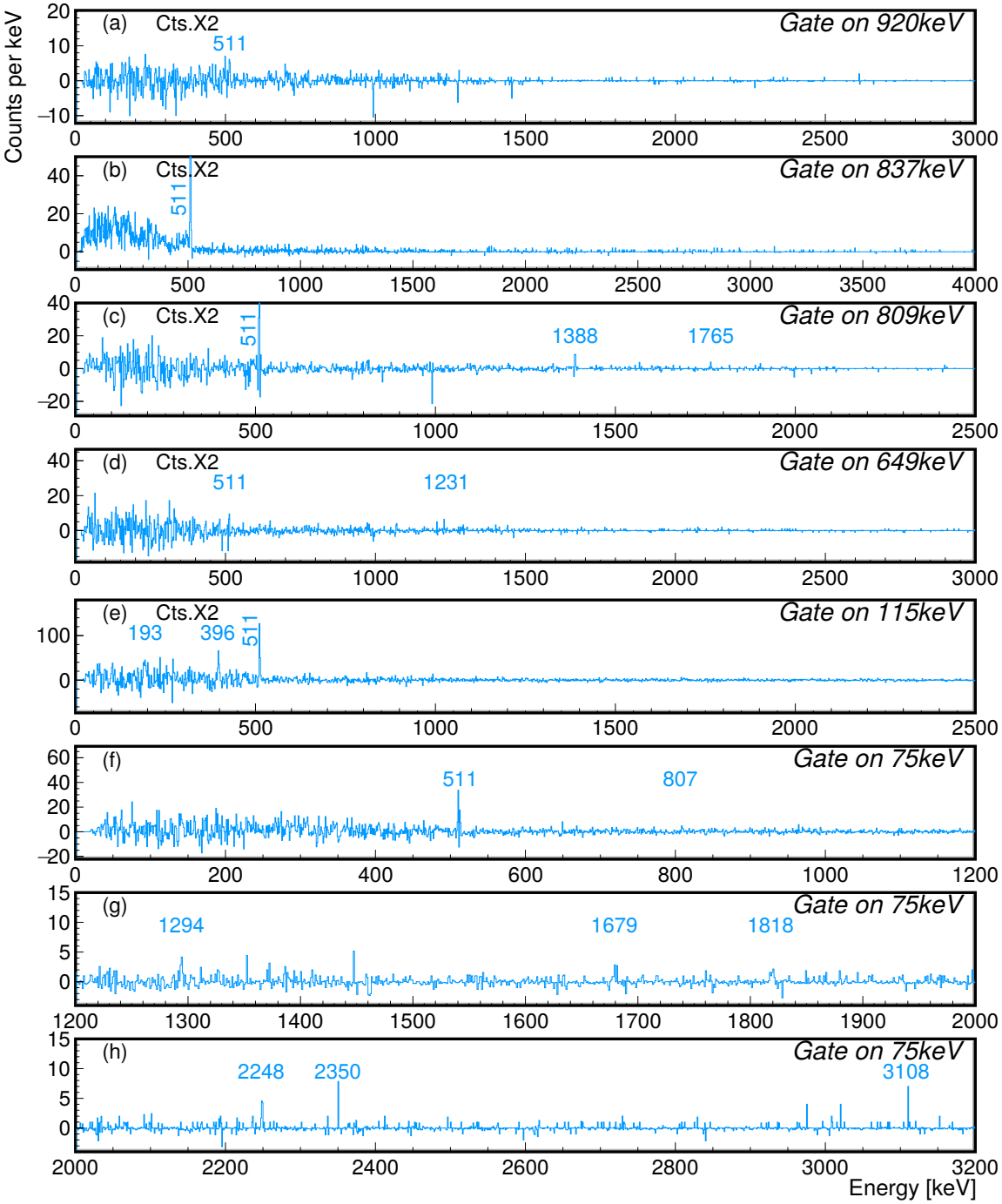

Figure 6.54: γ-γ background subtracted coincidence spectra for the ^{66}Se decay, requiring coincidences with: (a) 920 keV, (b) 837 keV, (c) 809 keV, (d) 649 keV, (e) 115 keV, (f) 75 keV, (g) 75 keV (continuation) and (h) 75 keV (continuation).

6.5.6. ^{66}Se half-life determination using beta-gamma coincidence conditions

In the γ-ray spectrum for ^{66}Se decay shown in Fig. 6.50, there are two γ-rays with enough intensity to be used in the half-life measurement for ^{66}Se. They are the 836.9 keV and the 2249.9 keV peaks. The β-delayed γ-ray time correlation window was set within $[0, 0.8] \ominus [-80, -40]$ ms for the EURICA HPGe array DGF-times. The γ-ray energy window was set within $[833.8, 839.9] \ominus [818.752, 833.835] \ominus [839.9, 855.0]$ keV for the 836.9 keV, and within $[2244.7, 2255.1] \ominus [2218.7, 2244.7] \ominus [2255.1, 2270.6] \ominus [2277.2, 2281.0]$ for the 2249.9 keV peak.

The implantation-decay time correlations were fitted using the solution for the Bateman equations considering only the mother nucleus activity, within a 10 s symmetrical time correlation window, avoiding the first millisecond. In this decay the total activity $A(t)$ was fitted considering the activity of ^{66}Se $A_0(t;^{66}\,\mathrm{Se})$ and a constant background a_0. The function used to fit the implantation-decay correlations was,

$$A(t) = a_0 + (1 - DT)\,\varepsilon_{\beta\gamma}\,A_0(t;^{66}\,\mathrm{Se}) \tag{6.15}$$

where $\varepsilon_{\beta\gamma} = \varepsilon_\beta \varepsilon_\gamma$ corresponds to the beta-gamma gated efficiency and $DT = 16.6(11)\%$ is the measured dead-time. The fit results are summarised in Table 6.21.

Parameter/Energy	836.9 keV	2249.9 keV
$N_0(^{66}\text{Se})$	3847800	4809750
$T_{1/2}(^{66}\text{Se})$ms	60.3(22)	61.7(22)
Dead-time	0.166085	
$\varepsilon_{\beta\gamma}(^{66}\text{Se})$	$3.423(87) \times 10^{-3}$	$3.404(87) \times 10^{-3}$
$Br(\beta(^{66}\text{As})$	1	
A_0 (bg.)	6.958(54)	8.935(68)
Bins/ms	0.25	
χ^2_i/NDF	5286/4995	4235/3997
Fit Method	RN	
Range ms	$[-10000, 10000] \ominus [-2, 2]$	

Table 6.21: Summary for the half-life measurement using β-γ coincidence windows. Fitted parameters are shown in blue. Parameters fixed during the fit, such as the number of implantations N_0 or dead-time DT, are shown in black. Parameters common to both measurements are shown in the centre of the row.

6.5.7. ^{66}Se half-life determination using the whole decay members

In this section, the half-life for ^{66}Se will be obtained by adjusting the implantation-decay time correlations introduced in Section 6.5.2. The half-life of the daughter nucleus ^{66}As was measured in Section 6.4.4 to be $T_{1/2} = 95.31(77)$ ms, and was used as a fixed parameter in the fit of the solution of the Bateman equations.

According to the discussion in Section 6.5.2, the implantation-decay time correlations were obtained using a symmetrical 10 s time correlation window in Fig. 6.55, where these correlations were fitted using the solution of the Bateman equations. The implantation-decay correlations were fitted considering the activity of ^{66}Se $A_0(t;^{66}\,\text{Se})$, the beta decay daughter ^{66}As $A_1(t;^{66}\,\text{As})$, the beta decay granddaughter ^{66}Ge $A_2(t;^{66}\,\text{Ge})$, the beta decay great-granddaughter ^{66}Ga $A_3(t;^{66}\,\text{Ga})$, and a linear background $a_0 + a_1\,t$. The function used to fit the implantation-decay correlations was,

$$A(t) = a_0 + a_1\, t + (1 - DT)\, \varepsilon_\beta \left(A_0(t; {}^{66}\mathrm{Se}) + A_1(t; {}^{66}\mathrm{As}) + A_2(t; {}^{66}\mathrm{Ge}) + A_3(t; {}^{66}\mathrm{Ga}) \right) \tag{6.16}$$

where ε_β corresponds to the beta efficiency and $DT = 16.6(11)\%$ is the measured dead-time. In Table 6.22 results of the fits are summarised.

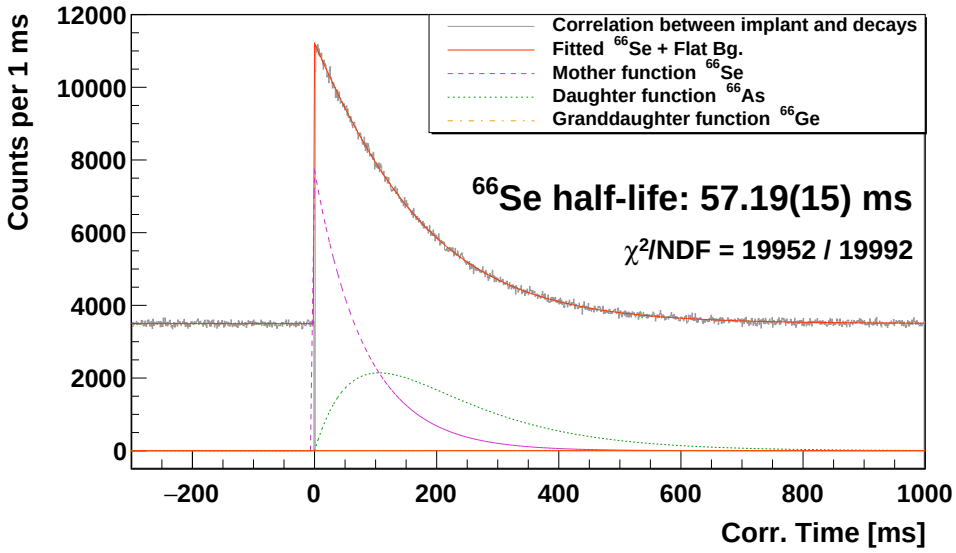

Figure 6.55: Half-life for ^{66}Se using all decay members of the nuclear decay chain. The daughter half-life for ^{66}As was fixed to our value measured in Section 6.4.4. The results of the fits are summarised in Table 6.22.

Nucl.	N_0	$T_{1/2}$	ε_β	DT
^{66}Se	961950	57.19(15)ms	0.7928(11)	0, 166085
^{66}As	0	95.77ms	0.7928(11)	0, 166085
^{66}Ge	0	135600ms	0.7928(11)	0, 166085
^{66}Ga	0	34164000ms	0.7928(11)	0, 166085

(a) Fitted parameters corresponding to Bateman equations.

Parameter	Comment
a_0	3498.50(88)
a_1	$-8.6(15) \times 10^{-4}$
Bins/ms	1
χ^2_i/NDF	19952/19992
Fit Method	RMIELN

(b) Fitted statistics and background adjusted parameters.

Table 6.22: The result of the fitting for ^{66}Se half-life in Fig. 6.55. Parameters fixed during the fit are shown in black, and fitted parameters are shown in blue. Parameters common to all fits are shown in the centre of the row.

Part IV

Discussions

Chapter 7

Level scheme construction using previously reported Q_β values

The main objective of this thesis is to obtain the beta decay Gamow-Teller transition strengths for the $T_z = -2$ ^{64}Se and the $T_z = -1$ ^{66}Se. In Chapter 6 the analysis of the nuclei of interest and their descendants was detailed, where the half-lives ($T_{1/2}$) and transition intensities for protons and γ-rays were obtained. To obtain the beta decay strengths for the decays of these nuclei it is necessary to use the Q_β values, which have not been measured in our experiments. They can be found in [WAK+17, AKW+17]. In the case of ^{64}Se and ^{64}As they are only to be found as theoretical extrapolations. In this work it was possible to estimate the Q_β value for the ^{64}Se and the ^{64}As using the **I**sobaric **M**ass **M**ultiplet **E**quation (IMME).

The discussion of the levels schemes is organised as follows. In Section 7.1 the level scheme for ^{63}Ge decay will be presented. Then scheme for ^{64}As decay will be discussed in Section 7.2, followed by the discussion of the scheme for ^{64}Se decay in Section 7.3, both decays analyzed using the previously reported AME2016 [WAK+17] Q_β values. For the $A = 66$ nuclei a similar logic is followed, with the discussion of

first the ^{66}As decay scheme then the ^{66}Se decay scheme in Section 7.5.

Following the discussion of the level schemes using the previously reported Q_β values, in Chapter 8 we will turn to the estimation of the Q_β values using the data from this experiment. In Section 8.1 Q_β values will be estimated using the energies of protons and γ-rays emitted in the ^{64}Se beta decay, the previously reported mass excess for ^{63}Ge, and the **I**sobaric **M**ass **M**ultiplet **E**quation (IMME). Finally, in Sections 8.2 and 8.3 the beta decay strengths will be calculated using our estimates of the Q_β values for ^{64}As decay and ^{64}Se decay, respectively.

7.1. The decay scheme of ^{63}Ge

In this section, using the experimental results from previous sections such as γ-ray intensities, γ-ray coincidences, and half-lives, together with the Q_β = 9626(40) keV reported in AME2016 [WAK+17], the level scheme for ^{63}Ge decay will be obtained together with the beta decay strengths.

In Nubase2016 [AKW+17] the ^{63}Ga$^{\mathbf{g.s.}}$ is reported as $J^\pi = 3/2^{(-)}$. Indeed in [B+91, W+01] it was reported to be $J^\pi = 3/2^-$. Since the ^{63}Ga is the mirror nucleus of ^{63}Ge, we assume $\mathbf{J^\pi = 3/2^-}$ for ^{63}Ge$^{\mathbf{g.s.}}$. In Table 7.1 a summary of the selection rules for this beta decay is presented.

The γ-rays with energies of 75.0 keV, 442.8 keV, and 722.2 keV appear both in Balamuth et. al. [B+91] and in Weiszflog et. al [W+01] as direct γ-ray transitions to the g.s. of the ^{63}Ga from excited states with energies **75.0 keV**, **442.8 keV**, and **772.2 keV** respectively. The 75 keV γ-ray corresponds to the transition from first excited state $J^\pi = 5/2^-$ with energy **75 keV** [B+91, W+01], to the ground state. analogously for the 443 keV and 772 keV.

J^π mother	Transition	L	S	Type	$\Delta\pi$	ΔJ	J^π daughter
$3/2^-$	Allowed	0	0	F	No	0	$3/2^-$
$3/2^-$	Allowed	0	1	GT	No	$0,1$	$1/2^-,\ldots,5/2^-$
$3/2^-$	First-Forbidden	1	0	F	Yes	$0,1$	$1/2^+,\ldots,5/2^+$
$3/2^-$	First-Forbidden	1	1	GT	Yes	$0,1,2$	$1/2^+,\ldots,7/2^+$
$3/2^-$	Second-Forbidden	2	0	F	No	$0,1,2$	$1/2^-,\ldots,7/2^-$
$3/2^-$	Second-Forbidden	2	1	GT	No	$0,\ldots,3$	$1/2^-,\ldots,9/2^-$
$3/2^-$	Third-Forbidden	3	0	F	Yes	$0,\ldots,3$	$1/2^+,\ldots,9/2^+$
$3/2^-$	Third-Forbidden	3	1	GT	Yes	$0,\ldots,4$	$1/2^+,\ldots,11/2^+$

Table 7.1: Selection rules for the ^{63}Ge beta decay. Since $J^\pi = 3/2^-$ was prior reported [AKW+17], and taking into account the mirror symmetry, the ground state of the ^{63}Ge was assumed $J^\pi = 3/2^-$.

7.1.1. Analysis of gamma-gamma coincidence projected spectra for ^{63}Ge decay

During the analysis of the ^{63}Ge in Section 6.1.4 we presented the total γ-ray coincidence projection spectrum correlated with ^{63}Ge implants, Fig. 6.6. Then in Section 6.1.5 we showed the γ-γ coincidence spectrum for all γ-rays observed in ^{63}Ge decay. The results are presented in Table 7.2. The decay scheme is discussed in the following section and presented in Fig. 7.1.

The energy difference between the previously reported states at **75.0 keV** and **442.8 keV** is 367.5 keV. We observed a γ-ray with this energy. Moreover, from Table 7.2 we see that the γ-rays with energies 75.0 keV and 367.5 keV are in coincidence while the 367.5 keV is not in coincidence with the 442.8 keV. This suggests that the 367.5 keV is a γ-transition between the excited states at **442.8 keV** and **75.0 keV**.

The 367.5 keV and 442.8 keV γ-rays are both emitted from the excited state at **442.8 keV**. Both γ-rays are in coincidence with γ-rays with energies 2765.1 keV

Energy gate keV	**Spectrum number**	**γ-ray coincidence energy keV**
75.0	6.10(s), 6.10(t), 6.10(u)	367.5, 482.4, 627.0, 636.3, 647.4, 650.7, 709.1, and 2765.1.
367.5	6.10(q), 6.10(r)	75.0, *144*, 482.4, 2765.1 and 2971.4
373.1	6.10(p)	*138* and 627.0
442.8	6.9(n), 6.10(o)	482.4 and 2765.1
482.4	6.9(m)	442.8 and 367.5
627.0	6.9(l)	373.1
641.2	6.9(k)	709.1, and 722.2
647.4	6.9(j)	75.0, and *722.2*
709.1	6.8(g), 6.9(h), 6.9(i)	75.0, 641.2, 647.4, *678*, *709.1*, 722.2, *1277*, and *1495.1*
722.2	6.8(f)	641.2
954.2	6.8(d)	1332.9
2765.1	6.8(a)	367.5, 442.8

Table 7.2: Summary of the γ-ray coincidence projected spectra for the ^{63}Ge decay. The 925.0 keV, the 1363.6 keV, and the 2485.4 keV do not shown any γ-ray coincidences. γ-rays written in italic are γ-rays observed in the γ-γ coincidence projected spectra but not in the γ-ray spectrum, or have low intensity.

and 482.4 keV, and vice-versa (see Table 7.2). This suggests that the γ-rays of 482.4 keV and the 2765.1 keV feed the **442.8 keV** level, and are emitted from excited states at **925.1 keV** and **3207.9 keV**, respectively. In addition the γ-ray with energy 925.0 keV is consistent with the existence of an excited state at **925.1 keV**.

The 722.2 keV γ-ray energy is reported as being a γ-transition emitted from excited state **722.2 keV** to the ground state in ^{63}Ga. The 647.4 keV γ-ray matches the energy difference between the excited states at **772.2 keV** and **75.0 keV**. This is also confirmed by the γ-ray coincidence between the γ-rays with energies 75.0 keV and 647.4 keV.

The 627.1 keV γ-ray was previously reported as a γ-transition to the g.s. from excited state at **627.1 keV**. As the γ-rays with energies 627.1 keV and the 373.1 keV are in coincidence, the last one should be emitted from excited state at

1000.1 keV to the **627.0 keV**.

The 722.2 keV γ-ray is in coincidence with the γ-ray with energy 641.2 keV. This suggest the existence of a level at **1363.6 keV**. Moreover, there is a strong γ-ray transition with this energy, which is therefore assigned as the ground state transition from this level.

The 709 keV γ-ray is in coincidence with the γ-ray with energy 641.2 keV. However, the coincidence between the 1363.6 keV and the 709 keV is not clear. This can be due to the lower efficiency of the detectors for the 1363 keV γ-ray. In this work we consider this γ-ray as a transition between the excited states at **2072.6 keV** and at **1363.5 keV**.

Finally the 954.3 keV and the 2485.4 keV γ-ray do not present any γ-γ coincidence, but considering their intensities in the γ-ray spectrum they are tentatively assigned as transitions from excited states at **954.3 keV** and at **2485.4 keV** to the ground state.

7.1.2. Beta decay strength calculation using the AME2016 $\mathbf{Q}_\beta$ values and decay scheme for ^{63}Ge

Once the γ-γ coincidences are clarified, the balance of intensities can be found for each level. The γ-ray intensities were presented in Table 6.2 as the number of counts C_γ over the γ-ray efficiency ε_γ, corresponding to the relative intensity. The absolute intensities are obtained according to the Eq. (5.6), taking into account the dead-time for the ^{63}Ge decay DT = 0.176922 as shown in Fig. D.3 in Appendix D.2, the time correlation windows correction $C_w(^{63}\text{Ge}) = 0.98682(17)$, and the number of implantations $N_{\text{impl}}(^{63}\text{Ge}) = 3620209$ of ^{63}Ge in the second DSSSD as shown in Table D.1. As this nucleus decays by positron emission the trigger efficiency for these

γ-rays correspond to the beta efficiency $\varepsilon_\beta = 0.8277(12)$. With these ingredients the normalization factor for the relative intensities corresponds to $4.1088(60) \times 10^{-7}$. Using this factor, the relative intensities of γ-rays in Table 7.3 were normalised and tabulated in the fourth column of the Table 7.3.

Initial State	Final State	Energy keV	I_β[%]	logf	logt	logft	Strength	Type
g.s.	3207.9(2)	6419(40)	0.17(2)	3.57(2)	1.95(6)	5.52(6)	0.012(3)	GT
g.s.	2485.4(3)	7142(40)	0.20(3)	3.83(1)	1.89(6)	5.72(6)	0.007(2)	GT
g.s.	2072.6(1)	7554(40)	0.27(2)	3.96(1)	1.75(3)	5.71(3)	0.008(1)	GT
g.s.	1363.5(1)	8264(40)	0.86(4)	4.17(1)	1.25(2)	5.42(3)	0.015(2)	GT
g.s.	1000.1(1)	8627(40)	0.18(4)	4.27(1)	1.93(9)	6.20(9)	0.002(1)	GT
g.s.	954.2(1)	8673(40)	0.13(1)	4.28(1)	2.06(4)	6.35(4)	0.0017(4)	GT
g.s.	925.1(1)	8702(40)	0.66(4)	4.29(1)	1.36(2)	5.65(3)	0.009(1)	GT
g.s.	722.2(1)	8905(40)	1.00(5)	4.35(1)	1.18(2)	5.53(2)	0.011(1)	GT
g.s.	627.0(1)	9000(40)	0.19(4)	4.37(1)	1.91(9)	6.28(9)	0.0020(9)	GT
g.s.	442.8(1)	9184(40)	4.6(2)	4.42(1)	0.52(1)	4.94(2)	0.045(4)	GT
g.s.	75.0(1)	9552(40)	1.3(1)	4.51(1)	1.06(4)	5.57(4)	0.010(2)	GT
g.s.	g.s.	9627(40)	90.4(2)	4.53(1)	-0.773(1)	3.75(1)	1.11(3)	F+GT

Table 7.3: Summary of transition intensities, logf, logt, logft, and strength for transitions in ^{63}Ge decay (see text).

The absolute intensity corresponds to the feeding to each particular state with energy E_l by the beta decay. Then, using the intensity the partial half-life can be calculated as $t_l = T_{1/2}/I_l$ corresponding to the sixth column of the Table 7.3. The logf value is obtaining by calculating the Fermi integral. The strength is calculated as indicated by the Eq. (1.26) for Gamow-Teller transition for all states except for the ground state that can be populated both by Gamow-Teller and Fermi transition. The strength to the g.s. in Table 7.3 and in Fig. 7.1 corresponds to the $B(F) + \lambda^2 B(GT)$. The level scheme obtained in this work is shown in Fig. 7.1, where the previously reported levels by Balamuth et. al. [B+91] and Weiszflog et. al. [W+01] are shown in black, and where the levels and γ-rays observed for the first time in this work are shown in red.

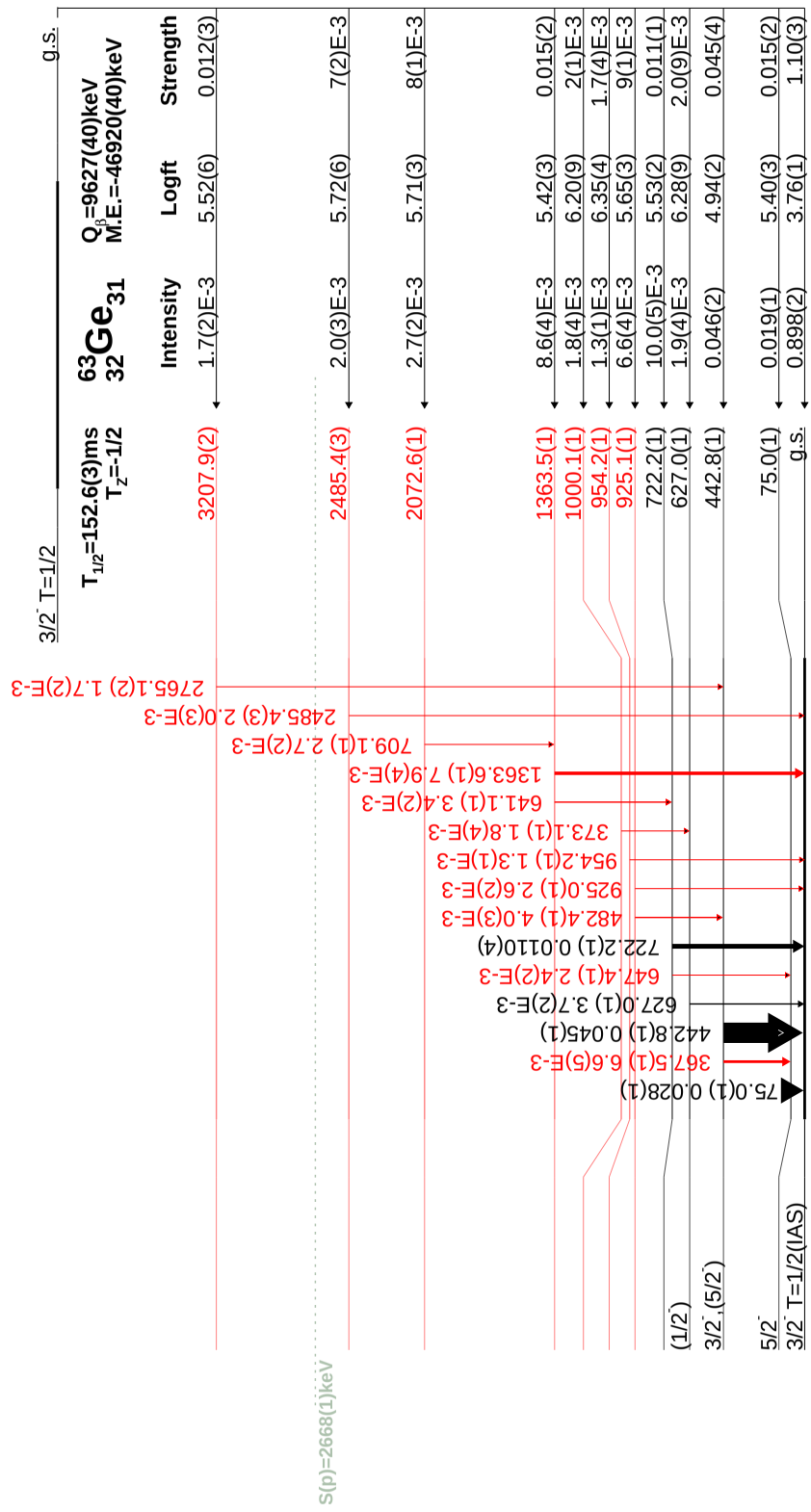

Figure 7.1: Level scheme for ^{63}Ge decay using AME2016 [WAK+17] mass excess and Q_β values. To construct this scheme we have used the ε_β and $T_{1/2}$ obtained in Sec. 6.1.7. Colour on line represent γ-rays and states observed by the first time. Also the proton separation energy $S(p)$ from AME2016 [WAK+17] is shown.

7.2. Decay scheme for ^{64}As using previous reported Q_β values

In order to obtain the ^{64}As β decay strengths to excited states in ^{64}Ge, results obtained in previous sections such as γ-ray intensities, γ-ray coincidences, γ-p coincidences and half-life, together with the $Q_\beta = 14785(200)\#$ keV reported in AME2016 [WAK+17], will be used to construct the level scheme for ^{64}As decay.

Then, in Table 7.4 a summary with the selection rules for this beta decay is presented, taking into account $J^\pi = 0^+$ for the ^{64}As ground state.

J^π mother	Transition	L	S	Type	$\Delta\pi$	ΔJ	J^π daughter
0^+	Allowed	0	0	F	No	0	0^+
0^+	Allowed	0	1	GT	No	0, 1	~~0^+~~, 1^+
0^+	First-Forbidden	1	0	F	Yes	0, 1	$0^-, 1^-$
0^+	First-Forbidden	1	1	GT	Yes	0, 1, 2	~~0^-~~, $1^-, \ldots, 2^-$
0^+	Second-Forbidden	2	0	F	No	0, 1, 2	$0^+, \ldots, 2^+$
0^+	Second-Forbidden	2	1	GT	No	$0, \ldots, 3$	~~0^+~~, $1^+, \ldots, 3^+$
0^+	Third-Forbidden	3	0	F	Yes	$0, \ldots, 3$	$0^-, \ldots, 3^-$
0^+	Third-Forbidden	3	1	GT	Yes	$0, \ldots, 4$	~~0^-~~, $1^-, \ldots, 4^-$

Table 7.4: Selection rules for the ^{64}As beta decay. Since the Gamow-Teller is a pseudo-vector operator, $0 \rightarrow 0$ transitions are excluded.

Since this nucleus is a β-delayed proton emitter, the level scheme reconstruction must be carried on in two parts, one analyzing the γ-ray transitions for excited states below the proton separation energy $S(p) = 5057(4)$ keV [WAK+17] (Section 7.2.1), and those above it (Section 7.2.2). Then the level scheme will be shown in Section 7.2.3.

7.2.1. Analysis of the projected gamma-gamma coincidence spectra for ^{64}As decay

The 901.4 keV, 676.9 keV, 576.2 keV, and 1578.6 keV γ-ray energies were previously reported by Ennis et al. [ELG+91] and by Farnea et al. [FEA+03]. The γ-rays with energies 901.4 keV, and the 1578.6 keV were previously reported as γ-transitions to the ground state from excited states with energies **901.4 keV**, and 1578.4 keV. The 576 keV γ-ray appears only in Farnea et. al. [FEA+03] being emitted from a state **2154.7 keV** and feeding the **1578.4 keV** level, then this level de-excites emitting two γ-rays, either the 1578.6 keV γ-ray to the ground state, or the 676.9 keV γ-ray to the excited state **901.4 keV**.

During the analysis of ^{64}As the γ-ray coincidence spectrum correlated with ^{64}As implantations was presented in Fig. 6.18. The coincidence gates were presented in Figs. 6.20 to 6.23. In Table 7.5 we present a summary of the γ-ray coincidences founded in each coincidence gate.

The γ-ray with energy 1264.9 keV is in coincidence with the 901.4 keV, but not with the 676.9 keV, the 1578.6 keV, or the 576.2 keV γ-rays. This suggests that the γ-ray cascade 1265.9 keV, 1300.5 keV, and 1495.1 keV feeds the **901.4 keV** state. On the other hand, the 1312.0 keV γ-ray is in coincidence with the γ-ray cascade emitted from the excited state at **2154.6 keV**, and the 1495.1 keV γ-ray. Indeed we noticed that the 1312.0 keV γ-ray feeding the level at **2154.6 keV**, and the 1300.5 keV γ-ray feeding the level at at **2166.3 keV** are consistent with an excited state at **3466.9 keV**. In this scenario the excited state at **2166.3 keV** emits the 1264.9 keV γ-ray to the excited state at **901.4 keV**. Also the γ-ray with energy 2565.8 keV matches the energy difference between the excited states at **3466.9 keV** and **901.4 keV**. Moreover, the 1888.4 keV γ-ray corresponds to a transition between

Energy gate keV	**Spectrum number**	**γ-ray coincidence energy keV**
442.8	6.23(d)	901.4
576.2	6.23(c)	*324*, 676.9, 901.4, 1312.0, 1495.1
676.9	6.22(h), 6.23(a), 6.23(b)	576.2, 901.4, *1293*, 1312.0, 1495.1, 1888.4
901.4	6.22(e), 6.22(f), 6.22(g)	576.2, 676.9, 1264.9, *1293*, 1300.5, 1312.0, 1495.1, 1888.4, 2565.8
1264.9	6.22(c), 6.22(d)	*229*, 901.4, 1300.5, 1495.1
1300.5	6.22(b)	901.4, 1264.9, *1293*, 1495.1
1312.0	6.22(a)	*314*, 576.2, 676.9, 901.4, *1293*, 1495.1
1315.1	6.21(g), 6.21(h)	676.9, 901.4, 3648.0
1377.5	6.21(f)	676.9, 901.4, *1495.1*
1412.5	6.21(e)	2565.8
1495.1	6.21(b), 6.21(c), 6.21(d)	576.2, 676.9, 901.4, 1264.9, *1293*, 1300.5, 1312.0, 1578.6, 1888.4, 2565.8
1578.6	6.21(a)	1495.1, 1888.4
1888.4	6.20(h)	676.9, 901.4, *1293*, 1495.1, 1578.6
2005.9	6.20(g)	676.9, 901.4, 1495.1, 1888.4
2054.4	6.20(f)	901.4, *1495.1*, *1888.4*
2397.6	6.20(e)	*168*, *177*, 676.9, 901.4
2565.8	6.20(d)	901.4, *1293*, 1495.1
3136.0	6.20(c)	901.4, 1315.1
3648.0	6.20(b)	1315.1
4236.7	6.20(a)	901.4

Table 7.5: Summary of the γ-ray coincidence projected spectra for the ^{64}As decay. γ-rays written in italic are γ-rays observed in the γ-γ coincidence projected spectra but not in the γ-ray spectrum, or are only seen with low intensity. The 4460.8 keV, 4852 keV, 5259.4 keV, 5268 keV, 5359.6 keV, 5366.3 keV, and the 5374.0 keV γ-rays do not have γ-γ coincidences and are too weak to be assigned to a direct ground state transition.

the excited states at **3466.9 keV** and at **1578.4 keV**.

In addition an excited state at **2955.8 keV** emitting both the 2054.4 keV and the 1377.5 keV, is confirmed by coincidences with the 901.4 keV and the 676.9 keV γ-rays respectively.

The 1495.2 keV γ-ray is placed between the **4962.0 keV** and **3466.9 keV** states. Similarly, the **4962.0 keV** level de-excites by the 1315.1 keV and then feeding the ground state by emitting the 3648.0 keV cascade to the ground state.

The 4236.7 keV γ-ray is emitted from the **5138.1 keV** level and is in coincidence with the 901.4 keV transition.

The case of the 1293 keV γ-ray is special since it cannot be observed in the projection, but it was observed in coincidence with 2565.8 keV, 1888.4 keV, 1495.1 keV, 1312.0 keV, 901.4 keV and 676.9 keV γ-rays. A level at **6255 keV** has been tentatively placed in the level scheme decaying by the 1293 keV γ-ray. This is consistent with all of these observed coincidences.

Since the 2397 keV γ-ray is in coincidence with the 676.9 keV and the 901.4 keV γ-rays it is consistent with it being placed as a transition to the **1578.4 keV** level from the **3975.9 keV** level. However these γ-rays could be in coincidence with the 1495.1 keV γ-ray. In order to fulfill this condition, a 511 keV γ-ray should be emitted. If it does exists it overlaps with the positron annihilation photo-peak.

7.2.2. Analysis of the proton spectrum and gamma-proton coincidence projected spectra for ^{64}As decay

Since the proton spectrum has poorer resolution ($\sim$ 200keV) than the γ-ray spectrum ($\sim$ 1keV) it is a challenging task to determine which states in ^{64}Ge are proton emitters. In Section 6.2.6 the γ-p coincidence spectra were shown, and coincidences with the γ-rays de-exiting levels in the ^{63}Ga were observed. The γ-rays observed had energies of 75.0 keV, 442.8 keV, 722.2 keV, and 925.1 keV. Nevertheless these coincidences are not clear enough to determine the energy of the corresponding proton. In spite of all these difficulties, a tentative level scheme will be presented.

In order to find the energy of the states in mother nucleus ^{64}Ge which are candidates to be proton emitters after the β^+ decay of ^{64}As, we have taken into account all possible combination between the states in ^{63}Ga and the measured proton

energies. In Fig. 7.2 we have presented a diagram to explain this methodology. Considering the proton separation energy $S_p = 5057(4)$ keV [WAK+17] of ^{64}Ge, the excitation energy E_s of the daughter state in ^{63}Ga and the energy of the proton E_p, we can estimate the excitation energy of the state in ^{64}Ge that emit that proton as:

$$E_{ex} = S_p + E_s + E_p \ . \tag{7.1}$$

If we calculate the excitation energy using all possible daughter states in ^{63}Ga, we would find five candidates for mother states in ^{64}Ge per proton. To show these candidates, we construct a plot where in the abscissa is the excitation energy in ^{64}Ge and in the ordinates is the multiplicity of that energy in arbitrary units. This multiplicity represents the probability of the existence of a state at E_x. In Fig. 7.2 for simplicity we show only two protons p_1 and p_2 and three states in ^{63}Ga, the ground state, the **75 keV** and the **442 keV**, giving arise to the excitation energies in ^{64}Ge: $E^{p_1}_{ex1}$, $E^{p_1}_{ex2}$ and $E^{p_1}_{ex3}$ using proton p_1 and $E^{p_2}_{ex1}$, E^{p2}_{e2} and $E^{p_2}_{ex3}$ using proton $p2$. As values involved in Eq. 7.1 came from experimental measurements, each one has its own precision that can be propagated to the mother excitation energy. Then, it is natural that the probability to find the state at E_{ex} could be represented as a Gaussian function (in arbitrary units), centred at E_{ex} and width given by the propagated error,

$$\Delta E_{ex} = \sqrt{\Delta S_p^2 + \Delta E_s^2 + \Delta E_p^2} \quad . \tag{7.2}$$

These Gaussian functions corresponding to a particular combinations of protons and daughter states are drawn in Fig. 7.2 and 7.3 in blue (and green).

As explained earlier, the energy resolution of the proton spectra is around ~ 200 keV in this experiment, then it is no easy to assign directly a proton emitter state in daughter nucleus ^{64}Ge after the beta decay of the mother nucleus ^{64}As.

Although it is physically possible to have almost the same proton energy emitted from two different states, this would be very improbable and this scenario was neglected for the rest of analysis by selecting only one decay channel per proton energy.

Returning to the example shown in Fig.7.2, in blue is represented the possible contributors of proton energies, as a Gaussian function centred in E_{ex} and width ΔE_{ex} (Eq. 7.2). The height of the Gaussian functions is related with an occurrence probability in arbitrary units, where one combination will have occurrence probability one. In Fig. 7.2 the red line represent all possible combinations added together. Then, we may end up into one of these cases:

- Peaks with similar occurrence probability around one.
- There is a favoured energy where the total occurrence probability is higher than the neighbours.

Cases with total occurrence probability around one are assigned as transitions to the ground state, considering protons as being emitted from different excited states. On the other hand, cases where there is one favoured value in the total occurrence probability, the protons are assigned as being emitted from a common level in ^{64}Ge as can be seen in Fig. 7.2.

Now in Fig. 7.3 we present all combinations separated by the proton energy. For each proton, the each possibility populating a state in daughter nucleus is drawn in blue. Also in each plot corresponding to a proton energy we show also the total multiplicity in red. When a proton have regular multiplicity around its candidate peaks, is then assigned to the ground state in daughter nucleus ^{63}Ga and indicated with a yellow ellipse. Cases where there is a favoured energy by two or more protons are then assigned to a common state and those peaks are indicated with a yellow

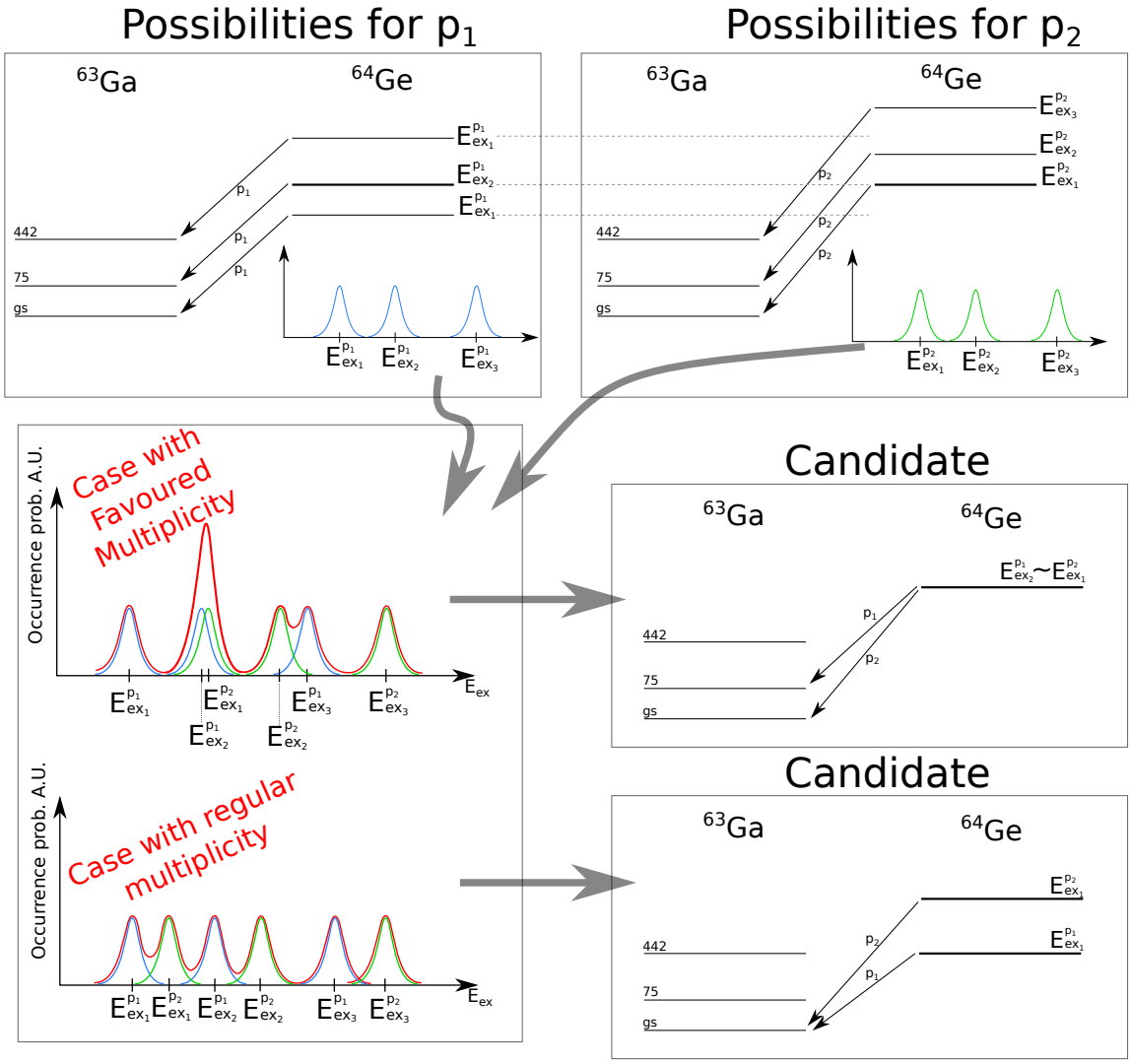

Figure 7.2: Example for the selection of the excitation states in ^{64}Ge emitting protons. We favour those states that could explain the major number of the proton emission (see text). For simplicity we shown only three states in ^{63}Ga.

filled ellipse.

The proton with energy 1493 keV in Fig. 7.3(a) populating the excited state with energy of 722.2 keV in ^{63}Ga, could be emitted from a state at **7276 keV**, the same state as the proton with an energy of 2224 keV, populating the ground state, Fig. 7.3(c).

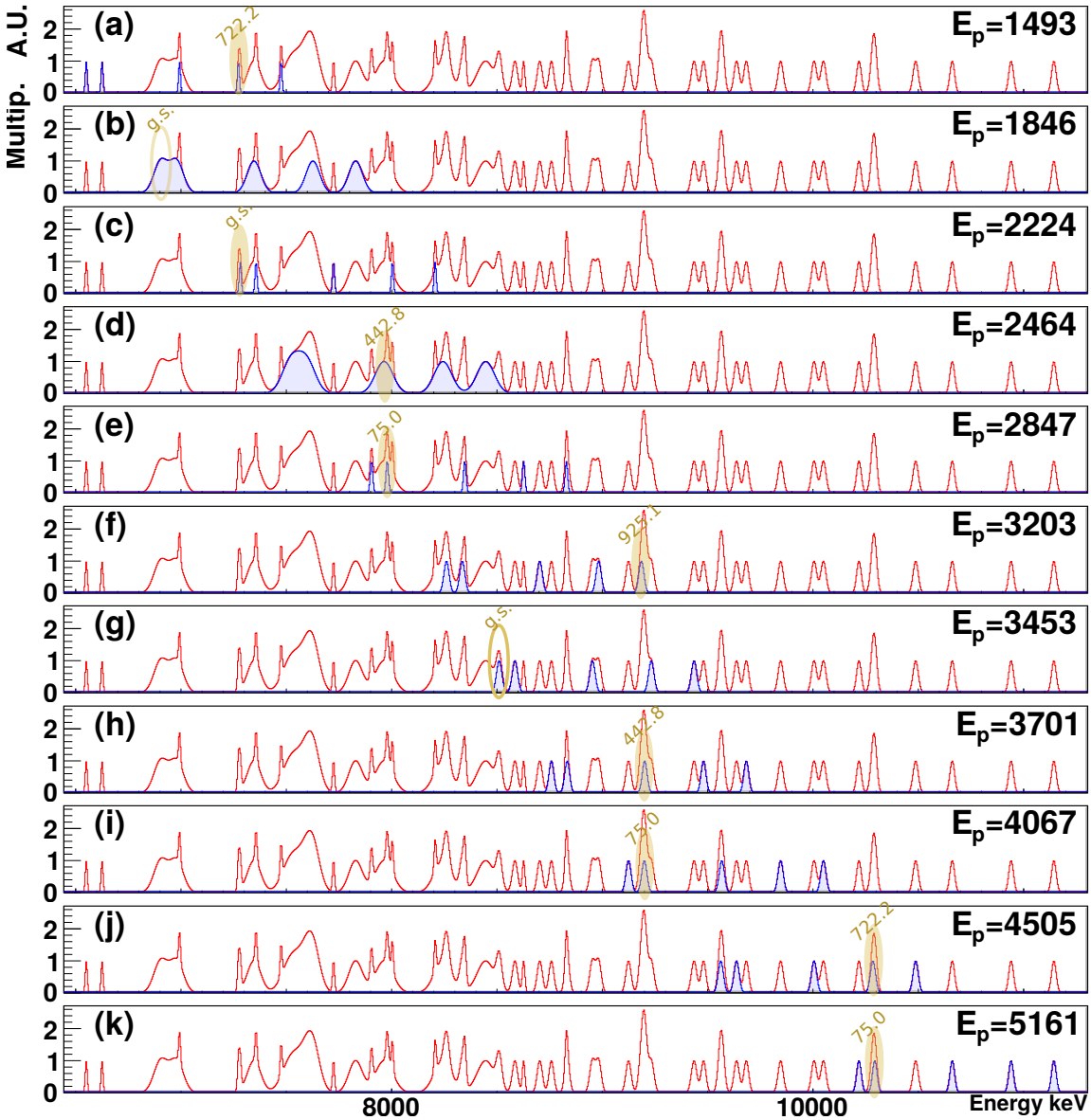

Figure 7.3: All possible energies of the excited states on ^{64}As, using the AME2016 [WAK+17] mass tables, formed taking into account the proton separation energy $S(p)$, the energy of the state in ^{63}Ga, and the proton energy. Higher multiplicities are candidates to the level scheme in ^{64}Ge. for: (a) 1493 keV, (b) 1846 keV, (c) 2224 keV, (d) 2464 keV, (e) 2847 keV, (f) 3203 keV, (g) 3453 keV, (h) 3701 keV, (i) 4067 keV, (j) 4505 keV, (k) 5161 keV. . Our election for the states is marked with a ellipse labelled with the corresponding excitation energy in ^{63}Ga.

The proton with energy 1846 keV in Fig. 7.3(b) was assigned as a ground state transition. The other possibility was that this proton populates the **75.0 keV** in ^{63}Ga, and the 1493 keV populates the 722.2 keV. However the proton with energy 1493 keV is in better agreement with the proton with energy 2224 keV.

The proton with energy 2464 keV in Fig. 7.3(d) populating the excited state at **442.8 keV**, is in agreement with the proton with energy of 2847 keV in Fig. 7.3(e) populating the **75.0 keV**, both emitted from an excited state at **7978 keV**.

The protons with energies 3203 keV, of 3701 keV and 4067 keV are consistent with proton emission from an excited state at **9195 keV**, populating the excited states in ^{63}Ga at **925.1 keV**, **442.8 keV**, and **75.0 keV** level respectively.

Finally, the protons with energies 4505 keV and 5161 keV, are consistent with proton emission from an excited state at **10.3 MeV**, populating excited states in ^{63}Ga with energies **722.2 keV** and **75.0 keV**.

7.2.3. Beta decay strength calculation using the AME2016 $\mathbf{Q}_\beta$ value and decay scheme for ^{64}As

Once the level scheme is constructed in Sections 7.2.1 and 7.2.3, the intensities for the ^{64}As beta decay to states in ^{64}Ge and ^{63}Ge can be calculated. The beta decay intensity (beta feeding) for each excited state, can be calculated by adding the intensities of the γ-rays emitted from the excited state, and subtracting the total intensity of transitions entering the state,

$$I_\beta^{(i)} = \sum_j I_\gamma^{(i)\to(j)} + \sum_k I_p^{(i)\to(k)} - \sum_l I_\gamma^{(l)\to(i)} \ , \tag{7.3}$$

where $I_\gamma^{(i)\to(j)}$ is the intensity of the γ-ray transition between the state (i) to the state (j) in ^{64}Ge, $I_p^{(i)\to(k)}$ is the intensity of the proton transition between the state (i) in ^{64}Ge to the state (k) in ^{63}Ga, and $I_\gamma^{(l)\to(i)}$ is the γ-transition between the states (l) and (i) in ^{64}Ge. In Table 7.6, the beta feeding calculations are presented for all states in the level scheme for ^{64}As decay.

Initial State	Final State	β transition energy keV	I_β[%]	logf	logt	logft	Strength	Type
g.s.	10289(20)	4496(200)	0.21(2)	2.7(1)	1.48(3)	4.2(1)	0.3(2)	GT
g.s.	9195(20)	5590(200)	0.64(5)	3.23(9)	1.00(3)	4.23(9)	0.2(1)	GT
g.s.	8510(30)	6275(200)	0.21(3)	3.51(8)	1.48(7)	5.0(1)	0.04(2)	GT
g.s.	7978(20)	6807(200)	1.40(9)	3.71(7)	0.65(3)	4.36(8)	0.17(6)	GT
g.s.	7276(10)	7509(200)	1.50(9)	3.94(6)	0.62(3)	4.57(7)	0.11(3)	GT
g.s.	6903(80)	7882(200)	1.00(8)	4.05(6)	0.80(3)	4.85(7)	0.05(2)	GT
g.s.	6255(2)	8530(200)	3.6(5)	4.24(5)	0.25(7)	4.49(9)	0.13(5)	GT
g.s.	5138.1(4)	9647(200)	1.2(2)	4.52(5)	0.70(5)	5.23(7)	0.023(8)	GT
g.s.	4962.0(1)	9823(200)	54(2)	4.57(5)	-0.94(1)	3.63(5)	1.5(2)	F
g.s.	4879.3(2)	9906(200)	0.9(1)	4.58(5)	0.85(6)	5.44(7)	0.014(5)	GT
g.s.	3975.9(4)	10809(200)	0.6(1)	4.78(4)	1.01(8)	5.80(9)	0.006(3)	GT
g.s.	3648.0(1)	11137(200)	0.3(3)	4.85(4)	1.3(5)	6.2(5)	0.003(6)	GT
g.s.	3466.8(1)	11318(200)	12(2)	4.89(4)	-0.26(8)	4.63(9)	0.09(4)	GT
g.s.	3136.0(4)	11649(200)	1.0(1)	4.96(4)	0.79(5)	5.74(7)	0.007(2)	GT
g.s.	2955.8(2)	11829(200)	1.9(2)	4.99(4)	0.52(4)	5.51(6)	0.012(3)	GT
g.s.	2166.3(1)	12619(200)	0.5(5)	5.14(4)	1.1(4)	6.2(4)	0.002(5)	GT
g.s.	2154.5(1)	12630(200)	-0.7(3)	-	-	-	-	GT
g.s.	1578.3(1)	13207(200)	1(2)	5.24(3)	1(2)	6(2)	0.00(1)	GT
g.s.	901.4(1)	13884(200)	4(3)	5.35(3)	0.2(3)	5.6(3)	0.01(1)	GT
g.s.	g.s.	14785(200)	15(4)	5.49(3)	-0.4(1)	5.1(1)	0.03(2)	GT

Table 7.6: Summary of transition intensities, logf, logt, logft, and strength for each level in ^{64}As decay using the AME2016 values for Q_β values.

Taking into account both the intensities of the beta decay to each state, and the selection rules for this beta decay in Table 7.4, we conclude that the excited state with energy **4962.0 keV** in ^{64}Ge corresponds to the $T = 1$, $J^\pi = 0^+$ IAS of the ^{64}As ground state.

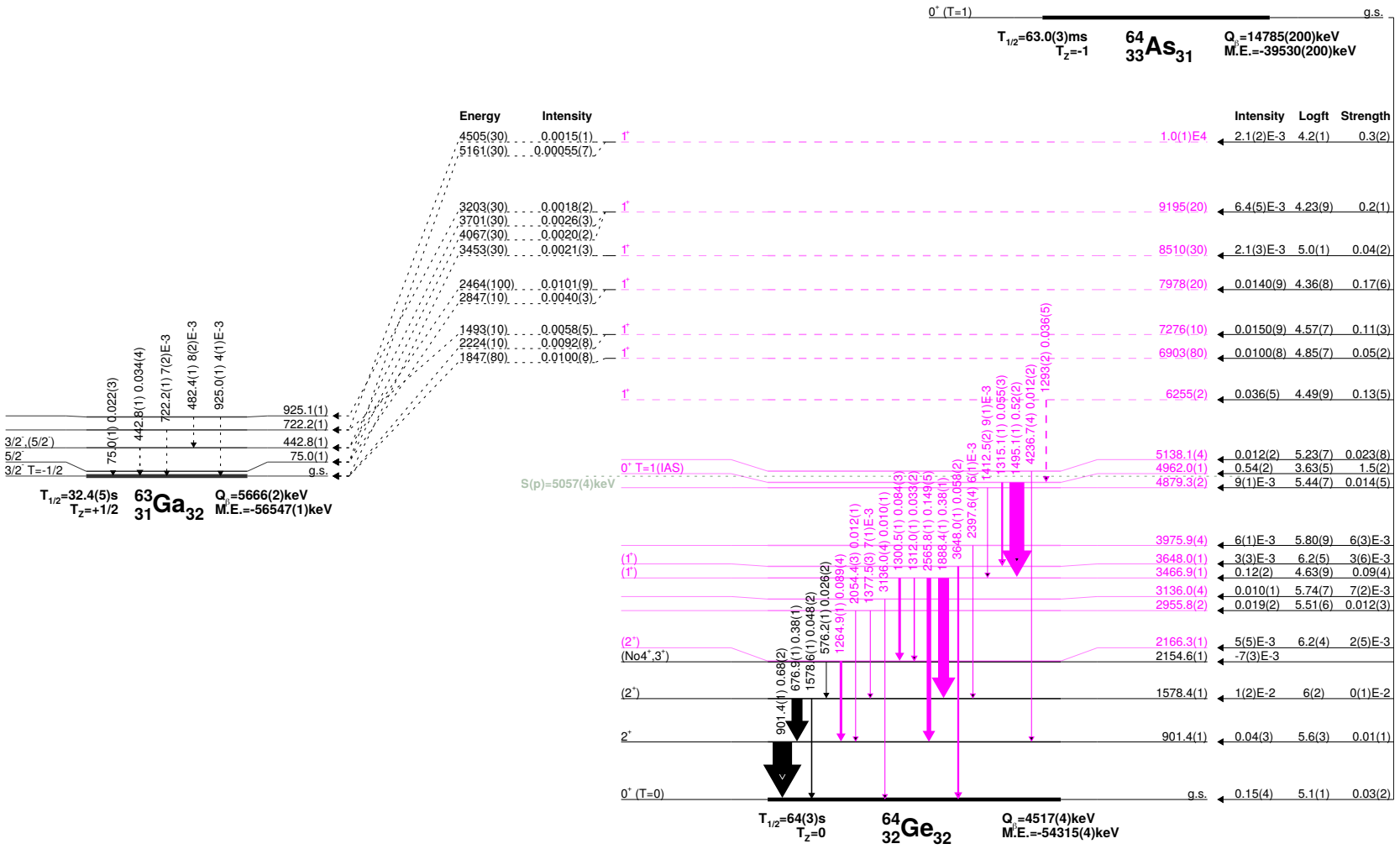

Figure 7.4: Level scheme for ^{64}As decay using the AME2016 [WAK+17] for the mass excess and Q_β values.

7.3. Decay scheme of ^{64}Se using previously reported Q_β values

Using the results for ^{64}Se decay from previous sections such as the γ-ray spectrum (see Section 6.3.4), the p-spectrum (see Section 6.3.5), the γ-γ coincidences (see Section 6.3.6), the γ-p coincidences (see Section 6.3.7), the half-life value and the Q_β = 12830(500)# keV taken from AME2016 [WAK+17], the level scheme for ^{64}Se decay was constructed.

In the literature the ground state of ^{64}As is reported as a $J^\pi = (0^+)$. Then the selection rules for this beta decay can be seen in Table 7.7.

J^π mother	Transition	L	S	Type	$\Delta\pi$	ΔJ	J^π daughter
0^+	Allowed	0	0	F	No	0	0^+
0^+	Allowed	0	1	GT	No	0, 1	~~0^+~~, 1^+
0^+	First-Forbidden	1	0	F	Yes	0, 1	$0^-, 1^-$
0^+	First-Forbidden	1	1	GT	Yes	0, 1, 2	~~0^-~~, $1^-, \ldots, 2^-$
0^+	Second-Forbidden	2	0	F	No	0, 1, 2	$0^+, \ldots, 2^+$
0^+	Second-Forbidden	2	1	GT	No	$0, \ldots, 3$	~~0^+~~, $1^+, \ldots, 3^+$
0^+	Third-Forbidden	3	0	F	Yes	$0, \ldots, 3$	$0^-, \ldots, 3^-$
0^+	Third-Forbidden	3	1	GT	Yes	$0, \ldots, 4$	~~0^-~~, $1^-, \ldots, 4^-$

Table 7.7: Selection rules for ^{64}Se beta decay. Since the Gamow-Teller is a pseudo-vector operator, transitions from $0 \rightarrow 0$ are excluded.

7.3.1. Analysis of the gamma-gamma coincidences for ^{64}Se decay

During the analysis of ^{64}Se in Section 6.3.6 the projected γ-ray coincidence spectrum was presented in Fig. 6.33. The gated coincidence spectra were presented in Fig. 6.34. In Table 7.8 we present a summary of the γ-ray coincidences observed in these gates.

Gate energy keV	**Spectrum number**	**γ-ray coincidence energy keV**
149.7	6.34(g)	358.7
358.7	6.34(f)	149.7, *306*
507.1	6.34(d)	*1449.2*
697.4	6.34(c)	1259.2
1259.2	6.34(b)	697.4
1449.2	6.34(a)	507.1

Table 7.8: Summary of γ-rays coincidences gating on transitions in ^{64}As populated in the decay of ^{64}As. Gamma-rays with low intensity or observed only in the γ-γ coincidence spectrum are written in italic font. The 418 keV γ-ray does not shown any γ-γ coincidences.

There is tentative evidence of 697.4 keV-1259.2 keV coincidences with one count in the 1259.2 keV gate and two in 697.4 keV gate. This can be interpreted in terms of the decay of a state at **1956.4 keV** by the 1259.2 keV γ-ray to a state **697.4 keV** since the 697.4 keV γ-ray is the more intense of the two.

The existence of the **1956.4 keV** state is supported by the observation of 1449.2 keV-507.1 keV coincidences. The 507.1 keV is not fully resolved from the 511 keV annihilation line but the excited state at **507.1 keV** is confirmed by th coincidences between 148.7 keV and 358.7 keV γ-rays.

7.3.2. Analysis of the proton spectrum and gamma-proton coincidences spectra for the ^{64}Se decay

As in the ^{64}As decay case, the low resolution of the proton peaks in comparison with the γ-rays makes the determination of the states which are proton emitters a challenging task.

In Section 6.3.7 we showed the coincidences between protons and the 417.5 keV γ-ray. This could be due to either the γ-p decay or the p-γ decay processes. We

note that in this experiment it is not possible to determine which one of the two processes occurs, however, we do not favour the γ-p process taking into account the mirror symmetry of ^{63}Ge. In Fig. 7.5 the $T_z = -1/2$ ^{63}Ge and its mirror nucleus $T_z = +1/2$ ^{63}Ga are shown where the energy corresponding to the Coulomb interaction was removed. From this point of view, a state with energy **417.5 keV** in ^{63}Ge

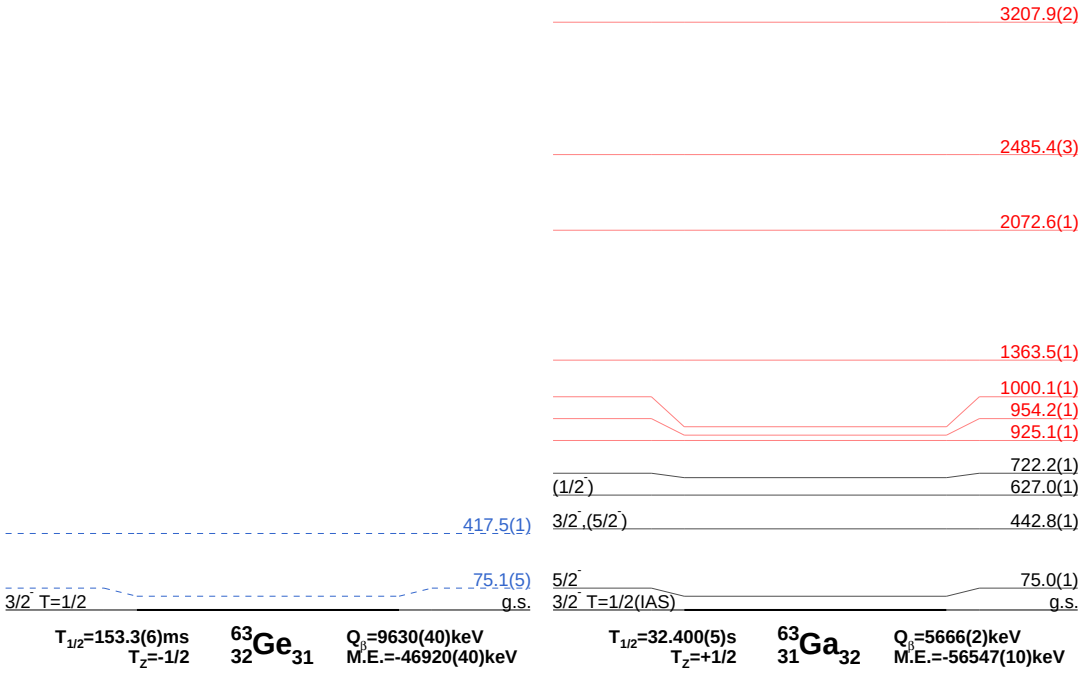

Figure 7.5: $A = 63$ isobaric doublet comparison.

can be seen as the counterpart of the **442.8 keV** state in ^{63}Ga, as can be seen in Fig. 7.5.

In this scenario, the proton with energy 1582 keV populates the excited state 417.5 keV in the ^{63}Ge. This is consistent with energy 1982 keV being emitted from the same state in ^{64}As and populating the g.s. in ^{63}Ge. As these are the protons with the highest intensity, they may correspond to the proton emission from the IAS $T = 2$ state in ^{64}As with an energy of **1956.4 keV**.

In order to determine the states in ^{64}As from which the rest of the observed protons were emitted, an analysis similar to that proposed for ^{64}As decay can be carried out by considering all possible combinations between proton energies and the energies in the ^{63}Ge. A proton with energy E_p populating a daughter state in ^{63}Ge emitted from the mother nuclide ^{64}As from the level at,

$$E_x = S_p + E_s + E_p \ . \tag{7.4}$$

where $S_p = -101(200)\#$ is the proton separation energy of the ^{64}As from AME2016 [WAK+17]. Taking into account all possible combinations between protons and daughter states in ^{63}Ge we can see if there are excitation energies that are favoured with higher multiplicity assigning those protons to a common state, or, if the total multiplicity is regular we assign the protons as independent transitions to the ground state. In Fig. 7.6 we present an example of the cases with favoured multiplicity and those with a regular total multiplicity.

Using this analysis, it can be seen that the protons with energies 1582 keV and 1982 keV are emitted from the same state in ^{64}As at **1956.4 keV** as it was shown previously with the proton-gamma coincidences. Indeed other two protons are candidates to be emitted from the same excited state in ^{64}As with energy **3581 keV**, the 3245 keV and 3705 keV. These cases are indicated in Fig. 7.7 with yellow filled ellipses. The remaining protons with energies 1139 keV, 2994 keV, 3990 keV, and 4663 keV, are not candidates for being emitted from a common state and are placed as tentative transitions to the ground state in ^{63}Ge emitted from states at **1038 keV**, **2893 keV**, **3889 keV** and **4562 keV**, marked with a yellow ellipse.

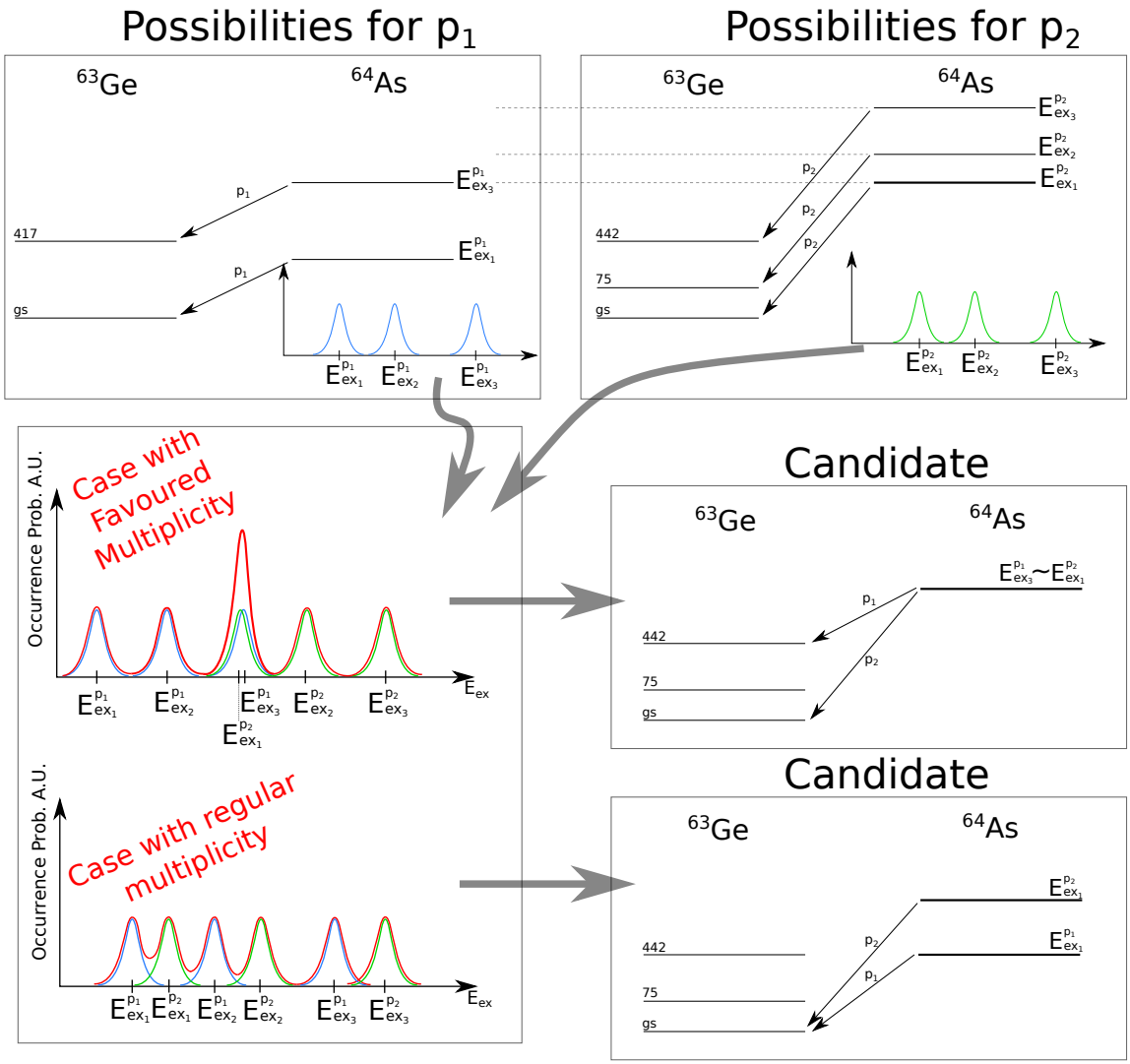

Figure 7.6: Example for the selection of the excitation states in ^{64}As emitting protons. We favour those states that could explain the major number of the proton emission (see text).

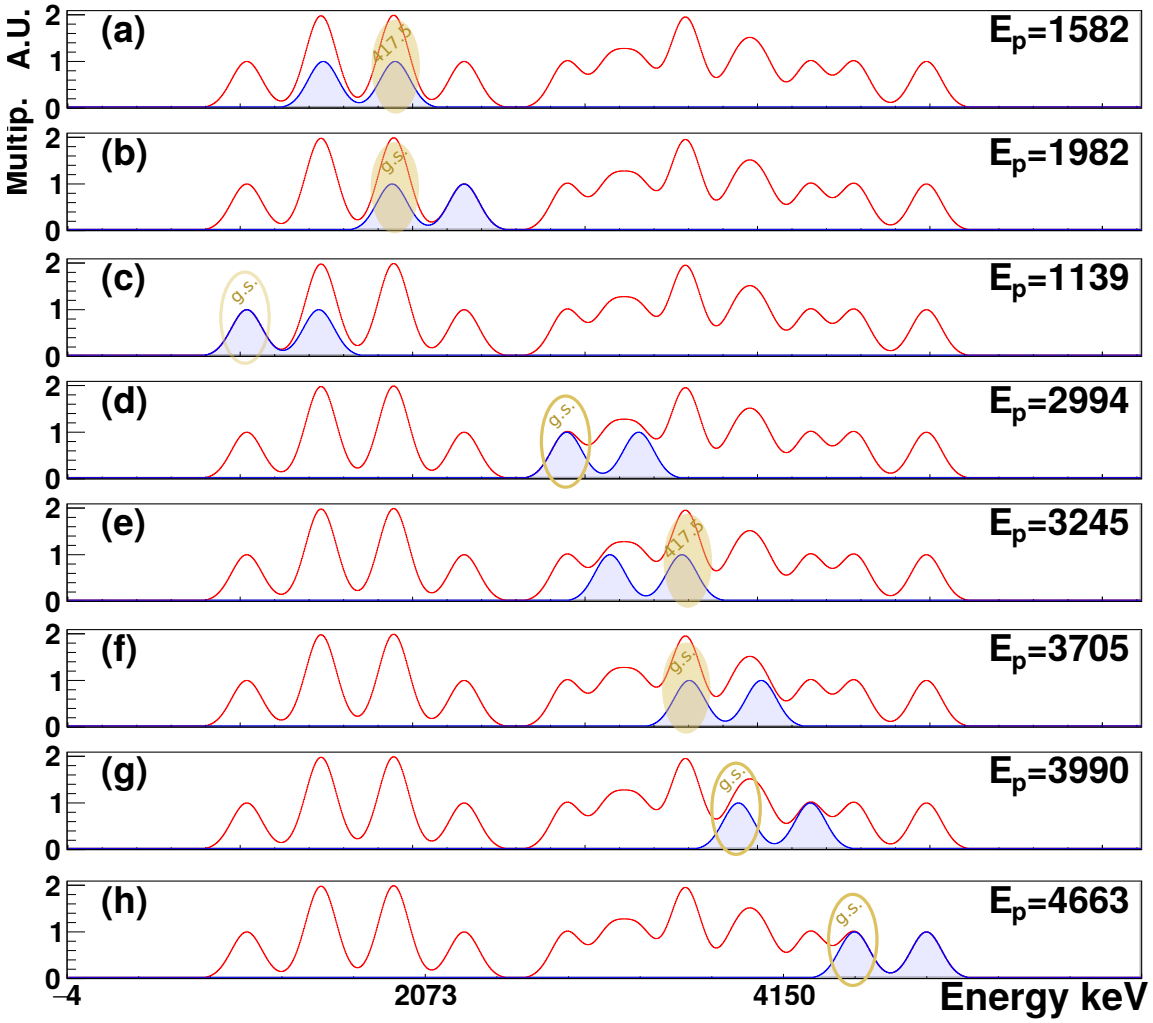

Figure 7.7: All possible energies of the excited states on the ^{64}Se, formed taking into account the proton separation energy $S(p)$, the energies of the states in ^{64}As, and the proton energies.

7.3.3. Beta decay strength calculation using the AME2016 Q_β values and decay scheme for ^{64}Se

After constructing the level scheme in previous sections, the beta decay intensities can be obtained by subtracting the total intensity of the transitions populating the state from the sum of the intensities of the de-exciting transitions. This gives,

$$I_\beta^{(i)} = \sum_j I_\gamma^{(i)\to(j)} + \sum_k I_p^{(i)\to(k)} - \sum_l I_\gamma^{(l)\to(i)} \ , \tag{7.5}$$

where $I_\gamma^{(i)\to(j)}$ is the intensity of the γ-ray transition between the state (i) to the state (j) in ^{64}As, $I_p^{(i)\to(k)}$ is the intensity of the proton transition between the state (i) in ^{64}As to the state (k) in ^{63}Ge, and $I_\gamma^{(l)\to(i)}$ is the γ-transition between the states (l) and (i) in ^{64}As. In Table 7.9, the beta feedings were calculated for each state populated in ^{64}As decay.

Using the values obtained in previous sections for the half-life and beta detection efficiency, and taking the Q_β value from AME2016 [WAK+17], the decay scheme was constructed for ^{64}Se in Fig. 7.8.

Initial State	Final State	Energy keV	I_β[%]	logf	logt	logft	Strength	Type
g.s.	4562(200)	8268(600)	1.00(7)	4.2(2)	0.35(3)	4.5(2)	0.11(9)	GT
g.s.	3889(300)	8941(600)	0.85(6)	4.4(2)	0.42(3)	4.8(2)	0.06(5)	GT
g.s.	3581(200)	9249(600)	4.3(2)	4.5(1)	-0.29(3)	4.2(1)	0.3(2)	GT
g.s.	2893(200)	9937(600)	2.0(1)	4.6(1)	0.05(3)	4.7(1)	0.08(6)	GT
g.s.	1038(300)	11792(600)	1.16(8)	5.0(1)	0.29(3)	5.3(1)	0.02(1)	GT
g.s.	1956.4(2)	10874(500)	60(3)	4.8(1)	-1.43(3)	3.4(1)	2.5(7)	F
g.s.	697.4(1)	12133(500)	1(2)	5.1(1)	0.2(7)	5.3(7)	0.02(7)	GT
g.s.	507.1(1)	12323(500)	16(4)	5.1(1)	-0.8(1)	4.3(2)	0.2(1)	GT
g.s.	148.7(2)	12681(500)	4(1)	5.2(1)	-0.2(2)	5.0(2)	0.04(4)	GT
g.s.	g.s.	12830(500)	10(6)	5.2(1)	-0.6(3)	4.6(3)	0.1(1)	GT

Table 7.9: ^{64}Se beta decay strengths using AME2016 values.

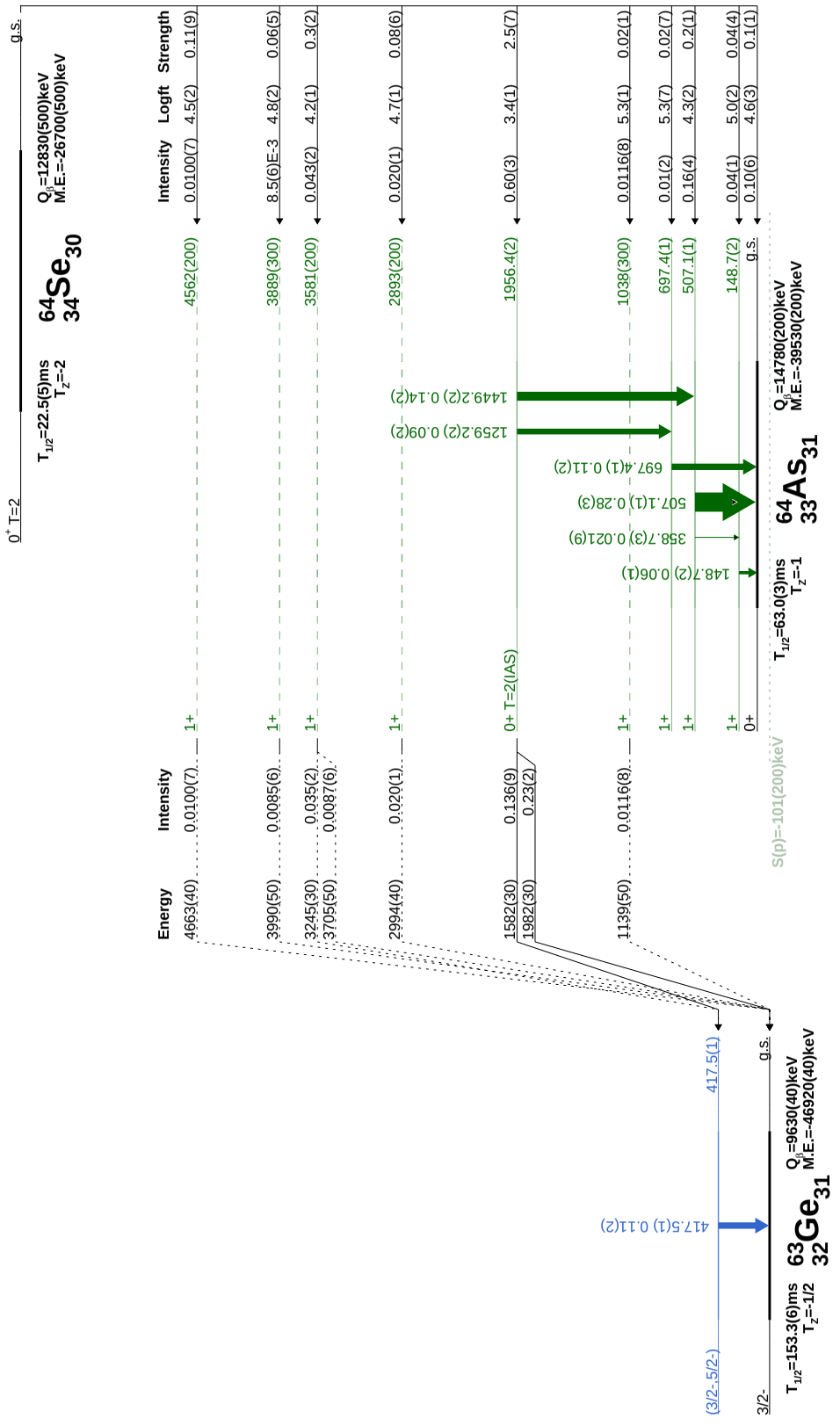

Figure 7.8: Level scheme for ^{64}Se using the half-life in Table 6.16, our measured half-life for the ^{64}As and ^{63}Ge and mass excess and Q_β values from AME2016 [WAK+17].

7.4. Decay scheme of ^{66}As

In this section the level scheme for ^{66}As will be constructed using the half-life value measured in this work, and the AME2016 [WAK+17] reported values for the mass excess and Q_β values, $M(^{66}\text{As}) = -52025(6)$ keV and $Q_\beta = 9582(6)$ keV. For this decay, in NUBASE2016 [AKW+17] the ground state of ^{66}As is reported as having $J^\pi = 0^+$, $T = 1$, and also $J^\pi = 0^+$ for the ground state of the ^{66}Ge.

Unlike the previous cases such as ^{63}Ge, ^{64}As, and ^{64}Se decays, in this nucleus no γ-rays were observed as was discussed in Section 6.4.3. This may means that no excited state is populated in the decay with the ground state being populated in 100% of the decays. In Table 7.10 the strength was obtained assuming 100% of the intensity in the ground state to ground state beta decay. Then a decay scheme is drawn in Fig. 7.9.

Initial State	Final State	Energy keV	I_β[%]	logf	logt	logft	Strength	Type
g.s.	g.s.	9582(7)	100	4.508(2)	-1.0(4)	3.5(4)	2(2)	F

Table 7.10: Transition intensity, logf, logt, logft, and strength for ^{66}As decay. In this case the beta decay of ^{66}As populated only the ground state in the ^{66}Ge.

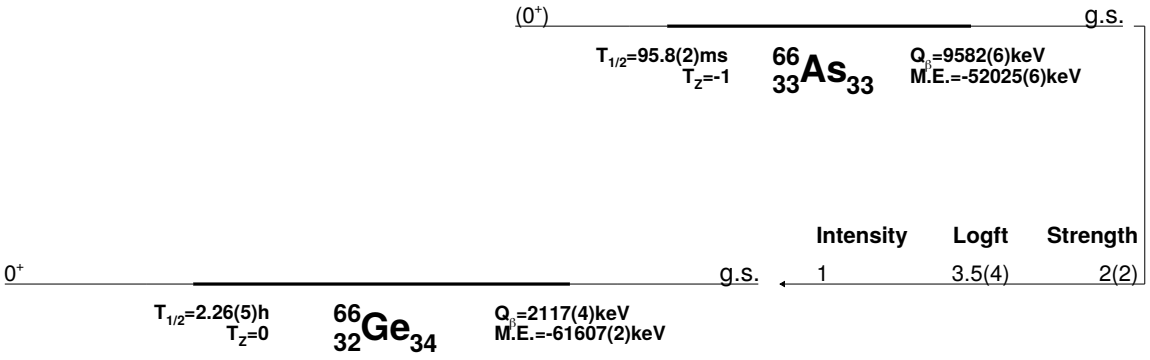

Figure 7.9: Decay scheme for ^{66}As using the half-life reported in Section 6.4.4, and the AME2016 [WAK+17] reported values for the mass excess and Q_β.

7.5. Decay scheme of ^{66}Se

In this section the decay scheme for ^{66}Se will be constructed using the half-life ($T_{1/2}$) and detection efficiency (ε_β) measured in Section 6.5.7 and the Q_β = 10370(200)# keV value taken from the AME2016 [WAK+17].

In the literature [G+98, G+01], the 836.9(1) keV and the 963.6(1) keV are assigned as direct transitions to the ground state from states with energies **837.1 keV** and **963.3 keV**. In this thesis we will use the γ-ray energies measured in this experiment. Thus the excitation energies for these two states are **836.9 keV** and **936.6 keV**. Grzywacz et al. [G+01] have suggested tentative values for J^π=1^+ and 2^+ for the **836.9 keV** and **963.6 keV**. Other levels reported in the literature have too high J^π to be populated directly in β decay and thus they are not observed in this experiment. Then, in Table 7.11 a summary with the selection rules for this beta decay is presented, taking into account $J^\pi = 0^+$ for ^{66}Se ground state.

J^π mother	Transition	L	S	Type	$\Delta\pi$	ΔJ	J^π daughter
0^+	Allowed	0	0	F	No	0	0^+
0^+	Allowed	0	1	GT	No	0, 1	~~0^+~~, 1^+
0^+	First-Forbidden	1	0	F	Yes	0, 1	$0^-, 1^-$
0^+	First-Forbidden	1	1	GT	Yes	0, 1, 2	~~0^-~~, $1^-, \ldots, 2^-$
0^+	Second-Forbidden	2	0	F	No	0, 1, 2	$0^+, \ldots, 2^+$
0^+	Second-Forbidden	2	1	GT	No	$0, \ldots, 3$	~~0^+~~, $1^+, \ldots, 3^+$
0^+	Third-Forbidden	3	0	F	Yes	$0, \ldots, 3$	$0^-, \ldots, 3^-$
0^+	Third-Forbidden	3	1	GT	Yes	$0, \ldots, 4$	~~0^-~~, $1^-, \ldots, 4^-$

Table 7.11: Selection rules for the ^{64}As beta decay. Since the Gamow-Teller operator is a pseudo-vector, $0 \rightarrow 0$ transitions are excluded.

7.5.1. Analysis of gamma-gamma coincidence projected spectra for ^{66}Se decay

During the analysis of ^{66}Se in Section 6.5.5 the γ-ray coincidence projected spectra were obtained for γ-rays observed in the γ-spectrum for this beta decay in Fig. 6.50. In Table 7.12 a summary of the observed coincidences is shown. Peaks observed in the γ-γ projected spectra but not in the γ-ray spectrum are written in italics, but they were not placed in the decay scheme.

Energy gate keV	**Spectrum number**	**γ-ray coincidence energy keV**
74.9	6.54(f), 6.54(g), 6.54(h)	808.6, *1294*, 1681.6, *1818*, 2249.9, *2350*, *3108*
114.9	6.54(e)	*193*, *396*
649.4	6.54(d)	*1231*
808.6	6.54(c)	*1388*, 1765.8
963.6	6.53(g)	*1286*, 1309.4, 1765.8
1309.4	6.53(f)	963.6
1681.6	6.53(e)	*2246*
1737.8	6.53(c)	*1720*
1765.8	6.53(a)	963.6, *991*
2000.8	6.52(h)	*119*, *306*, *879*
2216.8	6.52(g)	*992*
2249.9	6.52(e)	74.9, *690*
2273.8	6.52(d)	*947*, *1007*, 1765.8
2305.7	6.52(c)	*270*, *991*
2725.9	6.51(g)	*890*
2730.6	6.51(f)	*360*
2862.4	6.51(d)	74.9, *228*, *384*
3117.8	6.51(c)	*847*

Table 7.12: Summary of the γ-ray coincidence results for ^{66}Se decay. γ-rays written in italics are γ-rays observed in the γ-γ coincidence projected spectra but not in the γ-ray spectrum, or are only seen in low intensity. The γ-rays with energies of 3771 keV, 3367 keV, 2854 keV, 2376 keV, 2320 keV, 2314 keV, 2228 keV, 1743 keV, 1705 keV, 956 keV, 920 keV and 837 keV do not show any γ-γ coincidences.

The γ-ray with energy 963.6 keV is emitted from the state at **963.6 keV** [G$^+$95, G$^+$98, G$^+$01]. This γ-ray is in coincidence with the γ-rays with energies 1309.4 keV, 1766.3 keV and 1286 keV. The 1309.4 keV and 1766.3 keV γ-rays are not in coincidence with each other and this suggests they both populate the state at **963.6 keV** and originate in states at **2273.6 keV** and **2730.5 keV**. This is strongly supported by the γ-rays with energies of 2273.9 keV and 2730.6 keV that match the energies corresponding to the de-excitation to the ground state from levels at **2273.6 keV** and **2730.5 keV**. The peak at 1286 keV in coincidence with 963.6 keV gate would be emitted from an excited state at **2249.9 keV**.

Although it was not observed in the γ-spectrum in Fig. 6.50 for ^{66}Se decay, the γ-ray with energy 1286 keV appears clearly in the 963.6 keV gate. Its energy fits the difference in energy between the 2249.9 keV and 963.6 keV level. It is tentative placed there and is drawn as a dashed line.

The 2725.9 keV and 3117.8 keV γ-rays do not show γ-γ coincidences, and they are placed with dashed lines as direct transitions to the ground state from the excited states at **2725.9 keV** and **3117.8 keV**. Other peaks in the γ-ray spectrum in Fig. 6.50 are too weak to be considered in this thesis.

7.5.2. Beta decay strength calculation and decay scheme for ^{66}Se

The beta decay intensities for ^{66}Se decay can be obtained by balancing the intensity emitted from each excited state with the intensity fed by other excited states, then the beta decay intensity for each excited state $I_\beta^{(i)}$ is

$$I_\beta^{(i)} = \sum_j I_\gamma^{(i)\to(j)} - \sum_l I_\gamma^{(l)\to(i)} \ , \tag{7.6}$$

where $I_\gamma^{(i)\to(j)}$ is the intensity of the γ-ray transition between the state (i) to the state (j) in ^{66}As and $I_\gamma^{(l)\to(i)}$ is the γ-transition between the states (l) and (i) in ^{66}As. In Table 7.13, the beta feedings were calculated for each state in level scheme of ^{66}Se decay. Then in Fig. 7.10 the decay scheme for ^{66}Se is shown.

Initial State	Final State	Energy keV	I_β[%]	logf	logt	logft	Strength	Type
g.s.	3117.8(4)	7247(200)	0.42(7)	3.85(8)	1.13(7)	5.0(1)	0.04(2)	GT
g.s.	2730.5(1)	7635(200)	1.9(1)	4.00(6)	0.48(3)	4.48(7)	0.13(4)	GT
g.s.	2725.9(5)	7639(200)	0.34(7)	4.00(6)	1.23(9)	5.2(1)	0.02(1)	GT
g.s.	2273.6(1)	8091(200)	1.25(9)	4.14(6)	0.66(3)	4.80(7)	0.06(2)	GT
g.s.	2249.9(1)	8115(200)	7.3(3)	4.15(6)	-0.10(2)	4.04(6)	0.4(1)	GT
g.s.	963.6(1)	9401(200)	0.6(2)	4.49(5)	1.0(1)	5.5(1)	0.013(7)	GT
g.s.	836.9(1)	9528(200)	6.0(2)	4.53(5)	-0.02(2)	4.51(5)	0.12(3)	GT
g.s.	g.s.	10365(200)	82.2(4)	4.72(5)	-1.158(2)	3.57(5)	1.7(2)	F

Table 7.13: Summary of transition intensities, logf, logt, logft and beta strength for ^{66}Se decay.

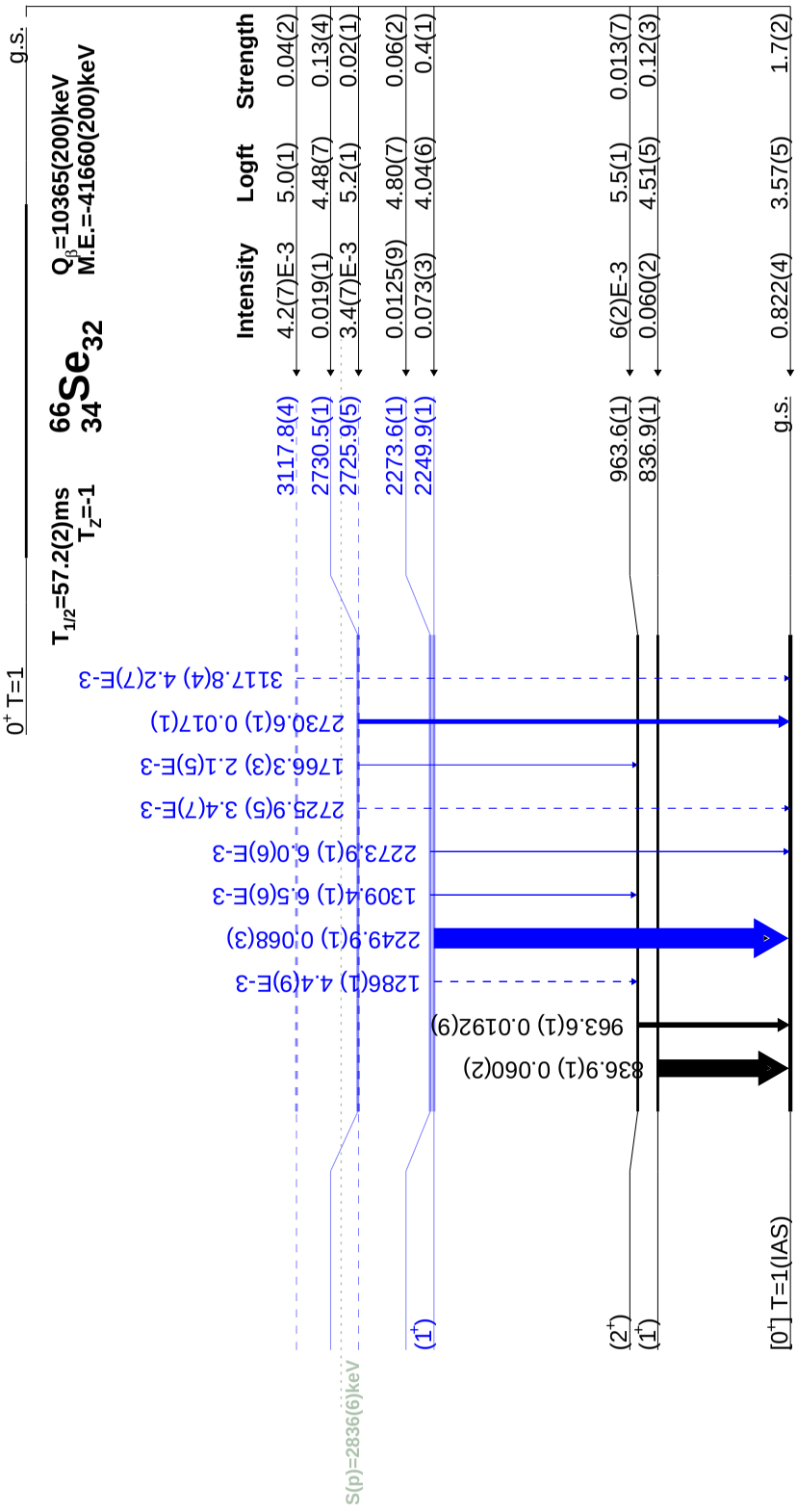

Figure 7.10: Level scheme for ^{66}Se using the half life in Table 6.22, our measured half life for ^{66}As and mass excess and Q_β values from AME2016.

Chapter 8

Decay scheme reconstruction for ^{64}Se and ^{64}As using Q_β values obtained from the IMME

In chapter 7 the Q_β value necessary for the calculation of the Fermi function (see Chapter 1) was taken from the AME2016 [WAK+17] database. Although the values reported there summarise all the results up to 2016, the values provided for the Q_β values for ^{64}Se, ^{64}As and ^{66}Se correspond to extrapolations. According to our knowledge, there are no new experimental values for these quantities since 2016 until now. However, for $A = 64$ nuclei, the beta-delayed proton emission of ^{64}Se may give information about the mass of the nuclei using the Isobaric Mass Multiplet Equation. This information will be used in order to obtain both the Mass excess and Q_β values for ^{64}Se and ^{64}As using data from this experiment. In the next section this procedure will be described.

8.1. Determination of ^{64}Se and ^{64}As mass excesses using the Isobaric Mass Multiplet Equation (IMME)

The **I**sobaric **M**ass **M**ultiplet **E**quation (IMME) was first proposed by Wigner [Wig57] and later derived with more mathematical rigour by Weinberg and Treiman [WT59]. To first order, the mass excess of IAS states for an isobaric multiplet lies in a parabola [LB09],

$$M^{(\mathrm{IAS})} = a + bT_z + cT_z^2 \tag{8.1}$$

where a, b, and c are parameters depending on the particular multiplet case.

The $T = 2$ multiplet is formed by five isotopes, three of them (^{64}Ge, ^{64}Ga, and ^{64}Zn) have experimental mass excess values, and the remaining two (^{64}Se and ^{64}As) has only have estimated values. The $T = 2$ multiplet is formed by the ground state in the $T_z = \pm 2$ members (^{64}Zn and ^{64}Se), excited states $\sim$ 1900 keV in $T_z = \pm 1$ members (^{64}Ga and ^{64}As), and the $T = 2$ state in ^{64}Ge at higher energy. The $T_z = 0$ ^{64}Ge IAS with $T = 2$ cannot be observed in this experiment since the mother state (g.s. of ^{64}As) is a 0^+ $T = 1$ state, and the Fermi transition to the 0^+, $T = 2$ state is forbidden. In Table 8.1 literature masses are summarized for $A = 64$ multiplet members, together with the IAS $T = 2$ excitation energy.

To obtain the IMME for the $A = 64$ multiplet, the mass excess of three states are needed, in our case we will use the ground state of ^{64}Zn, the IAS ($T = 2$) of ^{64}Ga, and the IAS ($T = 2$) of ^{64}As. The mass excess of the ground state for ^{64}Zn is reported in the literature [WAK+17]. The mass excess of the $T = 2$, IAS for ^{64}Ga can be obtained by adding the energy of the excited state measured in the charge exchange reaction [DFF+19] to the mass excess of the ground state of ^{64}Ga. The

T_z	-2	-1	0	+1	+2
Isotope	^{64}Se	^{64}As	^{64}Ge	^{64}Ga	^{64}Zn
E_{ex} keV	G.S.	1956.4	Unknown	1922	G.S.
M.E. [WAK+17]	$-26700\#(500)$	$-39530\#(200)$	-54315_{4}	-58832.8_{14}	-66004.0_{6}
M.E. [MGA+12]	$-26930\#(500)$	$-39650\#(300)$	-54315_{4}	-58832.8_{14}	-66003.8_{7}
M.E. [AWT03]	-	$-39520\#_{360}$	-54350_{30}	-58834.3_{20}	-66003.6_{7}
Q_β [WAK+17]	12830#(540)	14780#(200)	4517(4)	7171.2(15)	–
Q_β [MGA+12]	12720#(590)	14660#(300)	4517(4)	7171.0(15)	–
Q_β [AWT03]	-	14830#(360)	4480(30)	7169.3(21)	–

Table 8.1: Mass excess for g.s. and Q_β values for the members of the $A = 64$ $T = 2$ multiplet, obtained from atomic mass evaluation AME2016 [WAK+17], AME2012 [MGA+12], AME2003 [AWT03].Values obtained using extrapolation are marked with #. For each isotope the IAS $T = 2$ excitation energy (E_{ex}), the g.s. mass excess (M.E.) and Q_β value are shown in keV.

mass excess of the IAS $T = 2$ for ^{64}As was not known prior to our work, however, it can be obtained from our measurements of the proton-emission and γ-rays in the decay of ^{64}Se as shown in Fig. 8.1.

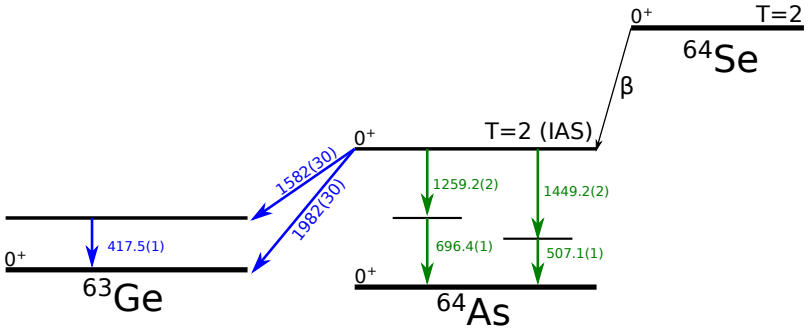

Figure 8.1: Diagram for the calculation of the ^{64}As g.s. and IAS state mass excess. The experimental values for the mass excess of ^{63}Ge were used together with the ^{64}As IAS p-emission (shown in blue) and the excitation energy of the IAS. The excitation energy of the IAS was obtained as the sum of the 1259 keV and the 696 keV energies (shown in green) seen in coincidence. The level was further confirmed by the 1449 keV and 507 keV coincidences. The spin-parity assignment to the level was made based on the information in the ^{64}Ga mirror nucleus [DFF+19].

Since the mass excess for the ^{63}Ge is known [WAK+17] (see Table 8.1), if we

add the averaged energy of the protons and the γ-ray shown in blue in Fig. 8.1 with the mass excess of ^{63}Ge, the mass excess of the $T = 2$ IAS in ^{64}As can be obtained. Then, the mass excess of the ground state of ^{64}As is obtained by subtracting the energy of the $T = 2$ IAS. The energy of the $T = 2$ IAS in ^{64}As was measured averaging the γ-ray cascade shown in green in Fig. 8.1.

The mass excess of the $T = 2$ IAS in $T_z = -1, +1, +2$ nuclei were fitted in order to obtain the IMME for this multiplet. The results of the fitting are shown in Table 8.2. In Fig. 8.2 the IMME obtained using these three points is shown, together with the IMME for lower masses multiplets measured by Orrigo et. al. [ORF+16].

a keV	b keV	c keV
−47473(24)	−9644(36)	189(12)

Table 8.2: The results of the fitting of the IMME in the $A = 64$ $T = 2$ multiplet. The input values are the mass excess of the ^{64}Zn g.s., ^{64}Ga IAS $T = 2$, and the ^{64}As IAS $T = 2$. The mass excess of the ^{64}Zn ground state and ^{64}Ga IAS $T = 2$ were previously reported in the literature [WAK+17, DFF+19]. The mass excess for ^{64}As was obtained using the protons and γ-rays observed in this experiment and the mass excess of ^{63}Ge reported in AME2016 [WAK+17].

In Table 8.3 mass excess values are presented for each member of the $A = 64$ $T = 2$ multiplet together with the g.s. masses, when known.

Mass excess keV	^{64}Se	^{64}As	^{64}Ga	^{64}Zn
Ground state	−27429(88)	−39597(44)	−58833(44)	−66004(88)
IAS $T = 2$	−27429(88)	−37640(44)	−56928(44)	−66004(88)

Table 8.3: Mass excess value for the $A = 64$ $T = 2$ multiplet. For ^{64}Ga and ^{64}Zn, literature values are used, for ^{64}As we report our deduced value (see text) and for ^{64}Se, and for ^{64}Se and ^{64}Ge results from the IMME formula are presented.

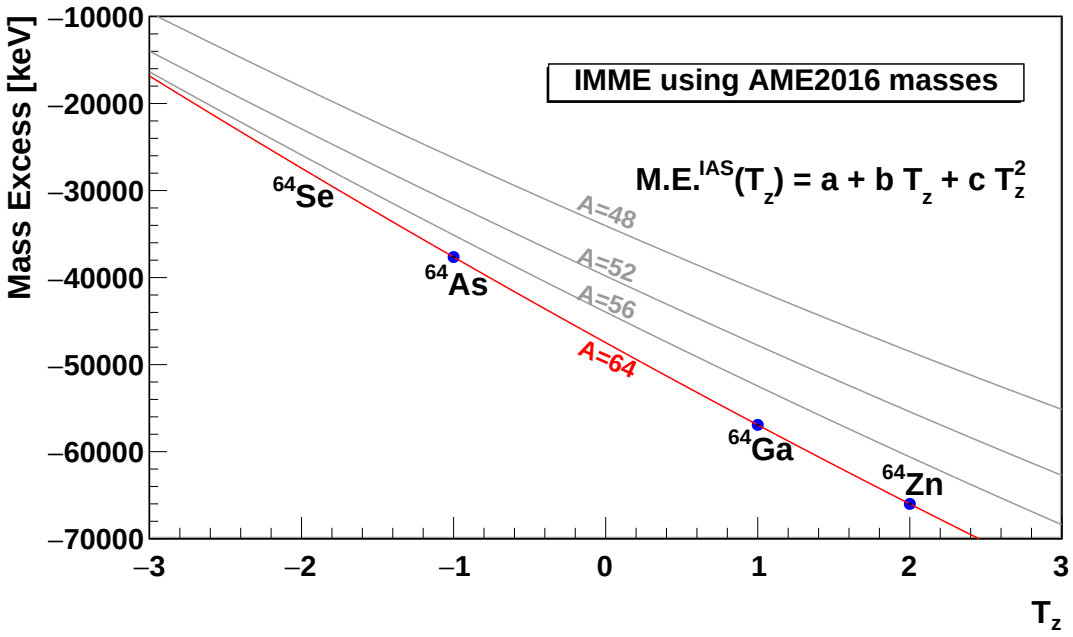

Figure 8.2: IMME fit using literature [WAK+17] values for the mass excess in ^{64}Zn and ^{64}Ga. The energy of the ^{64}As 0^+, $T = 2$ state was obtained using the ^{63}Ge mass excess in [WAK+17], proton energy measured with WAS3ABi, and the excitation energy of the IAS from the γ-ray energies. The IMME curves for lighter $T = 2$ multiplets were previously reported by Orrigo et. al [ORF+16] are shown coloured gray.

Once the mass excess values were obtained using the IMME, the Q_β value can be obtained by subtracting the mother mass excess ($M^{(moth.)}$) from the daughter mass excess ($M^{(daug.)}$),

$$Q_\beta = M^{(moth.)} - M^{(daug.)} \tag{8.2}$$

then, the Q_β values obtained using the IMME mass excess are Q_β (^{64}Se) = 12168(99) keV and Q_β (^{64}As) = 14718(44) keV.

8.2. Decay scheme of ^{64}As based on our new Q_β value results and the IMME estimated value

The decay scheme of ^{64}As in Section 7.2 was constructed using the Q_β reported in AME2016 [WAK+17]. As discussed in Section 7.2, the $T = 1$ IAS ($J^\pi = 0^+$) in ^{64}Ge has an energy of **4962.0 keV**, and can be populated only by a Fermi transition. The Fermi strength in this case should be $B(F) = N - Z = 2$, however $B(F) = 1.5(2)$ was obtained. In this section the beta decay strengths will be calculated using the $Q_\beta^{\text{IMME}} = 14718(44)$ keV, in order to investigate if the deficit in beta decay strength in IAS is related to the reported $Q_\beta^{\text{AME2016}} = 14780\#(200)$ [WAK+17].

In Table 8.4 the strength values obtained using the Q_β^{IMME} instead the Q_β^{AME2016} are shown. There is no big difference in the value obtained for the strength to the IAS $T = 2$. Then in Fig. 8.3 these results are shown in the decay scheme for ^{64}As.

Initial State	Final State	Energy keV	I_β[%]	logf	logt	logft	Strength	Type
g.s.	10289(20)	4429(50)	0.21(2)	2.65(3)	1.48(3)	4.13(4)	0.29(6)	GT
g.s.	9195(20)	5523(50)	0.64(5)	3.20(2)	1.00(3)	4.20(4)	0.25(4)	GT
g.s.	8510(30)	6208(60)	0.21(3)	3.49(2)	1.48(7)	4.97(7)	0.04(1)	GT
g.s.	7978(20)	6740(50)	1.40(9)	3.68(2)	0.65(3)	4.34(3)	0.18(3)	GT
g.s.	7276(10)	7442(50)	1.50(9)	3.92(1)	0.62(3)	4.54(3)	0.11(2)	GT
g.s.	6903(80)	7815(90)	1.00(8)	4.03(3)	0.80(3)	4.83(4)	0.06(1)	GT
g.s.	6255(2)	8463(40)	3.6(5)	4.22(1)	0.25(7)	4.47(7)	0.13(4)	GT
g.s.	5138.1(4)	9580(40)	1.2(2)	4.51(1)	0.70(5)	5.21(6)	0.024(6)	GT
g.s.	4962.0(1)	9756(40)	54(2)	4.55(1)	-0.94(1)	3.61(2)	1.53(6)	F
g.s.	4879.3(2)	9839(40)	0.9(1)	4.57(1)	0.85(6)	5.42(6)	0.015(4)	GT
g.s.	3975.9(4)	10742(40)	0.6(1)	4.770(9)	1.01(8)	5.78(8)	0.006(2)	GT
g.s.	3648.0(1)	11070(40)	0.3(3)	4.839(9)	1.3(5)	6.2(5)	0.003(6)	GT
g.s.	3466.8(1)	11251(40)	12(2)	4.876(9)	-0.26(8)	4.61(8)	0.09(4)	GT
g.s.	3136.0(4)	11582(40)	1.0(1)	4.942(9)	0.79(5)	5.73(5)	0.007(2)	GT
g.s.	2955.8(2)	11762(40)	1.9(2)	4.977(9)	0.52(4)	5.49(4)	0.012(2)	GT
g.s.	2166.3(1)	12552(40)	0.5(5)	5.125(8)	1.1(4)	6.2(4)	0.002(5)	GT
g.s.	2154.5(1)	12563(40)	-0.7(3)	-	-	-	-	GT
g.s.	1578.3(1)	13140(40)	1(2)	5.228(8)	1(2)	6(2)	0.00(1)	GT
g.s.	901.4(1)	13817(40)	4(3)	5.342(7)	0.2(3)	5.6(3)	0.01(1)	GT
g.s.	g.s.	14718(40)	15(4)	5.484(7)	-0.4(1)	5.1(1)	0.03(2)	GT

Table 8.4: Summary of transition intensities, logf, logt, logft and beta strength for ^{64}As decay using the IMME values for mass excess and Q_β values.

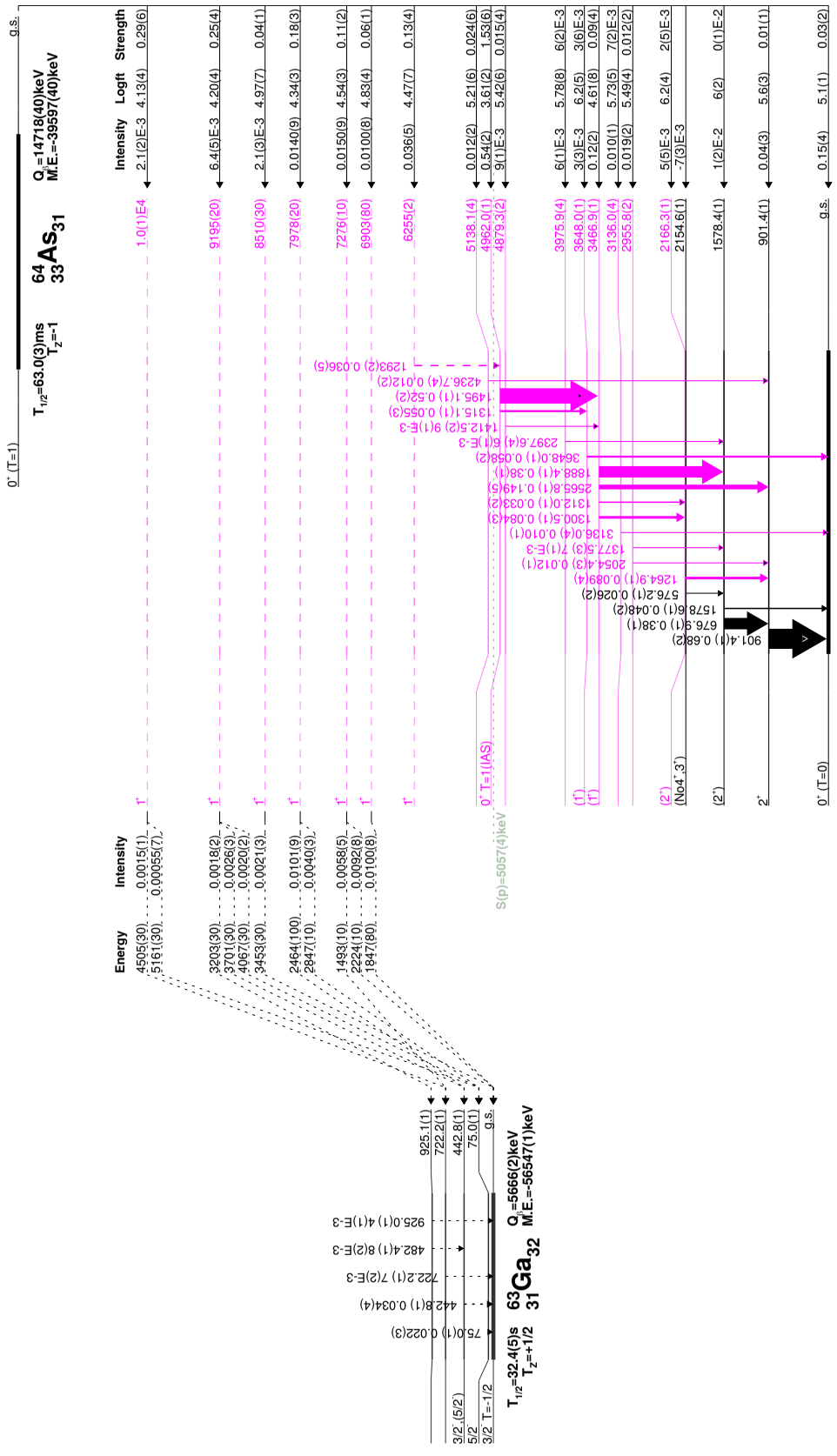

Figure 8.3: Level scheme for ^{64}As decay using mass excess and Q_β values deduced using the IMME (see text).

8.3. Decay scheme of ^{64}Se using our Q_β values estimated by the IMME

As in the decay of ^{64}As, in this section the decay scheme of ^{64}Se constructed in Section 7.3 will be recalculated using the Q_β value obtained using the IMME.

The $T = 2$ IAS ($J^\pi = 0^+$) in ^{64}As has an energy of **1956.4 keV**, and can be populated only by a Fermi transition. The Fermi strength in this case should corresponds to $B(F) = N - Z = 4$, however $B(F) = 2.5(9)$ was obtained.

In Table 8.5 beta decay strengths were calculated using the $Q_\beta^{\text{IMME}} = 12168(99)$ keV instead of $Q_\beta^{\text{AME2016}} = 12830\#(540)$ estimated in [WAK+17], in order to study the observed deficit in the beta decay strength to the IAS $T = 2$ in ^{64}As.

Initial State	Final State	Energy keV	I_β[%]	logf	logt	logft	Strength	Type
g.s.	4629(100)	7539(100)	1.00(7)	3.97(4)	0.35(3)	4.32(5)	0.18(5)	GT
g.s.	3956(100)	8212(100)	0.85(6)	4.18(4)	0.42(3)	4.60(5)	0.10(2)	GT
g.s.	3647(70)	8521(100)	4.3(2)	4.26(3)	-0.29(3)	3.98(4)	0.41(8)	GT
g.s.	2960(100)	9208(100)	2.0(1)	4.45(4)	0.05(3)	4.50(5)	0.12(3)	GT
g.s.	1105(100)	11063(100)	1.16(8)	4.87(3)	0.29(3)	5.16(4)	0.027(6)	GT
g.s.	1956.4(2)	10212(100)	60(3)	4.69(2)	-1.43(3)	3.26(3)	3.5(3)	F
g.s.	697.4(1)	11471(100)	1(2)	4.96(2)	0.2(7)	5.2(7)	0.03(9)	GT
g.s.	507.1(1)	11661(100)	16(4)	5.00(2)	-0.8(1)	4.2(1)	0.3(1)	GT
g.s.	148.7(2)	12019(100)	4(1)	5.07(2)	-0.2(2)	4.9(2)	0.05(4)	GT
g.s.	g.s.	12168(100)	10(6)	5.10(2)	-0.6(3)	4.5(3)	0.1(2)	GT

Table 8.5: ^{64}Se beta decay strengths using IMME values.

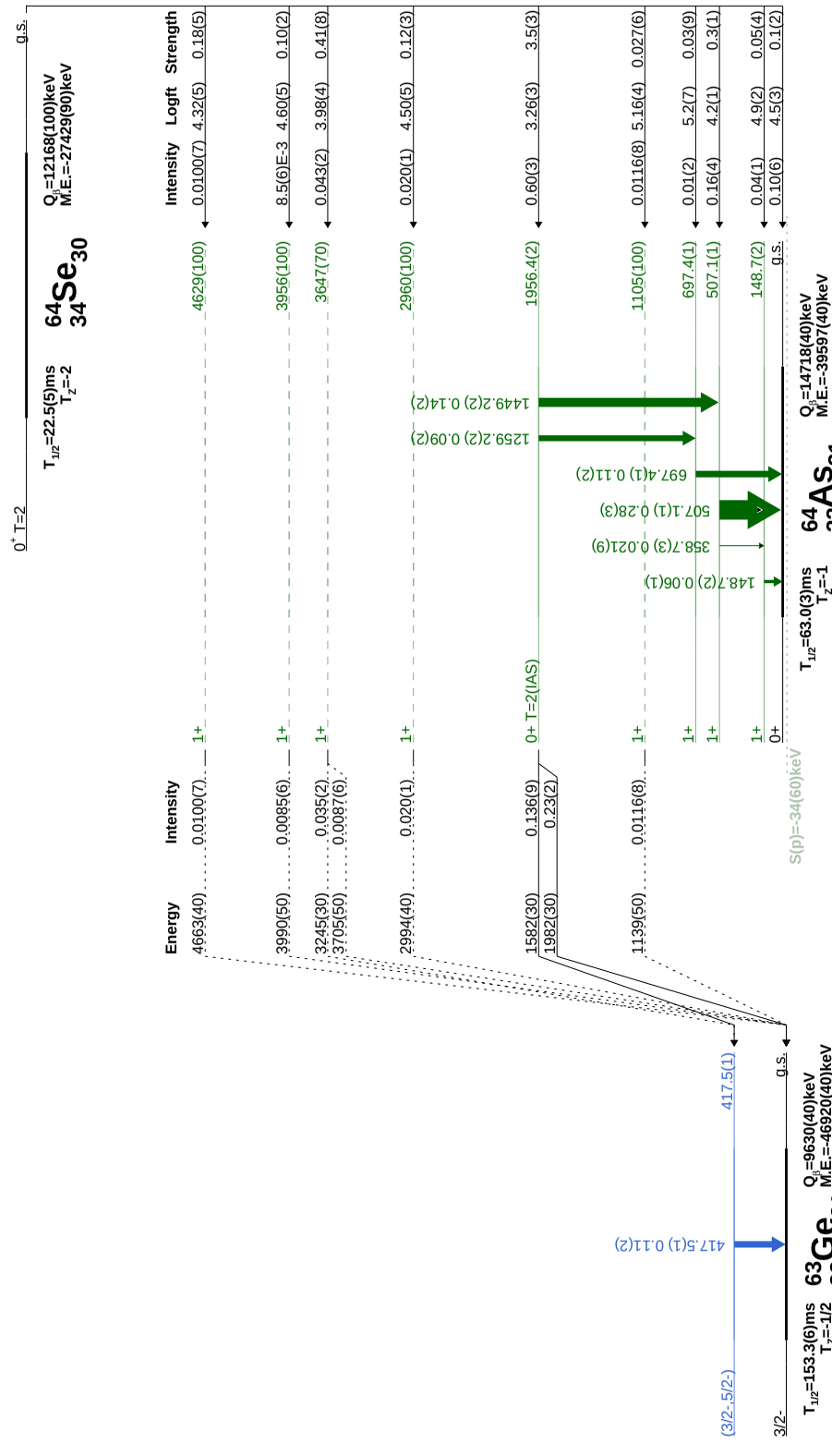

Figure 8.4: Level scheme for ^{64}Se using the half-life in Table 6.16, our measured half-life for ^{64}As and ^{63}Ge, and mass excess and Q_β values from our IMME estimations.

Using the Q_β^{IMME} obtained in the analysis of the IMME in Section 8.1 instead of the literature value Q_β^{AME2016} for ^{64}Se the beta decay strength to the IAS $T = 2$ in ^{64}As increases from 2.5(9) to 3.5(3). Unlike the case of ^{64}As using our estimate for the Q_β value makes a big difference in the strength obtained.

Chapter 9

Mirror symmetry comparison for ^{64}Se and ^{64}As decays

Once the decay schemes are constructed, the discussion now turns to the comparison in terms of mirror symmetry. First the decay of ^{64}Se will be compared with the charge exchange reaction ^{64}Zn(^{3}He, t)^{64}Ga results measured by F. Diel [DFF+19, Die15]. Then we present the $A = 64$ quintuplet with $T = 2$ formed by ^{64}Se, ^{64}As, ^{64}Ge, ^{64}Ga and ^{64}Zn. Finally we present an energy comparison for the decay of ^{63}Ge which involves its own beta decay daughter ^{63}Ga.

9.1. Comparison of the $|T_z| \leq 2$ members of the multiplet with A=64

The ^{64}Se ($T_z = -2$) beta decay populates states in ^{64}As ($T_z = -1$). On the other hand the charge exchange reaction (mirror process of the beta decay) in the ^{64}Zn ($T_z = +2$) [DFF+19] populates states in ^{64}Ga ($T_z = +1$). If isospin is a good quantum number, the beta decay of ^{64}Se and the charge exchange in ^{64}Zn should populate analogue states in the corresponding daughter nuclei, and with the same

strength. In Fig. 9.1, mirror nuclei $T_z = \pm 1$ are shown, aligned with the ground state.

In Fig. 9.1 the charge exchange reaction and the decay of ^{64}Se are shown. Then in Fig. 9.3 the strength comparison for these decays are shown.

In the same way, the comparison for the decay of ^{64}Se obtained using the Q_β obtained using the IMME in Section 8.1, is shown in 9.1 and 9.3.

Finally in Fig. 9.5 the quintuplet composed by ^{64}Se ($T_z = -2$), ^{64}As ($T_z = -1$), ^{64}Ge ($T_z = 0$), ^{64}Se ($T_z = +1$) and ^{64}Zn ($T_z = +2$) is shown. In this figure the states with $T = 2$ IAS are shown aligned for ^{64}Se, ^{64}As, ^{64}Ga and ^{64}Zn. The case of ^{64}Ge is different since the state with $T = 2$ is not populated in this experiment, and it was aligned with the $T = 1$ IAS.

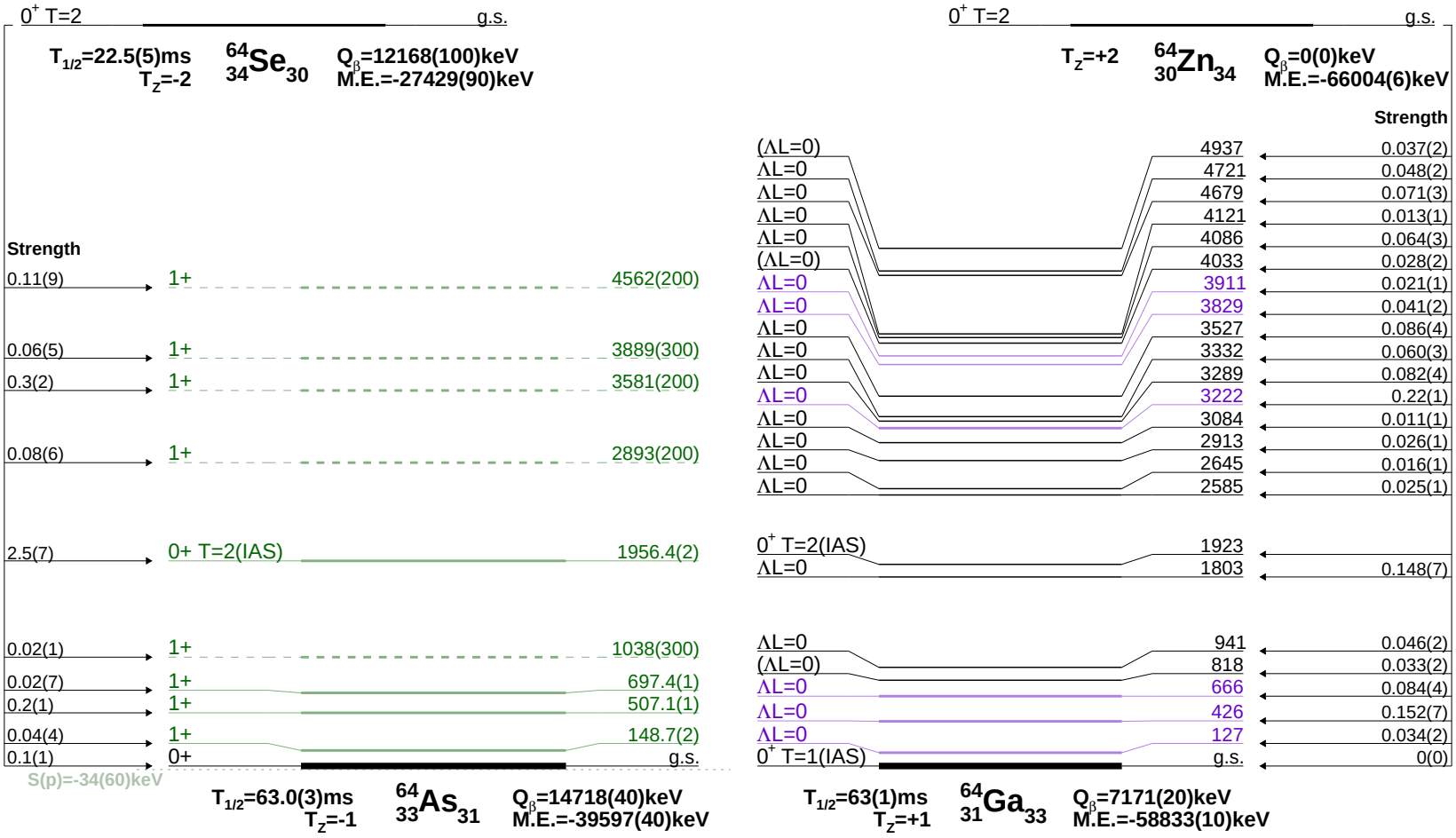

Figure 9.1: $T_z = \pm 1$ members ^{64}As and ^{64}Ga, of the isobaric multiplet obtained from the beta decay experiment (using AME2016 [WAK+17] mass excess and Q_β values) and charge exchange reaction [DFF+19].

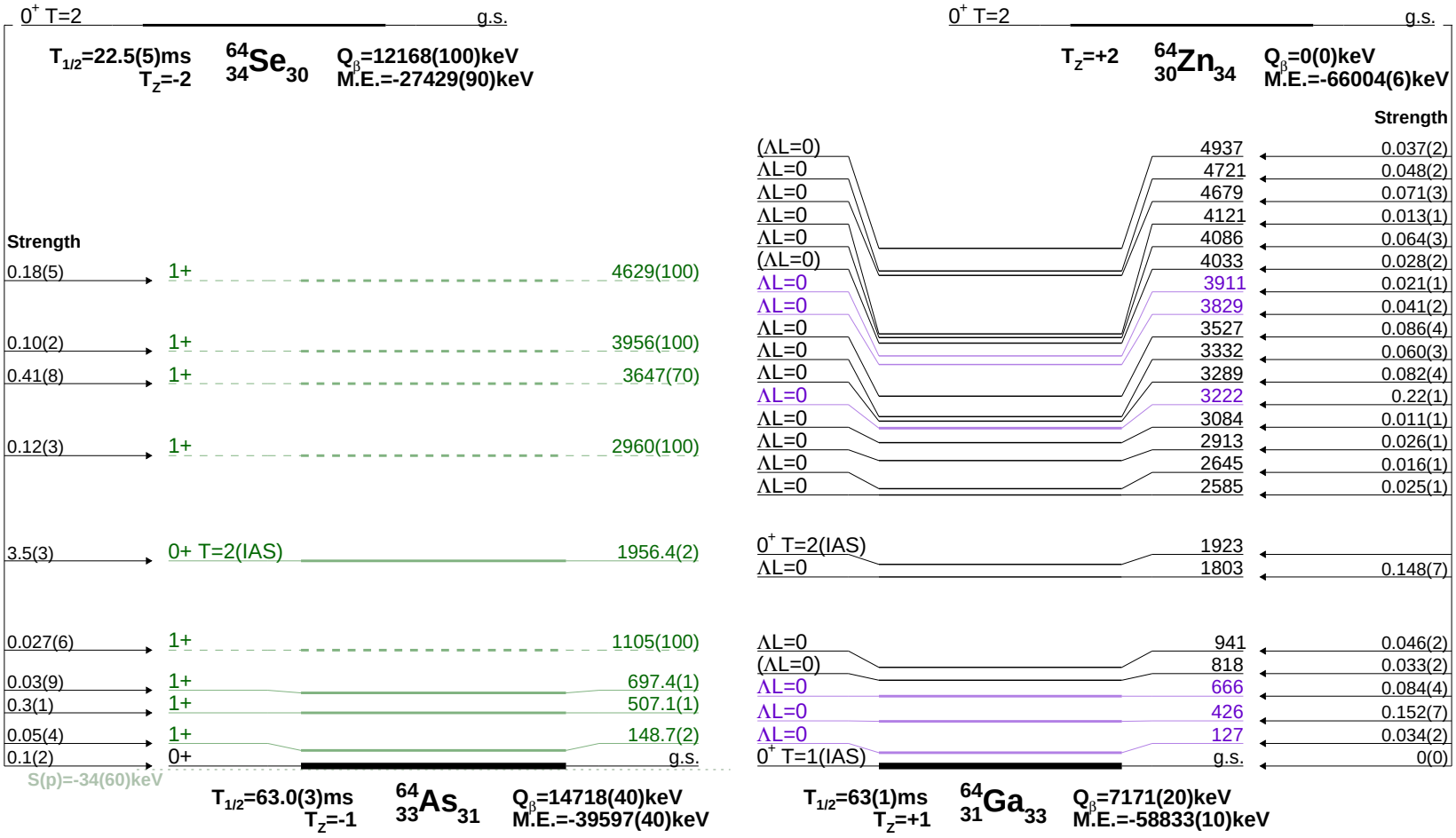

Figure 9.2: $T_z = \pm 1$ members ^{64}As and ^{64}Ga, obtained from this beta decay experiment (using our IMME mass excess estimations) and charge exchange reaction [DFF+19], respectively.

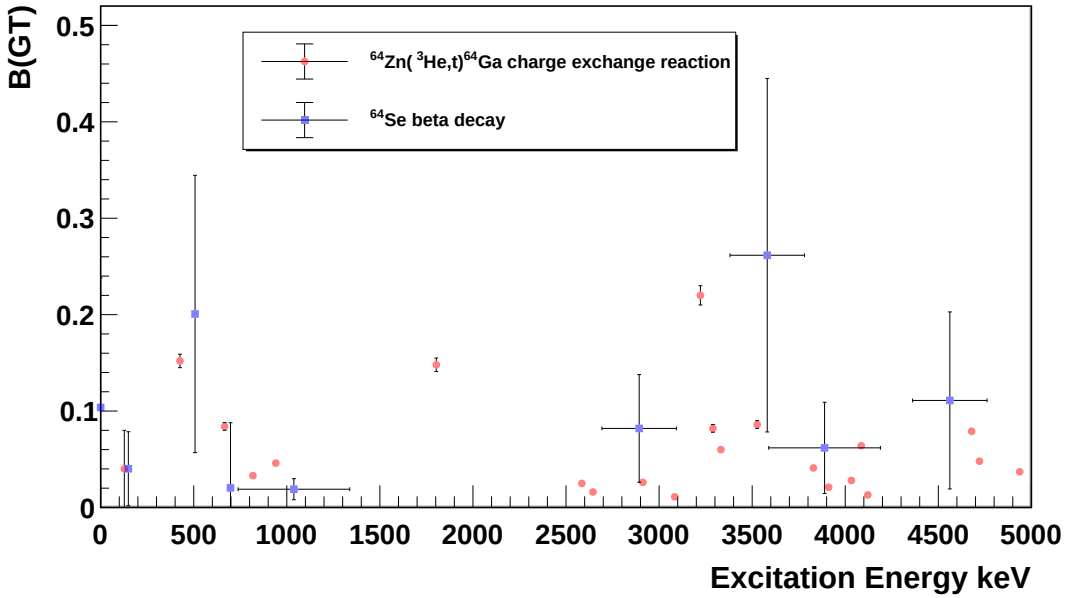

Figure 9.3: $A = 64$ strength comparison between the beta decay of ^{64}Se obtained using the $Q_\beta^{\mathrm{AME206}}$, and the charge exchange reaction ^{64}Zn(^{3}He,t)^{64}Ga.

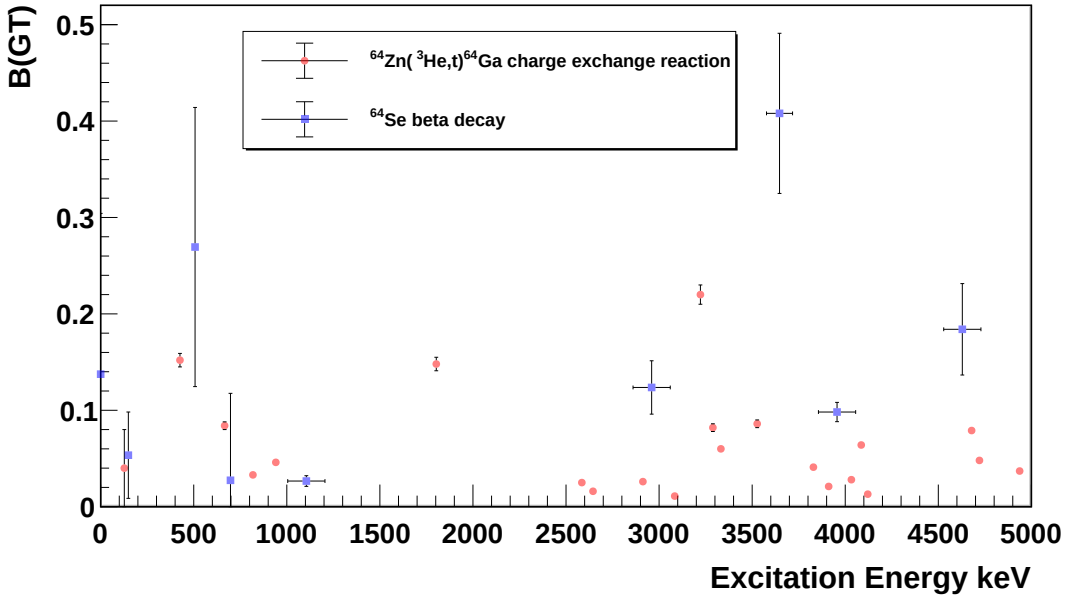

Figure 9.4: $A = 64$ strength comparison between the beta decay of ^{64}Se obtained using the Q_β^{IMME}, and the charge exchange reaction ^{64}Zn(^{3}He,t)^{64}Ga.

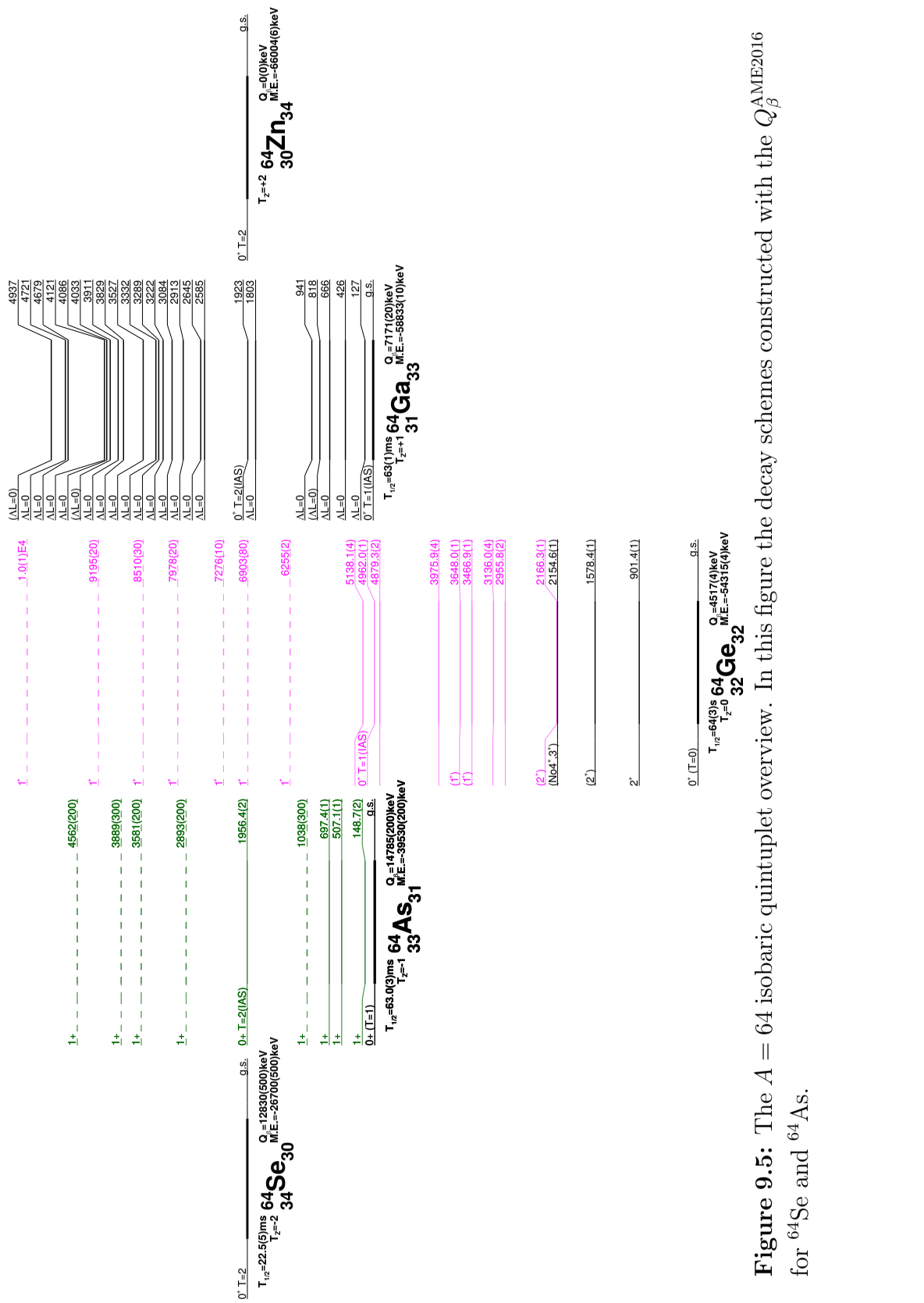

Figure 9.5: The $A = 64$ isobaric quintuplet overview. In this figure the decay schemes constructed with the Q_β^{AME2016} for ^{64}Se and ^{64}As.

Part V

Summary and conclusions

Chapter 10

Summary overview

In this thesis the decays of ^{64}Se, ^{64}As, ^{63}Ge, ^{66}Se and ^{66}As were studied. In two of them, ^{64}Se and ^{64}As, beta-delayed proton emission was observed. This work presents the first beta decay study of these nuclei, ^{64}Se and ^{64}As.

Knowledge of some of the excited states in the beta decay daughter ^{63}Ga came from two in-beam experiments in ^{63}Ga by Balamuth et. al and Weiszflog et. al. [W$^+$01,B$^+$91]. The states populated in these in-beam experiments can be different from the states populated in the beta decay. Fortunately four of the γ-rays observed in-beam were also observed in the present experiment giving a starting point for the construction of the decay scheme. Fifteen γ-rays were observed in the decay of ^{63}Ge, where four were previously reported in literature [W$^+$01, B$^+$91] and eleven were observed for the first time. This allowed us to expand the level scheme of ^{63}Ga with seven new excited states with energies of **925.1 keV**, **954.2 keV**, **1000.1 keV**, **1363.5 keV**, **2072.6 keV**, **2485.4 keV** and **3207.9 keV**, observed for the first time in this work.

With respect to the half-life of ^{63}Ge, $T_{1/2}$ = 142(8) ms was reported in NUBASE2016 [AKW$^+$17]. In this thesis the half-life was determined in two ways,

using first the 442.8 keV γ-ray as gate for the implantation-decay correlations, and secondly taking into account all decay members without any γ-ray gate including cases where we have ground state to ground state transitions. In the first case, using the 442.8 keV γ-ray we obtain $T_{1/2} = 152.7(28)$ ms. Using the whole decay chain we obtain $T_{1/2} = 152.60(33)$ ms. The two results agree and $T_{1/2} = 152.60(33)$ ms was used in the construction of the decay scheme for ^{63}Ge.

For ^{64}As decay, we observe for the first time the beta-delayed proton emission, which populates states in ^{63}Ga. This provide us the opportunity to investigate the ^{63}Ga either by the beta decay of ^{63}Ge or by the proton emission of ^{64}As. The beta decay daughter of ^{64}As is ^{64}Ge. As in the case of ^{63}Ga, previous knowledge of its excited states in this nucleus came from in-beam experiments carried out by Ennis et. al [ELG+91] and by Farnea et. al [FEA+03]. In the present experiment nineteen γ-rays were identified in ^{64}As decay, four of which were previously observed in the in-beam experiments. Gamma-rays coincidences and intensities allowed us to determine ten new excited states in ^{64}Ge with energies of **2166.3 keV**, **2955.8 keV**, **3136.0 keV**, **3466.9 keV**, **3648.0 keV**, **3975.9 keV**, **4879.3 keV**, **4962.0 keV**, **5138.1 keV** and **6255 keV**.

In the decay of ^{64}As it was possible to determine eleven proton energy peaks emitted in the beta-delayed proton emission. Some of these protons may be in coincidence with γ-rays in ^{63}Ga such as 75.0 keV, 442.8 keV, 482.4 keV, 722.2 keV and 925.0 keV. The number of ^{64}As ions was not enough to identify the gamma-proton coincidences. Nevertheless in this work we suggest a plausible scenario with six excited states in ^{64}Ge which are at **6903 keV**, **7276 keV**, **7978 keV**, **8510 keV**, **9195 keV** and **10 MeV**. These excited states were obtained by considering all possible excited state combinations, favouring those that appear in more than one

proton-gamma combination of energies.

The half-life of ^{64}As could be determined in three ways: using the implantation-proton correlations as a correlation gate, using the implantation-γ rays as correlation gate, using the implantation-beta correlations and taking into account the full decay chain. Using the proton condition we obtain $T_{1/2} = 63.46(60)$ ms and a proton branching of $B_p = 4.4\%$, where $\varepsilon_p = 100\%$ of proton efficiency was assumed. Then using the proton branching obtained with the proton condition, we obtain $T_{1/2} = 63.03(29)$ ms and a beta efficiency of $\varepsilon_\beta = 83.6\%$. Using the γ-ray gates we obtain values between 61.39(72) keV and 63.31(67) keV. In Fig. 10.1 a summary of these values is shown. The half-life weighted by the errors corresponds to $\bar{T}_{1/2} = 62.69(71)$ ms shown in Fig. 10.1 by the horizontal red lines. The average error of the half-lives is shown with dashed red lines as an accuracy reference. However we favour the half-life obtained using the full decay chain since it has the lowest error among the measurements, and is in agreement with the weighted value.

The study of the beta decay of ^{64}Se was one of the main goals of this thesis. It completes the study of $T_z = -2$ nuclei in the fp-shell where the decay still proceeds by a combination of beta-delayed p and beta-delayed γ-rays. The next $T_z = -2$ nucleus ^{68}Kr is expected to decay only by protons, and the experimental value is 89^{+11}_{-10} % [Goi17]. Moreover, ^{64}Se is the last case where the beta decay can be compared with the mirror CE reaction since ^{68}Ge is not stable. With only an upper limit for the half-life ($>$ 180ns) as previous knowledge, we were able to obtain the decay scheme and its half-life. Seven γ-rays were identified in the decay of ^{64}Se, six in ^{64}As and one in ^{63}Ge. Four excited states could be located using the γ-γ coincidence relations, energies and intensities, at **148.7 keV**, **507.1 keV**, **697.4 keV** and **1956.4 keV**. In this thesis it was shown that ^{64}Se is a proton emitter. Indeed

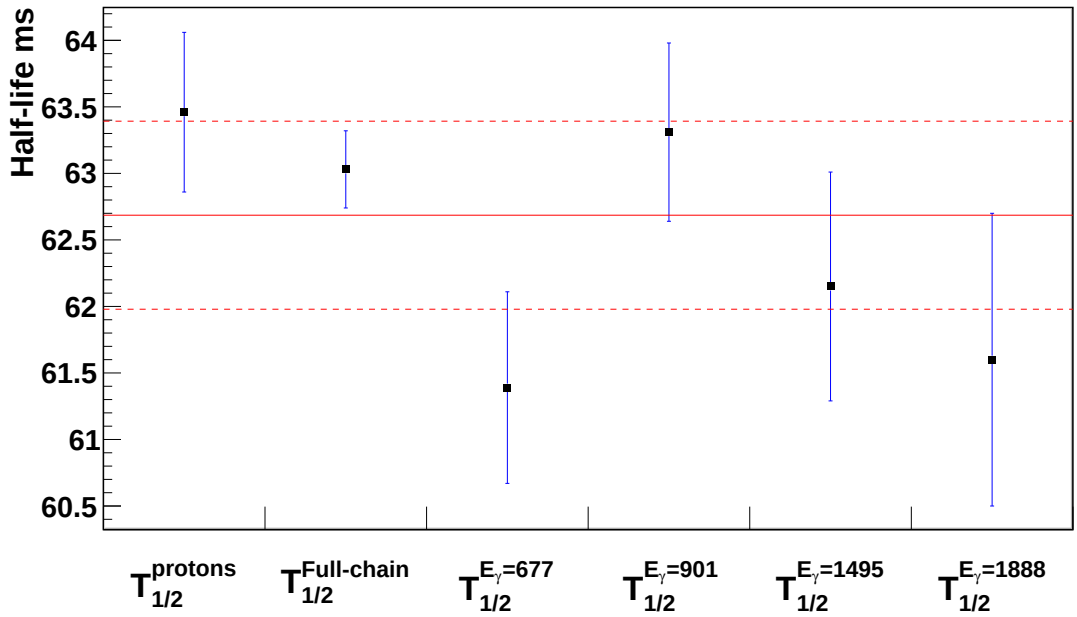

Figure 10.1: Half-lives for ^{64}As obtained using implantation-proton correlations, the implantation-beta taking into account the full decay chain, and the implantation-γ ray correlations. The mean value ($\bar{T}_{1/2} = 62.69(71)$ ms)) is shown with a horizontal red line. The confidence interval shown with red dashed lines was obtained as the error average.

eight protons peaks were observed in this decay, two of them, the 1982 keV and the 1582 keV energy protons, were identified as being emitted from the $T = 2$ IAS state at **1956.4 keV** in ^{64}As. For the other six protons, we proceed as in the case of ^{64}As decay, taking into account all possible combinations between the states in ^{63}Ge and the protons. We decided in favour of states with the largest number of combinations. The suggested proton emitting states in ^{64}As have the energies of **1038 keV**, **2893 keV**, **3581 keV**, **3889 keV** and **4562 keV**.

The half-life of ^{64}Se was determined using the implantation-proton correlations, implantation-beta correlations taking into account the full decay chain, and implantation-γ-ray correlations. Using the protons as gate for the correlations we ob-

tain $T_{1/2} = 23.32(62)$ ms and a proton branching $B_p = 48.02(89)\%$, where $\varepsilon_p = 100\%$ of proton detection efficiency was assumed. Then using the proton branching obtained with the proton condition, we use three γ-rays the 697 keV, 1259 keV and 1449 keV in combination as gate for the implantation-decay correlations. Using the γ-ray condition we obtain $T_{1/2} = 20.0(31)$ ms. Then using the full decay chain we obtain $T_{1/2} = 22.47(60)$ ms and a beta efficiency of $\varepsilon_\beta = 86.7(15)\%$, which was the value that was used in the construction of the decay scheme. In Fig. 10.2 these results are summarized. The averaged half-life value weighted by errors for ^{64}Se, shown by a horizontal red line, is $\bar{T}_{1/2} = 22.6(14)$ ms, which is in good agreement with the value obtained using all decay chain. The average error is shown with horizontal dashed red lines as an accuracy reference.

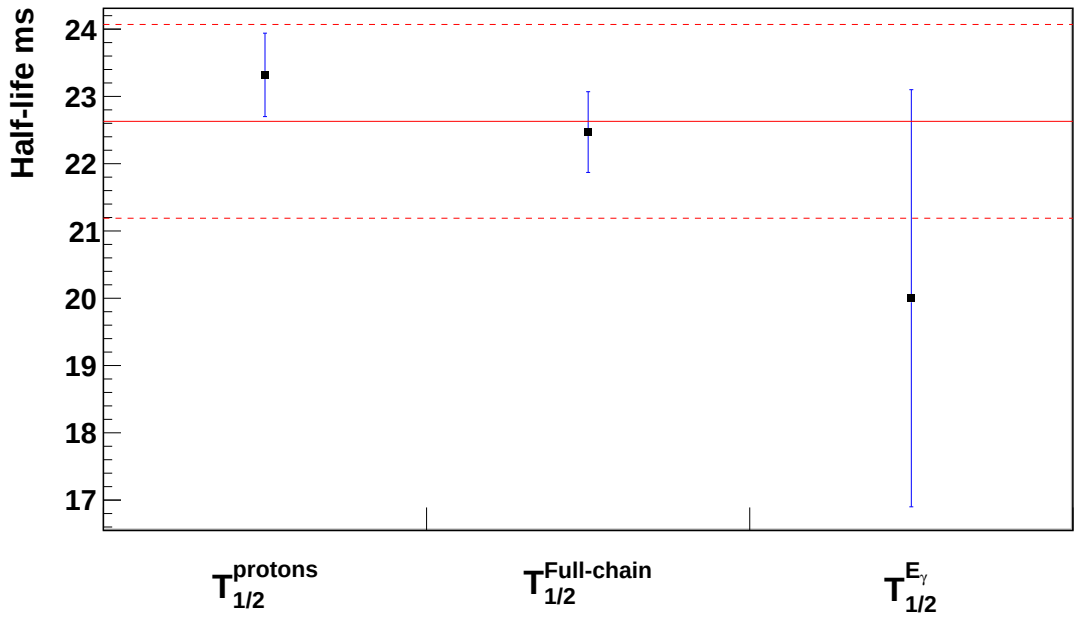

Figure 10.2: Half-life for ^{64}Se obtained using the full decay chain, the proton gate and the γ-ray gates. The mean value ($\bar{T}_{1/2} = 22.6(14)$ ms) is shown as a horizontal red line. The confidence interval shown with red dashed lines was obtained as the error average.

For ^{66}As the previously reported half-life was $T_{1/2} = 95.77(23)$ ms [AKW+17]. Using the whole decay chain we obtain $T_{1/2} = 95.31(77)$ ms which is in good agreement with the literature value. Also a beta efficiency of 76.5(4)% was determined during the fitting of the half-life. In this decay no γ-rays were observed, and we assume 100% of intensity for the g.s.-to-g.s. beta decay feeding as expected for a superallowed Fermi transition from 0^+ to 0^+.

The decay of ^{66}Se populates states in ^{66}As. This nucleus was previously studied in-beam by Grzywacz et. al [G+95, G+98, G+01]. Ten γ-rays were observed in the present work, where two of them, the 836.9 keV and the 963.6 keV, were also observed in the in-beam experiments. With the γ-ray coincidence analysis it was possible to expand the level scheme of the ^{66}As with five new excited states with energies of **2249.9 keV**, **2273.6 keV**, **2725.9 keV**, **2730 keV** and **3117.8 keV**.

The half-life of ^{66}Se was determined using the 836.9 keV and 2249.9 keV γ-rays, and then using the full decay chain. Using the γ-rays we obtain $T_{1/2}^{837} = 60.3(22)$ ms and $T_{1/2}^{2250} = 61.7(22)$ ms. Using the whole decay chain we obtained $T_{1/2} = 57.19(15)$ ms. The average half-life value weighted by errors in this case corresponds to $\bar{T}_{1/2} = 57.6(15)$ ms. However in the level scheme we use the half-life determined using the whole decay chain since it has a significantly lower error that the obtained in implantation-γ rays correlations. In Fig. 10.3, a summary of these measurements is shown, where the average half-life value is shown with an horizontal red line. The average errors are shown with horizontal dashed red lines as an accuracy reference.

In the decay of ^{64}Se and ^{64}As the calculation of decay strength required the Q_β values for those decays. The Q_β values for these nuclei have not been measured previously and only an estimated value taken from the AME2016 [WAK+17] was

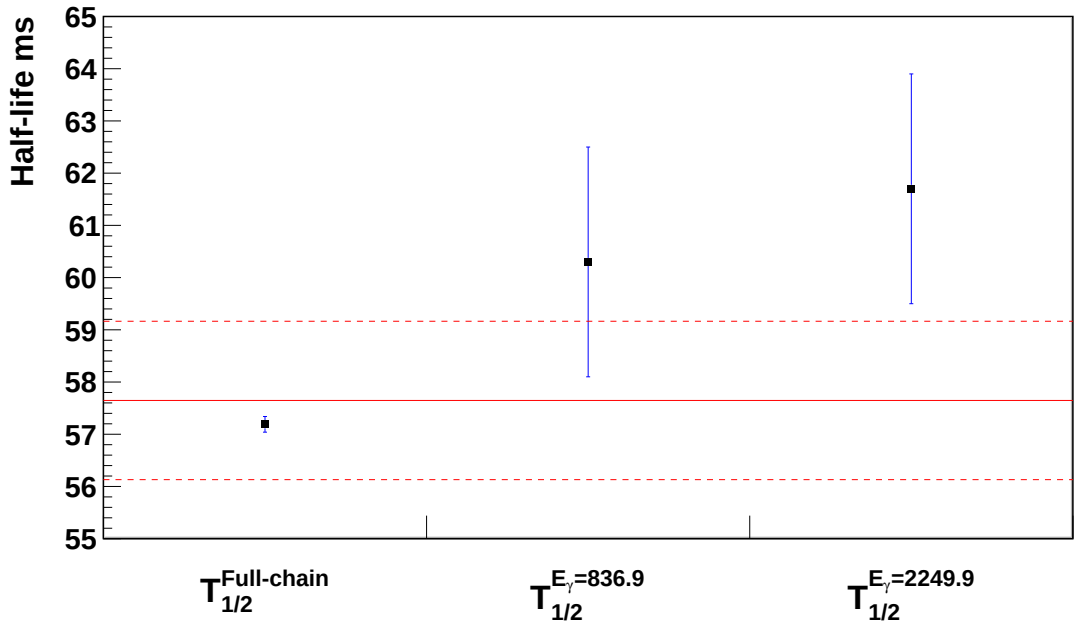

Figure 10.3: Half-live for the ^{66}Se obtained using full decay chain and the γ-ray gates. The mean value ($\bar{T}_{1/2} = 57.6(15)$ ms)) is shown with a horizontal red line. The confidence interval shown with red dashed lines was obtained as the error average.

available. Fortunately ^{64}Se is a beta-delayed proton emitter, and we could use the mass excess of ^{63}Ge in combination with the proton and the γ-ray energies, observed for the first time in this work, to estimate the mass excess for the ^{64}As. Then, using the ^{64}As, ^{64}Ga and ^{64}Zn members of the $T = 2$ multiplet, and the IMME equation we could obtain an estimate of the mass excess of ^{64}Se. We note that these estimates are based on the data from this experiment as well as literature values, and no nuclear model was involved. Using the mass excess for ^{64}Se estimated using the IMME, and our experimental value for the mass of ^{64}As the Q_β values could be obtained for these nuclei and its beta decay strength was recalculated.

In the decay of ^{64}Se the obtained beta decay strength to the IAS $T = 2$ in ^{64}As at **1956.4 keV**, using the AME2016 Q_β value was $B(F) = 2.7(7)$, while using

the Q_β from the IMME we obtain $B(F) = 3.5(3)$. In both cases there is a deficit with respect to the expected strength of $B(F) = N - Z = 4$ for this nucleus. One of the possible causes could be the estimated value for the ^{64}Se mass value used in the strength calculation. This can be tested only with a measurement of the mass of ^{64}Se.

On the other hand, the transition from the ^{64}Se $J^\pi = 0^+$ $T = 2$ ground state to the $J^\pi = 0^+$ ground state in ^{64}As $T = 1$ should be isospin forbidden. However we observe an intensity of 10(6)% in this transition. As the ground state feeding is obtained discounting all feeding to excited states, this intensity would correspond to transitions to excited levels in ^{64}As that were not observed. If we consider the intensity to the ground state in ^{64}As as belonging to the $T = 2$ IAS at **1956.4 keV** as radiation not detected, then the intensity to the IAS would be $I_\beta = 70\%$. In this exercise, the strength to the IAS in ^{64}As would correspond to 2.8 if we use the $Q_\beta^{\text{AME2016}} = 12830\#(500)$ keV value, and $B(F) = 3.9$ if we use the $Q_\beta^{\text{IMME}} = 12168(100)$ keV value, and the half-life obtained using the full decay chain $T_{1/2} = 22.5(5)$ ms. A similar exercise can be done, calculating the half-life value necessary to obtain the correct Fermi strength to the IAS. Considering the $I_\beta^{\text{IAS}} = 60(3)\%$, using the Q_βAME2016 = 12830#(500) keV the half-life should be $T_{1/2} = 13.4$ ms. However, if we consider the Q_βIMME = 12168(100) keV the half-life should be $T_{1/2} = 18.9$ ms. Any of these hypotheses or a combination of them may explain the observed deficit in the beta decay strength. However, with the present set of data, it is impossible to decide which one of the reasons given above is responsible for the deficit in the Fermi strength.

Part VI

Appendices

Appendix A

Symmetry conservation in gamma transitions

A gamma transition connect states in the same nucleus emitting a photon. The initial and final states have a definite angular momentum and parity and the photon must conserve both. Photons carry integer units of angular momentum ($\ell\hbar$) and a definite parity and the hole system must conserve both, angular momentum and parity. If the initial state has a intrinsic spin of $I_i\hbar$ and the final state has intrinsic spin $I_f\hbar$, the photon connecting them must carry a $\ell = \Delta I = (I_i - I_f)\hbar$ angular momentum. The photon carry at least one unit ($\hbar$) of angular momentum so the $\Delta I = 0$ is forbidden. The angular momentum coupling for this system can be written as in Eq. (A.1).

$$|\hbar(I_i - I_f)| \leq \ell \leq \hbar(I_i + I_f) \tag{A.1}$$

The transition may change the charge distribution of the nucleus (orbital change) generating an electric field, or a change in the current distribution of the nucleus (orbital direction change) generating a magnetic field, and these phenomenona give the parity of the photon emitted. In electric transitions $E\ell$ the electric dipole

($E1$) radiation has odd parity, while in the magnetic transitions the magnetic dipole ($M2$) radiation has even parity. Without entering in the electromagnetic theory, the parity of ℓ-order electric and magnetic transitions can be summarised as,

$$\Pi(E\ell) = (-1)^{\ell} , \qquad \ell = 1, 2, \ldots \tag{A.2}$$

$$\Pi(M\ell) = (-1)^{\ell+1} . \qquad \ell = 1, 2, \ldots \tag{A.3}$$

To fulfil these parity requirements in γ-ray transitions we must consider the parity of the final state, if it is the same that the initial state ($\Delta\pi$ = no) or different ($\Delta\pi$ = yes). In Tab. A.1 angular momentum, parity and character, electric or magnetic, are shown for γ-ray transitions with $\ell \leq 4$.

Type	Name	$\ell = \Delta I$	$\Delta\pi$
E1	Electric dipole	1	yes
M1	Magnetic dipole	1	no
E2	Electric quadrupole	2	no
M2	Magnetic quadrupole	2	yes
E3	Electric octupole	3	yes
M3	Magnetic octupole	3	no
E4	Electric hexadecapole	4	no
M4	Magnetic hexadecapole	4	yes

Table A.1: Gamma-ray multipolarity as a function of the angular momentum ℓ and parity carried by the photon.

Appendix B

Calibration of WAS3ABi using ^{207}Bi EC source

The energy calibration of the WAS3ABi active stopper was done using a ^{207}Bi calibration source as explained in Section 3.1.1. As this source is a conversion electron emitter, these electrons are mono-energetic and allowed us to calibrate in energy each strip of the WAS3ABi active stopper. The energies of the electrons emitted in ^{207}Bi EC decay are known in literature [KL11] and can be seen in Table B.1.

The calibration was performed placing the ^{207}Bi source in front of each DSSSD as shown in Fig. 3.5. In this way the spectra of ^{207}Bi were obtained for each strip of the DSSSDs. In Fig. B.1 the calibrated spectrum adding all strips in the corresponding DSSSD of the WAS3ABi active stopper are shown.

Type	Energy keV	Intensity %	Type	Energy keV	Intensity %
Auger L	7.97	54.4(14)	CE L	881.91(12)	$4.07(17) \times 10^4$
Auger K	56.7	2.9(3)	CE M	893.92(12)	$9.5(4) \times 10^5$
CE K	240.10(12)	$1.88(17) \times 10^4$	CE K	975.651(3)	7.08(17)
CE L	312.24(12)	$3.2(3) \times 10^5$	CE L	1047.795(3)	1.84(5)
CE M	324.25(12)	$7.5(7) \times 10^6$	CE M	1059.805(3)	0.44(3)
β^+	382.99(93)	0.0380(22)	CE K	1354.20(20)	$3.55(8) \times 10^4$
CE K	481.6935(21)	1.537(22)	CE L	1426.34(20)	$6.13(13) \times 10^5$
CE L	553.8372(21)	0.442(6)	CE M	1438.35(20)	$1.44(3) \times 10^5$
CE M	565.8473(21)	0.111(5)	CE K	1682.224(9)	0.0238(12)
CE K	809.77(12)	0.00246(10)	CE L	1754.367(9)	0.0034(5)

Table B.1: Literature values for ^{207}Bi [KL11] decay radiation obtained from the NNDC Brookhaven web page.

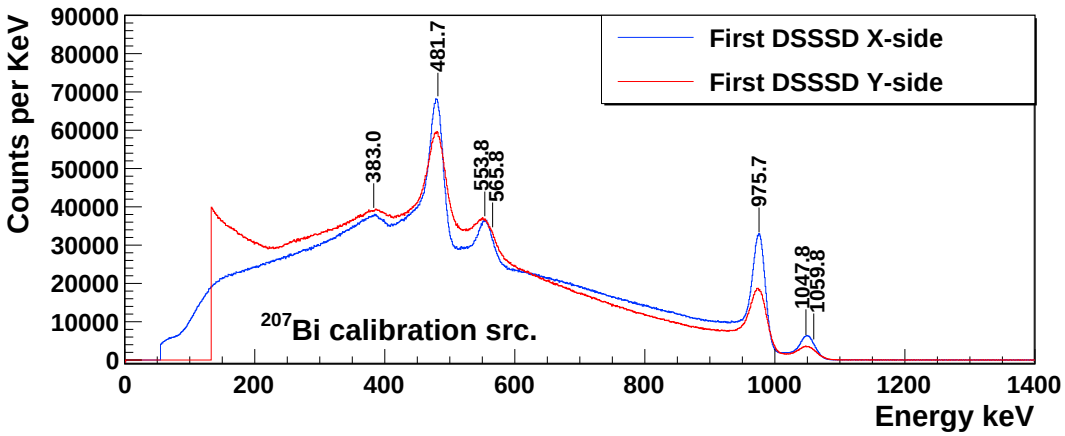

(a) ^{209}Bi calibration spectrum at first DSSSD.

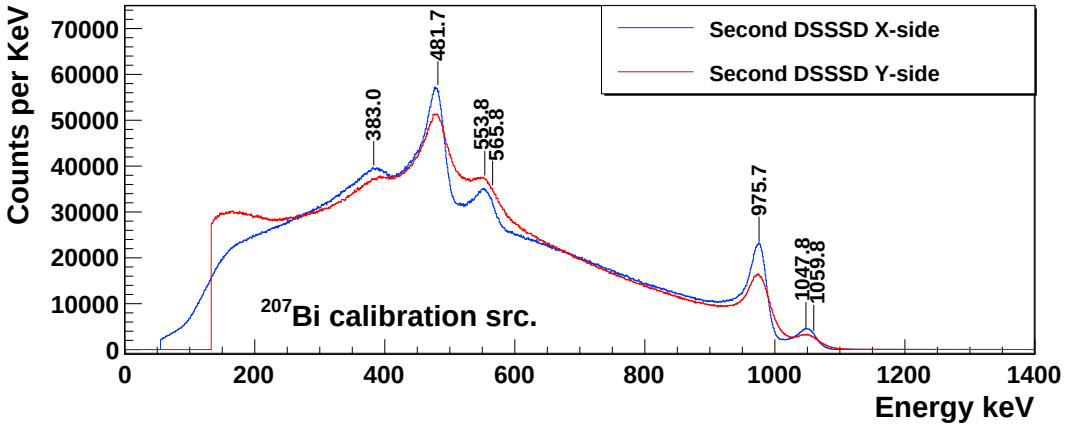

(b) ^{209}Bi calibration spectrum at second DSSSD.

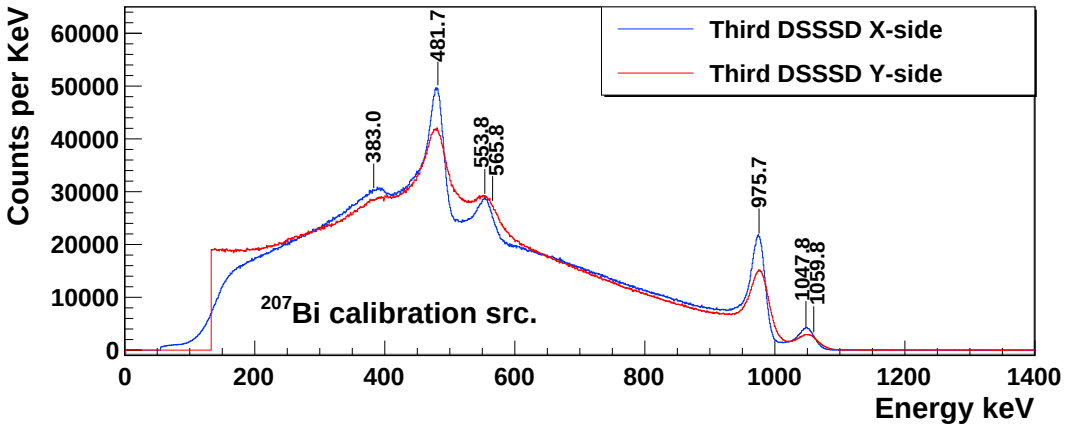

(c) ^{209}Bi calibration spectrum at third DSSSD.

Figure B.1: Spectrum of ^{209}Bi calibration source, constructed adding all strips of the corresponding DSSSD. Literature values [KL11] are shown for the most intense peaks.

Appendix C

Calibration of EURICA

EURICA HPGe array and its calibration procedure were described in Chapter 3.2. Each HPGe detector in this array was calibrated using two calibration sources ^{152}Eu [Mar13] and ^{133}Ba [KRK11]. These sources allow one to obtain an energy calibration within 121.8 keV to 1528.2 keV. In this section the calibration of the EURICA HPGe array using these sources will be shown.

The sources were placed above the top cover of the WAS3ABi active stopper. This allowed us to measure the γ-ray spectrum for each crystal and identify the peaks with the highest intensities. In Fig. C.1 the calibrated spectrum for ^{152}Eu obtained by adding the spectrum from all crystals is shown. Then, the area of each peak was obtained by fitting using a Gauss function and a polynomial background. Measured values for energy, FWHM and number of counts for each peak are summarised in Tables C.1 and C.2. In order to obtain the calibration below 121.8 keV, a ^{133}Ba source was used. As in ^{152}Eu case, the peaks with higher intensities were fitted using Gauss functions. In Fig. C.2 the calibrated spectrum for ^{133}Ba using all crystals is shown. Measured values of energy, FWHM and number of counts for each peak are summarised in Table C.3.

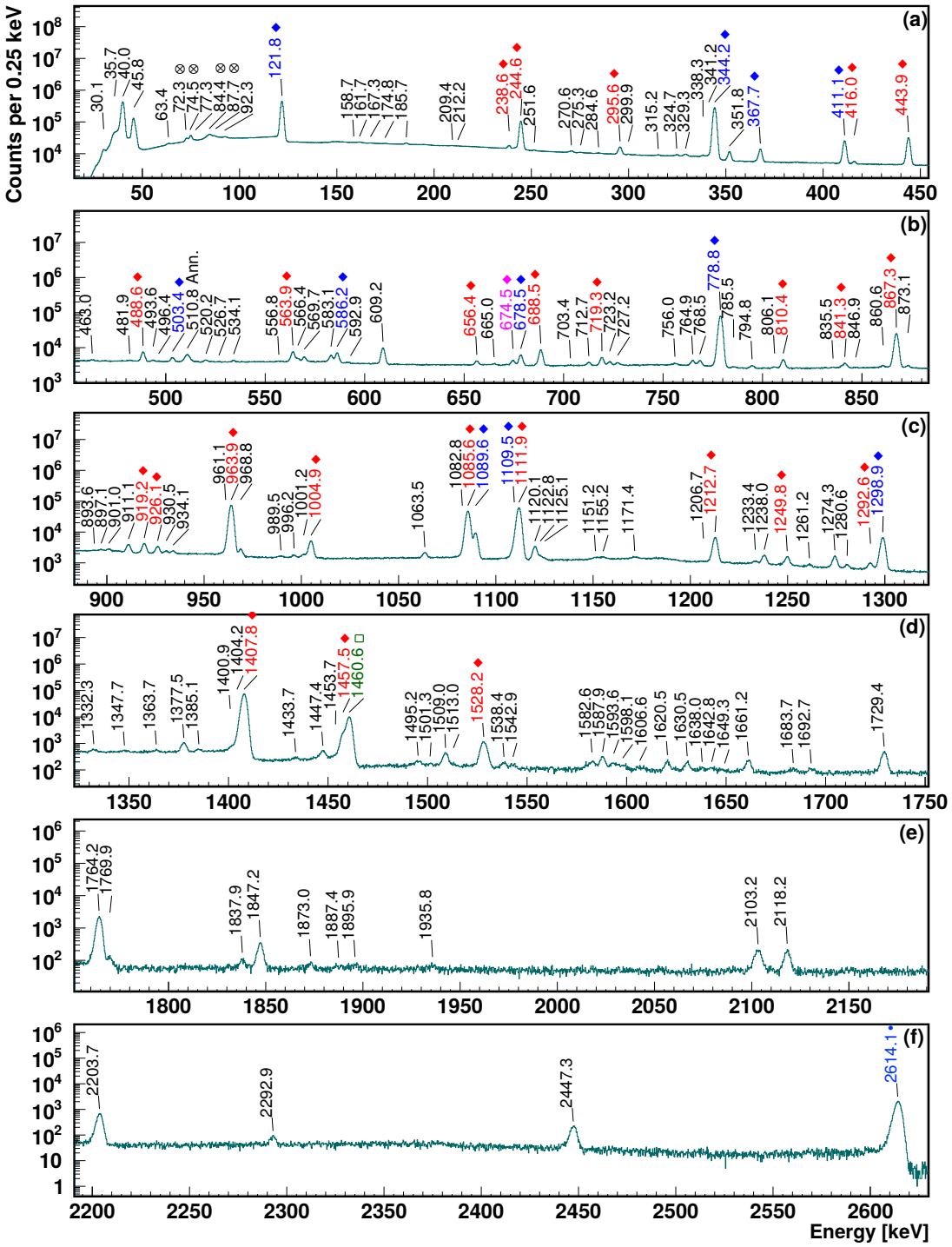

Figure C.1: EURICA γ-ray energy for the ^{152}Eu calibration. The most intense γ-rays from the ^{152}Eu decay are marked with blue and red labels. The ^{152}Eu β^- decay γ-rays are marked with ♦, the ^{152}Eu EC decay is marked with ♦, the ^{40}K decay is marked with □, the ^{208}Tl decay is marked with •, and the Pb x-rays are marked with ⊗.

Center keV	FWHM keV	Counts	Comments
30.1(1)	1.79(1)	1.7(1)E4	-
35.7(1)	1.79(1)	2.6(1)E5	-
40.0(1)	1.79(1)	2.9(1)E6	-
45.8(1)	1.79(1)	8.1(1)E5	^{210}Pb β^- decay
63.4(1)	1.8(1)	1.3(1)E4	-
72.4(2)	3.29(4)	1.1(2)E4	-
74.5(1)	3.29(4)	1.2(1)E5	-
77.3(1)	3.29(4)	0(3)E1	-
84.4(1)	3.29(4)	1.6(1)E5	-
87.7(1)	3.29(4)	7.7(1)E4	-
92.3(1)	3.29(4)	5.6(1)E4	-
121.8(1)	1.75(1)	2.8(1)E6	^{152}Eu β^- decay
158.7(2)	1.84(8)	6322(600)	-
161.7(1)	1.84(8)	1.1(1)E4	-
167.3(3)	1.84(8)	640(500)	-
175(1)	1.84(8)	0(4)E2	-
185.7(1)	1.84(8)	1.3(1)E4	^{226}Ra, ^{235}U, α decay
209.4(2)	2.0(3)	3286(600)	-
212.2(7)	2.0(3)	2288(500)	-
238.6(1)	1.75(1)	2.8(1)E4	^{152}Eu EC decay
244.6(1)	1.75(1)	6.6(1)E5	^{152}Eu EC decay
251.6(1)	1.75(1)	1763(400)	-
270.6(1)	1.92(2)	1.1(1)E4	-
275.3(1)	1.92(2)	2835(400)	-
284.5(1)	1.92(2)	2714(300)	-
295.6(1)	1.92(2)	5.4(1)E4	^{152}Eu EC decay
299.9(1)	1.92(2)	1907(400)	-
315.2(1)	1.78(1)	3426(300)	-
324.7(1)	1.78(1)	6184(300)	-
329.3(1)	1.78(1)	1.0(1)E4	-
338.3(1)	1.78(1)	5669(400)	-
341.2(1)	1.78(1)	1.2(1)E4	-
344.2(1)	1.78(1)	2.1(1)E6	^{152}Eu β^- decay
351.8(1)	1.78(1)	4.3(1)E4	-
367.7(1)	1.78(1)	6.4(1)E4	^{152}Eu β^- decay
411.1(1)	1.83(1)	1.6(1)E5	^{152}Eu β^- decay
416.0(1)	1.83(1)	6719(300)	^{152}Eu EC decay
443.9(1)	1.86(1)	2.1(1)E5	^{152}Eu EC decay
463.0(1)	1.9(2)	2515(300)	-
481.9(2)	2.17(2)	2422(300)	-
488.6(1)	2.17(2)	2.9(1)E4	^{152}Eu EC decay
493.6(1)	2.17(2)	2557(300)	-
496.4(5)	2.17(2)	273(300)	-
503.4(1)	2.17(2)	1.0(1)E4	^{152}Eu β^- decay

(a) Part 1.

Center keV	FWHM keV	Counts	Comments
510.8(1)	2.17(2)	2.4(1)E4	$e^+ + e^-$
520.2(1)	2.17(2)	3823(300)	-
526.7(9)	2.17(2)	0(9)E2	-
534.1(1)	2.17(2)	2877(300)	-
556.8(4)	1.98(2)	529(200)	-
563.9(1)	1.98(2)	3.0(1)E4	^{152}Eu EC decay
566.4(1)	1.98(2)	7449(300)	-
569.7(1)	1.98(2)	1.2(1)E4	-
583.1(1)	1.98(2)	1.8(1)E4	-
586.2(1)	1.98(2)	2.7(1)E4	^{152}Eu β^- decay
592.9(1)	1.98(2)	0(2)E2	-
609.2(1)	1.99(1)	5.5(1)E4	-
656.4(1)	2.06(1)	8626(200)	^{152}Eu EC decay
665.0(1)	2.06(1)	2884(200)	-
674.5(1)	2.06(1)	1.0(1)E4	^{152}Eu EC, β^- decay
678.5(1)	2.06(1)	2.6(1)E4	^{152}Eu β^- decay
688.5(1)	2.06(1)	4.8(1)E4	^{152}Eu EC decay
703.4(5)	2.06(1)	219(200)	-
712.7(1)	2.06(1)	5573(200)	-
719.3(1)	2.06(1)	1.8(1)E4	^{152}Eu EC decay
723.2(1)	2.06(1)	7237(200)	-
727.2(1)	2.06(1)	5232(200)	-
756.0(1)	2.16(1)	3467(200)	-
764.9(1)	2.16(1)	9760(200)	-
768.5(1)	2.16(1)	9409(200)	-
778.8(1)	2.16(1)	6.9(1)E5	^{152}Eu β^- decay
785.5(1)	2.16(1)	2106(200)	-
794.8(1)	2.16(1)	4111(200)	-
806.1(1)	2.16(1)	2138(200)	-
810.4(1)	2.16(1)	1.8(1)E4	^{152}Eu EC decay
835.5(3)	2.24(1)	599(200)	-
841.3(1)	2.24(1)	8373(200)	^{152}Eu EC decay
846.9(1)	2.24(1)	0(1)E2	-
860.6(1)	2.24(1)	3428(200)	-
867.3(1)	2.24(1)	2.1(1)E5	^{152}Eu EC decay
873.1(1)	2.24(1)	4144(200)	-
893.6(9)	2.25(3)	889(200)	-
897.1(1)	2.25(3)	2613(200)	-
901.0(1)	2.25(3)	3786(200)	-
911.1(1)	2.25(3)	1.8(1)E4	-
919.2(1)	2.25(3)	2.1(1)E4	^{152}Eu EC decay
926.1(1)	2.25(3)	1.3(1)E4	^{152}Eu EC decay
930.5(1)	2.25(3)	3869(200)	-
934.1(1)	2.25(3)	4124(200)	-

(b) Part 2.

Table C.1: The result of the fits for the ^{152}Eu (see Fig. C.1) calibration source. The energy, FWHM, and number of counts were obtained by fitting a Gauss function for each peak in ^{152}Eu spectrum using all crystals. (Continue in Table C.1).

Center keV	FWHM keV	Counts	Comments
961.1(1)	2.29(1)	1.2(1)E4	-
963.9(1)	2.29(1)	7.0(1)E5	^{152}Eu EC decay
968.8(1)	2.29(1)	1.2(1)E4	-
989.5(1)	2.46(2)	2139(200)	-
996.2(1)	2.46(2)	3535(200)	-
1001.2(1)	2.46(2)	5000(200)	-
1004.9(1)	2.46(2)	3.9(1)E4	^{152}Eu EC decay
1063.5(1)	2.34(8)	6879(200)	-
1082.8(1)	2.37(1)	8638(300)	-
1085.6(1)	2.37(1)	4.6(1)E5	^{152}Eu EC decay
1089.6(1)	2.37(1)	7.7(1)E4	^{152}Eu β^- decay
1109.5(1)	2.33(1)	2.9(1)E4	^{152}Eu β^- decay
1111.9(1)	2.33(1)	5.9(1)E5	^{152}Eu EC decay
1120.1(1)	2.33(1)	2.3(1)E4	-
1122.8(1)	2.33(1)	4930(300)	-
1125.1(2)	2.33(1)	2251(300)	-
1151.2(2)	3.7(3)	3013(200)	-
1155.2(1)	3.7(3)	3462(200)	-
1171.4(1)	3.7(3)	2850(300)	-
1206.7(3)	2.55(1)	568(100)	-
1212.7(1)	2.55(1)	5.9(1)E4	^{152}Eu EC decay
1233.4(1)	2.55(1)	2434(100)	-
1238.0(1)	2.55(1)	9437(200)	-
1249.8(1)	2.55(1)	8095(200)	^{152}Eu EC decay
1261.2(1)	2.55(1)	1026(100)	-
1274.3(1)	2.55(1)	9855(100)	-
1280.6(1)	2.55(1)	1947(100)	-
1292.6(1)	2.55(1)	4188(100)	^{152}Eu EC decay
1298.9(1)	2.55(1)	6.5(1)E4	^{152}Eu β^- decay
1332.3(1)	2.69(6)	1101(100)	-
1347.7(1)	2.69(6)	545(100)	-
1363.7(1)	2.69(6)	739(100)	-
1377.5(1)	2.69(6)	6566(100)	-
1385.1(1)	2.69(6)	1336(100)	-
1400.9(1)	2.67(1)	1883(100)	-
1404.2(1)	2.67(1)	1.9(1)E4	-
1407.8(1)	2.67(1)	8.2(1)E5	^{152}Eu EC decay
1433.7(2)	2.67(1)	372(50)	-
1447.4(1)	2.67(1)	3077(100)	-
1453.7(1)	2.67(1)	1189(90)	-

(a) Part 3.

Center keV	FWHM keV	Counts	Comments
1457.5(1)	2.67(1)	2.3(1)E4	^{152}Eu EC decay
1460.6(1)	2.67(1)	1.1(1)E5	^{40}K EC decay
1495.2(1)	2.67(1)	821(60)	-
1501.3(1)	2.67(1)	239(20)	-
1509.0(1)	2.67(1)	3286(80)	-
1513.0(3)	2.67(1)	129(50)	-
1528.2(1)	2.67(1)	1.3(1)E4	^{152}Eu EC decay
1538.4(1)	2.67(1)	543(50)	-
1542.9(1)	2.67(1)	300(30)	-
1582.6(1)	3.19(7)	1471(70)	-
1587.9(1)	3.19(7)	2621(80)	-
1593.6(1)	3.19(7)	1140(60)	-
1598.1(2)	3.19(7)	739(50)	-
1606.6(2)	3.19(7)	391(40)	-
1620.5(1)	3.19(7)	1309(60)	-
1630.5(1)	3.19(7)	1215(60)	-
1638.0(2)	3.19(7)	342(40)	-
1642.8(1)	3.19(7)	431(40)	-
1649.3(1)	3.19(7)	143(50)	-
1661.2(1)	3.19(7)	1826(70)	-
1683.7(2)	3.19(7)	366(40)	-
1692.7(2)	3.19(7)	439(40)	-
1729.4(1)	2.98(5)	4938(90)	-
1764.2(1)	3.04(2)	2.7(1)E4	-
1769.9(1)	3.04(2)	908(50)	-
1837.9(1)	3.02(7)	581(40)	-
1847.2(1)	3.02(7)	3579(80)	-
1873.0(2)	3.6(6)	352(50)	-
1887.4(7)	3.6(6)	194(50)	-
1895.9(3)	3.6(6)	287(50)	-
1935.8(4)	3.8(9)	248(50)	-
2103.2(1)	3.70(8)	2610(70)	-
2118.2(1)	3.70(8)	2092(60)	-
2203.7(1)	3.38(4)	8706(100)	-
2293.0(1)	3.0(2)	563(40)	-
2447.3(1)	3.62(8)	2898(60)	-
2614.1(1)	3.74(2)	3.1(1)E4	^{208}Tl β^- decay
2694.1(5)	5(2)	66(10)	-
3196.7(4)	4.1(8)	65(10)	-

(b) Part 4.

Table C.2: Continuation of Table C.1, results of the fits for ^{152}Eu calibration source in Fig. C.1.

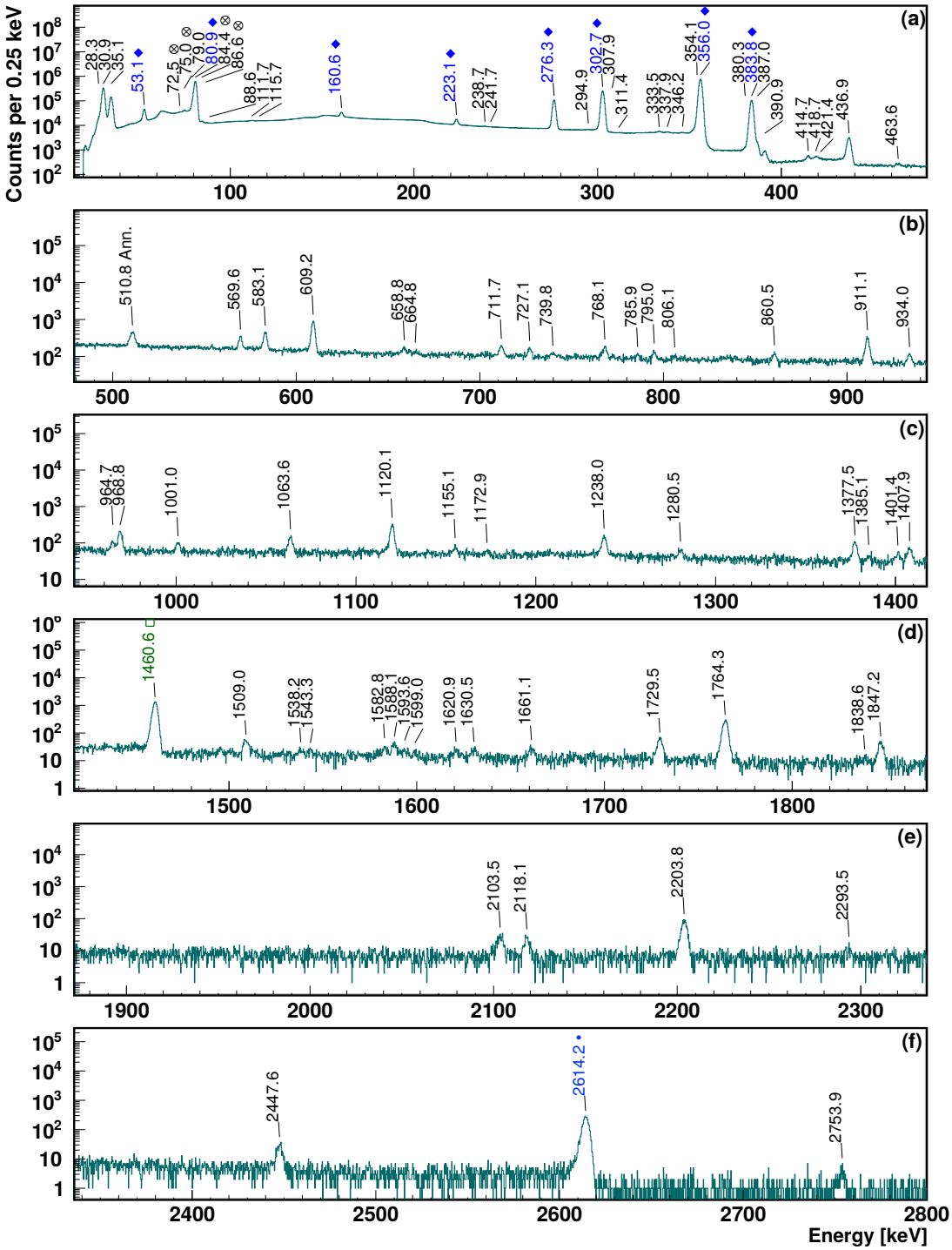

Figure C.2: EURICA γ-ray energy for the ^{133}Ba calibration. The most intense γ-rays from ^{133}Ba decay are marked with blue labels, this is, the ^{133}Ba EC decay are marked with ♦, the ^{40}K decay is marked with □, the ^{208}Tl decay is marked with •, and the Pb x-rays are marked with ⊗.

Center keV	FWHM keV	Counts	Comments
28.3(1)	1.77(1)	1.2(1)E5	-
30.9(1)	1.77(1)	2.3(1)E6	-
35.1(1)	1.77(1)	1.1(1)E6	-
53.1(1)	1.75(1)	2.2(1)E5	^{133}Ba EC decay
72.5(1)	1.75(1)	3852(800)	Pb x-ray
74.9(1)	1.75(1)	2.9(1)E4	Pb x-ray
79.0(1)	1.75(1)	1.1(1)E5	-
80.9(1)	1.75(1)	4.3(1)E6	-
84.4(1)	1.75(1)	5.6(1)E4	Pb x-ray
86.6(1)	1.75(1)	2.7(1)E4	Pb x-ray
88.6(1)	1.75(1)	1.4(1)E4	Pb x-ray
111.7(1)	2.3(2)	7422(700)	-
115.7(3)	2.3(2)	2306(500)	-
160.6(1)	1.75(1)	8.1(1)E4	^{133}Ba EC decay
223.1(1)	1.75(1)	5.1(1)E4	^{133}Ba EC decay
238.7(1)	1.75(6)	2524(300)	-
241.7(2)	1.75(6)	1174(300)	-
276.3(1)	1.75(1)	7.4(1)E5	^{133}Ba EC decay
294.9(1)	1.75(1)	0(3)E1	-
302.7(1)	1.75(1)	1.8(1)E6	^{133}Ba EC decay
307.9(1)	1.75(1)	3170(400)	-
311.4(1)	1.75(1)	2112(300)	-
333.5(1)	1.77(1)	6310(300)	-
337.9(1)	1.77(1)	3043(300)	-
346.2(1)	1.77(1)	0(3)E1	-
354.1(1)	1.77(1)	1.0(1)E5	-
356.0(1)	1.77(1)	5.7(1)E6	^{133}Ba EC decay
380.3(1)	1.85(1)	3888(100)	-
383.8(1)	1.85(1)	8.1(1)E5	^{133}Ba EC decay
387.0(1)	1.85(1)	1.2(1)E4	-
390.9(1)	1.85(1)	4933(100)	-
414.7(1)	2.35(2)	1963(90)	-
418.7(1)	2.35(2)	1726(90)	-
421.4(2)	2.35(2)	634(90)	-
436.9(1)	2.35(2)	2.7(1)E4	-
463.6(2)	2.5(4)	512(80)	-
510.8(1)	2.95(9)	3254(100)	-
569.6(1)	1.99(6)	1510(60)	-
583.1(1)	1.99(6)	2521(70)	-
609.2(1)	2.01(3)	6489(100)	-
658.8(2)	3.5(5)	646(70)	-
665(2)	3.5(5)	256(60)	-
711.7(1)	2.1(1)	837(50)	-
727.1(1)	2.1(1)	568(50)	-

(a) Part 1.

Center keV	FWHM keV	Counts	Comments
739.8(2)	2.1(1)	238(40)	-
768.1(1)	2.2(1)	850(50)	-
785.9(2)	2.2(1)	196(40)	-
795.0(1)	2.2(1)	385(40)	-
806.1(2)	2.2(1)	136(30)	-
860.4(1)	1.9(2)	363(40)	-
911.1(1)	2.32(7)	2405(70)	-
934.0(1)	2.2(2)	497(40)	-
964.7(1)	2.31(7)	440(40)	-
968.8(1)	2.31(7)	1445(50)	-
1001.0(1)	2.2(2)	429(40)	-
1063.6(1)	2.5(1)	969(50)	-
1120.1(1)	2.40(6)	2619(60)	-
1155.1(2)	2.6(5)	286(40)	-
1172.9(3)	2.6(5)	132(30)	-
1238.0(1)	2.7(1)	1181(50)	-
1280.5(2)	2.6(4)	276(40)	-
1377.5(1)	2.8(1)	860(40)	-
1385.1(2)	2.8(1)	149(30)	-
1401.4(2)	2.8(1)	254(30)	-
1407.9(1)	2.8(1)	497(30)	-
1460.6(1)	2.77(2)	1.5(1)E4	^{40}K EC decay
1509.0(1)	2.8(2)	464(30)	-
1538.2(3)	2.7(4)	114(20)	-
1543.3(2)	2.7(4)	97(20)	-
1582.8(2)	3.1(2)	188(20)	-
1588.1(1)	3.1(2)	328(30)	-
1593.6(3)	3.1(2)	132(20)	-
1599.0(4)	3.1(2)	70(20)	-
1620.9(3)	3.1(2)	135(20)	-
1630.5(3)	3.1(2)	155(20)	-
1661.1(2)	3.1(2)	200(20)	-
1729.5(1)	2.9(1)	646(30)	-
1764.3(1)	3.05(5)	3413(60)	-
1838.6(3)	3.0(2)	73(10)	-
1847.2(1)	3.0(2)	479(30)	-
2103.5(1)	3.5(2)	340(20)	-
2118.1(1)	3.5(2)	253(20)	-
2203.8(1)	3.4(1)	1115(40)	-
2293.5(5)	4(1)	71(20)	-
2447.6(1)	3.3(2)	357(20)	-
2614.2(1)	3.73(5)	4151(60)	^{208}Tl β^- decay
2753.9(3)	2(3)	19(6)	-

(b) Part 2.

Table C.3: Fit results for the ^{133}Ba calibration source in Fig. C.2. The energy, FWHM, and number of counts were obtained by fitting a Gauss function for each peak in ^{133}Ba spectrum using all crystals.

Appendix D

Settings of BigRIPs

In Chapter 2.2 the BigRIPS fragment separator was described and its role in the identification of nuclei was explained. As the experiment was designed to produce mainly four nuclei, more than one configuration was used to optimize the production rate and implantation depth for each case, as explaned in Sec. 2.3. In this section these settings used in BigRIPs will be shown.

D.1. Details of each setting

During the Kr2015-Campaign at RIKEN Nishina Center, several configurations for the mass separator BigRIPs were used, depending on the isotope of interest of each experiment. The data was divided into files labeled with a run number. Typically, a new file was created after 1 h or after changing the implantation configuration. Table D.1 summarise the configuration used in each setting. After been identificated, to select only fragments implanted at any of the three DSSSD placed after F11 focal plane, it is necessary to merge the BigRIPs file and WASSSABi file, and look only for ions fulfilling our implant condition. Table D.2 summarizes the

number of ions for each setting when the cleaning conditions are applied for the nuclei of interest in this experiment.

Configuration Subject	**Run Number Range**	**Observations**
Calibration Beam of ^{58}Ni	2002 - 2005	First runs for this setting.
	2006 - 2007	Degrader at F11 adjusted
	2008	Degrader at F11 adjusted
	2009	Degrader at F11 adjusted Threshold of Third DSSSD increased.
	2010 - 2012	Degrader at F11 adjusted Coarse gain in Qbeta plastic amplifier changed.
	2013	Degrader at F11 adjusted
	2014 - 2015	Degrader at F11 adjusted Primary beam increased in 50%
	2016 - 2017	Degrader at F11 adjusted Coarse gain in Qbeta plastic amplifier changed.
	2018 - 2022	Degrader at F11 adjusted
Setting optimized for ^{65}Br	2101	First run with for this setting.
	2102 - 2109	Degrader at F11 adjusted
	2110 - 2143	Degrader at F11 adjusted
	2144 - 3188	Degrader at F11 adjusted
Setting optimized for ^{60}Ge	3001 - 3019	Degrader at F11 adjusted
	3020 - 3042	Degrader at F11 adjusted
Setting optimized for ^{64}Se	3043	First run with for this setting.
	3044 - 3050	Slits adjusted.
	3051 - 3109	Slits adjusted.
Setting optimized for ^{66}Se	3110	First run for this setting.
	3111	Degrader at F11 adjusted
	3112	Degrader at F11 adjusted
	3113 - 3139	Degrader at F11 adjusted

Table D.1: Settings used in the Kr15 campaign. This table shows the run number of files with a common experimental configuration for BigRIPs and the upstream degrader of WASSSABi.

Table D.2: Numbers of ions in agreement with each cleaning condition applied to the data. The total number of implants corresponds to events with a valid F11 plastic signal and implanted in one of DSSSDs.

Nuc.	Runs	Before Merging		After Merging					Total
		No Cond.	Trigger F11 Cond.	No Cond.	Implant DSSSD1	Implant DSSSD2	Implant DSSSD3	Q_β and Veto	Implanted at DSSSDs.
$^{64}_{34}Se_{30}$	All	14.471	14.471	11.694	599	8.994	715	863	10.308
	2101	5.359	5.359	4.331	307	3.299	223	315	3.829
	3001	9.112	9.112	7.363	292	5.695	492	548	6.479
$^{64}_{33}As_{31}$	All	673.664	673.657	536.162	21.054	442.489	13.439	42.534	481.896
	2101	32.730	32.729	26.433	6.829	15.618	460	1.497	23.446
	3001	639.022	639.021	508.430	14.201	426.116	12.812	40.918	457.474
	3110	1.912	1.907	1.299	24	755	167	119	976
$^{63}_{32}Ge_{31}$	All	5.467.352	5.467.340	4.330.924	125.735	3.620.209	115.028	333.879	3.860.972
	2101	165.725	165.724	134.250	27.910	86.904	2.245	7.181	117.059
	3001	5.295.738	5.295.732	4.192.692	97.757	3.530.886	112.472	326.406	3.741.115
	3110	5.889	5.884	3.982	68	2.419	311	292	2.798
$^{66}_{34}Se_{32}$	All	1.675.026	1.674.974	1.196.133	44.520	961.950	35.728	51.615	1.042.198
	2101	17.338	17.338	13.896	6.857	4.507	174	625	11.538
	3001	115.375	115.375	92.197	9.053	68.081	1.500	6.211	78.634
	3110	1.542.313	1.542.261	1.090.040	28.610	889.362	34.054	44.779	952.026
$^{66}_{33}As_{33}$	All	420.339	420.317	285.058	12.718	221.486	8.629	10.811	242.833
	2101	3.055	3.053	1.696	1.128	81	23	68	1.232
	3001	10.029	10.028	5.522	1.332	1.300	44	376	2.676
	3110	407.225	407.236	277.840	10.258	220.105	8.562	10.367	238.925

Nuc.	Runs	Before Merging No Cond.	Before Merging Trigger F11 Cond.	After Merging No Cond.	After Merging Implant DSSSD1	After Merging Implant DSSSD2	After Merging Implant DSSSD3	Q_β and Veto	Total Implanted at DSSSDs.
$^{60}_{31}Ga_{29}$	All	1.437.172	1.437.163	1.092.880	15.213	443.530	434.710	100.267	893.453
	2101	899.829	899.824	683.651	9.233	265.212	294.763	62.861	569.208
	3001	535.419	535.417	408.010	5.959	178.144	139.400	37.259	323.503
	3110	1.924	1.922	1.219	21	174	547	147	742
$^{60}_{32}Ge_{30}$	All	.	.	22.381	233	3.943	12.487	2.397	16.663
	2101	.	.	14.198	153	2.355	8.355	1.549	3.343
	3001	.	.	8.183	80	1.588	4.132	848	5.800
	3110	-	-	-	-	-	-	-	-
$^{62}_{32}Ge_{30}$	All	.	.	2.776.186	48.435	1.150.903	1.209.594	235.787	2.408.932
	2101	.	.	353.416	6.355	268.186	38.177	25.892	312.718
	3001	.	.	2.420.459	42.034	881.752	1.170.833	209.683	2.094.619
	3110	.	.	2.311	46	965	584	212	1.595
$^{57}_{30}Zn_{27}$	All	1.410.846	1.410.837	977.173	10.688	6.424	366.811	260.256	383.923
	2101	1.258.001	1.257.993	873.170	9.703	5.269	334.989	245.577	349.961
	3001	152.845	152.844	104.003	985	1.155	31.822	14.679	33.962
$^{61}_{32}Ge_{29}$	All	877.821	877.817	673.194	7.953	299.541	242.342	61.462	549.836
	2101	514.426	514.423	397.299	4.487	171.473	159.070	36.116	335.030
	3001	363.395	363.394	275.895	3.466	128.068	83.272	25.346	214.806
$^{65}_{34}Se_{31}$	All	.	364.810	293.085	30.748	222.470	5.984	21.763	259.202
	2101	.	55.366	45.159	15.067	22.924	719	2.598	38.710
	3001	.	309.444	247.926	15.681	199.546	5.265	19.165	220.492
	3110	-	-	-	-	-	-	-	-

D.2. Dead-time measurement

The acquisition dead-time was monitored during the experiment to quantify the number of events loosed when the acquisition system was busy. The length of each event depends on the length of the time window established in the BigRIPs fragment separator, the WA3ABi active stopper and EURICA HPGe array, after receiving a trigger signal as discussed in Sec. 3.1.

Dead-time was monitored using scalers connected to acquisition trigger. Scalers internally compare the total number of the accepted and rejected triggers at each channel, which is related to the acquisition dead-time.

Dead-time depends on the implantation ratio which is given by the particular configuration used by BigRIPs fragment separator, discussed in Section D.1 and tabulated in Table D.1. The production rate of each individual nuclide may changes drastically depending on the configuration used in BigRIPs, for this reason, dead-time correction was measured for each nuclide and configuration used in BigRIPS, as can be seen in Figs. D.1 to D.5). Then, the total dead-time for each nuclide was obtained as an average over all implantations of that nuclear specie.

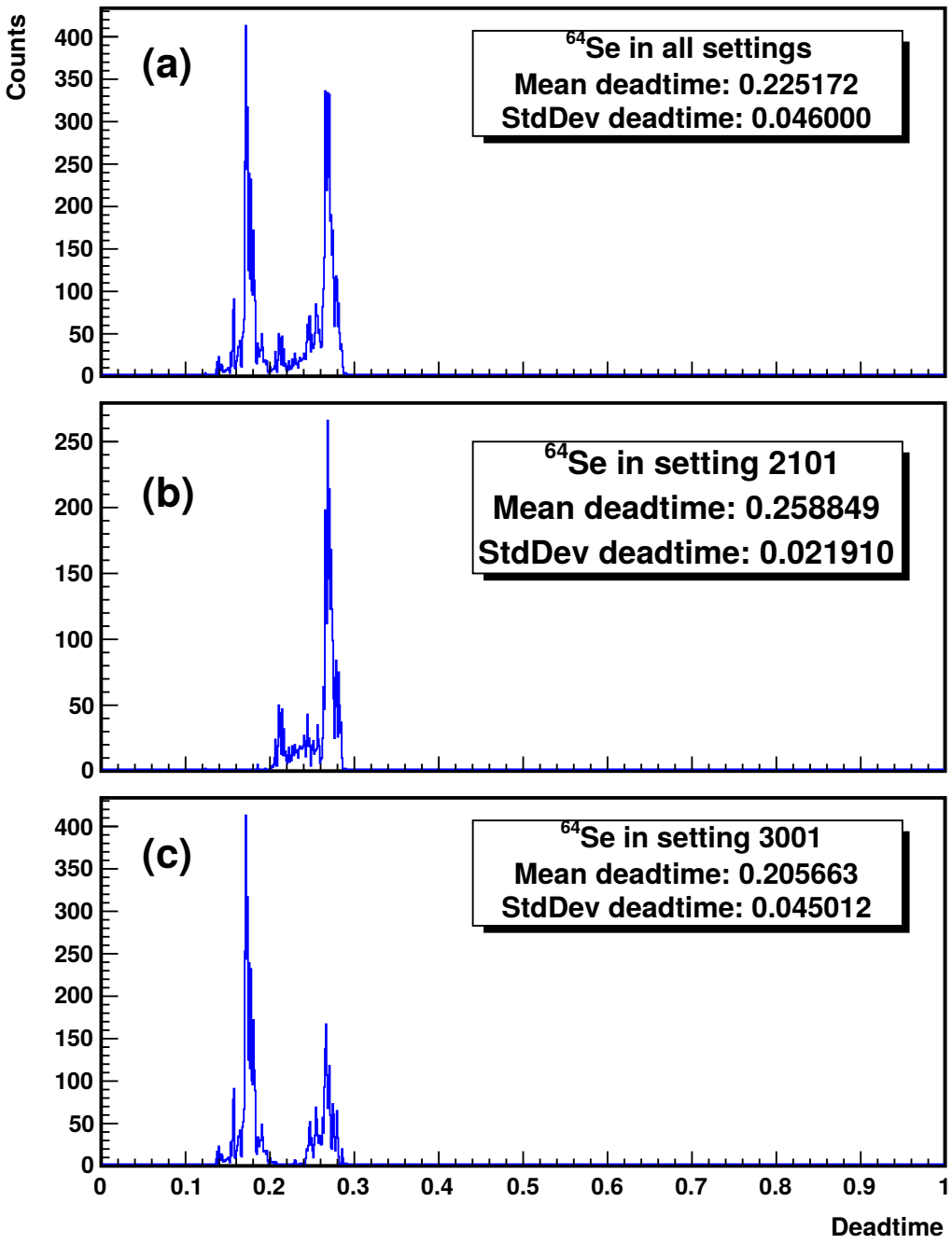

Figure D.1: Dead-time measured during ^{64}Se implants in: (a) all settings, (b) 2101 setting, and (c) 3001 setting.

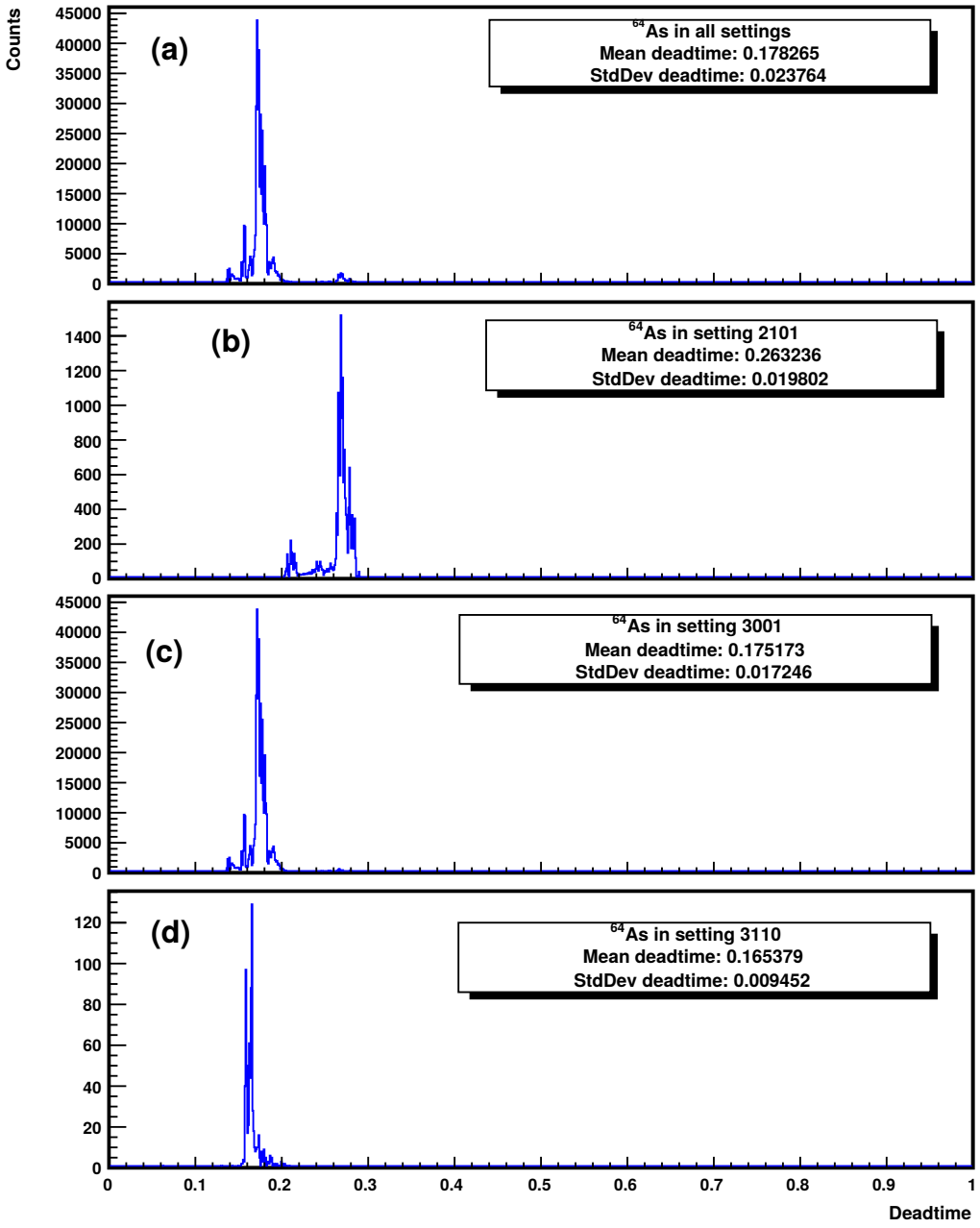

Figure D.2: Dead-time measured during ^{64}As implants in: (a) all settings, (b) 2101 setting, (c) 3001 setting, and (d) 3110 setting.

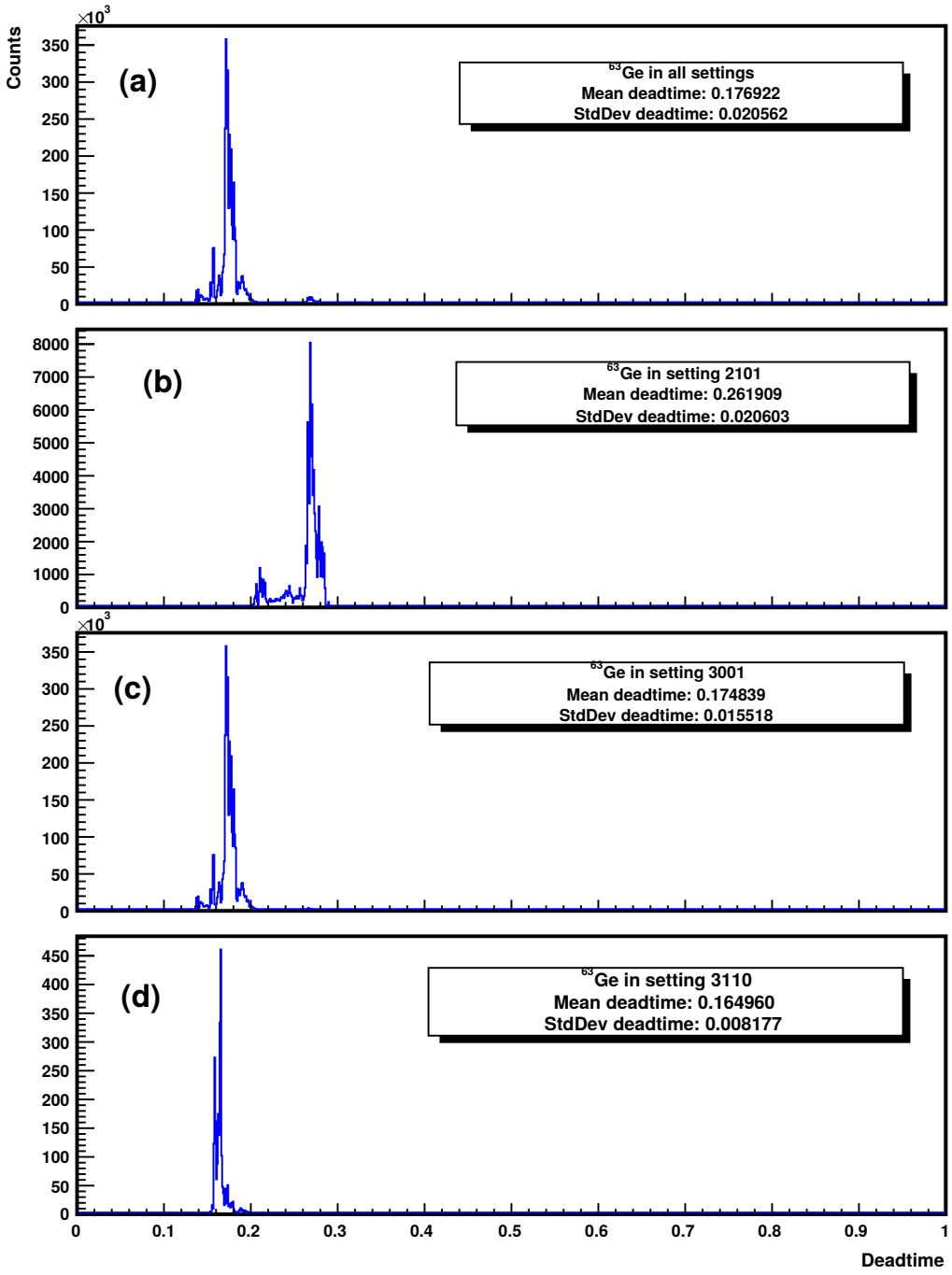

Figure D.3: Dead-time measured during ^{63}Ge implants in (a) all settings, (b) 2101 setting, (c) 3001 setting, and (d) 3110 setting.

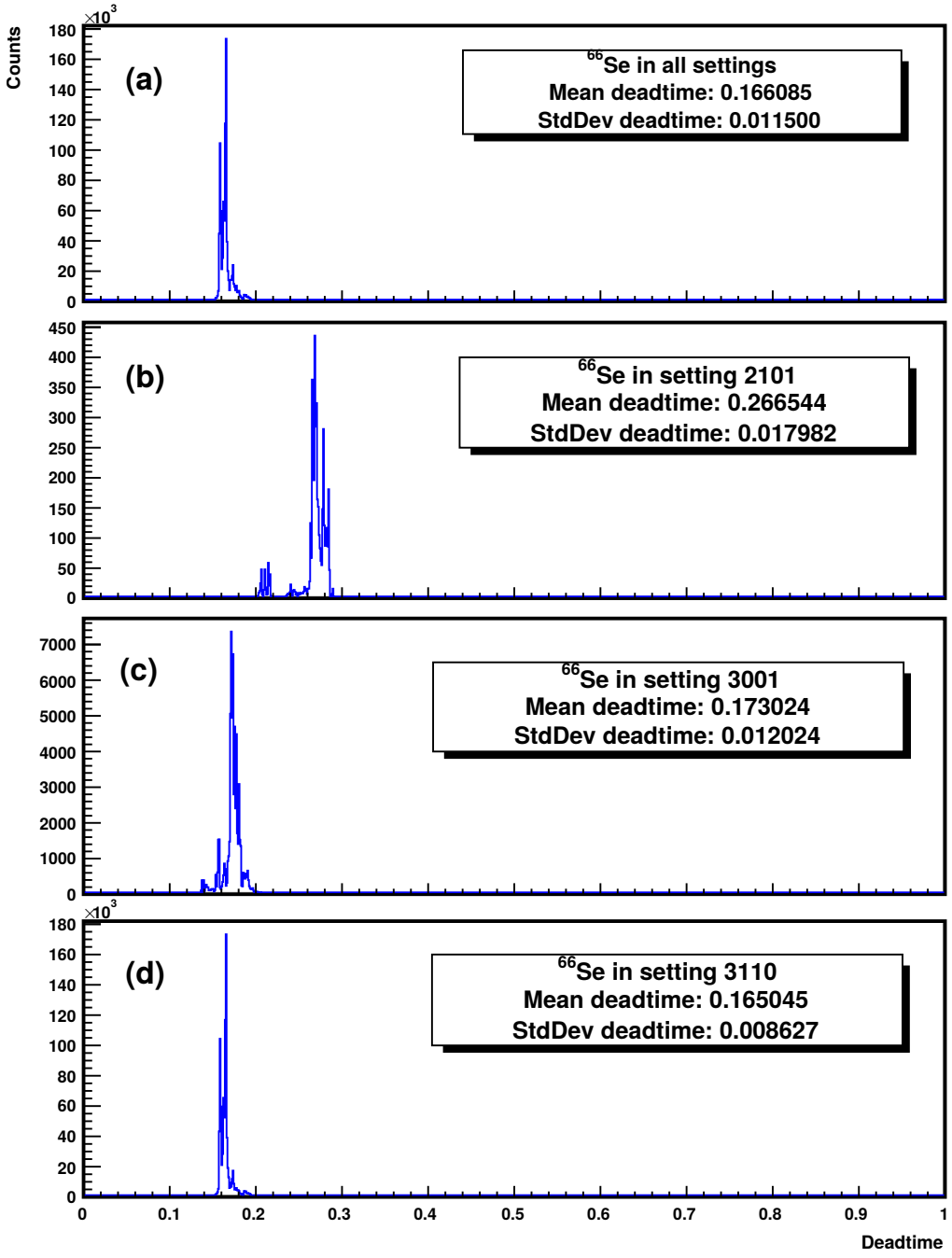

Figure D.4: Dead-time measured during ^{66}Se implants in (a) all settings, (b) 2101 setting, (c) 3001 setting, and (d) 3110 setting.

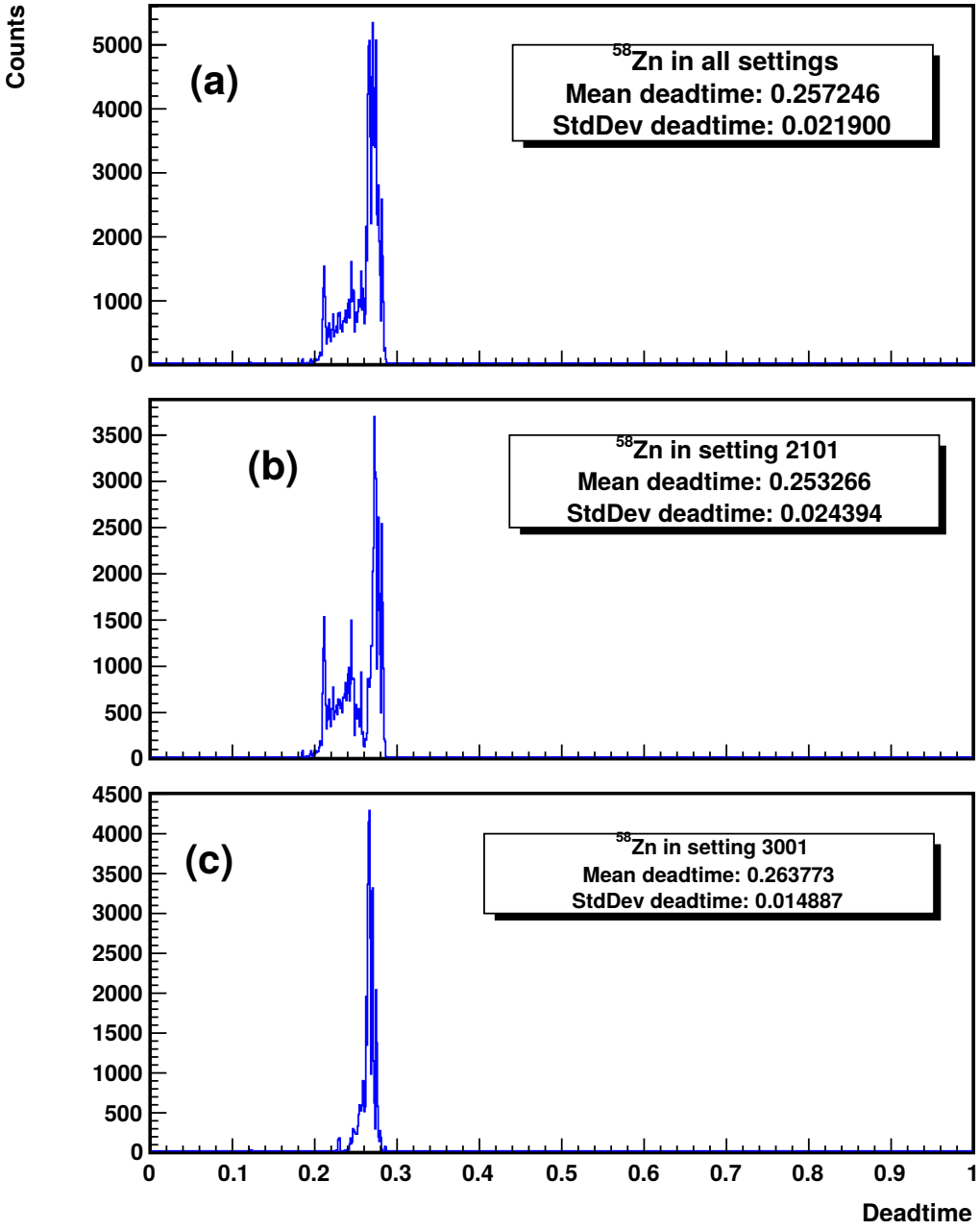

Figure D.5: Dead-time measured during ^{58}Zn implants in (a) all settings, (b) 2101 setting, and (c) 3001 setting.

Appendix E

Parametric functions to fit the proton and beta spectra

Beta spectra observed after correlation procedures in the WAS3ABi active stopper corresponds to the ΔE deposited by the beta particle in a strip. Its shape could be summarized as:

- In low energies, it has a stiffer rising, starting at some specific point.
- In higher energies, it decreases exponentially.

On the other side, as the protons are always emitted in coincidence with a beta particle, its distribution changes from a Gauss-like distribution to an asymmetrical distribution with a exponential-like decrease at higher energies. In order to be able to fit the beta and proton spectrum, parametric functions were defined. In this chapter, these functions will be described.

E.1. Parametric function for beta spectrum

The beta spectrum is composed with the energy deposited by beta particles in each strip. These deposition of energy corresponds, most of the times, to a small fraction of the total energy carried by a beta particle. The amount of energy depends of several factors, such as the Q_β value from mother nuclide, the implantation position and the geometry of each DSSSD, among others. All nuclei studied in this work decay by β^+, nevertheless, two of them (^{64}Se and ^{64}As) also are beta-delayed proton emitters, thus the parametric function must be flexible enough to allow fitting each spectra.

In order to take into account these characteristics we take an exponential tail ($e^{-x/b}$) multiplied by a inverted Gaussian, similar to the one often used in the tail of the γ-ray peaks [Kra87]:

$$\bar{f}(x;b,c) = e^{-x/b}\left(1 - e^{-(x/c)^2}\right) \ . \tag{E.1}$$

The normalization of this functions is given by the integral,

$$\int_{-\infty}^{\infty} e^{-x/b}\left(1 - e^{-(x/c)^2}\right)dx = b - \frac{c\sqrt{\pi}}{2}e^{c^2/4b^2}\mathrm{Erfc}\left(\frac{c}{2b}\right) \ . \tag{E.2}$$

This integral was obtained using Mathematica 11, where Erfc is the complementary error function defined as:

$$\mathrm{Erfc}(x) = \frac{c}{\sqrt{\pi}}\int_x^{\infty} e^{-t^2}dx \ . \tag{E.3}$$

Using the equations in (E.1) and (E.2), the β function f_β could be written as:

$$f_\beta(E;A,b,c,x_0) = \frac{A}{b - \frac{c\sqrt{\pi}}{2}e^{c^2/4b^2}\mathrm{Erfc}\left(\frac{c}{2b}\right)} \cdot e^{-(x-x_0)/b}\left(1 - e^{-((x-x_0)/c)^2}\right) \ , \tag{E.4}$$

where the x_0 was included as a translation.

An example of this functions can be found in Fig. E.1.

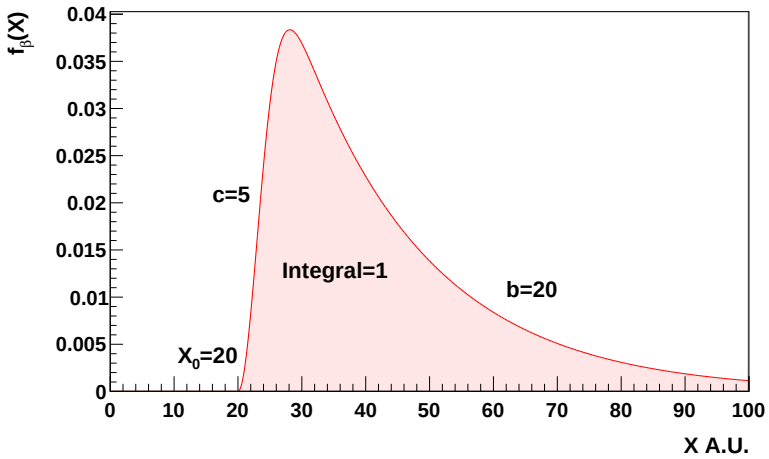

Figure E.1: Example of the parametric f_β function used during the fit of the beta spectrum.

E.2. Functions for the adjustment of proton spectra

Proton spectrum measured in the WAS3ABi active stopper are always in coincidence with the β particle and exhibits an energy distribution that may correspond to a Gauss-like distribution with an exponential-like tail to high energies. As it was explained in Sec. 5.1.3, in some cases the proton may not deposit all of its energy in one pixel, giving arise to a deformed tail to low energies. Although the low energy tail is small compared to the peak, neglecting this effect may result in the inclusion of false peaks in the analysis. In next subsections, the functions used to fit the proton spectrum will be described.

E.2.1. Function for the incomplete charge collection in protons

Function described in Appendix E.1 is very flexible and can be modified depending on the particular requirements. In some cases the proton deposits energy in two pixels and it is necessary to have a similar function, but above zero between two points corresponding to the minimum energy x_0 and the maximum energy z_0 deposited by a beta particle.

This behaviour could be achieved if the exponential tail at higher energies $e^{-x/b}$ is slightly modified to $e^{-x/b} - e^{-z_0/b}$,

$$\bar{g}_\beta(x; b, c, z_0) = \left(e^{-x/b} - e^{-z_0/b}\right)\left(1 - e^{-(x/c)^2}\right) \tag{E.5}$$

As in previous case, using Mathematica 11 the normalization N_g could be obtained by integrating,

$$N_g = \int_0^{z_0} \bar{g}_\beta(E)\, dE = \frac{e^{-z_0/b}}{2}\left(2be^{z_0/b} - 2(b + z_0) + c\sqrt{\pi}\left(\mathrm{Erf}\left(\frac{z_0}{c}\right)\right.\right. \\ \left.\left. + e^{(c^2+4bz_0)/4b^2}\left(\mathrm{Erf}\left(\frac{c}{2b}\right) - \mathrm{Erf}\left(\frac{c}{2b} + \frac{z_0}{c}\right)\right)\right) . \tag{E.6}$$

Then, the normalized function could be written as:

$$g_\beta(x; A, b, c, x_0, z_0) = \frac{A}{N_g(c, b, z_0 - x_0)}\left(e^{-(x-x_0)/b} - e^{-(z_0-x_0)/b}\right)\left(1 - e^{-((x-x_0)/c)^2}\right) \tag{E.7}$$

A plot this function can be seen in Fig. E.2, where its parameters has been choosed to: $A = 1$, $b = 20$, $c = 5$, $x_0 = 20$, and $z_0 = 80$.

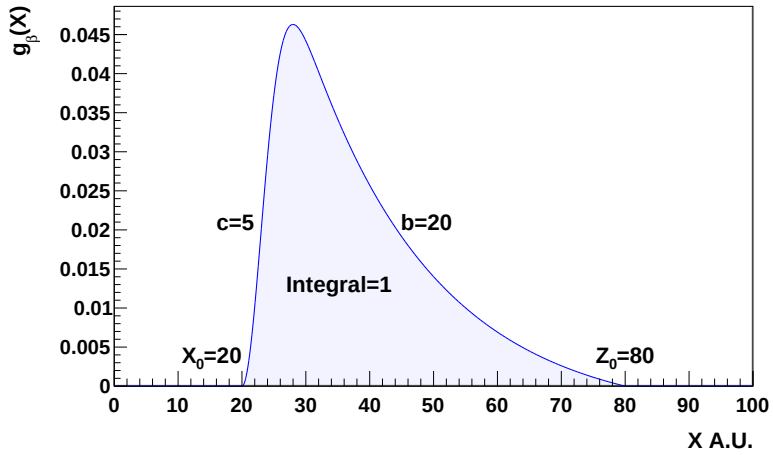

Figure E.2: Example of the parametric g_β function used during the fit of the beta spectrum.

E.2.2. Proton peak function

The function used in the fitting of proton spectra was constructed using a combination of three types of functions, Gauss function, beta function, and the function for the incomplete charge for protons. Taking into account the decays of ^{61}Ge and ^{57}Zn, measured during the experiment and analysed in Appendix F.1 and F.2, four components were used in the proton function f_p: G(E), Sng(E), Snl(E) and Snr(E),

$$f_p(E) = \mathrm{G}(E) + \mathrm{Sng}(E) + \mathrm{Snl}(E) + \mathrm{Snr}(E) \tag{E.8}$$

where G corresponds to a Gauss function, Sng and Snr corresponds to a beta function in Section E.1 and Snl corresponds to the function of incomplete charge of protons described in Appendix . E.2.1. In Fig. E.3, a plot of this function is shown.

Since there are three parameters in the Gauss function, four in the beta function (each) and five in the incomplete charge collection function, the number of free parameters in the fitting process should be reduced. Indeed, in order to

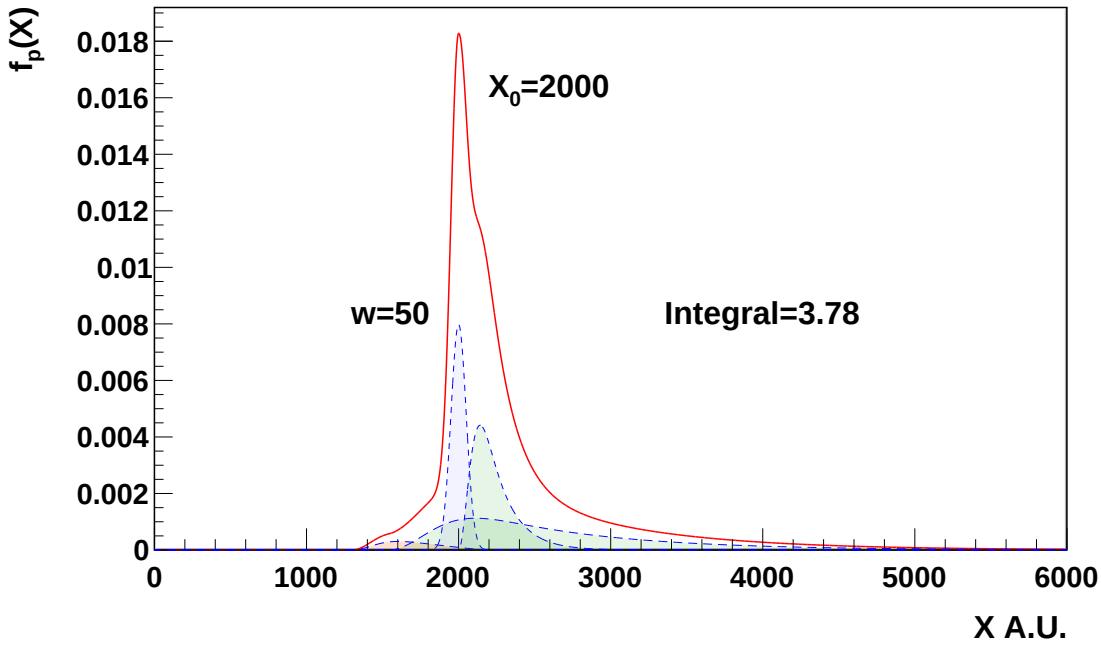

Figure E.3: Example of the parametric proton function used during the fit of the beta spectrum.

reduce the number of degrees of freedom, boundaries were setted for the parameters taking into account the decay of ^{57}Zn and ^{61}Ge discussed in Appendices F.1 and F.2). Parameters for the Sng, Snl, and Snr function were expressed in terms of the Gaussian function parameters: area A, FWHM w and centroid C,

1. The height of the Sng function was $1.193A$ in the second DSSSD, and $1.95A$ in the third DSSSD.

2. The height of the Snl function was $0.143A$ in the second DSSSd, and $0.220A$ in the third DSSSD.

3. The height of the Snr function was $1.446A$ in the second DSSSd, and $1.659A$ in the third DSSSD.

4. The difference between the center of the Gauss function, and the X_0 parameter

of the Snl function corresponds to the 730 keV in the second DSSSD, and to 709.9 keV in the third DSSSD.

5. The difference between the center of the Gauss function and the Z_0 parameter of the Snl was 162 keV in the second DSSSD, and 182 keV in the third DSSSD.

6. The difference between the center of the Gauss function and the X_0 parameter of the Snr function corresponds to 458 keV in the second DSSSD, and 428 keV in the third DSSSD.

Also the raising parameter c and the tail parameter b for the Sng, Snl, and Snr, were assigned independently from the width of the Gauss function. Taking into account these constrains, boundaries were setted to a range equivalent to two times the error width obtained in both DSSSDs.

Appendix F

Reconstruction algorithm for WAS3ABi events

As was explained in Sec. 3.1, the DSSSD event reconstruction procedure was optimized to obtain the highest beta efficiency possible and the best resolution in cases with proton emission. The reconstruction procedure was analysed using the decay of proton emitters such as ^{61}Ge and ^{57}Zn.

F.1. Analysis of ^{61}Ge decay

^{61}Ge [B^{+}07, H^{+}87] was produced during the experiment and implanted in second and third DSSSD of the WAS3ABi active stopper. This decay is very useful to study the proton energy shape as the mayor part goes through the 3.1MeV proton.

F.1.1. Adding comparison using the ^{61}Ge β-delayed proton decay

The ^{61}Ge proton spectrum was obtained using implant-decay correlation within 1 ms to 300 ms as can be seen in Fig. F.1. Random correlation background was subtracted using negative times -300 ms to -1 ms. In Fig. F.1 the reconstruction was performed using the D000 (same pixel for implant and maximum energy in decay), varying the thresholds for the A10 adding reconstruction from: no-adding (D000 only, green), 133 keV (A10E133, black), 500 keV (A10E500, blue), 700 keV (A10E700, red) and 1000 keV (A10E1000, pink). The D000 only proton spectrum have the best proton peak resolution, but also many events at lower energies corresponding to incomplete charge collection. Varying the adding threshold from 1000 MeV to 133 MeV, the incomplete charge collection decreases but decreasing the proton peak resolution. The best reconstruction is achieved using the A10E700 condition.

The ^{61}Ge was also used to study the dependency on the correlation distance in proton spectra. In Fig. F.2 three cases of distance correlation were selected where the maximum energy pixel in decay event and the implant pixel:

- are the same (D000).
- are at equal or less than one strip of distance in X and Y sides in the same DSSSD (D110).
- do not have a maximum distance but the implant pixel is next to one pixel fired in the decay event (NMD).

It can be seen that distance correlation condition do not alter the proton peak

resolution, but the NMD increase the beta efficiency almost in a factor of two.

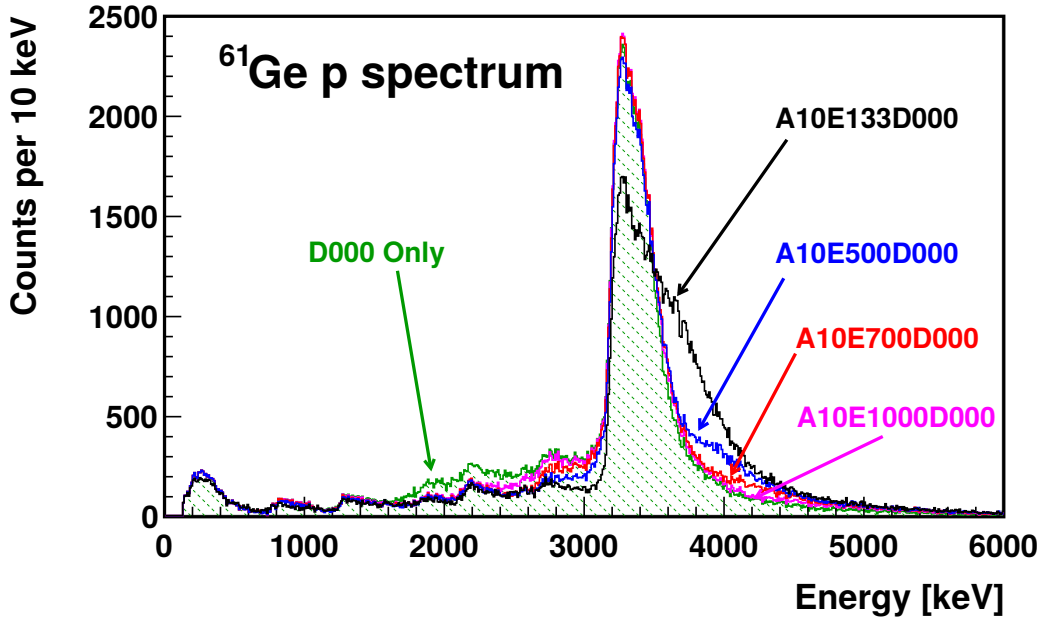

Figure F.1: ^{61}Ge decay proton spectrum, obtained with the implant-decay correlation within 1 ms to 300 ms, subtracting random correlations with negative times from −300 ms to −1 ms. Reconstruction adding comparison for the implant-decay distance conditions.

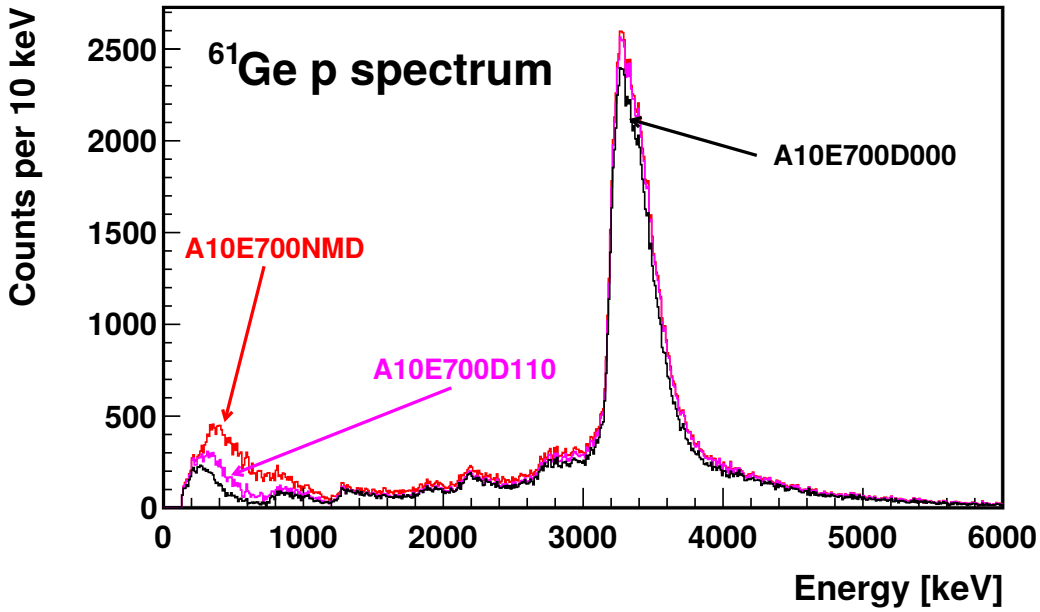

Figure F.2: ^{61}Ge decay proton spectrum constructed in the same way as that shown inFig. F.1. Reconstruction comparison for the implant-decay distance conditions, between D000, D110, and NMD condition.

F.2. Analysis of ^{57}Zn decay

^{57}Zn is a proton emitter [J+02, B+07] with energies between 1.1 MeV and 4.6 MeV. These proton peaks were used to study the WAS3ABi reconstruction algorithm and the fit of the proton peaks. This nuclide was implanted mainly in third DSSSD of WAS3ABi during the N1112-RIBF82 experiment.

F.2.1. Proton spectrum for the ^{57}Zn decay

The ^{57}Zn beta-delayed proton emission was studied using implant-decay correlations within 1 ms to 320 ms. Random correlation background was subtracted using negative times within −320 ms to −1 ms. In Fig. F.3 the proton spectrum for ^{57}Zn decay is shown as discussed in Section 5.1.2 using NMD correlation distance criteria and reconstructing the energy of the event using the A10E700 condition, this

is adding one Y-strip with a threshold of 700 keV. Proton spectrum was fitted using the parametric functions described in Appendix E for proton and beta particles.

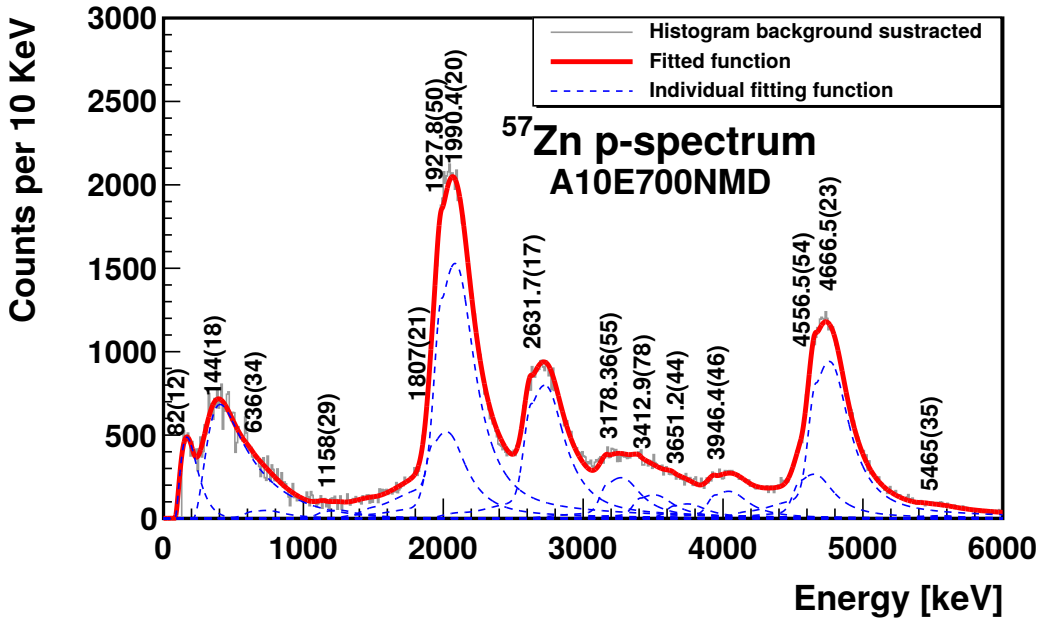

Figure F.3: Proton spectrum for ^{57}Zn decay within the correlation window $C_w = [1, 320] \ominus [-320, -1]$ms. The fitted energies are shown above each peak.

A comparison between the fitted energies for ^{57}Zn decay and the literature energies from Jokinen et al. [J+02] can be found in Table F.1. The 1158(29) keV is the only peak with a negative difference between the literature and our fitted value. Other peaks show an average energy shift of 99.44(19) keV. This shift is due to the sum of the energy deposited by a beta particle emitted in coincidence with a proton.

The ^{57}Zn is mainly implanted in the third DSSSD and the energy shift obtained is valid for this DSSSD. In order to quantify the energy shift for the second DSSSD, in Section F.3 the ^{65}Se decay will be analysed.

Fitted energy keV	Jokinen Energy keV	Energy shift keV
1158(29)	1168(15)	−10
1807(21)	1685(17)	122
1927.8(50)	1836(15)	92
1990.4(20)	1902(12)	88
2631.7(17)	2531(16)	101
3178.36(55)	3092(21)	86
3654(27)	3514(24)	140
3946.4(46)	3871(26)	105
4556.5(54)	4472(30)	85
4671.4(13)	4595(25)	76

Table F.1: Comparison between literature values [J+02] for ^{57}Zn decay and the energies fitted in the proton spectrum obtained in this experiment. The average energy deviation is 99.44(19) keV corresponding to the sum of the energy ΔE of a beta particle deposited in coincidence with a proton.

F.2.2. Distance condition comparison using the ^{57}Zn beta-delayed proton decay

Together with ^{61}Ge decay, the ^{57}Zn was used to compare the reconstruction algorithm performance, since is documented in literature [J+02, B+07] and the energies of protons cover most of DSSSD range. Decay of ^{57}Zn was used to compare the correlation distance between the maximum energy pixel in a decay event with the implantation pixel. As explained in Appendix F.1, three cases were selected where the maximum energy pixel in decay event and the implant pixel:

- are the same (D000).
- are at equal or less than one strip of distance in X and Y sides in the same DSSSD (D110).
- do not have a maximum distance but the implant pixel is next to one pixel

fired in the decay event (NMD).

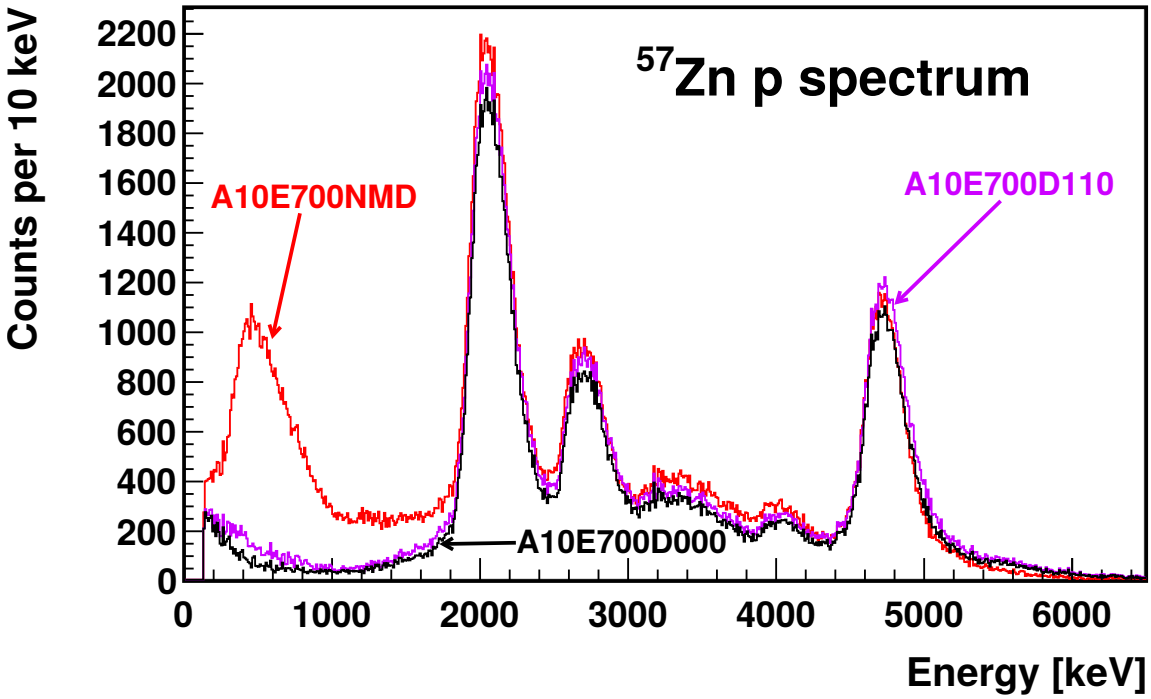

Figure F.4: Reconstruction comparison for the implant-decay distance conditions. Three cases are shown, all using the reconstruction A10E700 algorithm explained in Sec. 4.2, and varying the correlation distance in thesame pixel (D000, black), one neighbouring pixel (D110, purple), and close to one fire pixel only (NMD, red).

As in ^{61}Ge decay, the NMD distance correlation does not change the proton resolution, increasing the beta efficiency almost in a factor three.

F.3. Analysis of ^{65}Se decay

The ^{65}Se decay is an interesting case since it is a proton emitter reported in literature [RGL+11] which emits mainly two proton energies. In Fig. F.5 the level scheme from Rogers et al. is shown. The importance of this case goes beyond the proton energies, since this decay populates states in the daughter nucleus ^{64}Ge, which already was studied in this work in Section 6.2. This decay is was studied by T. Goigoux [Goi17]. We obtained the proton spectrum of this nucleus in order to measure the energy shift due to the sum with a beta particle in the second DSSSD.

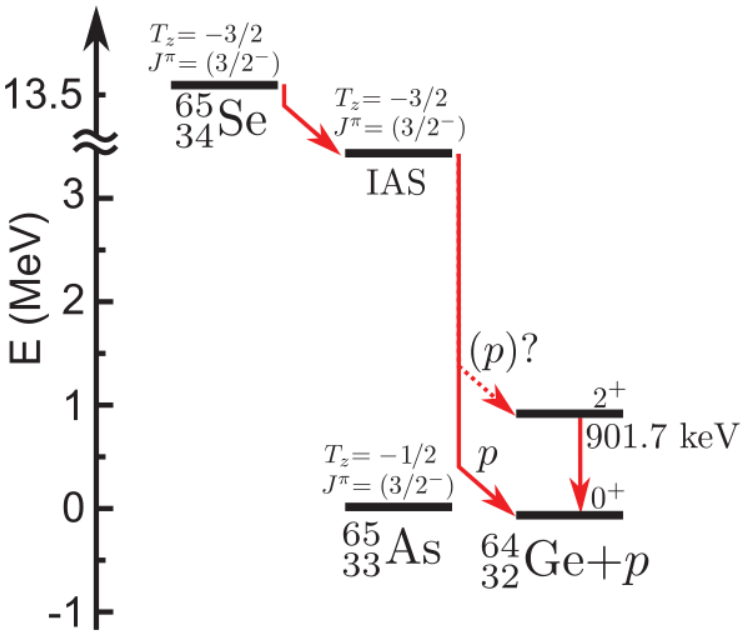

Figure F.5: Literature level scheme for ^{65}Se decay from Rogers et al. [RGL+11].

F.3.1. Proton spectrum for the ^{65}Se decay

The proton spectrum for ^{65}Se decay [RGL+11] was constructed using a implant-decay correlation time window within 1 ms and 250 ms. Random correla-

tions were subtracted using negatives correlation times within −250 ms and −1 ms.

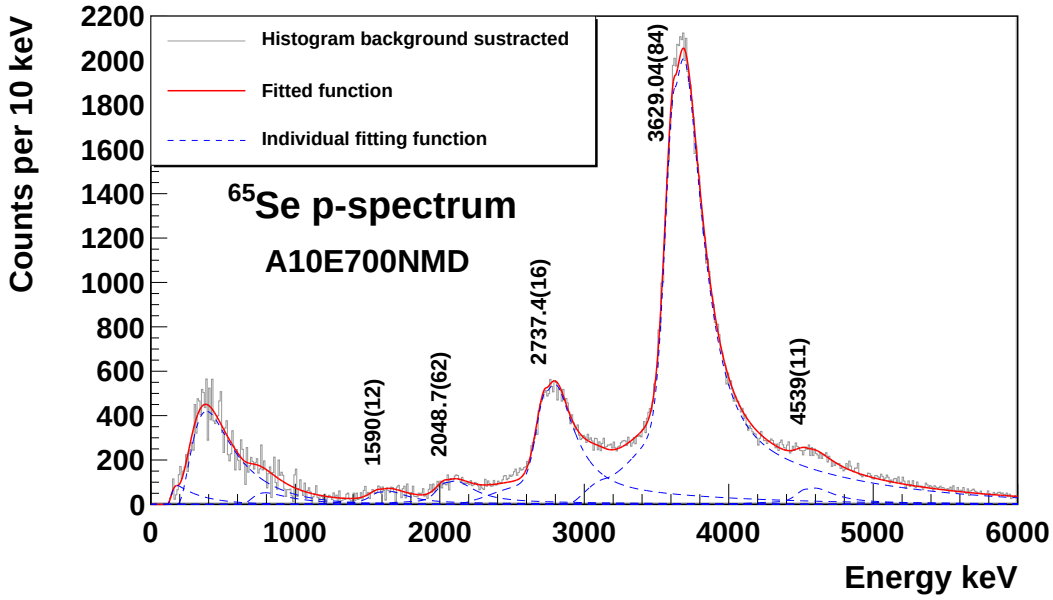

Figure F.6: Proton spectrum for ^{65}Se decay using the A10E700NMD algorithm. This proton spectrum has well defined proton peaks, also reported in the literature.

The main conclusion from this spectrum is that protons emitted with energies of 3629(29) keV and 2738(28) keV should correspond to the proton emission from the IAS in ^{65}As to the g.s. and 901.7 keV in the ^{64}Ge. Their proton energy difference is 891(40) keV which is in good agreement with the expected value of 901.7 keV from the level scheme in Fig. F.5. Rogers et al. [RGL+11] observed three proton peaks at 3.51(2) MeV (the most intense), and two weak peaks at 2.62(3) MeV and 3.77(3) MeV. In this work we observe only the 2.62(3) MeV and 3.51(2) MeV with energies of 2608(39) keV and 3499(40) keV respectively[1].

[1]Subtracting the energy shift $\Delta E = 130(27)$ keV due to the beta particle.

Appendix G

Comparison spectra using different correlation time windows sizes

Beta spectrum of an exotic nuclei is composed by the mother and daughters decays and depending on the half-lives values the spectrum may contain different ratio of each nuclei. To optimize the contribution of each nuclide, the decay of ^{64}Se and ^{57}Zn were studied using different length for the correlation window.

G.1. Number of decays compared to the window sizes

To catch all decay products it is necessary correlate up to extremely longer times. As this is not viable, the correlation window was chosen to maximize number of decays detected. In Tab. G.1 the correction factor C_w was calculated using different length of correlation windows. In this work a common criteria of $7 \cdot T_{1/2}$ was chosen to construct the spectra. In Sec. G.2 the ^{64}Se was analysed using different the correlation times, showing that in $7 \cdot T_{1/2}$ the mayor part of mother nuclei (proton emitter) are within this correlation window.

Corr. Time [ms]	$T_{1/2}$	$3T_{1/2}$	$5T_{1/2}$	$7T_{1/2}$	$9T_{1/2}$
C_w	0.5	0.875	0.969	0.992	0.998

Table G.1: Correction factor (C_w) for the correlation time as a function of the correlation time.

G.2. ^{64}Se decay proton spectrum constructed using different correlation time window length

The ^{64}Se decay is a proton emitter as discussed in Section 6.3.4), in the p spectrum protons appear above 1.4MeV (see Fig. 6.31a). To study the influence of the correlation window size, decay events with energy lower than 1.4MeV are considered beta particles and higher energy as protons. In Fig. G.1 and G.2 spectra using diferent window size are shown, starting from $[1, 24] \ominus [-24, -1]$ms, to $[1, 10000] \ominus [-10000, -1]$ms, in steps of 24ms, the size of correlation window was systematically increased.

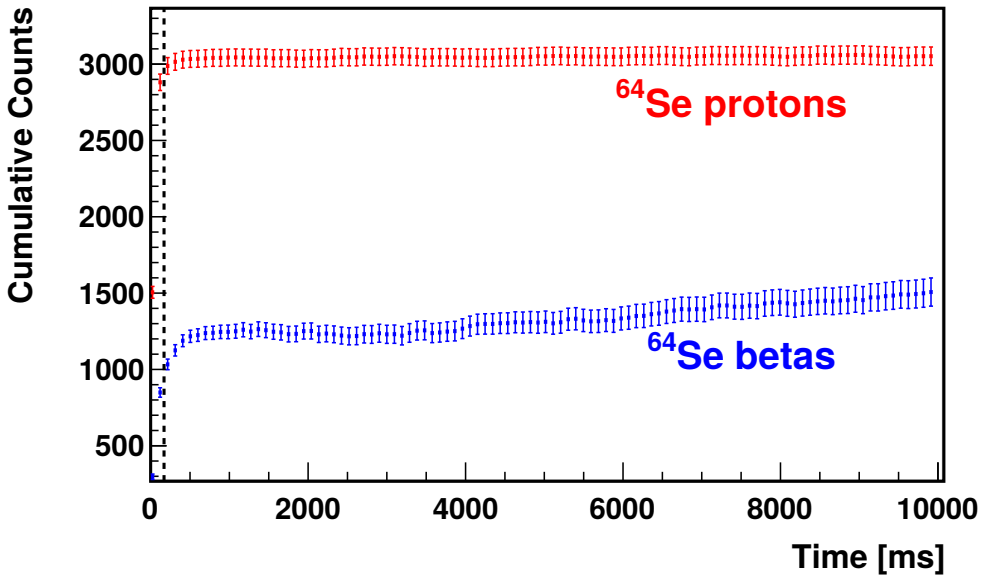

Figure G.1: ^{64}Se p spectrum using the D000 and the SIP condition. The vertical dashed line marks the seven half-lives limit used to obtain the p spectra.

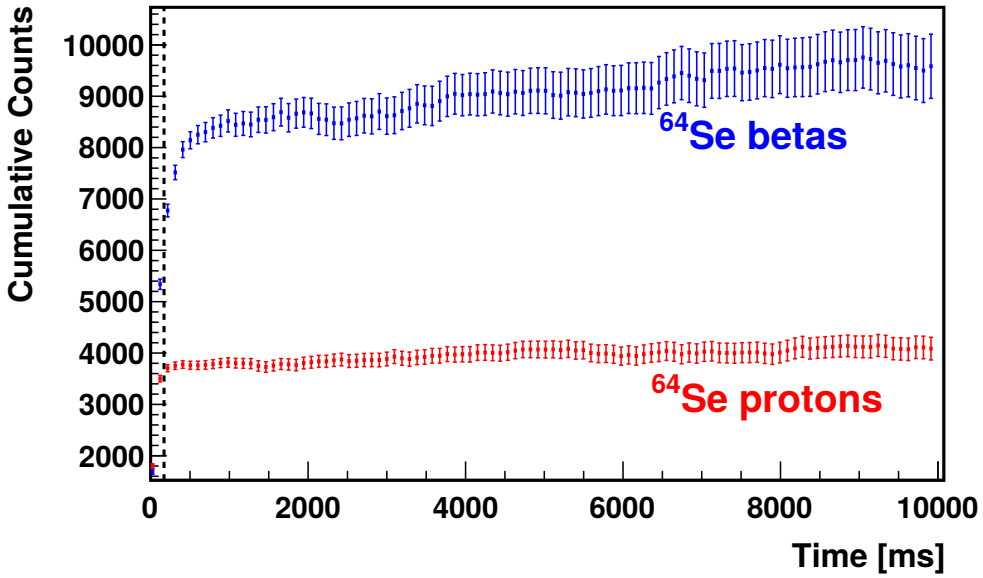

Figure G.2: ^{64}Se p spectrum using the NMD condition. The vertical dashed line marks the seven half-lives limit used to obtain the p spectra.

From Fig. G.1 and G.2 it is shown that using $7 \cdot T_{1/2}$ the main part of the protons is detected, this is the ^{64}Se decay, longer times daughter decays turns to be the major contributor to the correct correlations.

Appendix H

Bateman equations for half-lives

Radioactive decay population was first formulated by E. Rutherford in 1905 and then analytical solved by H. Bateman in 1910 [Bat10]. Relates the evolution of a nuclear specie. Many approach [TdO14, Skr74] has been applied to solve them.

The number of nuclei i decaying into the substance $i+1$ as a function of the time transforming into $i+1$ is given by:

$$\frac{dN^{(i)}}{dt}(t) = -\lambda^{(i)} N^{(i)}(t) \ , \tag{H.1}$$

where $\lambda^{(i)}$ is the decay constant. In the same way the population of daughter nucleus $N^{(i+1)}$ depends it own decay constant $\lambda^{(i+1)}$, and the amount of mother nuclei transforming into:

$$\frac{dN^{(i+1)}}{dt}(t) = -\lambda^{(i+1)} N^{(i+1)}(t) + \lambda^{(i)} N^{(i)}(t) \ , \tag{H.2}$$

Then we can write the activity $A_i(t)$ for the first three nuclei generations

$(i = 0, \ldots, 2)$ within the decay chain as

$$A_0(t) = \lambda_0 N_0 e^{-\lambda_0 \cdot t} \tag{H.3}$$

$$A_1(t) = \frac{\lambda_1 \cdot \lambda_0 \cdot N_0}{\lambda_0 - \lambda_1} \left(e^{-t\cdot\lambda_1} - e^{-t\cdot\lambda_0}\right) \tag{H.4}$$

$$A_2(t) = \frac{\lambda_0 \cdot \lambda_1 \cdot \lambda_2 \cdot N_0}{(\lambda_1 - \lambda_2)(\lambda_1 - \lambda_0)(\lambda_2 - \lambda_0)} e^{-t(+\lambda_0+\lambda_1+\lambda_2)} \left[\lambda_1 \left(e^{t\cdot(\lambda_1+\lambda_2)} - e^{t\cdot(\lambda_1+\lambda_0)}\right)\right. \tag{H.5}$$

$$\left. +\lambda_2 \left(e^{t\cdot(\lambda_2+\lambda_0)} - e^{t\cdot(\lambda_1+\lambda_2)}\right) + \lambda_0 \left(e^{t\cdot(\lambda_1+\lambda_0)} - e^{t\cdot(\lambda_2+\lambda_0)}\right)\right] \tag{H.6}$$

where the total activity is then,

$$A(t) = A_0(t) + A_1(t) + A_2(t) \tag{H.7}$$

The activity corresponds to the number of decays per second. In this experiment there are several factors that may decrease the detection such as the beta or proton efficiency and dead-time. These factors affect to all nuclei implanted in the WAS3ABi active stopper.

$$A(t) = (1 - DT)\left(\varepsilon_0 A_0(t) + \varepsilon_1 Br^{0\to1} A_1(t) + \varepsilon_2 Br^{1\to2} A_2(t)\right) \tag{H.8}$$

where the ε_i and $Br^{i\to k}$ with $i = 0, \ldots, 2$ correspond to the detection efficiency and branching for the transition from the nucleus i to the nucleus k. The branching ratio corresponds to the fraction of the total number of nuclei that decay through one decay mode. If only one decay mode is available, the branching ratio is then 100%. However cases such as the ^{64}Se or ^{64}As may decay beta or beta-delayed proton. In the following, consider the case where the mother nucleus decay to two daughter nuclei labelled $1a$ and $1b$, then these two nuclei decays to their corresponding daughter nucleus labelled $2a$ and $2b$ respectively. In this scenario the activities contribution could be summarised as:

Mother activity: The activity A_0 of the mother nucleus corresponds to:

$$(1 - DT)\,\varepsilon_0\,A_0(t) \tag{H.9}$$

Daughter activity: The daughter activity is composed by the activity of the two daughter nuclei A_{1a} and A_{1b}, with branching $Br^{0\to 1a}$ and $Br^{0\to 1b}$. The contribution of daughter activities to the total activity are given by

$$(1 - DT)\,\varepsilon_{1a}\,Br^{0\to 1a}\,A_{1a}(t)\,, \tag{H.10}$$

$$(1 - DT)\,\varepsilon_{1b}\,Br^{0\to 1b}\,A_{1b}(t)\,. \tag{H.11}$$

Granddaughter activity: The daughter activities populate granddaughter nuclei. The daughter $1a$ decays to $2a$ nucleus with $Br^{1a\to 2a} = 100\%$. On the other hand, the daughter $1b$ decays to $2b$ nucleus with $Br^{1b\to 2b} = 100\%$. In this case, the contributions of the granddaughter nuclei to the total activity are,

$$(1 - DT)\,\varepsilon_{2a}\,Br^{1a\to 2a}A_{2a}(t)\,, \tag{H.12}$$

$$(1 - DT)\,\varepsilon_{2b}\,Br^{1b\to 2b}A_{2b}(t)\,, \tag{H.13}$$

then the activity in this case can be written as,

$$\begin{aligned} A(t) = (1 - DT)\,\big(&\varepsilon_0\,A_0(t) + \varepsilon_{1a}\,Br^{0\to 1a}\,A_{1a}(t) + \varepsilon_{1b}\,Br^{0\to 1b}\,A_{1b}(t) \\ &= \varepsilon_{2a}\,Br^{1a\to 2a}A_{2a}(t) + \varepsilon_{2b}\,Br^{1b\to 2b}A_{2b}(t)\big) \end{aligned} \tag{H.14}$$

Same procedure was applied during the half-life determination for the nuclei of interest.

Appendix I

SRIM simulation for proton range in silicon

In earlier sections (see Sec. 5.1) it was explained the correlation analysis between implants and decays to obtain the decay spectra for the nuclei of interest. In this analysis, the random correlations can be reduced if temporal and spatial constrains are applied between implant and decay events.

In this work, p-delayed β decay was observed in many nuclei (for example in ^{64}Se decay and ^{64}As decay). The proton deposit the maximum of energy at the end of its path in the Bragg peak. This place is easily distinguishable in DSSSD events, in most of the cases would correspond to the pixel with the higher energy detected. However, the distance where the implant should be searched during the correlation procedure depends on the range of the proton, a longer range would increase the number of random correlation while a shorter range would decrease the number of true correlations observed.

The SRIM [ZZB10] code allow to perform range simulations for heavy ions in matter. In Tab. I.1, the results of the simulation for protons in silicon using

SRIM software are shown. In this simulation, the proton range was obtained as a function of the proton energy. From 100 keV up to 10 MeV the projected range is smaller than the half of the size of a strip of WAS3ABi, indicating that the implant should be searched in the neighbouring of the pixel where the maximum amount of energy was detected. Also the implant position relative to the center of the pixel is important, nuclei implanted near the border of the pixel could deposit the maximum energy in the neighbor strip. In order to measure the total energy of the protons, in Sec. **??** a reconstruction algorithm was described, in Sec. F.1.1 the algorithm is tested using the ^{61}Ge decay who emit one proton at 3.1 MeV.

Ion Energy	dE/dx Elec.	dE/dx Nuclear	Projected Range	Longitudinal Straggling	Lateral Straggling
100,00 keV	4,957E-01	8,673E-04	8692 Å	991 Å	1265 Å
200,00 keV	3,930E-01	5,030E-04	1,83 μm	1347 Å	1907 Å
300,00 keV	3,288E-01	3,624E-04	3,02 μm	1835 Å	2638 Å
400,00 keV	2,861E-01	2,862E-04	4,41 μm	2351 Å	3463 Å
500,00 keV	2,554E-01	2,379E-04	5,99 μm	3098 Å	4373 Å
600,00 keV	2,321E-01	2,043E-04	7,75 μm	3838 Å	5360 Å
700,00 keV	2,137E-01	1,795E-04	9,67 μm	4582 Å	6418 Å
800,00 keV	1,986E-01	1,604E-04	11,74 μm	5719 Å	7542 Å
900,00 keV	1,861E-01	1,452E-04	13,97 μm	6806 Å	8728 Å
1,00 MeV	1,755E-01	1,328E-04	16,33 μm	7871 Å	9972 Å
1,50 MeV	1,361E-01	9,392E-05	30,29 μm	1,32 μm	1,71 μm
2,00 MeV	1,124E-01	7,331E-05	47,69 μm	2,04 μm	2,56 μm
2,50 MeV	9,644E-02	6,042E-05	68,32 μm	3,07 μm	3,54 μm
3,00 MeV	8,486E-02	5,156E-05	92,05 μm	4,06 μm	4,66 μm
3,50 MeV	7,604E-02	4,507E-05	118,76 μm	5,07 μm	5,89 μm
4,00 MeV	6,906E-02	4,010E-05	148,36 μm	6,11 μm	7,24 μm
4,50 MeV	6,338E-02	3,616E-05	180,77 μm	7,86 μm	8,71 μm
5,00 MeV	5,866E-02	3,297E-05	215,93 μm	9,54 μm	10,29 μm
5,50 MeV	5,466E-02	3,031E-05	253,80 μm	11,19 μm	11,97 μm
6,00 MeV	5,124E-02	2,807E-05	294,32 μm	12,84 μm	13,76 μm
6,50 MeV	4,826E-02	2,616E-05	337,45 μm	14,50 μm	15,66 μm
7,00 MeV	4,564E-02	2,450E-05	383,14 μm	16,17 μm	17,66 μm
8,00 MeV	4,125E-02	2,177E-05	482,01 μm	21,92 μm	21,95 μm
9,00 MeV	3,771E-02	1,961E-05	590,78 μm	27,36 μm	26,64 μm
10,00 MeV	3,479E-02	1,786E-05	709,23 μm	32,70 μm	31,70 μm

Table I.1: Proton range in silicon as a function of the energy obtained with SRIM. The proton range is less than the width of the WAS3ABi strips, because of that, the protons are detected in the same pixel where the implantation took place.

Appendix J

Analysis of ^{58}Zn decay

^{58}Zn is one of the nucleus used to test the analysis procedure, it was produced during the experiment, its daughter is long lived and there is not proton emission. In this experiment this nucleus was studied by Daiki Nishimura (University of Tokyo) and the level scheme is already calculated .

J.1. Beta spectrum for ^{58}Zn decay

Beta spectrum was obtained by correlating implantation and decays within time difference in $[1, 600]$ms and random correlation background subtracted using negative correlation times $[-600, -1]$ms. For the decay events, the A10E700NMD condition was used to obtain the higher detection efficiency for γ-rays. In Fig. J.1 the β spectrum is shown, fitted using the parametric beta function in Eq. (E.4).

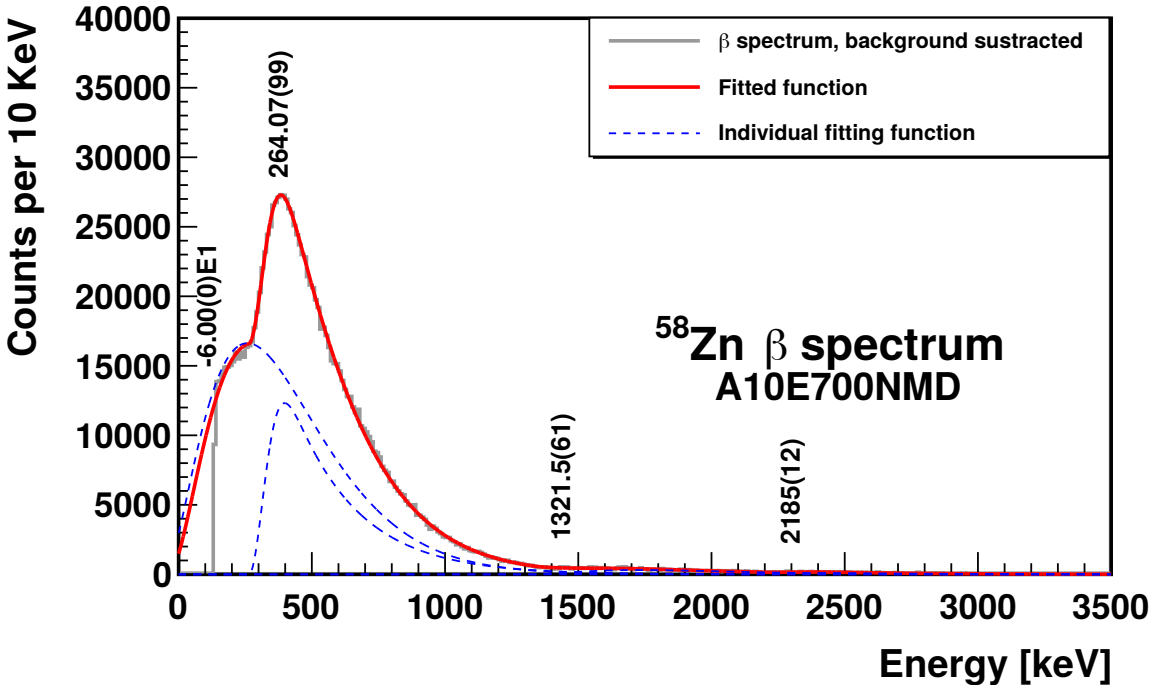

Figure J.1: Beta spectrum for ^{58}Zn decay within the correlation window $C_w = [1, 600] \ominus [-600, -1]$ms. The spectrum was fitted using the parametric beta function described in Eq. (E.4).

J.2. Prompt γ-ray spectrum for ^{58}Zn decay

The γ-ray spectrum was constructed using implantation-decay correlation within $[1, 600] \ominus [-600, -1]$ms and prompt condition imposed using β-γ coincidence within $[0, 0.8] \ominus [-80, 40][\mu s]$.

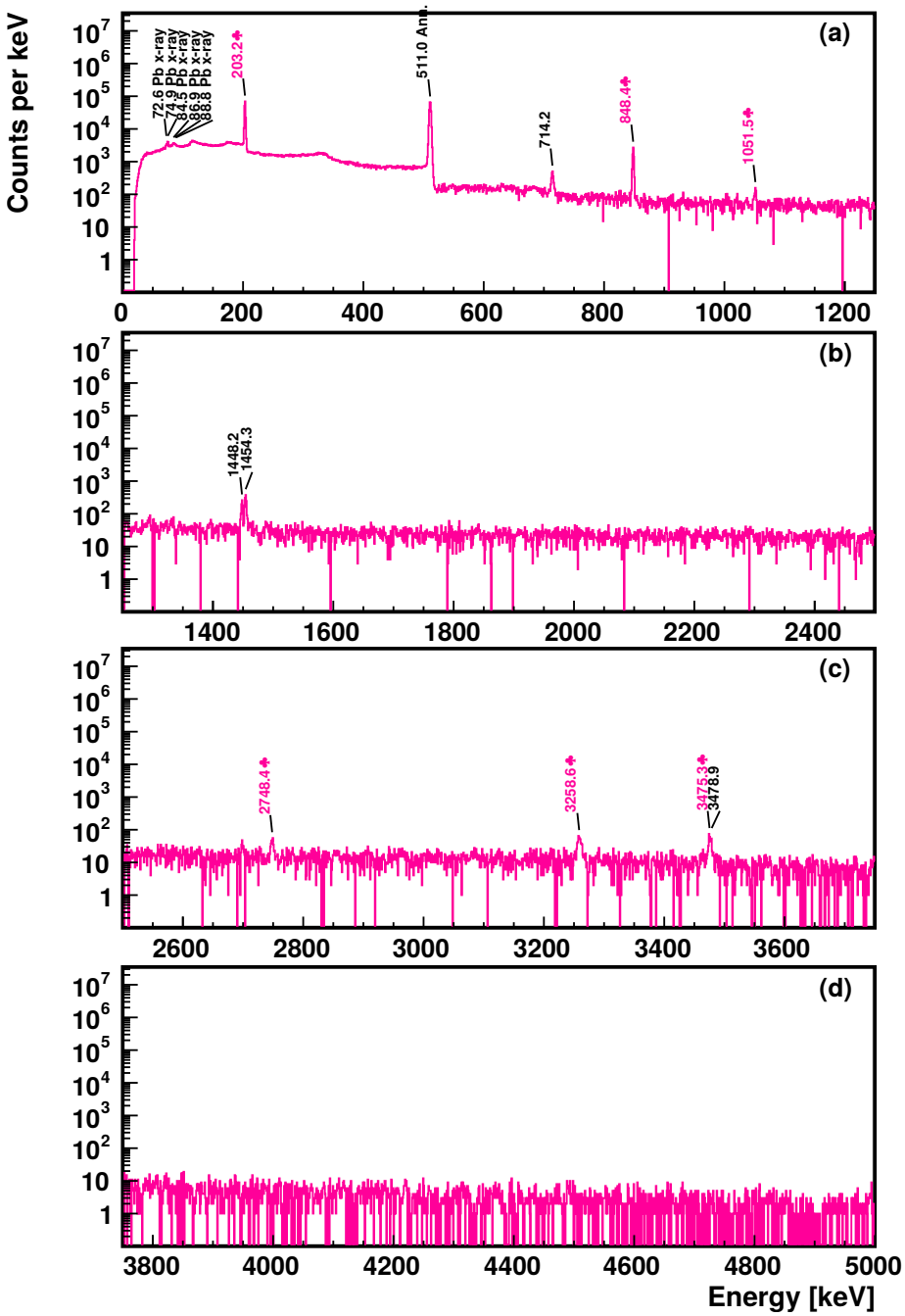

Figure J.2: γ spectrum for ^{58}Zn constructed with a β-implant correlation window $[1, 600] \ominus [-600, -1]ms$, and a β-γ coincidence window $[0, 0.8] \ominus [-80, -40]\mu s$. γs assigned to ^{58}Zn decay are drawn in pink and marked with ♣, also the Pb x-rays and the e^+ annihilation peak are marked. Unassigned γs are labelled in black.

J.3. Half-life measurement for ^{58}Zn decay using all decay members

The fit function was constructed using the Bateman equations taking into account the mother nucleus ^{58}Zn, daughter nucleus ^{58}Cu, and granddaughter nucleus ^{58}Ni. The number of nuclei was fixed from the number of implantations at third dsssd ($N_0(^{58}Zn) = 1.930.602$). Dead-time was measured by the scalers after each implantation ($DT(^{58}\text{Zn}) = 0.26015381$) and was fixed during the fit. In Tab. J.1 and Fig. J.3 the result of the fits are shown.

Nucl.	N_0	$T_{1/2}$	ε_β	DT
^{58}Zn	1.930.602	85.03_{18}ms	0.8509_{13}	$0, 26015381$
^{58}Cu	0	3.204ms	0.8509_{13}	$0, 26015381$

(a) Fitted parameters corresponding to Bateman equations.

Parameter	Comment
A_0	$2.669, 5_{32}$
χ^2_i/NDF	**1183/1191**
Fit Method	RMIELN

(b) Fitted statistics and background adjusted parameters.

Table J.1: The result of the fits of the correlation time using all decay members in Fig. J.2, parameters fixed during the fit are shown in black, and fitted parameters are shown in blue.

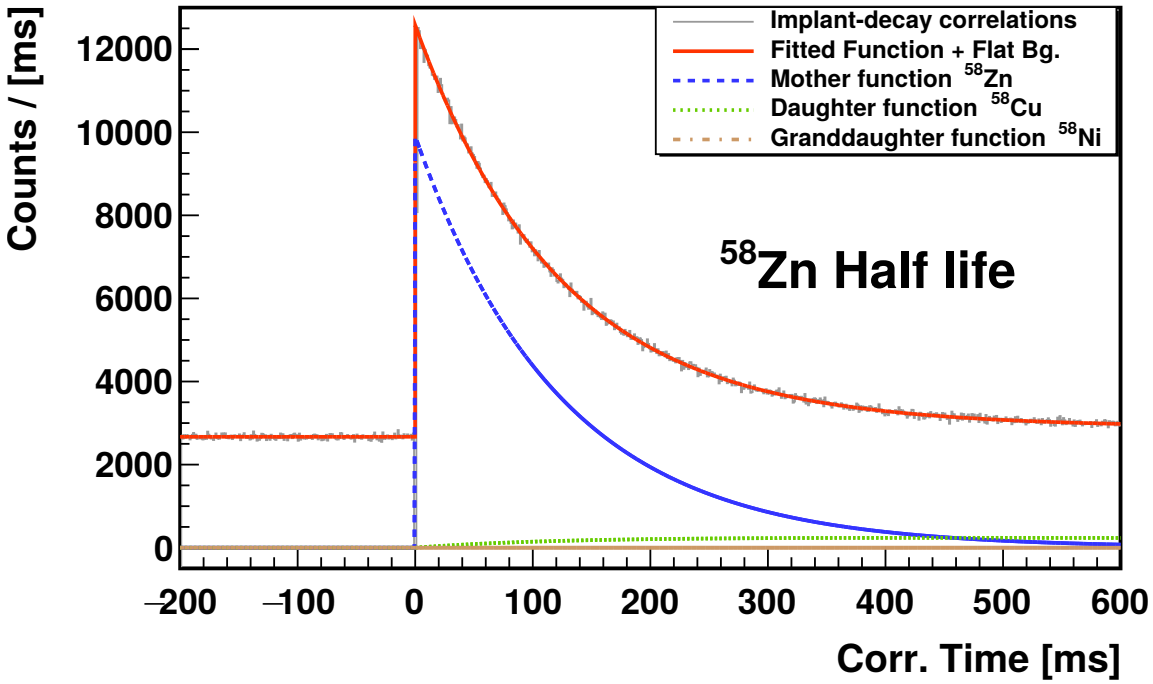

Figure J.3: Implant-decay correlation time taking into account the daughter and granddaughter nuclei of ^{58}Zn.

J.4. Half-life for ^{58}Zn using the E_γ=203 keV coincidence condition

The $E_\gamma = 203.1_1$keV (see Fig. J.2) was used to measure the half life for ^{58}Zn decay with γ-rays within the energy window $E_\gamma \in [201.0, 205.4] \ominus [189.3, 201.0] \ominus [205.4, 216.6] keV$.

Isotope	N_0	$T_{1/2}$	ε_β	DT
^{58}Zn	1.930.602	$84,60_{30}$ms	$0,10333_{29}$	0, 26015381
^{58}Cu	0	3.204ms	0	0, 26015381

(a) Fitted parameters corresponding to Bateman equations.

Parameter	Comment
A_0	$33,565_{36}$
χ^2_i/NDF	1235/1191
Fit Method	RMIELN

(b) Fitted statistics and background adjusted parameters.

Table J.2: Fit results of γ-gated spectrum in Fig. J.4, parameters fixed during the fit are shown in black, and fitted parameters are shown in blue.

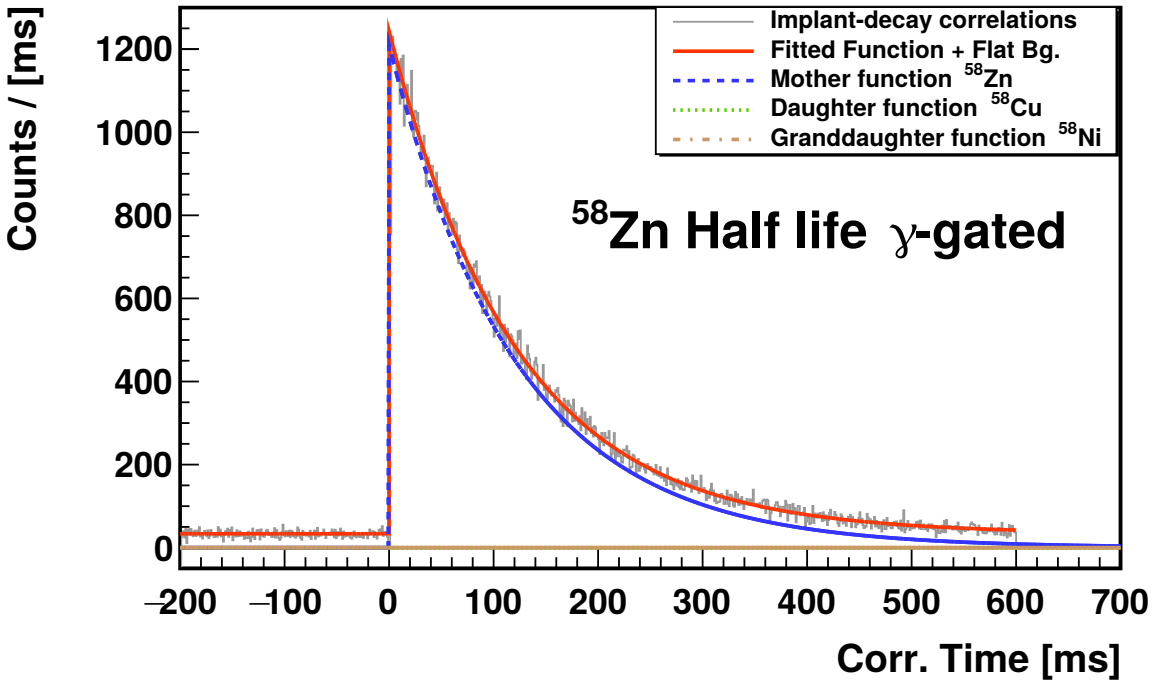

Figure J.4: Implant-decay correlation time gated on $E_\gamma = 203keV$. As this is a γ-gated spectrum, daughter and granddaughter nuclei do not contribute to the correlation curve.

J.5. Level scheme for ^{58}Zn decay

Level scheme was reconstructed for ^{58}Zn decay using the AME2016 [WAK+17] mass excess, Q_β value and half-life from the fit using all decay members in Appendix J.3. Then in Fig. J.5 the level scheme for ^{58}Zn decay is shown.

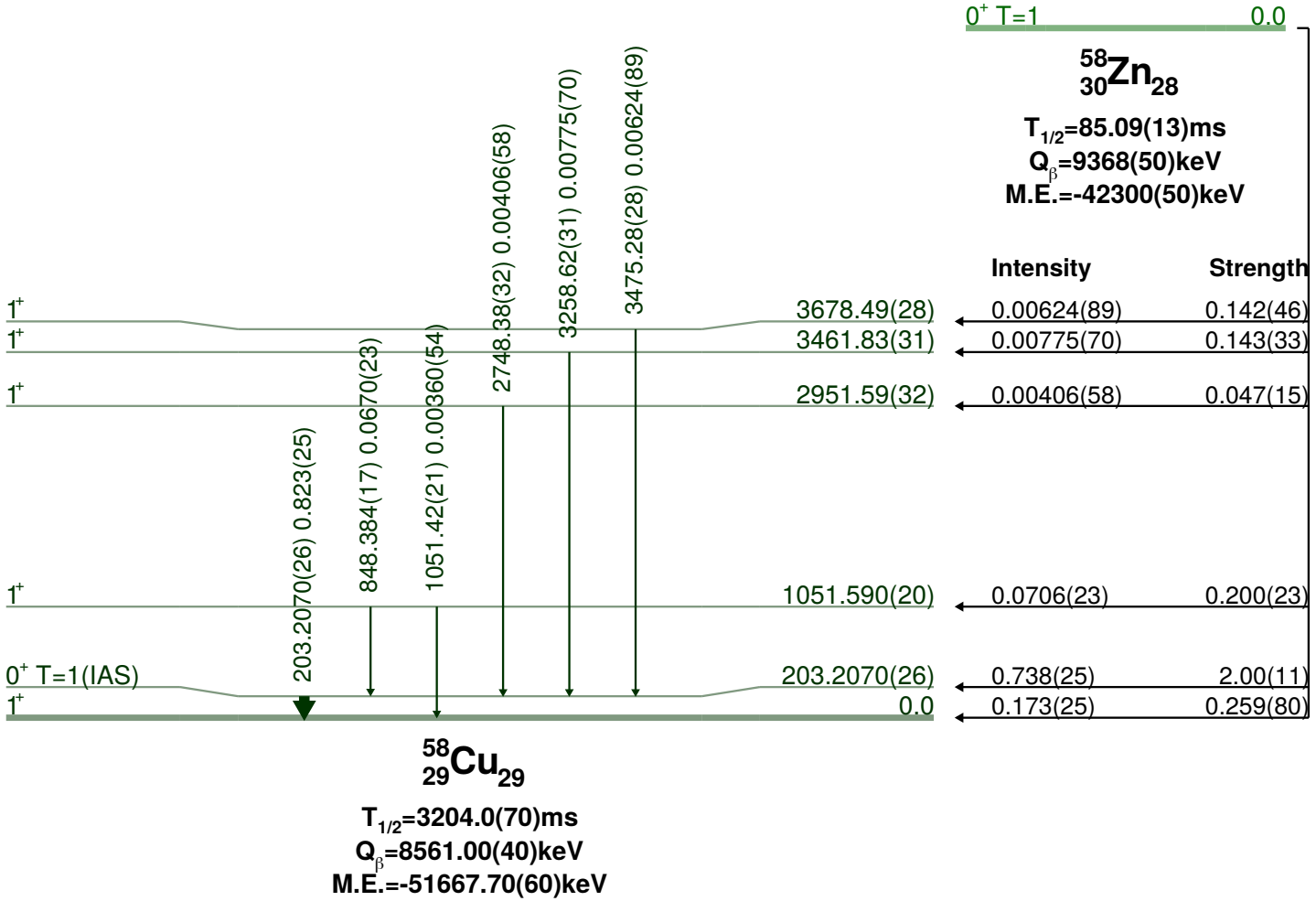

Figure J.5: Decay scheme for ^{58}Zn β^+ decay. γ-rays already reported in the literature are drawn in black while the γ observed in this experiment are shown in green.

Appendix K

Pb X-ray Energies and Intensities

X-ray can be emitted when an electron from an inner atomic shell is ejected from the atom. In this experiment, lead x-ray fluorescence was present in most of the γ-ray spectra.

Lead x-ray tables are wide available in literature for example in [Fir96]. In Table K.1 the most intense x-ray lines of lead are shown.

Siegbahn Notation	Energy [keV]	Intensity (per 100 K-Shell vacancies)
$k_{\alpha 1}$	74.969	46.2_9
$k_{\alpha 2}$	72.805	27.7_6
$k_{\alpha 3}$	72.144	0.0428_{13}
$k_{\beta 1}$	84.938	10.70_{22}
$k_{\beta 2}$	87.300	3.91_8
$k_{\beta 3}$	84.450	5.58_{11}

Table K.1: List of fluorescence X-rays for Lead obtained from [Fir96]. The Siegbahn notation corresponding in this case to $k_{\alpha 1} = K \rightarrow L_3$, $k_{\alpha 2} = K \rightarrow L_2$, $k_{\alpha 3} = K \rightarrow L_1$, $k_{\beta 1} = K \rightarrow M_3$, $k_{\beta 2} = K \rightarrow N_2 N_3$, and $k_{\beta 3} = K \rightarrow M_2$.

Bibliography

[AAB+02] H. Abele, M. Astruc Hoffmann, S. Baeßler, D. Dubbers, F. Glück, U. Müller, V. Nesvizhevsky, J. Reich, and O. Zimmer. Is the Unitarity of the Quark-Mixing CKM Matrix Violated in Neutron Beta Decay? *Physical Review Letters*, 88(21):4, 2002.

[AKW+17] G. Audi, F. G. Kondev, Meng Wang, W. J. Huang, and S. Naimi. The NUBASE2016 evaluation of nuclear properties. *Chinese Physics C*, 41(3):1–138, 2017.

[AWT03] Audi G., Wapstra A.H., and Thibault C. The Ame2003 atomic mass evaluation - (II). Tables, graphs and references. *Nuclear Physics A*, 729(1):337–676, 2003.

[B+91] D. P. Balamuth et al. In-beam γ-ray spectroscopy of the n=z+1 nucleus ^{63}Ga. *Phys. Rev. C*, 43(5):2082–2097, 1991.

[B+07] B. Blank et al. Production cross-sections of proton-rich 70Ge fragments and the decay of 57Zn and 61Ge. *Eur. Phys. J. A*, 31:267–272, 2007.

[B+10] H. Baba et al. New data acquisition system for the riken radioactive isotope beam factory. *Nucl. Inst. and Meth. in Phys. Res. A*, 616:65–68, 2010.

[B+15] H. Baba et al. Time-stamping system for nuclear physics experiments at riken ribf. *Nucl. Inst. and Meth. in Phys. Res. A: Accelerators, Spectrometers, Detectors and Associated Equipment*, 777:75–79, 2015.

[Bat10] H. Bateman. Solution of a differential equations occurring in the theory of radiactive transformations. *Proc. Cambridge Philos. Soc.*, 15:423–427, 1910.

[Bec96] Henri Becquerel. Sur les radiations émises par phosphorescence. *Comptes Rendus de l'Académie des sciences*, 1896.

[C+15] P.F.F. Carnelli et al. Multi-Sampling Ionization Chamber (MUSIC) for measurements of fusion reactions with radioactive beams. *Nucl. Instr. and Meth. in Phys. Res. A*, pages 197–202, 2015.

[Cha14] J. Chadwick. Intensitätsverteilung im magnetischen Spektrum von β-Strahlen von Radium B+C. *Verh. d. Deutsch. Phys. Ges*, 1914.

[DAA+07] C. Dossat, N. Adimi, F. Aksouh, F. Becker, A. Bey, B. Blank, C. Borcea, R. Borcea, A. Boston, M. Caamano, G. Canchel, M. Chartier, D. Cortina, S. Czajkowski, G. de France, F. de Oliveira Santos, A. Fleury, G. Georgiev, J. Giovinazzo, S. Grévy, R. Grzywacz, M. Hellström, M. Honma, Z. Janas, D. Karamanis, J. Kurcewicz, M. Lewitowicz, M. J. López Jiménez, C. Mazzocchi, I. Matea, V. Maslov, P. Mayet, C. Moore, M. Pfützner, M. S. Pravikoff, M. Stanoiu, I. Stefan, and J. C. Thomas. The decay of proton-rich nuclei in the mass A = 36 - 56 region. *Nuclear Physics A*, 792(1-2):18–86, 2007.

[DFF+19] F. Diel, Y. Fujita, H. Fujita, F. Cappuzzello, E. Ganioğlu, E. W. Grewe, T. Hashimoto, K. Hatanaka, M. Honma, T. Itoh, J. Jolie, Bin Liu, T. Otsuka, K. Takahisa, G. Susoy, B. Rubio, and A. Tamii. High-resolution study of the Gamow-Teller (GT) strength in the Zn64 (3He,t) Ga64 reaction. *Physical Review C*, 99(5):1–10, 2019.

[Die15] Felix Diel. *Study of $Tz = +2 \rightarrow +1$ Gamow-Teller transitions in a 64Zn(3He,t)64Ga reaction.* PhD thesis, University of Cologne, 2015.

[ELG+91] P.J. Ennis, C. J. Lister, W. Gelletly, H.G. Price, B.J. Varley, P.A. Butler, T. Hoare, S. Cwiok, and W. Nazarewicz. Triaxiality and Isospin-Forbidden E1 Decays in the N=Z Nucleus 64Ge. *Nuclear Physics A*, 535:392–424, 1991.

[F+13] N. Fukuda et al. Identification and separation of radioactive isotope beams by the BigRIPS separator at the RIKEN RI Beam Factory. *Nucl. Instr. Meth. B*, 317:323–332, 2013.

[FEA+03] Farnea, Others E, G De Angelis, A Gadea, P G Bizzeti, A Dewald, and J Eberth. Isospin mixing in the N=Z nucleus 64Ge. *Physics Letters B*, 551:56–62, 2003.

[Fer34] E. Fermi. Versuch einer Theorie der β-Strahlen. I. *Zeitschrift für Physik*, 88(3-4):161–177, 1934.

[Fir96] Richard B. Firestone. *Table of Isotopes.* Jhon Wiley & Sons, 8 edition, 1996.

[FRG11] Y Fujita, B Rubio, and W Gelletly. Spin-isospin excitations probed by strong, weak and electro-magnetic interactions. *Progress in Particle and Nuclear Physics*, 66(3):549–606, 2011.

[Fuj01] Y. Fujita. Isospin Symmetry-Structure Study at New High-Resolution Course of RCNP. *Nuclear Physics A*, 687:311c–320c, 2001.

[G+95] R. Grzywacz et al. Identification of μs-isomers produced in the fragmentation of a112Sn beam. *Physics Letters B*, 355(3-4):439–446, 1995.

[G+98] R. Grzywacz et al. Isomeric states in ^{66}As. *Phys. Lett. B*, 429:247–253, 1998.

[G+01] R. Grzywacz et al. In-beam study of the N=Z nucleus ^{66}As using the decay tagging technique. *Nuc. Phys. A*, 682:41c–47c, 2001.

[Goi17] Thomas Goigoux. *Study of 67Kr two-proton radioactivity and development of a time projection chamber*. PhD thesis, L'Université de Bordeaux, 2017.

[gro13] RIBFDAQ group. Anaroot. https://ribf.riken.jp/RIBFDAQ/index.php?Tools%2FAnalysis%2FANAROOT, 2013.

[H+87] M.A.C. Hotchkis et al. Beta-delayed proton decay of 61Ge. *Phys. Rev. C*, 35(1):315–319, January 1987.

[Hey99] K Heyde. *Basic Ideas and Concepts in Nuclear Physics an Introductory Approach*. Institute of Physics Publishing, 1999.

[HT15] J. C. Hardy and I. S. Towner. Superallowed 0+→0+ nuclear β decays: 2014 critical survey, with precise results for Vud and CKM unitarity. *Physical Review C - Nuclear Physics*, 91(2):1–27, 2015.

[Iso13] Tadaaki Isobe. Anaroot: new online/offline framework for ribf data analysis based on root. *RIBF User meeting*, 2013.

[J+02] A. Jokinen et al. Beta decay of 57Zn*. *EPJ direct*, 4(1):1–11, Dec 2002.

[K+12] Toshiyuki Kubo et al. BigRIPS separator and ZeroDegree spectrometer at RIKEN RI Beam Factory. *Prog. Theor. Exp. Phys.*, pages 1–11, 2012.

[Kam17] O. Kamigaito. Developments of linear accelerators at RI Beam Factory. *RIKEN Accel. Prog. Rep.*, pages S–54 – S–55, 2017.

[KL11] F. G. Kondev and S. Lalkovski. Nuclear Data Sheets for A = 207. *Nuclear Data Sheets*, 112(3):707–853, 2011.

[KOF+13] H. Kumagai, T. Ohnishi, N. Fukuda, H. Takeda, D. Kameda, N. Inabe, K. Yoshida, and T. Kubo. Developments of Parallel Plate Avalanche Counter (PPAC) for BigRIPS fragment separator. *Nucl. Instr. and Meth. in Phys. Res. B*, pages 717–727, 2013.

[Kra87] Kenneth S. Krane. *Introductory Nuclear Physics*. John Wiley & Sons, Oregon State Universiy, 1987.

[KRK11] Y. Khazov, A. Rodionov, and F. G. Kondev. Nuclear Data Sheets for A = 133. *Nuclear Data Sheets*, 112(4):855–1113, 2011.

[LB09] S.M. Lenzi and M.A. Bentley. Test of Isospin Symmetry Along the N=Z Line. *Lect. Notes Phys*, 764(2009):57–98, 2009.

[Mar13] M. J. Martin. Nuclear Data Sheets for A = 152. *Nuclear Data Sheets*, 114(11):1497–1847, 2013.

[MGA+12] M.Wang, G.Audi, A.H.Wapstra, F.G.Kondev, M.MacCormick, X.Xu, and B.Pfeiffer. The AME2012 atomic mass evaluation(II). Tables, graphs and references. *Chinese Physics C*, (12):1603–2014, 2012.

[Mol11] Francisco Molina. *Beta Decay of Tz=-1 nuclei and Comparison with Charge Exchange Reaction Experiments*. PhD thesis, Universidad de Valencia, 2011.

[Mor11] Ana Isabel Morales. *Beta-delayed gamma-ray spectroscopy of heavy neutron-rich nuclei produced by cold-fragmentation of 208Pb*. PhD thesis, Universidad de Santiago de Compostela, 2011.

[MRF+15] F. Molina, B. Rubio, Y. Fujita, W. Gelletly, J. Agramunt, A. Algora, J. Benlliure, P. Boutachkov, L. Cáceres, R. B. Cakirli, E. Casarejos, C. Domingo-Pardo, P. Doornenbal, A. Gadea, E. Ganioglu, M. Gascón, H. Geissel, J. Gerl, M. Górska, J. Grbosz, R. Hoischen, R. Kumar, N. Kurz, I. Kojouharov, L. Amon Susam, H. Matsubara, A. I. Morales, Y. Oktem, D. Pauwels, D. Pérez-Loureiro, S. Pietri, Zs Podolyák, W. Prokopowicz, D. Rudolph, H. Schaffner, S. J. Steer, J. L. Tain, A. Tamii, S. Tashenov, J. J. Valiente-Dobón, S. Verma, and H. J. Wollersheim. Tz=-1 $\rightarrow$ 0 β decays of Ni54, Fe50, Cr46, and Ti42 and comparison with mirror (He3,t) measurements. *Physical Review C - Nuclear Physics*, 91(1):014301, 2015.

[Nis12] Shunji Nishimura. Beta-gamma spectroscopy at RIBF. *Progress of Theoretical and Experimental Physics*, 2012(1):1–13, 2012.

[NLXW13] S. Nishimura, G. Lorusso, Z. Xu, and J. Wu. WAS3ABi: The beta-counting system for the EURICA project. *RIKEN Accel. Prog. Rep.*, 46:182, 2013.

[ORA+14] S. E. A. Orrigo, B. Rubio, J. Agramunt, A. Algora, F. Molina, Y. Fujita, B. Blank, P. Ascher, M. Gerbaux, J. Giovinazzo, S. Grévy, T. Kurtukian-Nieto, W. Gelletly, B. Bilgier, R. B. Cakirli, E. Ganioglu, H. C. Kozer, L. Kucuk, G. Susoy, L. Cáceres, O. Kamalou, C. Stodel, J. C. Thomas, H. Fujita, T. Suzuki, A. Tamii, L. Popescu, and A. M. Rogers. Beta decay of the exotic Tz=-2, 56Zn nucleus and half-life of various proton-rich Tz=-1 nuclei. *Acta Physica Polonica B*, 45(2):355–362, 2014.

[ORF+14] S. E. A. Orrigo, B. Rubio, Y. Fujita, B. Blank, W. Gelletly, J. Agramunt, A. Algora, P. Ascher, B. Bilgier, L. Cáceres, R. B. Cakirli, H. Fujita, E. Ganio, M. Gerbaux, J. Giovinazzo, S. Grévy, O. Kamalou, H. C. Kozer, L. Kucuk, F. Molina, L. Popescu, A. M. Rogers, G. Susoy, C. Stodel, and T. Suzuki. Observation of the Beta-Delayed Gamma-Proton Decay of 56Zn and its Impact on the Gamow-Teller Strength Evaluation. *Physical Review Letters*, 112(June):1–5, 2014.

[ORF+16] S. E.A. Orrigo, B. Rubio, Y. Fujita, W. Gelletly, J. Agramunt, A. Algora, P. Ascher, B. Bilgier, B. Blank, L. Cáceres, R. B. Cakirli, E. Ganioğlu, M. Gerbaux, J. Giovinazzo, S. Grévy, O. Kamalou, H. C. Kozer, L. Kucuk, T. Kurtukian-Nieto, F. Molina, L. Popescu, A. M. Rogers, G. Susoy, C. Stodel, T. Suzuki, A. Tamii, and J. C. Thomas. β decay of the exotic Tz=-2 nuclei Fe48, Ni52, and Zn56. *Physical Review C*, 93(4):1–18, 2016.

[Pau33] W. Pauli. *Rapports et Discussions du Septieme Conseil de Physique Solvay*. Institut international de physique Solvay, Brussels, 1933.

[Rad00] D.C. Radford. Notes on the use of the program gf3. https://radware.phy.ornl.gov/gf3/gf3.html#5.2., 2000.

[RG09] B. Rubio and W. Gelletly. Beta Decay of Exotic Nuclei. *Lect. Notes Phys*, 764:99–151, 2009.

[RGL+11] A.M. Rogers, J. Giovinazzo, C.J. Lister, B. Blank, et al. 69Kr beta-delayed proton emission: A Trojan horse for studying states in proton-unbound 69Br. *Phys. Rev. C*, 84:051306, 2011.

[SBF+05] A. Stolz, T. Baumann, N. H. Frank, T. N. Ginter, G. W. Hitt, E. Kwan, M. Mocko, W. Peters, A. Schiller, C. S. Sumithrarachchi, and M. Thoennessen. Discovery of 60Ge and 64Se. *European Physical Journal A*, 25(SUPPL. 1):335–338, 2005.

[SFF+14] N. Sakamoto, M. Fujimaki, N. Fukunishi, Y. Higurashi, O. Kamigaito, H. Okuno, K. Suda, T. Watanabe, Y. Watanabe, and K. Yamada. Performance of new injector rilac2 for riken ri-beam factory. *Proceedings of LINAC*, pages 1123–1126, 2014.

[Sim19] E. Simpson. The colorful nuclide chart. https://people.physics.anu.edu.au/~ecs103/chart/, 2019.

[Skr74] K. Skrable. A general equation for the kinetics of linear first order phenomena and suggested applications. *Health Physics*, 27:155–157, 1974. Analysis.

[SND+13] P. A. Söderström, S. Nishimura, P. Doornenbal, G. Lorusso, T. Sumikama, H. Watanabe, Z. Y. Xu, H. Baba, F. Browne, S. Go, G. Gey, T. Isobe, H. S. Jung, G. D. Kim, Y. K. Kim, I. Kojouharov, N. Kurz, Y. K. Kwon, Z. Li, K. Moschner, T. Nakao, H. Nishibata, M. Nishimura, A. Odahara, H. Sakurai, H. Schaffner, T. Shimoda, J. Taprogge, Zs Vajta, V. Werner, J. Wu, A. Yagi, and K. Yoshinaga. Installation and commissioning of EURICA - Euroball-RIKEN Cluster Array. *Nuclear Instruments and Methods in Physics Research, Section B: Beam Interactions with Materials and Atoms*, 317(PART B):649–652, 2013.

[Tap15] Jan Taprogge. *Decay Spectroscopy of Neutron-Rich Cadmium Isotopes*. PhD thesis, Universidad Autonoma de Madrid, 2015.

[TdO14] R. Thibes and Suzicleide L. de Oliveira. General solution to bateman's differential equations with direct index notation. *International Journal of Pure and Applied Mathematics*, 93(6):879–883, 2014.

[Tea19] BigRIPS Team. Technical information of bigrips, zerodegree, samurai beam line, and oedo beam line. http://ribf.riken.jp/BigRIPSInfo/, 2019.

[TH15] I. S. Towner and J. C. Hardy. Theoretical corrections and world data for the superallowed ft values in the β decays of Ti42, Cr46, Fe50, and Ni54. *Physical Review C - Nuclear Physics*, 92(5):1–9, 2015.

[W+01] M. Weiszflog et al. High-spin spectroscopy of ^{63}Ga and ^{65}Ga. *Eur. Phys. J. A*, 11:25–38, 2001.

[WAK+17] Meng Wang, G. Audi, F. G. Kondev, W.J. Huang, S. Naimi, and Xing Xu. The AME2016 atomic mass evaluation (II). tables, graphs and references. *Chinese Physics C*, 41(3):030003, 2017.

[Wig57] E. P. Wigner. Phys. rev. *Proceedings of the Robert A. Welch Conferences on Chemical Research*, 1:67, 1957.

[WT59] S. Weinberg and S. B. Treiman. Electromagnetic corrections to isotopic spin conservation. *Phys. Rev.*, 116:465–468, 1959.

[Xu15] Zhengyu Xu. *Beta-decay spectroscopy on neutron-rich nuclei in a range of Z = 26-32*. PhD thesis, University of Hong Kong, 2015.

[ZZB10] J. F. Ziegler, M. D. Ziegler, and J. P. Biersack. SRIM - The stopping and range of ions in matter (2010). *Nuclear Instruments and Methods in Physics Research B*, 268:1818–1823, June 2010.